ACCURATE 3D NUMERICAL MODELS FOR THE FIRE PERFORMANCE ON LSF PARTITION WALLS

Giovanna Lyssa da Costa Frizzera

Dissertation presented to the School of Technology and Management of Bragança to obtain the Master Degree in Construction Engineering.

Work oriented by:

Prof. Dr. Paulo Alexandre Gonçalves Piloto

Prof. Dra. Renata Gomes Lanna da Silva

Bragança

2024

ACCURATE 3D NUMERICAL MODELS FOR THE FIRE PERFORMANCE ON LSF PARTITION WALLS

Giovanna Lyssa da Costa Frizzera

Dissertation presented to the School of Technology and Management of Bragança to obtain the Master Degree in Construction Engineering.

Work oriented by:

Prof. Dr. Paulo Alexandre Gonçalves Piloto

Prof. Dra. Renata Gomes Lanna da Silva

Bragança

2024

Acknowledgment

I would like to express my sincere gratitude to all the individuals who contributed to the completion of this work and to my academic journey.

Firstly, I wish to thank my supervisors, Prof. Dr. Paulo Alexandre Gonçalves Piloto from IPB (Portugal) and Prof. Dra. Renata Gomes Lanna da Silva from CEFET (Brazil). Their guidance, valuable insights, and continuous support were fundamental to the development of this project.

To CEFET, I extend my heartfelt gratitude for the unique opportunity to undertake this exchange, along with all the support provided during my undergraduate studies. To IPB, for the warm welcome and the opportunity to conduct this research in its academic environment. The stimulating learning environment and resources offered by both institutions were essential to the success of this work.

To my friends, who shared moments of joy, challenges, and triumphs with me. You were incredibly important during this journey and made it even more meaningful.

To my family, Danieli, Giuliano, Daniel, and Clara, who have always been by my side, offering love, encouragement, and unwavering support. Your constant encouragement was the foundation upon which I built my academic dreams. Without you, none of this would be possible.

Finally, I would like to express my profound gratitude to all those who contributed in some way to this work and to my academic formation, especially Ana Caramelo, Daniel, Clara, Lucas Melo and Renato. This is just the beginning of a journey that will continue to be shaped by learning and the relentless pursuit of knowledge.

Abstract

The present study proposes a numerical model analysis of the fire performance of non-load bearing Light Steel Frame (LSF) walls under fire. Assessments were conducted under ISO 834 and hydrocarbon fire conditions, including the numerical validation of medium-scale experimental fire resistance tests.

Comparison between numerical and experimental results employed three different computational solution methods for walls without cavity insulation. The hybrid method (solution method 1) considers convection and radiation in the cavity region, using the experimental cavity temperature. To predict this temperature, solution method 2 employs interface elements for radiation heat transfer, while solution method 3 considers radiation and convection in the cavity region.

The analysis used the Root Mean Square Error (RMSE) to compare the temperature evolution at different locations on the wall section at specific time increments. The hybrid method (solution 1) presented a lower RMSE, providing a better approximation by considering phenomena such as cracks and material falls during the tests. The relative error was used to compare the fire resistance times obtained from numerical simulations and experimental tests.

A parametric study was developed to investigate the thermal effect of the thickness and type of the wall protection layer, as well as the density of the insulation material. The results allowed for the formulation of a new proposal to predict fire resistance for insulation, considering the parameters analysed.

Keywords: Fire resistance; LSF walls; Partition Wall; Numerical Simulation.

Resumo

O presente estudo propõe uma análise numérica do desempenho ao fogo de paredes de aço leve (LSF) não suportadas por carga. Avaliações foram conduzidas sob condições de incêndio de acordo com a ISO 834 e com fogo de hidrocarboneto, incluindo a validação numérica de testes experimentais de resistência ao fogo em escala média.

A comparação entre os resultados numéricos e experimentais empregou três diferentes métodos de solução computacional para paredes sem isolamento na cavidade. O método híbrido (método de solução 1) considera a convecção e a radiação na região da cavidade, utilizando a temperatura experimental da cavidade. Para prever essa temperatura, o método de solução 2 emprega elementos de interface para a transferência de calor por radiação, enquanto o método de solução 3 considera radiação e convecção na região da cavidade.

A análise utilizou o RMSE para comparar a evolução da temperatura em diferentes locais na seção da parede em incrementos de tempo específicos. O método híbrido (solução 1) apresentou um RMSE mais baixo, fornecendo uma melhor aproximação ao considerar fenômenos como fissuras e queda de material durante os testes. O erro relativo foi usado para comparar os tempos de resistência ao fogo obtidos a partir de simulações numéricas e testes experimentais.

Um estudo paramétrico foi desenvolvido para investigar o efeito térmico da espessura e tipo da camada de proteção da parede, bem como a densidade do material isolante. Os resultados permitiram a formulação de uma nova proposta para prever a resistência ao fogo para isolamentos, considerando os parâmetros analisados.

Palavras-chave: Resistência ao Fogo; Paredes de Aço Leve; Paredes Não Estruturais; Simulação Numérica.

Contents

List of Tables

List of Figures

Acronyms

APDL ANSYS Parametric Design Language.

CFS Cold-Formed Steel.

FEA Finite Element Analysis.

FEM Finite Element Model.

FRR Fire Resistant Ratings.

LSF Light Steel Frame.

RE Relative Error.

RMSE Root Mean Square Error.

Chapter 1

Introduction

The growing concern about fire safety in buildings is driven by recent accidents and their tragic consequences in terms of loss of lives and material damage. This scenario has heightened the importance of evaluating the fire performance of Light Steel Frame (LSF) walls. Figure 1.1 presents one of the last fire events in Valencia (Spain) in 2024, February 22nd, where fire spread in one hour through the 138 apartments and left at least ten dead people and up to 14 missing people. Their, one can see the partition walls failed and even the LSF deformed a lot, losing all the gypsum layers and protection.

Although regulations and simulations of the standard ISO 834 fire test are widely used to assess performance under fire conditions, this approach may not be entirely suitable for evaluating LSF walls. This discrepancy arises due to differences between the actual time and temperature curves in fires and those simulated by the ISO 834 test, especially regarding the maximum temperature reached and the time required to achieve it [1].

Hydrocarbon fires, common in facilities of oil, gas, and chemical complexes, can also occur in buildings, as evidenced by the attack on the Twin Towers on September 11, 2001, contributing to the total collapse of the structure [2], [3]. This event led to in-depth studies of fires under non-conventional conditions [4].

While the behaviour of LSF walls in standard fire scenarios is well-known, there is an urgent need to assess the insulation performance under fire in different sets of LSF walls subjected to various fire conditions. This is because materials and structures that

(a) Post fire inspection on Friday.

(b) Detail of the facade and interior of the building during the fire.

Figure 1.1: The fire in a building in Valencia (Spain) (photo from El Pais, Mònica Torres).

are effective under normal conditions may not provide the level of protection required in hydrocarbon fire situations [2]. The study of non-conventional conditions can significantly contribute to improving fire design rules, based on both performance and prescriptive criteria, for LSF constructions, ensuring their safety at elevated temperatures.

However, full-scale fire tests are time consuming and expensive. Therefore, Finite Element Analysis (FEA) emerges as a viable alternative to investigate the fire performance of LSF wall systems and understand their thermomechanical behaviour. The numerical models developed consider the fire temperature as a boundary condition in the model, evaluating the temperature distribution of the LSF walls to determine their fire performance.

1.1 Objectives

This work aims to comprehensively understand the behaviour of Light Steel Frame (LSF) walls when exposed to high temperatures. The proposed approach includes a detailed analysis of the fire resistance of these walls through thermal analyses. Using the Finite Element Model (FEM), simulations will be conducted to assess the average and maximum temperatures on the unexposed side of LSF walls during simulations, with the purpose of determining fire resistance through insulation.

1.1.1 Specific Objectives

Develop and implement numerical simulation models, using Ansys Mechanical ANSYS Parametric Design Language (APDL) software, to analyse the behaviour of LSF walls in different fire scenarios, encompassing both ISO 834 standard fire and hydrocarbon fire.

Conduct a comprehensive parametric study, investigating how variables such as fire intensity, cavity region filling, type, and dimensions of the fire protection board affect the behaviour of LSF walls.

Propose a simplified calculation method that allows for a practical assessment of the fire resistance of LSF walls.

These objectives aim to contribute to a deeper understanding of the behaviour of LSF walls in fire situations and provide practical tools for the evaluation and design of fire insulation systems in LSF structures.

1.2 Outline of Thesis

This dissertation is structured into six chapters.

Chapter 1: provides a brief introduction to the topic, outlines the general and specific objectives of the study, and presents the structure of the work.

Chapter 2: discusses the state of the art, introducing the concepts of Light Steel Frame, load bearing and non-load bearing walls, and providing a chronological review of studies related to LSF walls.

Chapter 3: defines the main characteristics of fire, along with the fire resistance structure. It presents the standard curves used to evaluate this phenomenon and discusses the theory of heat transfer.

Chapter 4: presents the mathematical models and the properties of materials used in the simulation. It includes the validation of numerical models through comparison with experimental tests.

Chapter 5: conducts the parametric study, where numerical models are developed with variations in the thickness and type of protection boards, as well as different densities

for the insulation material inside and outside the cavity. This chapter is followed by a discussion of the results.

Chapter 6: brings the final conclusions of the study and suggests possible directions for future developments.

Appendix A: presents the material properties.

Appendix B: provides details and representations of the studied LSF walls.

Chapter 2

State of the Art

This chapter aims to deepen the understanding of wall systems constructed using Light Steel Frame (LSF) in the context of investigating their performance in fire situations. LSF systems, characterised by an innovative approach in the construction industry, stand out for providing lightweight and efficient structures. The chapter will specifically address the different categories of LSF walls, exploring their application in various functionalities. Additionally, it will include an analysis of experimental and numerical research aimed at evaluating the behaviour of LSF walls in various fire scenarios.

2.1 Light Steel Frame Walls

Walls constructed using the Light Steel Frame (LSF) methodology reflect a meticulous integration of materials that not only redefine construction paradigms but also establish new standards for performance and safety. The backbone of this innovation lies in light steel profiles, whose precision in manufacturing ensures a robust and durable structure.

These structures are carefully planned and built with galvanised steel profiles, providing resistance to corrosion and essential stability. Furthermore, the true potential of LSF walls is revealed by incorporating additional materials to enhance thermal, acoustic performance, and structural safety, as illustrated in Fig. 2.1.

The cladding of LSF walls plays a crucial role in optimising thermal insulation.

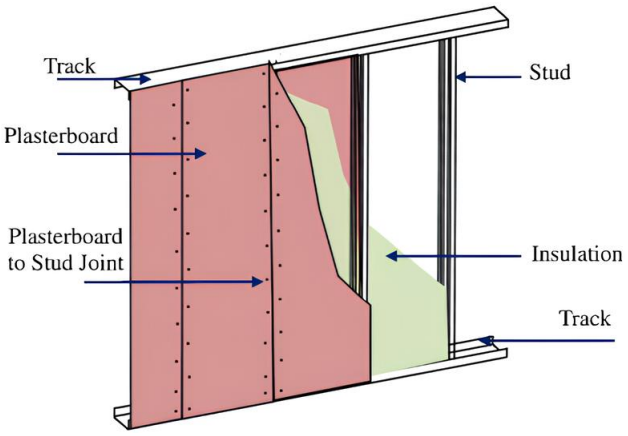

Figure 2.1: Light Steel Frame System [5].

Commonly used materials include plasterboard, calcium silicate boards, oriented strand boards, and steel sheets [6]. Their application not only serves as a surface prepared for finishes but also plays a vital role in protecting against direct exposure to fire and lateral containment of steel studs, contributing to structural stability [7].

Additionally, insulation materials such as rockwool, fiberglass, and cellulose fiber can be employed to improve acoustic and thermal control of walls due to their low heat transfer characteristics. However, using these materials within the cavity of walls provides lower fire resistance (R) compared to walls with empty cavities [8],[9]. On the other hand, using insulation between cladding sheets offers better fire protection [9], as will be presented in the validation of the results of this dissertation.

2.1.1 Partition Walls

A partition wall, in the context of civil construction, typically refers to an interior wall without structural support that is designed to divide a space, as opposed to walls that support the weight of the building. These structures can be constructed using a variety of materials, such as plasterboard, light steel structures, or modular panels. The choice of materials and construction methods depends on the specific needs of the environment and the architectural design.

Within the realm of fire performance research, Light Steel Frame (LSF) walls, when

employed as partitions in buildings, play a crucial role in spatial organisation. Their lightweight construction confers noteworthy advantages, offering flexibility in layout and adaptability to occupants' needs. In the investigation of these walls' behaviour in fire scenarios, it is crucial to consider not only structural integrity, but also the capacity to uphold compartmentalisation and slow down the propagation of fire.

Previous studies have devoted special attention to the analysis of the performance of (LSF) walls when used as partitions. For instance, Magaraboosha nam et al. [10] conducted full-scale experimental tests to investigate the fire resistance of LSF walls with single, double, and alternate studs, considering different cavity depths under non-load bearing conditions (Fig. 2.2). The results highlighted that two layers of gypsum coating and a wider cavity exhibited greater fire resistance. Furthermore, studies, like the one conducted by Gnanachelvam et al. [11] explored the fire resistance of non-load bearing Light Steel Frame (LSF) walls with cellulose insulation that incorporates phase change materials (PCM) through reduced-scale fire tests.

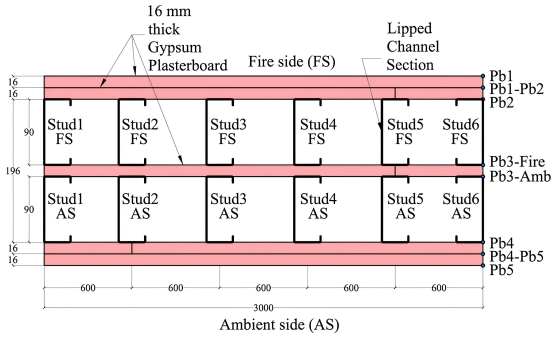

(a) Double stud wall.

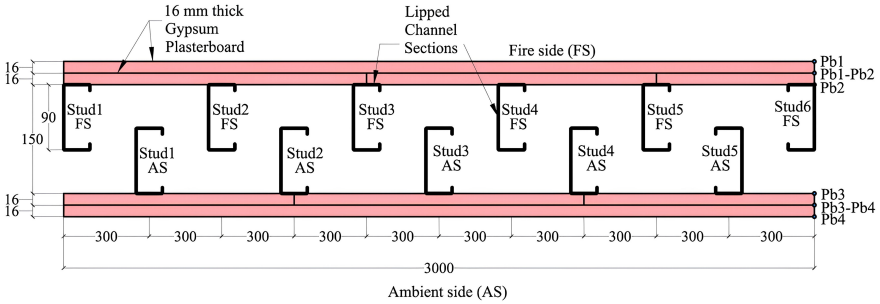

(b) Staggered stud wall.

Figure 2.2: Cross-section of LSF walls tested by Magaraboosha nam et al. [10].

2.1.2 Load Bearing Walls

Non-partition walls represent structural elements in a construction, playing a crucial role in support loads and preserving the overall stability of the structure. In contrast to partition walls, whose purpose is to segment internal spaces, non-partition walls are engineered to resist external forces and enhance the overall structural integrity of the building.

The selection of materials for the construction of non-partition walls is guided by specific structural requirements, taking into account factors such as the load to be supported, soil characteristics, and aesthetic demands of the architectural design. Materials such as concrete, steel, and masonry are commonly employed, each offering its own advantages in terms of strength and durability.

In the context of research dedicated to load bearing walls, the analysis encompasses not only the thermal performance of these structures but also their structural response under elevated temperature conditions. Notable studies include the one conducted by Gunalan et al. [12], who developed experimental and numerical tests [13] on Light Steel Frame (LSF) walls designed to support loads. These tests involved variations in the quantity of plasterboard, type and location of insulation (internal and external to the cavity), and applied load, with the aim of assessing the panels' performance in fire situations. The results indicated improvements offered by the new external insulation panel wall system compared to the conventional cavity insulation system. Moreover, the researchers proposed a simplified design method to predict the fire resistance rating, based on two equations. These equations aim to predict the temperature of the heated flange over time during a standard fire and the critical (failure) temperature of the hot flange as a function of load ratio for LSF wall systems with various configurations of plasterboard and insulation [14].

In 2015, the study conducted by Kesawan and Mahendran [5] is also noteworthy, suggesting the use of hollow flange channel (HFC) section studs in LSF walls to enhance their Fire Resistant Ratings (FRR). The results demonstrated that the new stud section (HFC) exhibited better performance in fire conditions compared to the conventional stud

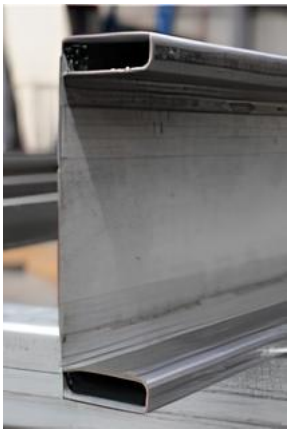

Figure 2.3: Hollow Flange Channel (HFC) section [5].

sections used.

2.2 Literature Review

Sultan [15], in 1996, presents a one-dimensional mathematical model designed to predict the fire resistance of unloaded non-insulated Cold-Formed Steel (CFS) stud wall assemblies protected with Type X gypsum plasterboards exposed to fire. The model considers various heat transfer mechanisms, including radiation, convection and conduction through the wall elements. The thermal properties of the plasterboard were determined experimentally. Although the model exhibited accuracy in predicting fire resistance, limitations were acknowledged, such as the omission of the thermal contribution of steel elements and the use of a one-dimensional heat transfer assumption. Analysis of the results showed that calcination of the plaster on the exposed surface occurred after around 17 minutes for assembly 1 (with 15.9 mm thick plasterboard) and approximately 11 minutes for assembly 2 (with 12.7 mm thick plasterboard).

Gerlich et al. [16], in 1996, investigated the performance of load bearing light steel frame (LSF) walls and to model their performance against ISO 834 and real fires in compartments. The study proposed methodologies for predicting structural behaviour at elevated temperatures, encompassing considerations for the reduction in steel strength and

stiffness, deflections resulting from temperature gradients, and the effects of axial loads on the bending behaviour of the system. The real fires represent a hydrocarbon pool fire with rapid growth, short duration and rapid decomposition phase, and a fuel-bed controlled timber crib fire with slow temperature rise, long duration and slow decomposition. Two-dimensional finite element models of LSF walls under realistic fire conditions were developed with the TASEF program. Three full-scale furnace tests were carried out to validate the proposed model. The furnace temperature followed the curve prescribed by ISO 834, except in the third test, where the furnace temperatures were modified to provide a more severe exposure after about 8 minutes. Although these models accurately predicted time-temperature histories, the authors suggested the need for refinements when modelling against fires of significantly higher temperatures than standard conditions.

Keerthan and Mahendran [17], in 2012, developed finite element thermal models for non-load bearing cold-formed light steel frame wall panels with cavity insulation, as well as for new composite wall panels with an outer insulation layer. The aim of this modelling was to simulate the thermal behaviour of these wall systems under normal and realistic fire conditions. The study proposed thermal properties for plasterboard, insulation materials and steel, based on a comparison of previous research and experimental results. Finite element models developed with SAFIR were validated by comparing their thermal analysis results with available fire test results. The numerical results showed that cavity insulation was detrimental to the fire rating of cold-formed light steel frame walls, while the use of external insulation offered superior thermal protection. The study also concluded that accurate finite element models can be used to simulate the thermal behaviour of cold-formed light steel frame walls with different configurations of insulation and plasterboard.

Ariyanayagam [18], in 2013, conducted an investigation into the fire resistance of Light Gauge Steel Frame (LSF) wall systems, both load bearing and non-load bearing. The study developed realistic fire time-temperature curves for modern residential and commercial buildings, employing full-scale fire tests and numerical analyses. The fire curves were based on the parametric Eurocode EN 1991-1-2:2002 [19] and the Barnett 'BFD' curve [20]. Finite element models of LSF walls under realistic fire conditions were

developed with ABAQUS and analysed under steady-state and transient fire. The study also develops two simplified methods to predict the fire resistance ratings of LSF walls exposed to realistic design fires as approaches based on the temperature of the hot flange and the energy-based time equivalence. Taking this into account, the author concludes that the hot flange temperature is the critical parameter that determines the failure of the LSF wall studs exposed to realistic design fires. He also concludes that the maximum temperature of the fire and the time in which it occurs significantly influenced the stud temperatures and therefore also the axial compressive strengths and failure times of LSF wall studs. Rapid fires only influenced the performance of LSF walls at higher load ratios, while prolonged fires also affected them at lower load ratios. The energy-based time equivalent method was developed on the basis of the principles of equal fire severity. It is applicable to prolonged fires and cannot be used for rapid fires.

Chen et al. [21], in 2019, identified a gap in research related to experiments on CFS walls exposed to hydrocarbon fires and external fire exposure. Their subsequent study explored the fire behaviour of non-load bearing CFS walls under four different design fire conditions, including ISO 834 fire curve, hydrocarbon fire curve, external fire curve, and a typical realistic design fire curve. CFS structures measuring 1.2 m long by 1.2 m wide were built with double layers of cladding on both sides, cavity insulation and thermal monitoring using 21 K-type thermocouples at half height. The researchers used C140 (140×50×13×1.2 mm) CFS lipped channel section studs and U142 (142×50×1.2 mm) CFS unlipped channel section tracks using 16 mm long self-drilling wafer head screws, two types of cladding (fire-resistant gypsum board and low-density calcium silicate board), rockwool with a thickness of 150 mm and a density of 60 kg/m^3 for cavity insulation and four different design fire curves. In addition, out-of-plane deformation (thermal buckling) of CFS studs was verified and a discussion was held on the applicability of time equivalence methods to predict the fire performance of non-load bearing CFS walls under different design fire curves.

The study concluded that the maximum temperature of the design fire curve is an important index to represent the severity of fire exposure, with hydrocarbon fire and

realistic design fire showing much more severe damage than ISO 834 or external fire. In addition, it was found that replacing the plasterboard of the fire-side base layer with a low-density calcium silicate board increases the performance of the insulation and structure of CFS walls in fire conditions. The authors recommend a temperature of 900°C on the unexposed surface of the plasterboard as the critical temperature to represent the fall of the plasterboard on the fire side. A simplified temperature distribution model and the critical drop temperature of the plasterboard on the fire side were recommended for the numerical modelling of CFS walls. The study also explored the time equivalence of different fire curves for CFS walls and concluded that neither the equal area method nor the energy-based method was suitable for the time equivalence of the fire resistance of CFS walls.

In 2020, Chen et al. [6] continued their research into the thermal behaviour of non-load bearing cold-formed steel walls with external insulation exposed to different fire conditions. To compare the fire performance of cavity-insulated CFS walls with externally insulated CFS walls, medium-scale experimental tests were conducted on unloaded CFS walls subjected to four different fire scenarios, including ISO 834 fire, external fire, hydrocarbon fire and typical realistic design fire. CFS structures 1.2 m long by 1.2 m wide were then built with insulation between the two layers of cladding on both sides, no insulation in the cavity and thermal monitoring using 29 K-type thermocouples at half height. The researchers used C140 (140×50×13×1.2 mm) CFS lipped channel section studs and U142 (142×50×1.2 mm) CFS unlipped channel section tracks, two types of cladding (fire resistant gypsum board and low density calcium silicate board), rockwool with a thickness of 24 mm and a density of 60 kg/m^3 for insulation between the cladding boards and four different design fire curves. The results were compared with the experiments carried out in the previous study [21]. Both studies will be used for the numerical validation of the models developed in this dissertation, as presented in Chapter 4.

The study identified an almost stable state of heat transfer in the final phase of exposure to external fire. Furthermore, two types of stud buckling under different fire conditions were identified, including local buckling of the entire stud section and local

buckling of the hot flange of the stud and the adjacent web. The research concluded that external insulation is a more reasonable configuration than cavity insulation to improve the fire resistance of CFS walls, since cavity insulation can delay heat transfer from the cavity to the ambient side and result in a reduction in the fire resistance time of CFS walls. However, if the cavity insulation is removed from the walls of CFS, the corresponding performance in terms of sound and thermal insulation would be significantly reduced.

In addition, a simplified one-dimensional finite difference method was developed that showed good accuracy and high efficiency for predicting the temperature dependent on time of the ambient surface of CFS walls. This method proposes to exclude steel uprights from the heat transfer model. For walls with external insulation, the temperatures of the cavity surfaces represent the hot and cold flaps of the uprights. For walls with insulation in the cavity, the temperature of the hot surface of the cavity still represents the hot flange of the upright, while the temperature of the cold flange is obtained statistically.

Chen et al. [22], in 2020, conducted experiments on cavity-insulated gypsum-sheathed cold-formed steel (CFS) walls in a full-scale (3.0 x 3.0 m) with and without load. The experiments were also subjected to four different fire conditions, just as in the previous research. The results show that the axial load has a negligible effect on the heat transfer of these walls in the event of a fire and provide a basis for the indirect coupling method of the thermomechanical analysis of the CFS walls, which is normally used to simplify the analysis of the fire resistance of these walls. In addition, the research proposes a new time equivalence method for CFS walls based on the same temperature as the hot flange as the equivalence principle. Both the equal area method and the energy-based method, which are two other commonly used time equivalence methods based on time temperature curves and energy equivalence, respectively, were modified with reference temperatures and gave a good prediction of the time equivalence of the fire resistance of CFS walls.

Upasiri et al. [23], in 2022, investigated the fire performance of LSF wall panels with lightweight concrete as cavity filler. The study employed finite element modelling to compare the fire behaviour of conventional LSF walls with and without cavity insulation

with lightweight concrete filled LSF walls under normal and hydrocarbon fire conditions. The frames consist of four vertical thin-walled steel channel sections with 600 mm centers and sheathing with one and two gypsum boards on each side (12.5 mm and 15 mm thick). Research compares the performance of various lightweight concrete fillers, including Autoclaved Aerated Concrete (AAC) with a density of 600 kg/m^3, Foam Concrete (FC) with densities of 650 kg/m^3 and 1000 kg/m^3 and rockwool filler. LSF walls filled with lightweight concrete show promising improvements in terms of insulation and fire resistance. Among the lightweight concrete materials considered, Foam Concrete with a density of 1000 kg/m^3 shows the best fire performance. Both two-dimensional and three-dimensional finite element numerical analyses were carried out using BAQUS CAE. However, a similar temperature variation was observed in the central plane of the wall for both analyses. Therefore, only 2D modelling was used for the parametric study. The authors simulated the region of the cavity developed only by radiation, as they concluded that radiation dominates over conduction and convection. Promising improvements in insulation and fire resistance ratings were observed, with foam concrete with a density of 1000 kg/m^3 demonstrating the best fire performance among the considered materials. However, lightweight concrete can be unfavourable to the overall weight of the wall.

In 2017, Piloto et al. [24] contributed significantly to the field by developing an accurate numerical model based on thermal analysis with air-structure interaction. Models predicted the ability of the unexposed side of the wall to maintain temperature, and their validity was confirmed by experimental tests conducted by other researchers [25]. Piloto et al. [26] also analysed the fire performance of LSF using simplified one-dimensional heat flow, comparing the results with a 2D finite element analysis.

In 2018, Piloto [27] presented a 3D sequential numerical model to investigate the fire resistance of LSF walls constructed with composite panels, employing a hybrid finite element model [28], [29]. In 2022, Alves et al. [30] presented research on double stud LSF walls with a new simplified method, producing results consistent with experimental observations. Piloto et al. [31] analysed the critical temperature on load bearing LSF walls.

In 2023, Torres et al. [32] investigated the fire behaviour of external LSF walls, while Piloto et al. [33] compared the fire performance of LSF walls with void cavities using three different computational solution methods. These methods considered: 1) air-structure interaction, 2) the existence of interface elements for the radiation heat transfer in the cavity region, enabling cavity temperature prediction, and 3) convection and radiation in the cavity region with a prescribed cavity temperature from experiments (hybrid).

The results of these investigations constitute a valuable contribution to understanding the thermal response of partition walls, as well as the thermal and mechanical response of load bearing walls in fire situations. These findings serve to guide improvements in materials and construction practices, providing a solid foundation for advancements in the realms of scientific and applied knowledge, particularly within the context of engineering and construction. However, the scarcity of studies analysing the performance of Light Steel Frame walls in fires is notable, different from those conventionally adopted in tests. Therefore, this dissertation aims to enhance knowledge in the analysis of walls subjected to standard and hydrocarbon fires.

Chapter 3

Fire Behaviour of LSF Walls

The Light Steel Frame (LSF) wall system is typically used as partitions and load bearing structural elements in buildings, effectively controlling the spread of fire to adjacent compartments for a specified period in the event of fires. The Fire Resistance Rating (FRR) assigned to these walls plays a crucial role in the structural stability design of buildings, being vital to ensure safe evacuation of occupants and reduce the risk of human losses [5].

The FRR, which evaluates the ability of LSF walls to delay the effects of fire, is intrinsically linked to the insulation (I), structural (R), and integrity (E) behaviour of these structures when exposed to fire conditions. Precision in evaluating fire resistance requires careful consideration of various factors, including the mechanical and thermal properties of the materials used, the severity of the fire, and the type of coating and insulation used.

In this context, exploring the complexities of these factors is essential for a comprehensive and accurate assessment of the safety provided by these structures in fire situations. Therefore, this chapter provides explanations of essential parameters in the analysis of the behaviour of LSF walls in different types of fires.

3.1 Natural Fire

Natural or real fire represents a time-temperature curve for a fire process within a compartment. The natural fire curve is characterised by three basic stages: ignition, heating, and cooling [34], as illustrated in Fig. 3.1.

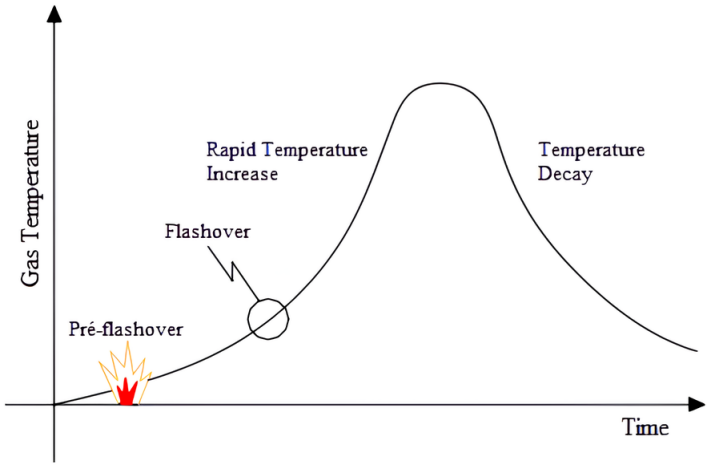

Figure 3.1: Evolution of Gas Temperature in a Fire. (Adapted from [35]).

Ignition: Represents the onset of inflammation, with a gradual increase in temperature and minimal impact on the characteristics of the compartment, such as the openings and compartment material. This stage poses no immediate risk to human life or structures, culminating in "flashover", where widespread inflammation occurs.

Heating: Characterised by a sudden increase in temperature, all combustible material in the compartment ignites, reaching gas temperatures exceeding 300°C and undergoing rapid growth.

Cooling: Signifies the gradual reduction of temperature after the extinguishment of combustible material during the heating phase.

Temperature during a fire is crucial, represented by standardised curves such as ASTM E-119 and ISO 834, commonly used in tests. However, these standard curves do not fully reflect the actual behaviour of fire in structures, as the furnace temperature continuously rises, not representing the cooling phase. Natural curves consider specific characteristics

of the burning environment, including the degree of ventilation, the characteristics of combustible materials, and the thermal properties of the compartmental material. Eurocode 1 Part 1.2 [19] prescribes a mathematical expression that incorporates the cooling phase and considers the combination of the mentioned characteristics.

However, for the development of this dissertation, these curves will not be relevant. Instead, standard fires and hydrocarbon fires will be analysed.

3.2 Standard Fire ISO 834

The ASTM E-119 and ISO 834 standard curves are the most widely disseminated temperature-time curves globally, commonly employed for conducting tests on structural elements and for the design of typical buildings (residential and commercial). These curves depict the increase in temperature over time in compartments where the fire load is composed of cellulosic materials. The ASTM E-119 curve exhibits behaviour similar to the ISO curve. Therefore, for this study, the ISO 834 curve, referenced in EN 1991-1-2 [19], will be used, calculated by the following expression

$$\theta_g = 20 + 345 \log_{10}(8t + 1) \tag{3.1}$$

Where θ_g is the gas temperature in the fire compartment [°C], and t is the time [min].

3.3 Hydrocarbon Fire

Unlike the standard fire curve, which demonstrates a gradual increase over time, hydrocarbon fires exhibit a rapid increase in temperature accompanied by a flame shock wave in structures, fire-resistant coatings, combustible finishes, and building materials [2]. The specific curve for this fire (see Fig. 3.2) reaches approximately 1100°C in about half an hour, maintaining a constant temperature from that point on.

The formulation for the hydrocarbon curve is provided by the expression EN 1991-1-2 [19]

$$\theta_g = 1080\left(1 - 0.325e^{-0.167t} - 0.675e^{-2.5t}\right) + 20 \tag{3.2}$$

Where θ_g is the gas temperature in the fire compartment [°C], and t is the time [min].

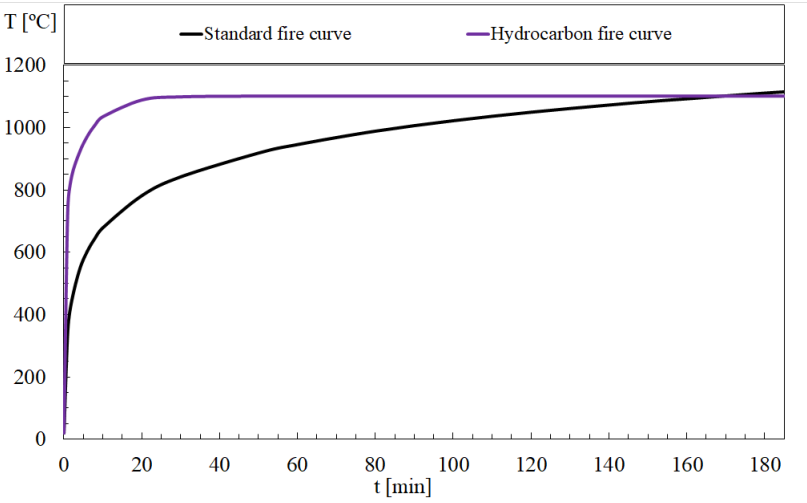

Figure 3.2: Standard fire and hydrocarbon curves.

3.4 Heat Transfer Mechanisms

Heat transfer can be defined as the thermal energy being transported within a medium, either through a vacuum or between mediums due to a spatial thermal gradient. Such a phenomenon occurs through one or more of its three distinct modes: conduction, convection, and radiation, typically quantified in terms of heat flux, i.e., the rate of thermal energy per unit area.

3.4.1 Conduction

Thermal conduction is a process that occurs in materials when one region has a higher temperature than the others. In this area, the agitation of particles increases, promoting a gradual transmission of heat between neighbouring particles without significant displacement. This mechanism requires a material medium to occur, and the effectiveness

of conduction is directly proportional to the contact between bodies at different temperatures. The lower heat conduction in gases, compared to solid materials, is explained by the greater distance between particles in gases, limiting efficient contact and, consequently, thermal transfer [35].

According to Fourier's Law, the general equation for heat flow by conduction [W] is expressed as

$$\dot{h}_c = -\lambda A \frac{dT}{dx} \tag{3.3}$$

Where, λ is the thermal conductivity of the material [W/mK], A is the cross-sectional area [m^2], and $\frac{dT}{dx}$ is the temperature gradient along the flow direction. The negative sign indicates the direction of heat flow, moving from the region of higher to lower temperature.

The Eurocode 1-Part 1-2 [19] describes the thermal effects used for temperature analysis. These effects are given by the net heat flux $\dot{h}_{net}$ [W/m^2] on the boundary surface of the element.

On a surface exposed to fire, the net heat flux is divided into two components: the first considers heat transfer by convection ($\dot{h}_{net,cv}$), and the second considers radiative heat transfer ($\dot{h}_{net,r}$), as shown below.

$$\dot{h}_{net} = \dot{h}_{net,cv} + \dot{h}_{net,r} \tag{3.4}$$

3.4.2 Convection

Convection is the process of heat transfer that occurs when a moving fluid, such as air or water, comes into contact with an object at different temperatures. This phenomenon can occur naturally, influenced by variations in fluid density, or it can be forced, induced by external elements such as fans. In natural convection, the localised increase in temperature causes an ascent of the warmer fluid as a result of a decrease in density. Heat transfer can be conceptualised as an exchange between hotter and less heated particles, layer by layer, forming a connection between the moving fluid and the surface in question.

Consequently, the temperature does not remain constant throughout the analysed region, showing a variation between the temperature of the medium and the temperature of the surface. This variation is fundamentally influenced by fluid flow, the thermal properties of the fluid and the surface, as well as the geometry of the system [35].

According to EN 1991-1-2 [19], the heat flux by convection between the medium and the surface under study [W/m^2] is expressed as

$$\dot{h}_{net,cv} = \alpha_{cv} \left(\theta_g - \theta_m\right) \tag{3.5}$$

Where, α_{cv} is the heat transfer coefficient [W/m^2K], θ_g is the temperature of the gas near the member exposed to fire [°C], and θ_m is the surface temperature [°C]. These parameters vary according to the fire curve used. For standard fires, Eurocode 1 standardises the value of the convective heat transfer coefficient as $\alpha_{cv} = 25$ [W/m^2K] and $\alpha_{cv} = 50$ [W/m^2K] for hydrocarbon fires.

3.4.3 Radiation

The propagation of heat through radiation is a mechanism that does not require the presence of a material medium, as energy is transmitted through electromagnetic waves. In precise terms, radiation is more effective in a vacuum because the existence of a material medium to be traversed results in the dissipation of exchanged energy between two distant bodies. The radiation process, in a simplified manner, involves the emission of electromagnetic waves by a heated body (radiant energy), which, when absorbed by a receiver, is converted into thermal energy. Upon reaching a receiving body, part of the generated heat is absorbed, part is dissipated into the internal environment of the receiver (through conduction through the body and convection at the interface with the internal medium), and part returns to the external environment through convection [35].

According to the EN 1991-1-2 standard [19], the net flow of radiative heat per unit area exposed to fire [W/m^2] is given by

$$\dot{h}_{net,r} = \emptyset \varepsilon_m \varepsilon_f \sigma[(\theta_r + 273)^4 - (\theta_m + 273)^4] \tag{3.6}$$

Where $\emptyset$ is the view factor, ε_f and ε_m are respectively the emissivity of the fire and the member's surface, σ is the Stefan-Boltzmann constant (5.67×10^{-8} [W/m^2K^4]), θ_r is the effective radiation temperature of the fire environment [°C], and θ_m is the temperature of the member's surface [°C].

Furthermore, the standard [19] makes some considerations, such as, on the non-exposed side to the fire, the net heat flux should assume $\alpha_c = 9$, [W/m^2] when considering the influence of radiation heat. If the standard does not specify the surface emissivity of the element (ε_m), it can be assumed that $\varepsilon_m = 0.8$. The emissivity to fire is generally considered as $\varepsilon_f = 1$. In the case of members fully engulfed by the fire, the radiation temperature θ_r can be represented by the gas temperature θ_g around that member. Additionally, the gas temperature θ_g can be used as a nominal temperature-time curve, for example, ISO 834 fire curve and hydrocarbon curve.

3.5 Fire Resistance Criteria and Testing Standards

Testing standards are crucial for rigorously assessing the performance of Light Steel Frame (LSF) walls during fires, establishing specific criteria and procedures for tests, including thermal resistance and structural integrity. Understanding these standards is vital to ensure consistency in performance studies, providing a solid foundation for interpreting results and guiding construction practices. Therefore, the appropriate application of these standards scientifically validates research and sets safety standards to promote the safe and continuous development of LSF structures in fire-prone environments. The European standards used to obtain the fire resistance of non-load bearing LSF walls are EN 1363-1 [36], EN 1364-1 [37] and EN 13501-2 [38].

3.5.1 EN 1363-1

The European standard EN 1363-1 (Fire Resistance Tests - General Requirements) outlines fundamental principles for assessing the fire resistance of various building elements when exposed to standardised fire exposure conditions. The objective is to establish specific procedures for the accurate determination of fire resistance, covering a variety of construction elements.

Effective test implementation requires the use of a specially designed furnace capable of subjecting the test specimen to rigorous and standardised conditions. This exposure is conducted under precise control of the furnace temperature, while a system monitors and controls the pressure of hot gases inside. The sample, inserted into a specific frame, undergoes appropriate heating, pressure, and support conditions. Loading and restraint of the sample are carefully planned, with specific devices, when necessary, to assess integrity and ensure compliance with performance criteria. In special cases, measuring the oxygen concentration in the furnace gases may also be required.

The procedure involves exposing one side of the wall sample to a standardised fire load, following the heating curve specified by ISO 834. At any time after the first 10 minutes of the test, the temperature recorded by any thermocouple in the furnace should not differ from the corresponding temperature of the standard temperature/time curve by more than 100 K.

Furthermore, the standard establishes essential failure criteria to assess the performance of the sample during the test.

Load bearing capacity (R) is defined as the time during which the LSF wall can maintain its load bearing ability during the test. Failure to support vertical load occurs due to the limitation of vertical contraction (C_{limit}) or the limitation of the rate of vertical contraction ($\frac{dC}{dt}$), expressed by the equations

$$C_{limit} = \frac{h}{100}\,[mm] \tag{3.7}$$

$$\frac{dC}{dt} = \frac{3h}{1000}\,[mm/min] \tag{3.8}$$

Where h is the initial height [mm] of the specimen after applying the load.

The Integrity (E) of the wall is assessed regarding its ability to prevent the passage of flames, smoke, or hot gases from the exposed side to the non-exposed side, measured in terms of time, duration, and location.

Finally, Insulation (I) is defined as the period during which the wall maintains its ability to resist temperature variations above ambient temperature on the non-exposed side to fire, considering the criteria:

Increase the average temperature above the initial average temperature by more than 140 K, or increase at any location (including the roving thermocouple) above the initial average temperature by more than 180 K.

3.5.2 EN 1364-1

The EN 1364-1 (Fire Resistance Tests for Non-load bearing Elements - Parte 1: Walls) is a standard that outlines specific procedures for conducting experimental tests to assess the fire resistance of non-load bearing walls. The primary purpose of these experiments is to analyse the ability of the wall to contain the spread of fire from one side to the other.

Regarding the execution of these experiments, the standard establishes detailed criteria. A rigid frame with high stiffness and reduced thermal expansion is required to secure the test specimen. The dimensions of this sample follow a specific rule: if the width or height of the construction element is less than 3 meters, the sample should be tested in its actual dimensions. If one of the dimensions exceeds 3 meters, it should not be less than 3 meters in the test.

Additionally, the standard provides detailed information about the instrumentation required for the experiments. Furnace temperature control should be conducted by plate thermocouples inside it, with the largest surface facing the furnace wall. The ratio is one thermocouple for every $1.5m^2$ of exposed surface to be tested. If the wall has expected

fire insulation exceeding 5 minutes, disc thermocouples should be installed on the non-exposed side to obtain the average and maximum developed temperature. It is suggested to position 5 thermocouples to measure the average temperature, with one in the center of the sample and the other 4 distributed in the center of each quarter of the wall. For measuring the maximum temperature, an additional 7 thermocouples are recommended.

3.5.3 EN 13501-2

The EN 13501-2 standard lays down procedures for classifying the fire resistance of construction products and building elements, aiming to ensure safety in the event of a fire.

Fire resistance classification is expressed in minutes, with specific periods of 15, 20, 30, 45, 60, 90, 120, 180, 240, or 360 minutes. These classifications are determined through a combination of letter designations, supplemented by the nearest time in minutes during which functional requirements are met, as well as by the specified load level.

In the context of partition walls, defined as non-structural elements, the standard requires fire resistance tests according to EN 1364-1 to determine their fire resistance classification. These walls play a crucial role in compartmentalising spaces within buildings, maintaining separation between adjacent areas during a fire.

Fire resistance tests assess the ability of partition walls to withstand fire for a specific period, taking into account criteria such as integrity and thermal insulation. This contributes to the safety of occupants and the protection of the building in emergency situations, ensuring that these walls remain intact and capable of fulfilling their fire containment function.

Additionally, the standard also establishes classifications for other important aspects, such as:

Radiation (W): The radiation classification shall be given by the time for which the radiation, measured as specified in the standard, does not exceed 15 kW/m^2.

Mechanical action (M): The element shall resist the impact as described in the test standard, without prejudice to the E and/or I performance.

Table 3.1: Classification of partition walls.

E		20	30		60	90	120		
EI	15	20	30	45	60	90	120	180	240
EI-M			30		60	90	120	180	240
EW		20	30		60	90	120		

The following classes are defined in Table 3.1.

These criteria and procedures ensure consistency and accuracy in fire resistance tests for non-load bearing elements, contributing significantly to the reliable assessment of a wall's ability to contain the spread of fire under standardised conditions.

Chapter 4

Finite Element Analyses of LSF Walls

This chapter outlines the methodology employed in the dissertation, focusing on the analysis of finite element models developed. These models were conceived based on walls used in experimental tests conducted by researchers. The adopted approach incorporates various methods to assess the fire resistance of non-load bearing Light Steel Frame (LSF) walls, considering both standard fire conditions and exposure to hydrocarbons.

Finite Element Analysis (FEA) is an effective computational technique for solving complex engineering problems with domains subjected to various boundary conditions. It has become essential in modelling physical phenomena in different states of matter, dealing with field variables that vary infinitely in the domain. FEA is based on decomposing the domain into elements, where a systematically approximate solution is constructed using variational or weighted residual methods. By dividing the domain into elements and expressing unknown field variables in terms of approximation functions, FEA simplifies the problem to a finite number of unknowns, making the analysis more feasible. These functions are defined in terms of the field variable values at nodes, located along the boundaries of the elements and connecting adjacent elements [39].

In the thermal context, using the ANSYS software, FEA is employed to analyse

transient heat transfer, capturing the temporal evolution of temperature distribution. The simulation covers fire test conditions, incorporating transient thermal analysis with temperature-dependent material properties. Validation of the results will be conducted through a comparison with experimental tests, ensuring the reliability of the models.

4.1 Validation of the Numerical Model

In this dissertation, the non-load bearing Cold-Framed Steel (CFS) walls to be validated include the test specimens "S1" and "S5", constructed by Chen et al. in 2019 [21], and the specimens "S9" and "S13", produced by Chen et al. in 2020 [6]. Additionally, these authors developed a simplified calculation method to obtain the steel structure's temperature profile, based on a one-dimensional finite difference method.

The medium-scale LSF wall specimens in both studies were manufactured with dimensions of 1.2 m in length by 1.2 m in width, as depicted in Fig. 4.1. The steel frames were constructed by assembling three C140 studs (140×50×13×1.2 mm) every 600 mm and two U142 tracks (142×50×1.2 mm), as illustrated in Fig. 4.2. The steel studs and tracks were fabricated from a galvanised steel sheet (Q345) with a nominal wall thickness of 1.2 mm and a nominal yield strength of 345 MPa. The structure was covered with two layers of gypsum board on both sides, each with a thickness of 12 mm. Two types of coatings were used: fire-resistant gypsum board (1200×1200×12 mm) and calcium silicate board (1200×1200×12 mm). However, only the walls coated with fire-resistant gypsum board were used to develop the numerical models.

For the light steel frame wall specimens "S1" and "S5", a 150 mm thick rockwool insulation (density of 60 kg/m^3) was used as insulation in the cavity of the steel frames, as depicted in Fig. 4.3. To monitor the thermal response of the LSF walls during the fire experiments, a total of 21 type K thermocouples were installed at mid-height sections of each specimen, as shown in Fig. 4.4.

For specimens "S9" and "S13", a 24 mm thick rockwool insulation (density of 60 kg/m^3) was used as external insulation between the gypsum boards. Simultaneously, two

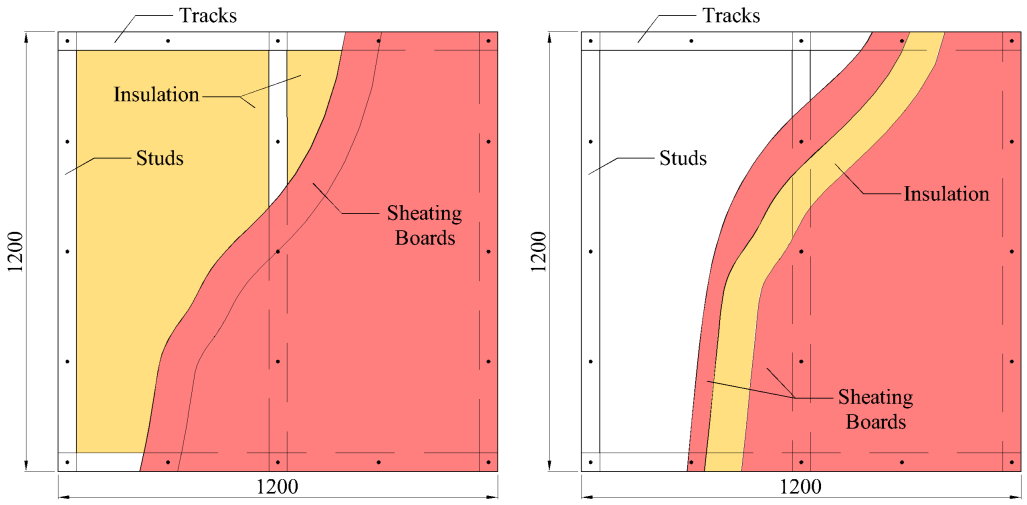

Figure 4.1: LSF wall Cavity-insulated and external insulated.

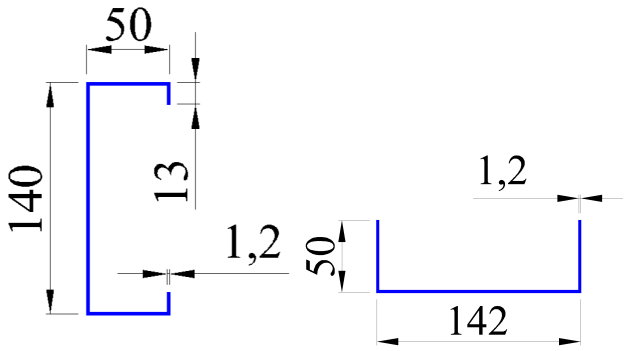

Figure 4.2: Steel stud and track sections.

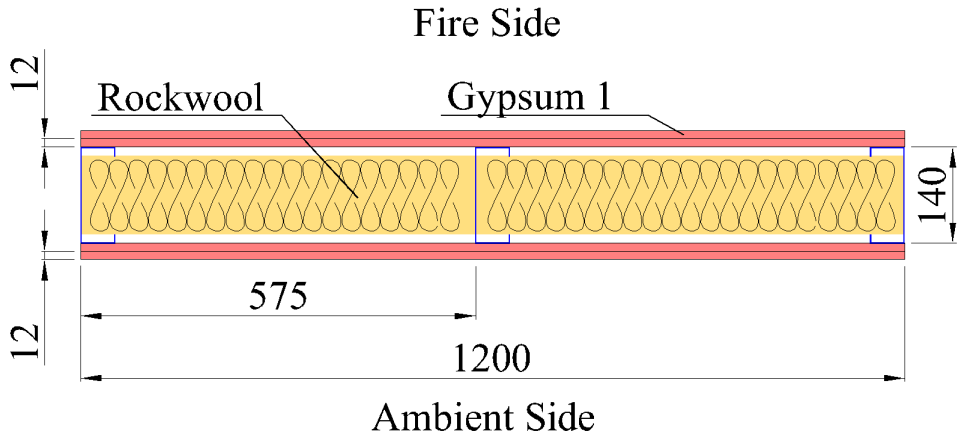

Figure 4.3: Cross section of wall specimen “S1” and “S5”.

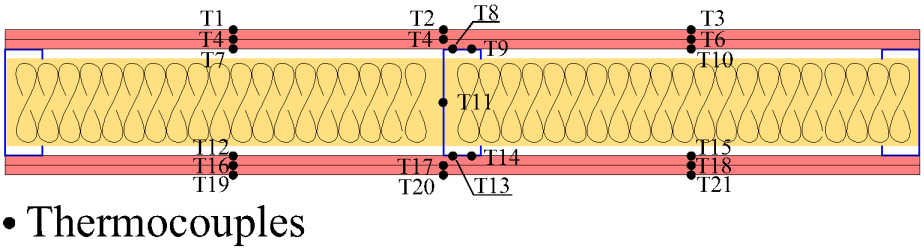

Figure 4.4: Thermocouples localisation on wall specimens “S1” and “S5”.

layers of gypsum strips are placed directly on the steel frame to prevent compression deformations and irregular joints on the wall surfaces, as shown in Fig. 4.5. Additionally, there are 29 type K thermocouples at mid-height sections of each specimen, as illustrated in Fig. 4.6.

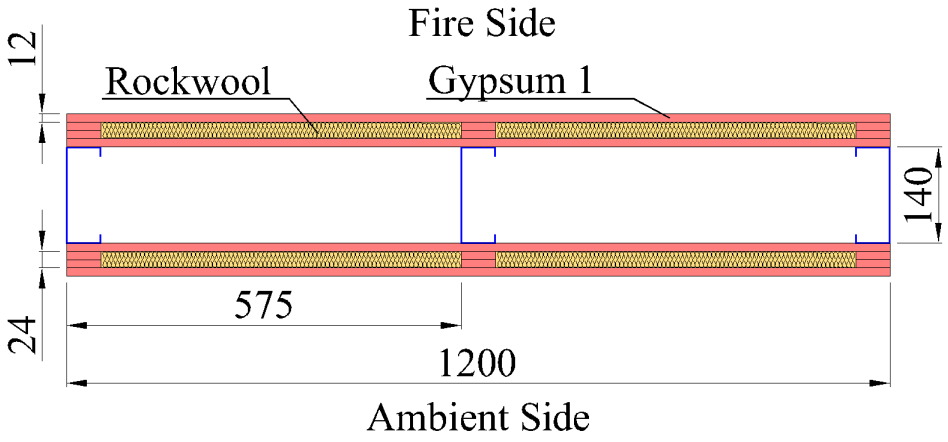

Figure 4.5: Cross section of wall specimen “S9” and “S13”.

4.2 Finite Element Method in Heat Transfer Analysis

Heat transfer analysis through the finite element method is a complex process, involving the solution of partial differential equations, iterative numerical methods, and advanced

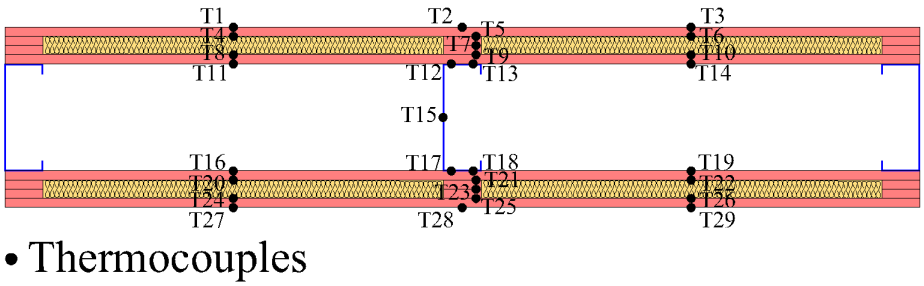

Figure 4.6: Thermocouples localisation on wall specimens “S9” and “S13”.

concepts from finite element theory. The finite element analysis software ANSYS Mechanical software is capable of conducting two types of thermal analyses: steady-state and transient.

Steady-state thermal analysis determines the temperature distribution and other thermal quantities under steady-state loading conditions, where variations in heat storage effects over time can be ignored. On the other hand, transient thermal analysis determines the temperature distribution and other thermal quantities under conditions that vary over time.

Based on the first law of thermodynamics, which considers thermal energy conservation, software ANSYS employs Fourier's Law of heat transfer to assess heat conduction. The third-order partial differential equation (PDE) 4.1 derived from Fourier's Law describes the transient behaviour of heat conduction in a material [40].

$$\rho C \frac{\partial T}{\partial t} = \frac{\partial}{\partial x}\left(\lambda \frac{\partial T}{\partial x}\right) + \frac{\partial}{\partial y}\left(\lambda \frac{\partial T}{\partial y}\right) + \frac{\partial}{\partial z}\left(\lambda \frac{\partial T}{\partial z}\right) + Q \tag{4.1}$$

Where T is the temperature, λ is the thermal conductivity of the material, Q is the amount of heat generated in the material per unit volume, ρ is the density, C is the specific heat capacity, and t is the time.

If there is no internal heat generation, the equation is further simplified to

$$\rho C \frac{\partial T}{\partial t} = \frac{\partial}{\partial x}\left(\lambda \frac{\partial T}{\partial x}\right) + \frac{\partial}{\partial y}\left(\lambda \frac{\partial T}{\partial y}\right) + \frac{\partial}{\partial z}\left(\lambda \frac{\partial T}{\partial z}\right) \tag{4.2}$$

The boundary conditions can be a known temperature and/or a known heat flux. For

this thesis, the initial temperature is specified as T=T_0.

This formulation is suitable for solution using the finite difference method but should be replaced by a variational formulation for Finite Element Analysis. For this purpose, a weighted residual method is typically employed [41].

4.2.1 Weighted Residuals Methods

The weighted residual method plays a fundamental role in finite element analysis, being crucial for obtaining discrete variational formulations. This method, often employed in transforming differential equations into forms more suitable for finite element analysis, utilises the Galerkin approach to simplify the variational formulation [41].

In the Galerkin approach, a test function is chosen to be identical to the weighting function. This implies that the variational formulation is simplified, as the test function facilitates mathematical manipulation. The variational formulation is obtained by multiplying the partial differential equation (PDE) by this test function and integrating over the domain [42].

Weighted residual method requires the weighted averages of the residual to be equal to zero. These weighted averages are calculated using a set of weighting functions, which may include global shape functions. These weighting functions play a crucial role in seeking approximate solutions and ensure the method is effective in finite element analysis.

The approximation function for the solution of the differential equation is expressed as a linear combination of unknown parameters and interpolation functions. This allows for an approximate representation of the solution, making it possible to apply the weighted residual method [41], [42].

In the Galerkin form of the weighted residual method, the weighting functions are chosen to match the shape functions. This contributes to the efficiency of the method, ensuring a consistent and coherent approach in finite element analysis.

4.2.2 Shape Functions

Shape functions, also known as interpolation functions, are crucial in the discretization of the domain in finite elements. They approximate the temperature distribution within each element. The shape functions are chosen to ensure continuity between elements and are often low-order polynomials [41]. In Section 4.3 below, the shape functions for the elements used in the modelling will be presented.

4.2.3 Transient Heat Transfer Problems

Finite element method requires the numerical integration of variational equations along each element. Consequently, the stiffness matrix and the load vector are assembled, considering the shape functions, and the solution is obtained by solving the resulting system of equations [40].

$$[M]\left\{\dot{T}\right\} + [\lambda]\, T = q \tag{4.3}$$

Where M is the system's thermal capacity matrix, $\dot{T}$ is the vector of temporal derivatives of the unknown nodal temperatures, λ is the global thermal conductivity matrix, T is the vector of unknown nodal temperatures, and q is the specified heat flux.

To address transient problems, transient analysis is implemented. The equation is discretized in time, and the Newton-Raphson method, an iterative method, is often employed. The solution for each time step is obtained by adjusting the temperature and material properties.

The iterative method involves starting with the initial temperature (T_0), obtaining a more accurate solution to solve the equation

$$[M]\left\{\dot{T}\right\}_1 + [\lambda\left(\{T\}_0\right)]\,\{T\}_1 = \{q\}_0 \tag{4.4}$$

Then repeating the iteration scheme until the solution converges

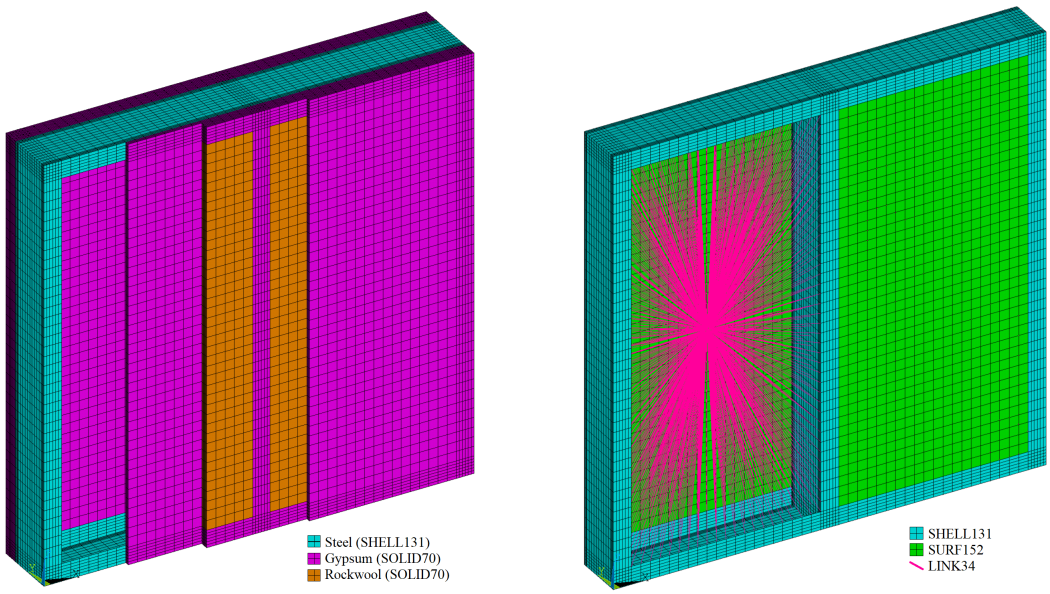

Figure 4.7: LSF wall Elements.

$$[M]\left\{\dot{T}\right\}_n + \left[\lambda\left(\{T\}_{n-1}\right)\right]\{T\}_n = \{q\}_{n-1} \tag{4.5}$$

The iteration is conducted until convergence is achieved.

4.3 Finite Element Model

For the thermal analysis of the walls, the following Element Types offered by the ANSYS Mechanical APDL software were selected (see Fig. 4.7):

SHELL131: Employed to model the steel studs and tracks of the walls.

SOLID70: Used to model the gypsum boards and rockwool insulation of the walls (represented in purple and orange, respectively).

SURF152: Applied in methods 2 and 3 to simulate the radiation effect occurring inside the cavity without insulation (represented in green).

LINK34: Exclusively used in method 3 to simulate the convection effect occurring inside the cavity without insulation (represented in pink).

The SHELL131 element in the ANSYS software is a tool designed to model thin

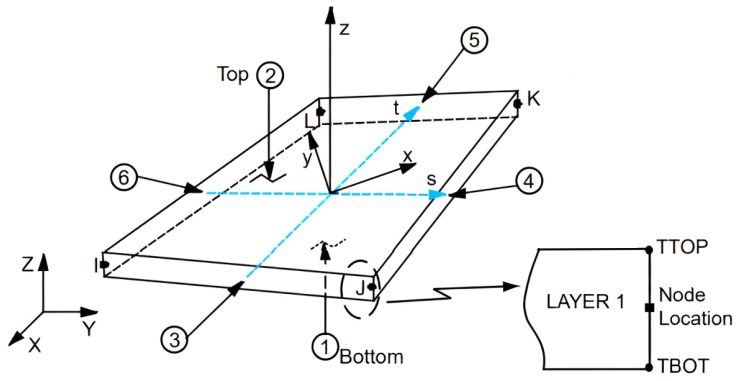

Figure 4.8: SHELL131 Geometry (Adapted from [40]).

structures where one dimension is significantly smaller than the other two dimensions. This three-dimensional shell element is particularly useful for steady-state or transient thermal analyses.

SHELL131 is capable of conducting thermal analysis both in-plane and through the thickness of the shell. With four nodes (Fig. 4.8), each having up to 32 degrees of freedom for temperature, this element provides a detailed representation of the thermal distribution in thin structures. This modelling capability is crucial in situations where thermal properties vary in different directions within the structure.

To define the SHELL131 element, four nodes, a layer thickness, a material angle for each layer, and material properties are required. In this specific study, the choice was made to use only one layer with a linear temperature variation through the thickness. This choice simplifies the model, making it more applicable to certain contexts. Additionally, a thickness of 1.2 mm was defined for the element (in accordance with the thickness of the steel profiles), except at the junction points between the steel studs and tracks, where a thickness of 2.4 mm was adopted, as shown in Fig. 4.9.

In the current study, the “Paint” option is utilised, replacing the variable TBOT with the variable TEMP. This substitution enables the direct bonding of the element to an underlying solid, eliminating the need for additional constraint equations.

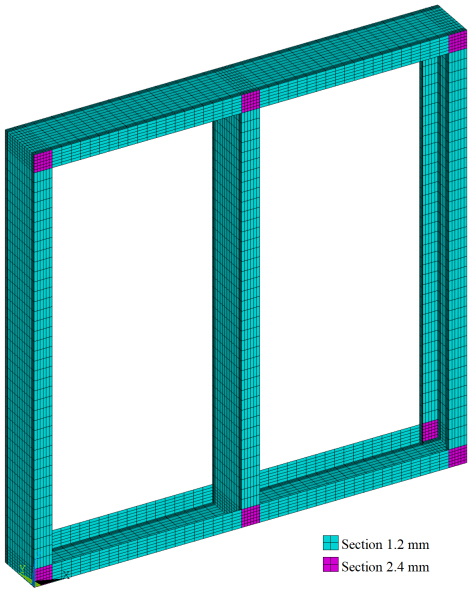

Figure 4.9: Shell sections.

Regarding specific configurations, the constant variable TEMP (T) is employed, applied only to one layer. The layer shape functions in the plane are defined by the mathematical expression

$$T = \frac{1}{4}((TI(1-s)(1-t) + TJ(1+s)(1-t) + TK(1+s)(1+t) + TL(1-s)(1+t)) \quad (4.6)$$

Where I, J, K, and L are the nodes of the SHELL131 element and s and t are the element natural coordinates. This equation reflects the linear temperature distribution within the layer.

Regarding the surface integration, points in the plane dimension are considered with a 2X2 configuration. This provides an effective representation of the thermal distribution along the structure under analysis. The integration in the thickness layer usually requires 3 integration points.

The SOLID70 element in ANSYS exhibits a notable three-dimensional thermal conductivity capacity, applicable to both steady-state and transient thermal analyses. Composed of eight nodes, as shown in Fig. 4.10, each with a single degree of freedom for

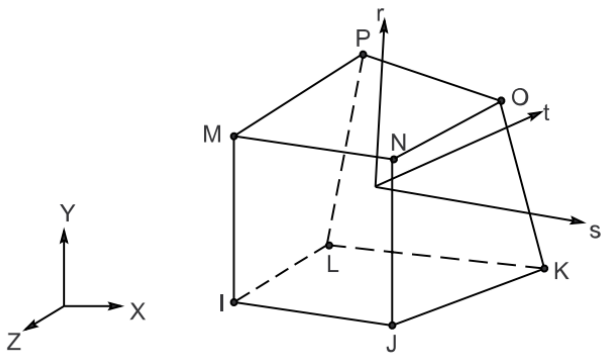

Figure 4.10: SOLID70 Geometry [40].

temperature TEMP (T), this element is designed to accurately and intricately represent the thermal distribution in complex solids. Its definition requires the specification of orthotropic material properties, enabling the modelling of varied thermal behaviours. Using a 2x2x2 configuration for integration points, SOLID70 ensures an effective representation during thermal analysis, capturing complex temperature variations. Its mathematical shape functions describe the linear temperature (T) distribution within its structure and are expressed as

$$\begin{aligned} T = \frac{1}{8}((&TI(1-s)(1-t)(1-r) + TJ(1+s)(1-t)(1-r) + TK(1+s)(1+t)(1-r) + \\ &TL(1-s)(1+t)(1-r) + TM(1-s)(1-t)(1+r) + TN(1+s)(1-t)(1+r) + \\ &TO(1+s)(1+t)(1+r) + TP(1-s)(1+t)(1+r)) \end{aligned} \tag{4.7}$$

Where I, J, K, L, M, N, O, and P represent the nodes of the element and s, t and r are the element natural coordinates.

The SURF152 element can be employed in various applications related to surface loads and effects. Specifically designed for three-dimensional thermal analyses, the SURF152 can be overlaid on a face of any 3D thermal element. Defining this element involves specifying four to ten nodes, as represented in Fig. 4.11, as well as material properties. It is crucial that these nodes share positions with the nodes of the underlying solid element. Additionally, it is possible to include an extra node, offset from the base element, to account for convection or radiation effects.

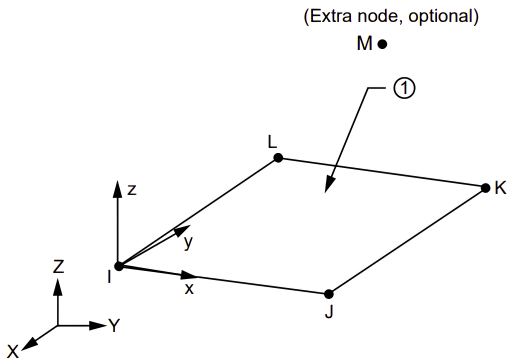

Figure 4.11: SURF152 Geometry (Adapted from [40]).

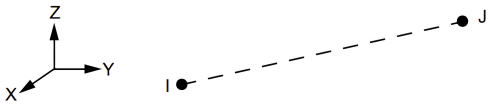

Figure 4.12: LINK34 Geometry [40].

During the use of SURF152, the essential nodes in this study are designated as I, J, K, and L, and the extra node as M, all possessing a degree of freedom represented by bulk temperature of the cavity (T). This element allows for the consideration of radiation between the modelled surface and the extra node, which is crucial for more accurate thermal simulations, especially in situations where the effects of convection or radiation cannot be fully defined a priori. Additionally, the extra node becomes particularly useful when the bulk temperature is unknown, providing flexibility in situations where thermal conditions may vary or not be entirely known. Similar to SHELL131, regarding surface integration, points in the plane dimension are also considered with a 2X2 configuration, presenting the same layer shape functions.

The LINK34 element is used to model uniaxial heat transfer, providing the unique capability of conducting thermal convection between its nodes. Specifically designed for thermal analyses, LINK34 is applicable in both two-dimensional (planar or axial) and three-dimensional contexts, covering steady-state and transient thermal analyses. Its configuration is defined by two terminal nodes, as shown in Fig. 4.12, designated as I and J, with a single degree of freedom associated with temperature TEMP (T) at each node.

Additionally, the element incorporates essential parameters, including a convective surface area, two empirical terms, and a film coefficient, to appropriately characterise convective heat transfer. This simplified approach is particularly effective in modelling thermal processes along a uniaxial direction, making it a valuable choice in scenarios where detailed analysis of heat transfer is crucial for understanding the thermal behaviour of a system.

4.4 Finite Element Mesh

In developing the finite element model in this dissertation, the mesh was strategically divided to ensure an accurate and efficient representation of the system under analysis. Carefully considering the specific requirements of the problem, as well as the geometric and thermophysical characteristics of the model, a higher density of elements was applied to critical areas to ensure adequate resolution. The choice of element types and mesh parameters aimed to balance result accuracy with computational efficiency, guided by the operational conditions and specific thermal phenomena of the study. Thus, the divisions used were developed as illustrated in Fig. 4.13.

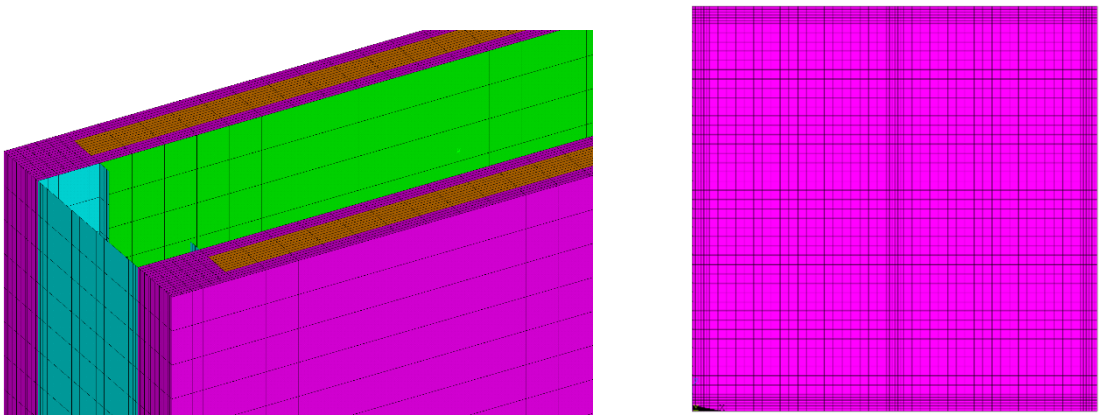

Figure 4.13: Finite element mesh of a LSF wall model.

The stud section mesh, represented in Fig. 4.13, was divided into 4 elements for Lip region, 6 for Flange, and 10 for Web. Additionally, in the gypsum board, 4 divisions were

made along the thickness, 20 in the horizontal region between the studs, and 40 in the vertical lines.

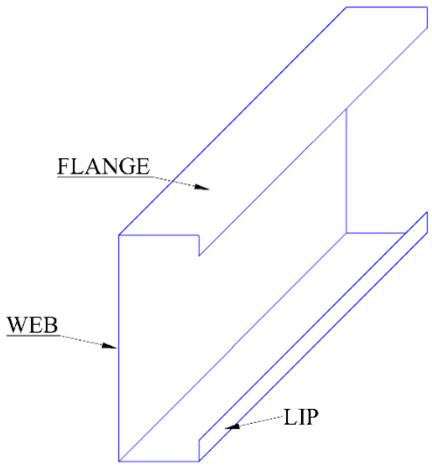

Figure 4.14: Steel stud components.

4.5 Solution Methods

Three distinct numerical solution methods were employed for a more accurate simulation of the performance of Light Steel Frame (LSF) walls without insulation in the cavities. The hybrid method (solution 1) incorporates convection and radiation in the cavity region based on the experimental cavity temperature (bulk temperature is introduced as a boundary condition. The second method (solution 2) considers interface elements for heat transfer exclusively by radiation, while the third method (solution 3) involves heat transfer by radiation and convection in the cavity region.

Additionally, a finite element model was developed to simulate the fire test on insulated LSF walls. Modifications to the thermal properties of the mineral wool (rockwool) insulation were implemented to simulate the fall of gypsum boards and the melting of rockwool during the test under hydrocarbon fire conditions. These adaptations aim to bring the numerical results closer to the experimental ones.

4.5.1 Initial and Boundary Conditions

To simulate heat transfers that occur when LSF walls are subjected to standard fire and hydrocarbon conditions, the following boundary conditions were applied:

For all models, an initial temperature of 5ºC was set at all nodes, chosen based on conducted experimental tests [6], [21]. Subsequently, conditions were applied for the side exposed to fire (FS), for the unexposed side (UNEX), and lastly, for the cavity (if necessary). According to EN 1991-1-2 [19], different values must be adopted for the convective heat transfer coefficient for different fire conditions on the exposed side. As for the rest of the properties, the same values can be adopted.

Exposed side to fire:

On surfaces exposed to fire, the heat flux considered both convection and radiation, calculated by Eq. 3.5,3.6. For radiation with flame emissivity, $\varepsilon_f = 1.0$ was assumed. The Stefan-Boltzmann constant was adopted as $\sigma = 5.67$ x $10^{-}8$ [W/m^2 K^4].

For models subjected to the standard temperature-time curve, a convective heat transfer coefficient of $\alpha_{cv} = 25$ [W/m^2K] and the average temperature determined by Eq. 3.1 were used. The gas temperature on the exposed side followed the ISO834 standard.

For the hydrocarbon fire curve, a convective heat transfer coefficient of $\alpha_{cv} = 50$ [W/m^2K] and the average temperature determined by Eq. 3.2 were used. The gas temperature on the exposed side followed the EN 1991-1-2 standard [19].

Unexposed side:

The heat flux must be determined using Eq. 3.4 with a convective heat transfer coefficient $\alpha_{cv} = 9$ [W/m^2K], assuming it encompasses the effects of radiation heat transfer.

Boundary conditions applied to the cavity region will be presented in the explanations for each solution method, considering that in walls with empty cavities, heat transfer in this region occurs through conduction, convection (movement of hot air within the wall cavity), and direct radiation. In cavities with insulation material, heat is transferred only through conduction, originating from the surface of the steel gypsum board and insulation [9]. Perfect contact between materials was considered in all models.

Transient and nonlinear thermal analyses were solved using the Newton-Raphson full solution option method, considering variations in thermal properties with temperature. This method allows for multiple corrections to be applied to obtain the final convergent solution. The chosen criterion for convergence is the heat flux, with a tolerance of $1.0x10^{-3}$ and a minimum reference value of $1.0x10^{-6}$. In this study, a time step of 60 seconds was established, constrained to a minimum and maximum of 1 and 60 seconds, respectively.

4.5.2 Solution Method 1

Solution Method 1 employs a hybrid finite element approach to simulate heat transfer through radiation and convection in the cavity region. This model is applicable for determining the fire resistance of Light Steel Framing (LSF) walls with empty cavities, based on the cavity temperature behaviour derived from previous experiments. The cavity temperature is calculated as the average between the inner faces in contact with the cavity, the most exposed (hot) layer, and the less exposed (cold) layer. In this study, this method was applied to model Specimens "S9" and "S13", as per the conducted experimental test [6].

According to Piloto et al. [28], the convection heat transfer coefficient in the cavity region can be determined by averaging the coefficients applied to exposed and unexposed surfaces. This assumption is considered physically acceptable, assuming that the cavity region is initially protected at the start of the fire test and fully exposed to the fire at the test's end. The application of convection and radiation should cover the surfaces in contact with the cavity, including the external surfaces of the studs and the internal surfaces of the gypsum boards for the analysed walls. Additionally, the bulk temperature should be determined through experimental tests, considering effects such as crack formation, board fall-off, material combustion, or any other heat release.

Therefore, the boundary conditions adopted for the cavity region, when the models are subjected to the standard temperature-time curve, include a convection heat transfer

coefficient of $\alpha_{cv} = 17$ [W/m^2K] and an average temperature determined from experimental tests. For models subjected to the hydrocarbon fire curve, a convection heat transfer coefficient of $\alpha_{cv} = 29.5$ [W/m^2K] and an average temperature also determined experimentally were used. Both models were subjected to the radiation boundary condition with an emissivity value of 1.

Additionally, the time at the end of the solution for the model subjected to the standard fire condition was set at 11100 s for experimental test validation. In the case of the model using the hydrocarbon fire, the time at the end of the solution was set at 5460 s.

4.5.3 Solution Method 2

In this method, the SURF152 element was employed to apply additional boundary conditions in the cavity region, assuming heat transfer by radiation among all internal faces. This model can predict the cavity temperature in the region simply by achieving thermal equilibrium of the internal faces in that region.

The finite element SURF152 was overlaid onto the internal areas of the SOLID70 element to define the heat flow by radiation between the surface of the protective plate and the temperature of the node inserted in the cavity, as illustrated in Fig. 4.15. The emissivity value for the SURF152 element was considered equal to 1, assuming the Stefan-Boltzmann constant with a value of $\sigma = 5.67$ x $10^{-}8$ [W/m^2K^4].

Subsequently, the time at the end of the solution for the model subjected to the standard fire condition was set to 11100 s for the validation of the experimental test. In the case of the model using hydrocarbon fire, the time at the end of the solution was established as 5460 s. Later, both final times for each solution were increased to obtain the fire resistance time of the models, as these exceed the times conducted in the experimental tests. Unlike Method 1, Methods 2 and 3 do not rely on experimental data to input boundary conditions into the models, thus allowing an increase in the time limit for the solutions.

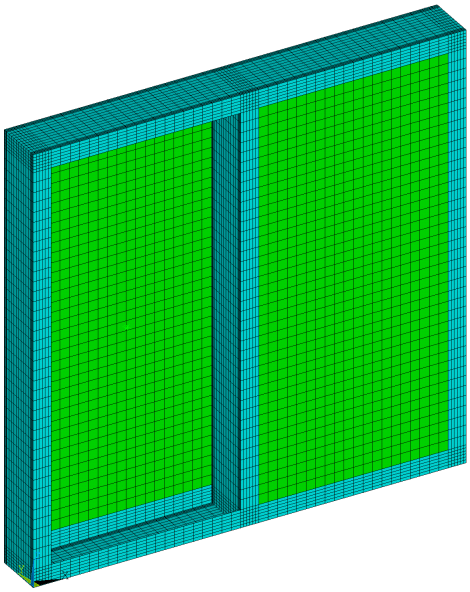

Figure 4.15: SURF152 applied on Solution Method 2.

4.5.4 Solution Method 3

Similar to Method 2, this method uses the finite element SURF152 to apply radiation boundary conditions in the cavity region. Additionally, this method incorporates the finite element LINK34 to impose convection boundary conditions also present in the cavity region. The LINK34 element facilitates uniaxial heat transfer, simulating thermal convection between the nodes of the internal areas of the plasterboard in contact with the cavity and the node inserted at the center of this region, as show in Fig. 4.7.

Therefore, the essential parameters of the LINK34 element to simulate the boundary conditions adopted for the cavity region were added according to each analysed fire curve. When the models are subjected to the standard curve, a convection heat transfer coefficient of $\alpha_{cv} = 17$ [W/m^2K] and a convection surface area according to the dimensions of the surfaces of the SURF152 element were adopted. For models subjected to the hydrocarbon fire curve, a convection heat transfer coefficient of $\alpha_{cv} = 29.5$ [W/m^2K] and a convection surface area, also according to the dimensions of the surfaces of the SURF152 element, were used.

Finally, increments in the final solution times were used, as in Method 2, to obtain

the fire resistance time of the models.

4.5.5 Solution Method for Cavity Insulated Walls

The finite element analysis (FEA) for models equipped with cavity insulation did not include the imposition of specific boundary conditions for this region, as heat transfer is exclusively by conduction. Therefore, additional finite elements such as SURF152 or LINK34, for simulating radiation and convection inside the walls, were not required.

However, during the comparison of numerical results with experimental data, the need to adjust the model for enhanced accuracy of the walls' behaviour during the fire resistance test became evident. Omitting phenomena in the numerical models, such as the appearance of cracks, plate fall, and material combustion, resulted in discrepancies compared to expectations. Thus, adjustments were made to the thermal properties of plasterboard and rockwool, aiming for better agreement with experimental results, simulating the increased heat transfer associated with these phenomena.

After each implemented modification, the error (RMSE) was calculated for each layer of the wall. To select the most appropriate change, the criteria adopted were the lowest average RMSE and the lowest RMSE in the layer not exposed to fire, as the latter is used in determining the fire resistance time by insulation (I) of Light Steel Framing (LSF) walls. The obtained results, along with the modifications made, will be detailed throughout this chapter.

4.6 Material Properties

Accuracy and reliability of any numerical modelling are directly related to the correct definition of the properties of the materials involved. In the context of simulating Light Steel Framing (LSF) walls, different materials were used, each contributing in a unique way to the system's integrity. It is important to note that the properties of these materials have a significant impact on the overall performance of LSF walls. The properties will be further detailed in Appendix A.

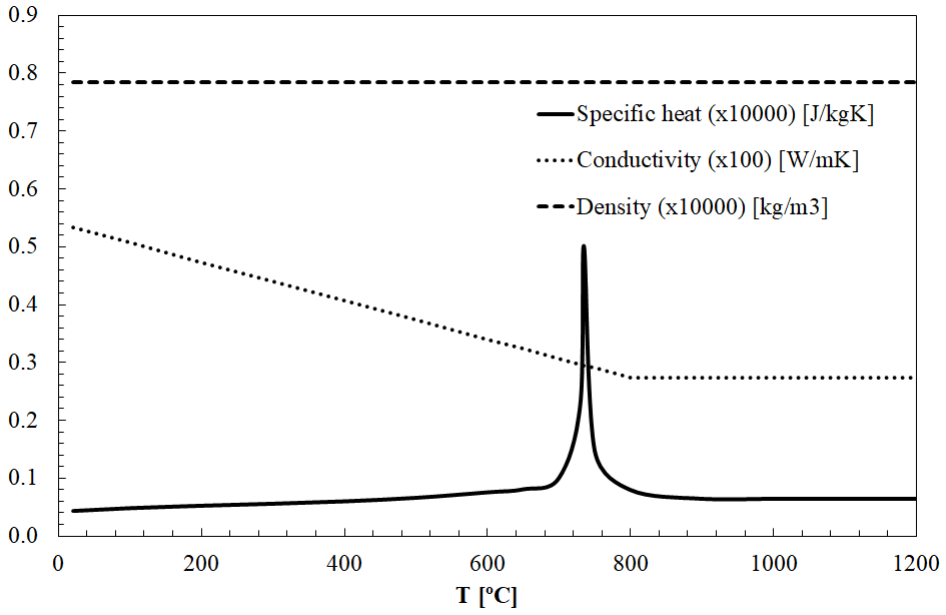

Figure 4.16: Thermal properties of carbon steel.

To ensure simulations as accurate as possible, the thermal properties of the materials used in the models were obtained from established standards [43], [44] as well as through experimental studies [15]. These properties include thermal conductivity, specific heat, density, and material emissivity, all of which are critical in determining the thermal performance of LSF walls. Additionally, the properties of these materials may vary with temperature. Therefore, it is essential to consider this variable when conducting simulations to accurately predict the behaviour of LSF walls under different conditions.

4.6.1 Carbon Steel

Thermal properties of carbon steel CFS elements are provided by the standard EN 1993-1-2 [43]. Fig. 4.16 illustrates the specific heat of carbon steel, thermal conductivity, and constant density, which remains at the value of 7850 kg/m^3. The emissivity of carbon steel is equal to 0.7, as specified by the standard EN 1991-1-2 [19].

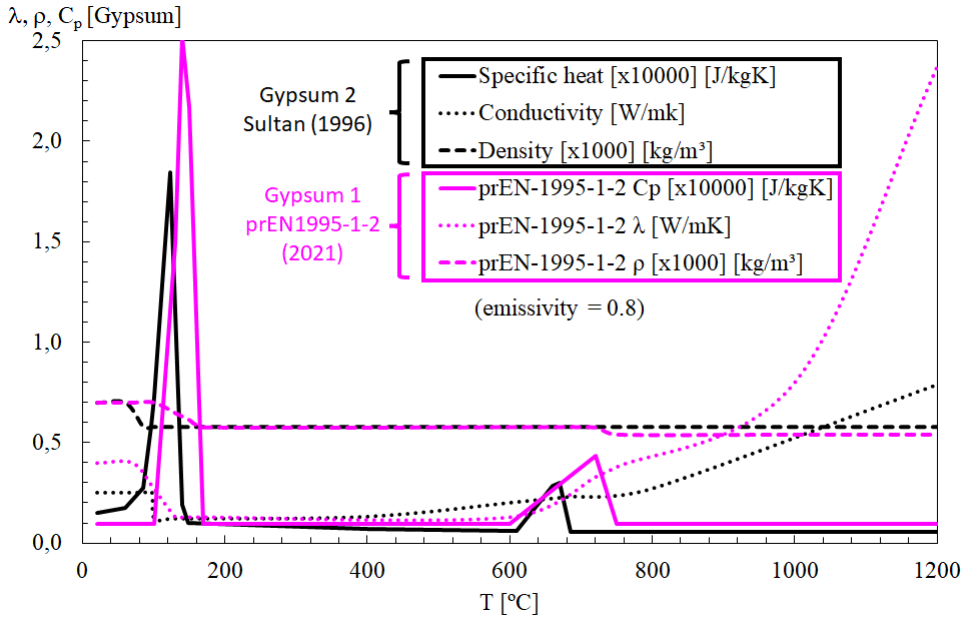

Figure 4.17: Thermal properties of Gypsum Type 1 and Gypsum Type 2.

4.6.2 Gypsum Plasterboards

Two distinct varieties of gypsum plasterboard, namely Gypsum Type 1 and Gypsum Type 2, were utilised in this thesis. Gypsum Type 1 was employed to validate the experimental tests, while both types of plasterboard were utilised in the development of the parametric study due to their representation of the most commonly used thermal properties for gypsum plates in Portugal.

For Gypsum Type 1, its thermal properties are defined by prEN 1995-1-2 [44], while the specifications for thermal properties are outlined by Sultan (1996) [15]. Fig. 4.17 illustrates the specific heat, thermal conductivity, density, and emissivity of the material for the two distinct gypsum types adopted.

4.6.3 Mineral wool (Rockwool)

Thermal properties of rockwool are specified by the standard prEN 1995-1-2 [44], as depicted in Fig. 4.18. The material density, obtained from experimental tests [6], [21], is 60 kg/m^3. The emissivity used is equal to 0.8, as prescribed by the standard EN

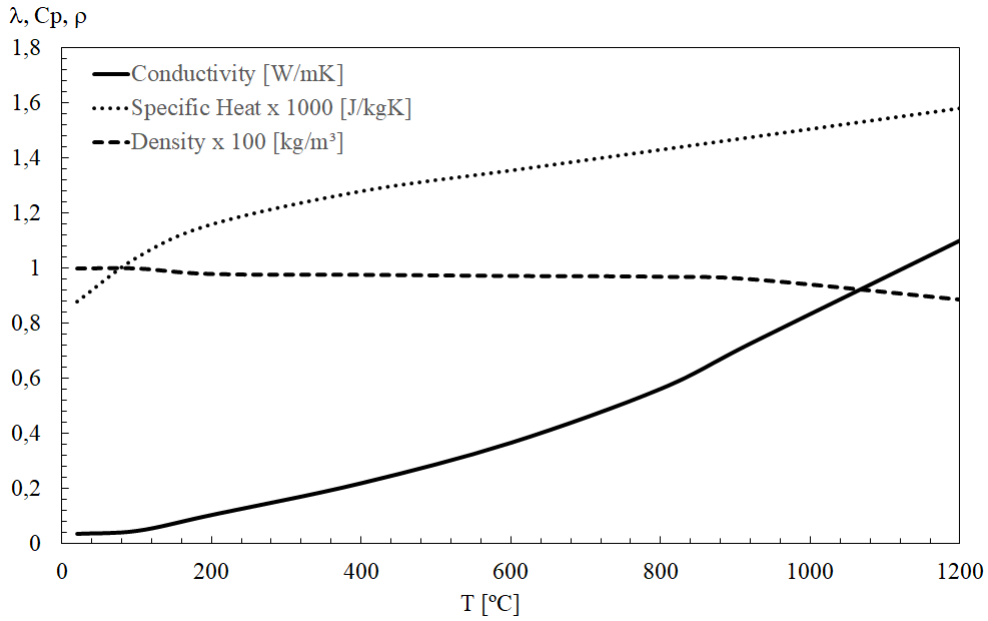

Figure 4.18: Thermal properties of Rockwool (60 kg/m^3).

1991-1-2[19].

4.7 Numerical Validation and Discussion

In this section, the numerical validation of the methodology employed in this work is presented. A comparison will be made between the temperatures obtained in the experimental tests conducted by Chen et al. [6], [21] and those extracted from selected nodes in the meshes of the finite elements modelled. To ensure the accuracy of the methods developed, considering the assumed modifications and material characterisation, each developed model will be verified against available experimental results.

The temporal variation of temperature across all layers of the walls was recorded by the thermocouples installed in the test experiments, as shown in Fig. 4.4 and 4.6. Therefore, the temperatures in the numerical models were extracted at the same locations as these thermocouples (see Fig. 4.19). In this study, a comparison is presented using the Root Mean Square Error (RMSE) for the temperature evolution of each component. Towards the end of the chapter, the Relative Error (RE) will be used to compare the fire

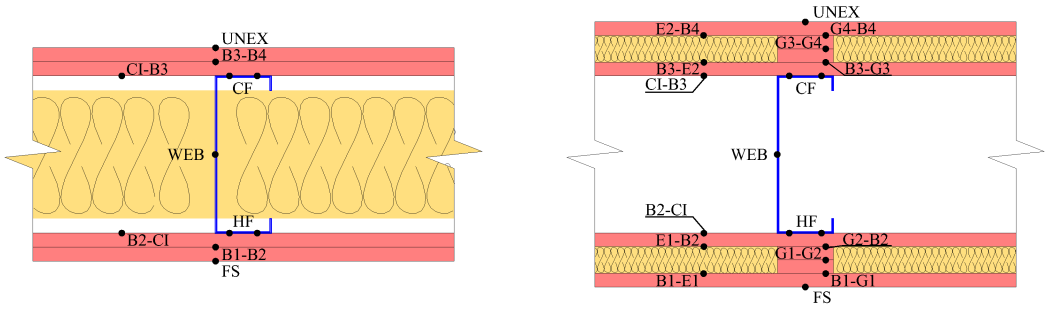

(a) Internal insulated wall. (b) External insulated wall.

Figure 4.19: Thermocouples positions on internal (a) and external (b) insulated walls.

resistance time for insulation (I). The RMSE [ºC] is the adopted method for validating the mathematical model, as presented in Eq. 4.8.

$$RMSE = \sqrt{\frac{1}{n}\sum_{i=1}^{n}(T_{exp} - T_{num})^2} \tag{4.8}$$

Where n is the number of instants to be compared, T_{exp} is the temperature from the experimental test, and T_{num} is the temperature from the finite element model. This error represents the relative difference between the two curves (FEA and test). In a perfect representation, RMSE would be equal to 0, signifying that the closer to 0, the better the finite element results.

The numerical validation will be presented in accordance with the order of the models developed during this dissertation. Initially, the walls with insulation in the cavity region, referred to as “S1” and “S5” in the experimental test, will be evaluated. Subsequently, the walls with insulation outside the cavity, located between the two gypsum board layers, “S9” and “S13”, will be examined. Furthermore, this study initiates the analysis of Light Steel Framing (LSF) walls exposed to hydrocarbon fires, followed by walls subjected to standard fire conditions.

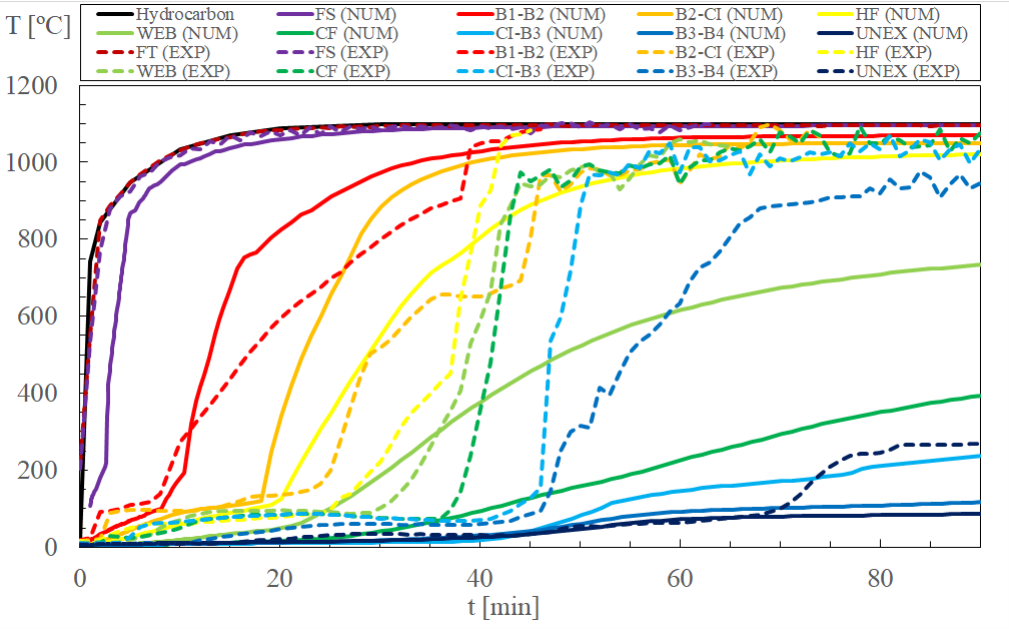

Figure 4.20: Experimental and numerical results for Specimen "S5".

4.7.1 Validation of cavity insulated walls specimens

Fig. 4.20 illustrates the comparison between the experimental results and the numerical outcomes for the "S5" specimen model. The graphical representation includes the average temperatures of each layer of the analysed walls.

This wall was subjected to a hydrocarbon fire condition. Its geometry consisted of two 12 mm gypsum boards with rockwool insulation in the cavity. This case underwent a 91-minute fire test. According to the authors [21], the failure of the insulation (I) for Specimen "S5" occurred due to the extrapolation of the average criterion temperature (140°C + ambient temperature) at 73 minutes. Failures in thermocouples were recorded during the fire test, approximately at 63 minutes for the fire-exposed surface (FS) and at 46 minutes for the thermocouples between the most exposed gypsum board layers (B1 and B2) and the hot flange of the stud (HF). Analysing the abrupt temperature increase in the graph at 38 minutes, the collapse of the first gypsum board layer exposed to the fire (B1) can be identified. After the test's conclusion, the authors observed the collapse of the GP boards on the fire-exposed face layer (B1) and the base layer (B2), as well as

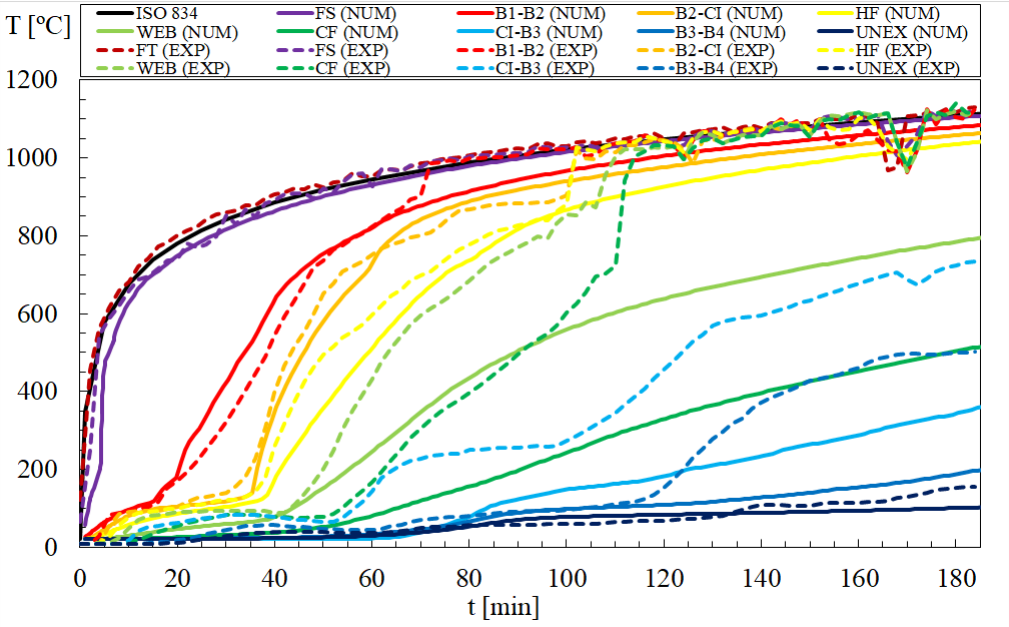

Figure 4.21: Experimental and numerical results for Specimen "S1".

the melting of the rockwool cavity insulation. Additionally, the steel stud oxidised and exhibited local buckling at the mid-height.

The authors also noted that the temperature of the B1-B2 layer rises slowly at the beginning of the fire exposure due to the dehydration of $CaSO4 \cdot 2H2O$ and the evaporation of moisture from the gypsum boards in the B1 layer on the fire exposed side. This process extracts a significant amount of heat from the gypsum board, resulting in a smooth development of the corresponding time-temperature curve. This phenomenon was observed in other tested specimens as well.

The comparison of experimental results with numerical outcomes for the Specimen "S1" model is depicted in Fig. 4.21.

This wall was subjected to a standard fire condition. Its geometry comprised two 12 mm gypsum boards with rockwool insulation in the cavity. This case underwent a 185-minute fire test. The furnace temperature curve was affected during the time interval of 169 minutes to 174 minutes due to the liquefied petroleum gas (LPG) tanks not being replaced promptly during the fire experiments. According to the authors [21], the failure of Specimen "S1" insulation occurred due to the extrapolation of the maximum criterion

temperature (180°C + ambient temperature). Cracks were observed in the gypsum board most exposed to the fire at approximately 10 minutes. Additionally, at around 70 and 100 minutes, drops in temperature were noted for the first and second gypsum boards most exposed to the fire, as evident from the sharp temperature increase in the mentioned time intervals. At 137 minutes into the test, the temperature of the surface not exposed to the fire at approximately 900 mm height reached 185.2°C (measured by a portable thermometer), exceeding the insulation failure criterion (I). The rockwool cavity insulation experienced a decrease in thickness due to partial melting of the material. Furthermore, oxidation and significant local crushing were observed at the mid-height of the steel pin structure, attributed to direct exposure to the fire.

Analysing the temperature-time curves obtained from the numerical tests of the two specimens, a discrepancy in results is apparent when gypsum board drops occur, as the numerical models do not assume this phenomenon throughout the analysis procedure. Additionally, imperfect contact may occur between the rockwool insulation and the internal surfaces of the boards and steel profile, creating void spaces in the region, leading to heat transfer through radiation in the cavity.

To address this, modifications were made to the thermal properties of the materials in accordance with Eq. 4.2 to simulate effects such as the emergence of cracks, board drops, material combustion, or any other heat release. The abrupt decrease in specific heat (C) and increase in thermal conductivity (λ) lead to a rapid increase in the heat conduction of the altered material, representing what would occur if the material disappeared during fire exposure. The modifications applied to each specimen are described in Tables 4.1 and 4.3. The modification temperature signifies that the thermal properties of that material were changed from the mentioned temperature.

After processing and extracting data from each implemented alteration, the obtained results were compared using RMSE, as shown in Table 4.2.

The selected option for Specimen “S5” was modification number 14 (see Fig. 4.22), as it has the lowest RMSE for the layer not exposed to fire (UNEX). To determine the wall’s insulation time, the maximum and average temperatures of the least exposed surface to

Table 4.1: Modification in thermal properties implemented in the numerical model of Specimen "S5".

Modification Number	Modified Material	Specific Heat [J/kgK]	Thermal Conductivity [W/mK]	Modification Temperature [ºC]
1	Gypsum	100	10	900
2	Rockwool	100	10	900
3	Rockwool	100	10	800
4	Rockwool	200	20	900
5	Rockwool	200	20	800
6	Rockwool	50	5	900
7	Rockwool	500	50	900
8	Rockwool	500	50	800
9	Rockwool	100	30	800
10	Rockwool	150	30	800
12	Rockwool	20	10	800
13	Rockwool	100	75	800
14	Rockwool	50	75	800
15	Rockwool	50	100	800
16	Rockwool	50	200	800

Table 4.2: Comparison of the RMSE values for the numerical results of Specimen "S5" with and without material modifications.

Modification	FS	B1-B2	B2-CI	HF	WEB	CF	CI-B3	B3-B4	UNEX	Average
0	111.4	148.5	191.8	181.4	272.7	559.1	581.6	483.2	75.9	289.5
1	113.4	324.5	406.4	614.6	254.9	461.5	529.6	467.0	74.2	360.7
2	112.4	144.0	180.3	181.0	156.6	428.6	361.6	434.8	69.6	229.9
3	112.5	142.2	180.2	194.9	160.7	296.5	202.6	326.8	54.2	185.6
4	112.4	143.8	184.9	182.8	139.1	395.4	323.1	411.7	68.2	217.9
5	112.5	142.5	189.2	200.0	176.6	259.3	194.1	296.6	46.4	179.7
6	112.4	144.1	178.9	179.7	183.8	468.9	423.7	457.0	71.3	246.6
7	112.4	144.0	191.6	185.5	123.4	354.0	310.9	392.1	66.8	209.0
8	112.6	143.1	201.9	205.4	194.3	234.0	198.5	283.7	44.4	179.8
9	112.5	142.7	159.9	202.4	184.5	244.9	195.5	287.5	44.8	175.0
10	112.5	142.8	194.3	202.5	184.9	245.1	195.0	287.1	44.9	178.8
12	112.5	142.2	180.0	195.1	160.8	294.8	203.5	327.3	54.8	185.6
13	112.5	143.4	204.3	208.4	202.0	222.5	196.8	279.1	44.6	179.3
14	112.5	143.3	204.0	208.1	201.5	222.3	196.6	277.6	44.3	178.9
15	112.5	143.6	207.1	210.3	206.3	214.0	194.8	278.2	44.8	179.1
16	112.6	143.8	211.4	215.4	218.3	201.4	190.4	275.8	44.6	179.3

Table 4.3: Modification in thermal properties implemented in the numerical model of Specimen "S1".

Modification Number	Modified Material	Specific Heat [J/kgK]	Thermal Conductivity [W/mK]	Modification Temperature [ºC]
1	Gypsum	100	10	900
2	Rockwool	100	10	900
3	Rockwool	50	75	800

Table 4.4: Comparison of the RMSE values for the numerical results of Specimen "S1" with and without material modifications.

Modification	FS	B1-B2	B2-CI	HF	WEB	CF	CI-B3	B3-B4	UNEX	Average
0	49.9	48.2	43.4	76.3	211.6	308.2	151.8	53.6	11.0	106.0
1	43.1	53.5	47.5	69.1	250.1	425.0	231.0	154.3	19.0	143.6
2	43.3	64.9	78.3	109.2	185.7	318.6	97.5	70.1	40.9	112.1
3	68.5	95.5	189.7	183.1	175.7	162.1	187.2	164.1	180.1	156.2

the fire are evaluated. Thus, it will be the criterion used to choose the best proposal for altering the properties of the materials used in the numerical models.

After processing and extracting data from each implemented alteration, the results obtained were compared using RMSE, as shown in Table 4.4.

The best option for Specimen "S1" was the starting guess "0", where none of the materials underwent modifications in their thermal properties, possibly due to the partial melting of rockwool insulation, unlike what occurred in Specimen "S5". Therefore, for the development of the parametric study on walls with cavity insulation when subjected to standard fire, no changes were made to the material properties. However, for walls subjected to a hydrocarbon fire curve, alterations will be made to the specific heat (C = 50) and conductivity ($\lambda = 75$) of rockwool when the material reaches temperatures above 800ºC.

4.7.2 Validation of external-insulated walls specimens

The comparisons between the experimental results and the numerical outcomes for the three solution methods employed in Specimen "S13" are depicted in Fig. 4.23, 4.24 and

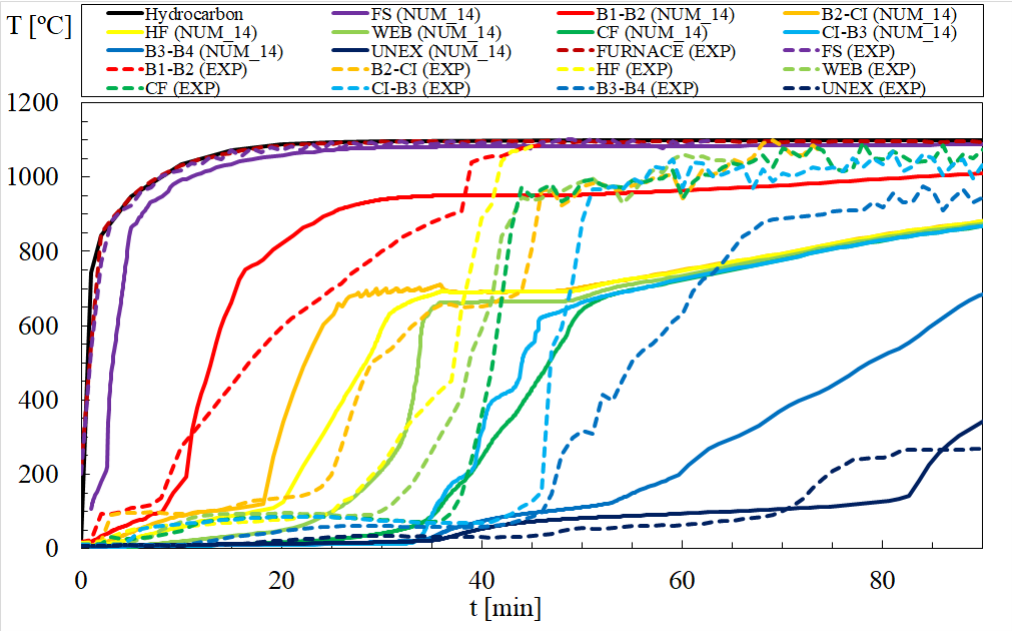

Figure 4.22: Experimental and numerical results for Specimen "S5" – Modification 14.

4.25. The average temperatures of each layer of the analysed walls were selected for the graphical representation.

The wall of Specimen "S13" was subjected to a hydrocarbon fire curve. Its geometry consisted of two 12 mm gypsum boards with rockwool insulation between the boards and no insulation in the cavity region. This case underwent a 91-minute fire test. For this insulation configuration, it was not possible to reach the insulation failure criteria during the experimental tests. Analysing the abrupt temperature increase in the graph that occurred in the B1-B2 layer at 85 minutes, it is possible to identify the collapse of the first gypsum board most exposed to the fire (B1). After the test concluded, cracks were observed in the second gypsum board (B2), and local buckling occurred at the mid-height of the steel stud.

After processing and data extraction, the results obtained for the three solution methods were compared using RMSE, as shown in Table 4.5.

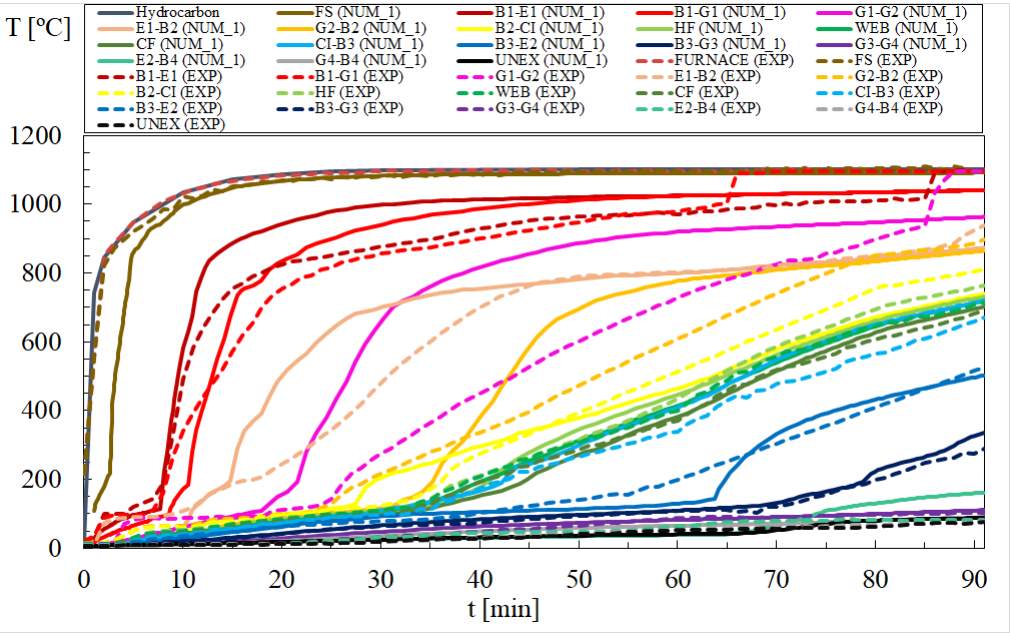

Figure 4.23: Experimental and numerical results for Specimen "S13" – Solution Method 1.

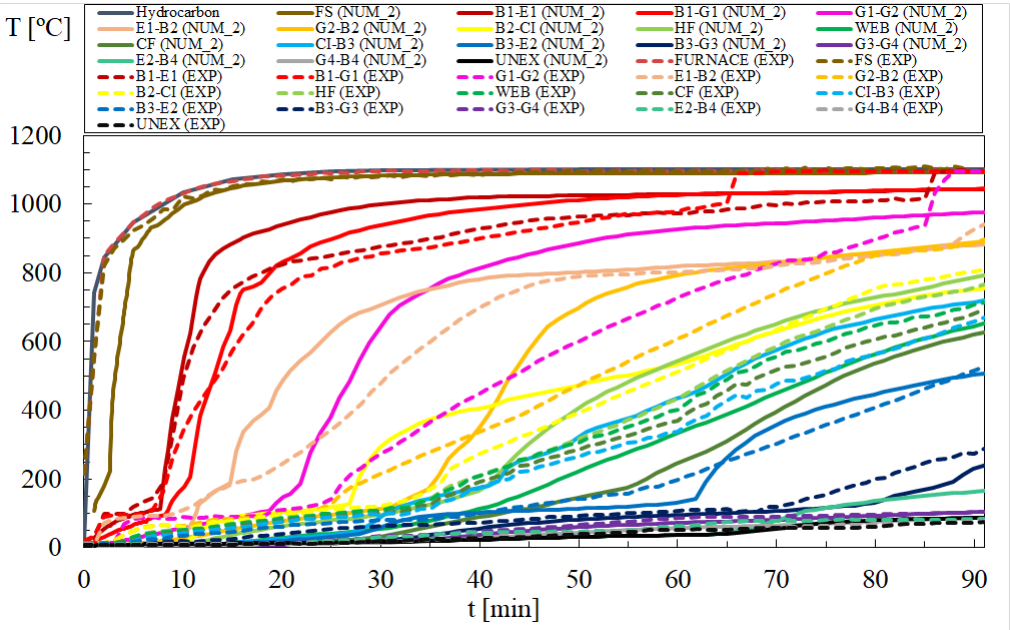

Figure 4.24: Experimental and numerical results for Specimen "S13" – Solution Method 2.

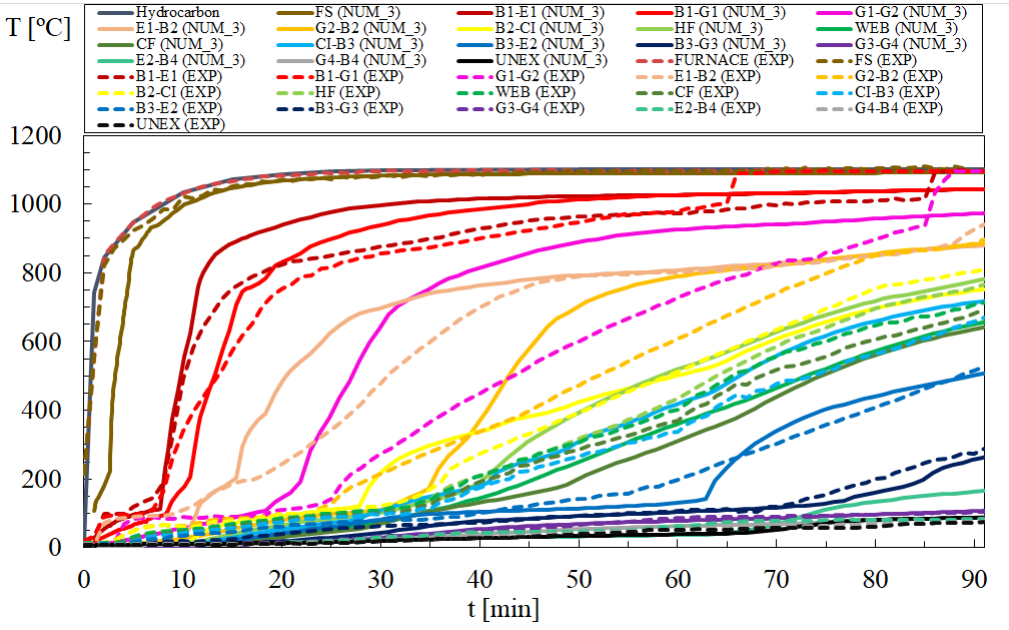

Figure 4.25: Experimental and numerical results for Specimen "S13" – Solution Method 3.

Table 4.5: Comparison of the RMSE values for the numerical results of Specimen "S13" for solution methods 1, 2, and 3.

Sol.	FS	B1-E1	B1-G1	G1-G2	E1-B2	G2-B2	B2-CI	HF	WEB	CF	CI-B3	B3-E2	B3-G3	G3-G4	E2-B4	G4-B4	UNEX	Ave.
1	96.5	79.5	72.5	216.3	113.4	103.8	49.4	21.3	9.9	17.6	46.4	28.2	13.1	9.6	28.6	12.8	8.8	54.6
2	96.4	80.3	70.4	214.3	114.9	109.9	79.9	56.1	74.2	94.5	65.3	34.4	33.8	8.8	31.1	4.9	9.4	69.3
3	96.4	79.1	70.8	214.9	110.8	109.3	50.9	43.6	57.6	56.8	55.1	29.7	18.7	4.4	30.1	8.4	8.9	61.5

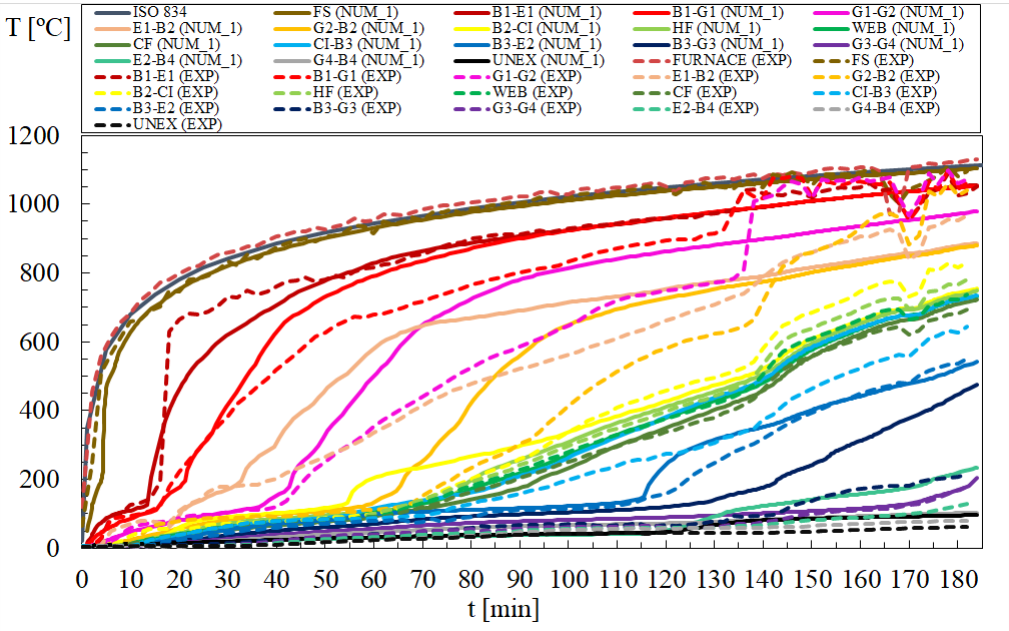

Figure 4.26: Experimental and numerical results for Specimen “S9” – Solution Method 1.

Fig. 4.26, 4.27, and 4.28 depict the comparisons between the experimental results and the numerical outcomes for Specimen “S9” using the three proposed calculation methods.

Similar to what occurred in the experimental test of Specimen “S1”, the furnace temperature of Specimen “S9” decreased at 169 minutes but later recovered because the gas fuel was not replaced in time. The wall of Specimen “S9” was subjected to a standard fire curve. Its geometry comprised two 12 mm gypsum boards with rockwool insulation between the boards and no insulation in the cavity region. This case underwent a 185-minute fire test, but it was not sufficient to reach the insulation failure criteria. The authors reported that at 15 minutes of fire exposure, there was cracking in the most exposed gypsum board (B1), but the board fell only around the 134-minute mark, where the B1 board and the strips from layer G1 fell. After the test, it was reported that part of the B2 board and rockwool insulation fell.

After processing and data extraction, the results obtained for the three solution methods were compared using RMSE, as shown in Table 4.6.

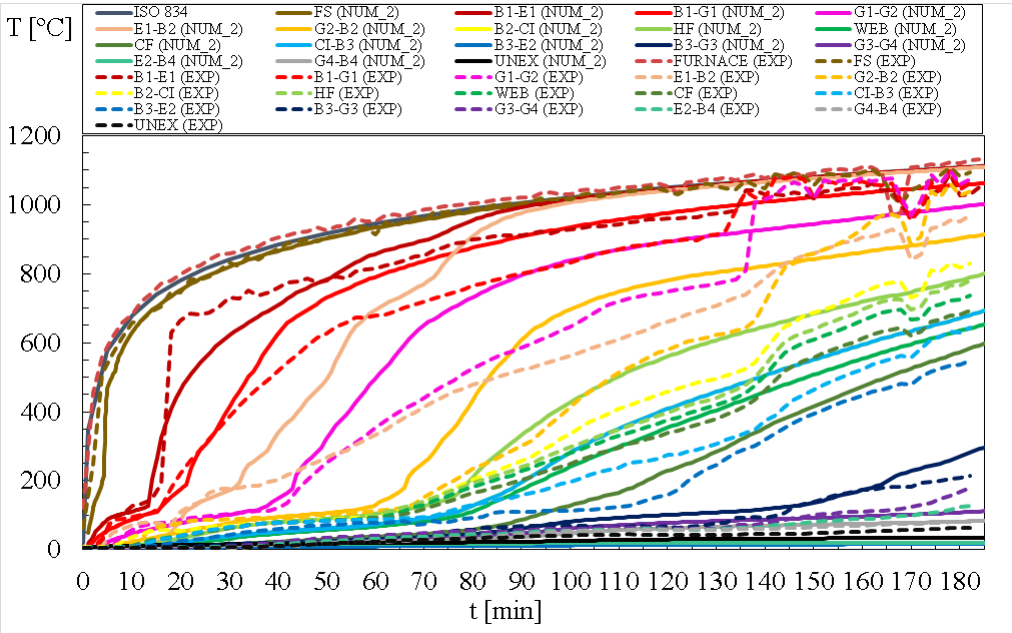

Figure 4.27: Experimental and numerical results for Specimen "S9" – Solution Method 2.

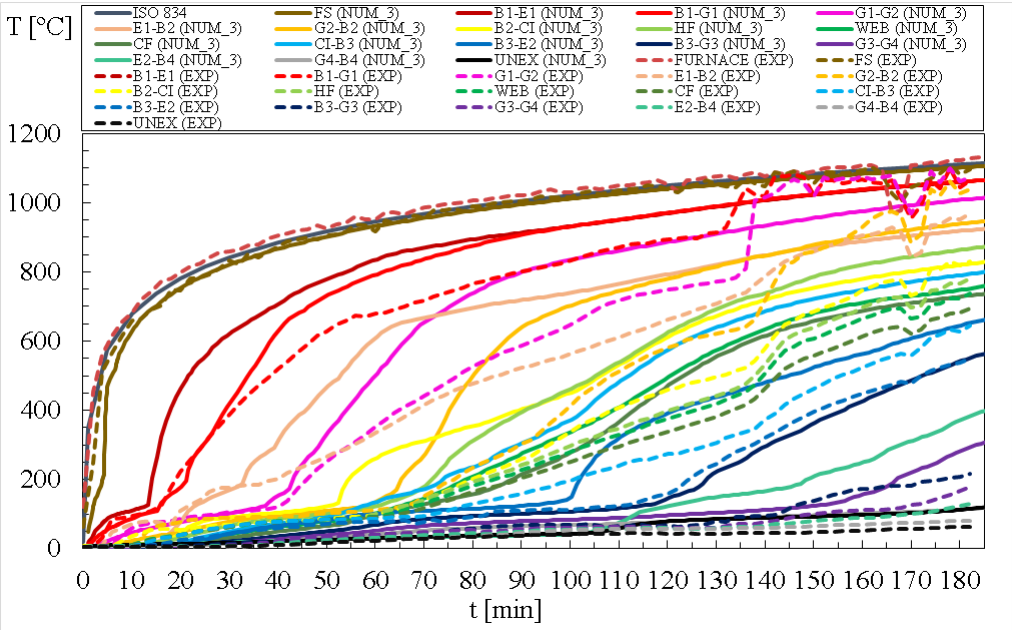

Figure 4.28: Experimental and numerical results for Specimen "S9" – Solution Method 3.

Table 4.6: Comparison of the RMSE values for the numerical results of Specimen "S9" for solution methods 1, 2, and 3.

Sol.	FS	B1-E1	B1-G1	G1-G2	E1-B2	G2-B2	B2-CI	HF	WEB	CF	CI-B3	B3-E2	B3-G3	G3-G4	E2-B4	G4-B4	UNEX	Ave
1	39.8	53.4	74.6	124.8	127.2	128.8	56.3	22.5	14.4	14.8	76.6	27.5	89.6	17.9	39.7	18.7	20.2	55.7
2	39.9	76.1	77.3	128.2	293.6	147.4	79.5	81	57.4	97	73.8	241.1	22.5	18.9	45	5.2	14.1	88.1
3	39.8	53.2	76.4	126.4	142.6	156.3	108.1	131.7	65.2	74.4	182.3	107.9	145.1	41.2	96.5	22	27.8	93.9

Comparing the obtained error results for the unexposed face (UNEX) and the overall mean error for Specimens "S13" and "S9", it can be concluded that all three methods provide a good prediction of the behaviour of the LSF wall over time during fire test experiments. Higher errors were found among the first layers of gypsum (G1-G2, E1-B2, and G2-B2), possibly due to the numerical model assuming that the B1 board and rockwool insulation remain in place throughout the simulation, and due to the perfect material contact assumption in the numerical simulations.

4.7.3 Conclusions

As mentioned in Chapter 3, the fire test standard EN 1363-1 [36] recommends that, after the initial 10 minutes of the test, the temperature recorded by any thermocouple in the furnace should not deviate by more than 100°C from the corresponding temperature in the standard fire curve. Therefore, the results obtained in this dissertation were deemed satisfactory if the RMSE value was less than 100°C for each analysed component.

To compare the fire resistance time for insulation (I), the Relative Error (RE) [%] will be used, given by the equation

$$RE = \frac{\left|tfi_{num} - tfi_{exp}\right|}{tfi_{exp}} \tag{4.9}$$

Where tfi_{num} represents the fire resistance time obtained from the numerical test, and tfi_{exp} represents the fire resistance time obtained from the experimental test.

As the fire resistance time for Specimen "S1" of 137 minutes was obtained through portable thermometer measurement, it was possible to identify the temperature across the entire surface, not limited to the thermocouple locations. Thus, a lower fire resistance time of 175.7 minutes was found than would be recorded by the thermocouples. Therefore, since the numerical model was restricted to the thermocouple locations, the fire resistance time from the experimental test will be considered as provided by the thermocouples.

For Specimen "S1", despite modification 1 presenting a lower RMSE, the RE for the fire resistance time was not the lowest among the other options. This occurred because

Table 4.7: Comparison of fire resistances by insulation for Specimen "S5" ($tfi_{exp} = 73$ min).

Modification	Tave [min]	Tmax [min]	Tfi [min]	Relative Error [%]
0	>100	>100	>100	-
1	>100	>100	>100	-
2	>100	>100	>100	-
3	86.76	87.37	86.76	18.85
4	99.55	>100	99.55	36.37
5	83.65	84.31	83.65	14.59
6	>100	>100	>100	-
7	94.03	93.99	93.99	28.75
8	82.5	83.09	82.5	13.01
9	82.72	83.3	82.72	13.32
10	82.87	83.46	82.87	13.52
12	86.94	87.36	86.94	19.1
13	82.24	82.97	82.24	12.66
14	82.11	82.73	82.11	12.48
15	82.6	83.29	82.6	13.15
16	82.08	82.69	82.08	12.44

Table 4.8: Comparison of fire resistances by insulation for Specimen "S1" ($tfi_{exp} = 175.7$ min).

Modification	Tave [min]	Tmax [min]	Tfi [min]	Relative Error [%]
0	224.75	214.45	214.45	22.05
1	221.04	208.64	208.64	18.75
2	166.44	166.27	166.27	5.37
3	131.35	131.53	131.35	25.27

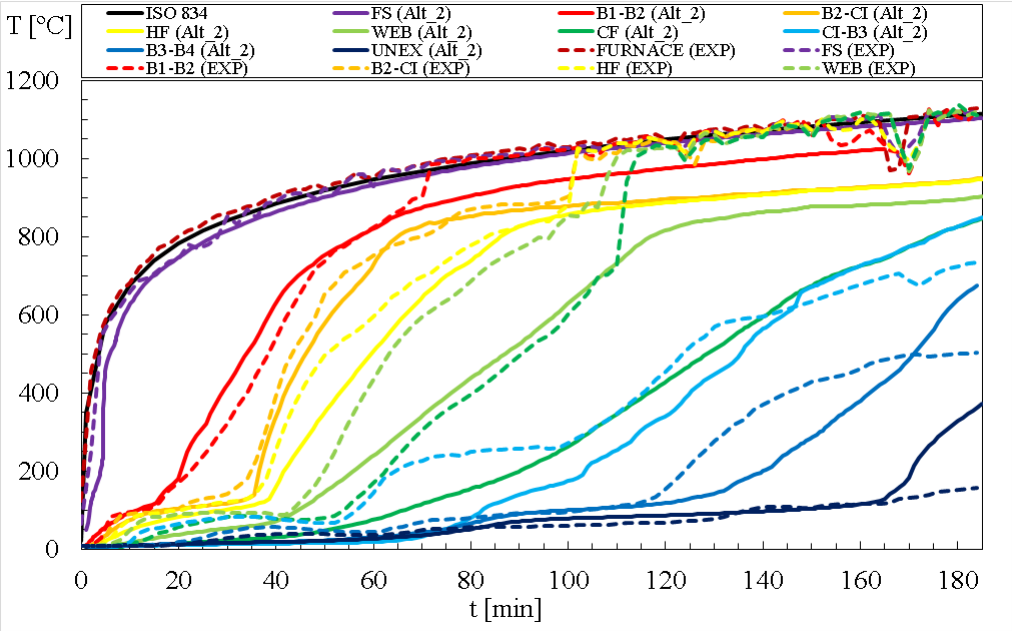

Figure 4.29: Experimental and numerical results for Specimen "S1" – Modification 2.

the modifications made to the materials antecipated the temperature increase on the unexposed face (UNEX), as shown in Fig. 4.29.

The results of the Finite Element (FE) models proved satisfactory for the unexposed face (UNEX). Therefore, with thermal properties modified at elevated temperatures, such as thermal conductivity and specific heat of the material, the FE model can be used to determine the insulation fire resistance time (I). However, additional analyses are desirable for a more accurate prediction of the temperature evolution along the wall section. The modification of material properties is crucial to minimise phenomena observed in fire experiments, which may result in the anticipation of the temperature growth curve.

In the case of Specimens "S9" and "S13", it was not possible to calculate the relative error (RE) since the criterion values for insulation fire resistance were not achieved in the experimental tests. Therefore, the Tables 4.9 and 4.10 solely compares the results obtained by each solution method used.

In solution method 1, comparing the fire resistance time is not feasible due to the absence of apparent temperature values after 91 and 185 minutes for the tests of Specimen "S13" and "S9", respectively.

Table 4.9: Comparison of fire resistances by insulation for Specimen "S13" ($tfi_{exp} = >91$ min).

Solution	Tave [min]	Tmax [min]	Tfi [min]	Relative Error [%]
1	>91	>91	>91	-
2	136.27	136.09	136.09	-
3	136.22	136.18	136.18	-

Table 4.10: Comparison of fire resistances by insulation for Specimen "S9" ($tfi_{exp} = >185$ min).

Solution	Tave [min]	Tmax [min]	Tfi [min]	Relative Error [%]
1	>185	>185	>185	-
2	>360	335.02	335.02	-
3	187.79	187.92	187.79	-

Solution method 2 exhibits a higher RMSE compared to the other methods for Specimen "S13". This can be explained by the absence of the convection component in the heat flow. The lack of this heat flow is responsible for the increase in temperature in the cavity region, resulting in greater discrepancies in HF, WEB, CF values, and in the temperatures of the plasterboards in contact with the cavity region.

However, for Specimen "S9", solution 3 yielded the highest error. A possible explanation for this result is that, due to the more gradual temperature increase in the ISO 834 fire, the omission of convection resulted in lower temperatures during the fire exposure, approaching the experimental results. The evolution of temperatures in the numerical simulations followed the fire curves rather than the furnace temperature curves. Therefore, for Specimens "S1" and "S9", the variations in experimental temperatures were not considered due to inadequate replenishment of liquefied petroleum gas (LPG), which could also lead to discrepancies in the numerical results. Moreover, in Fig. 4.30, 4.31, and 4.32, it is observed that the temperature developed uniformly on the unexposed surface (UNEX) in methods 1 and 3, while method 2 exhibited a higher concentration of heat in the stud region.

Additionally, besides thermal analyses for insulation criteria (I), it is observed that the

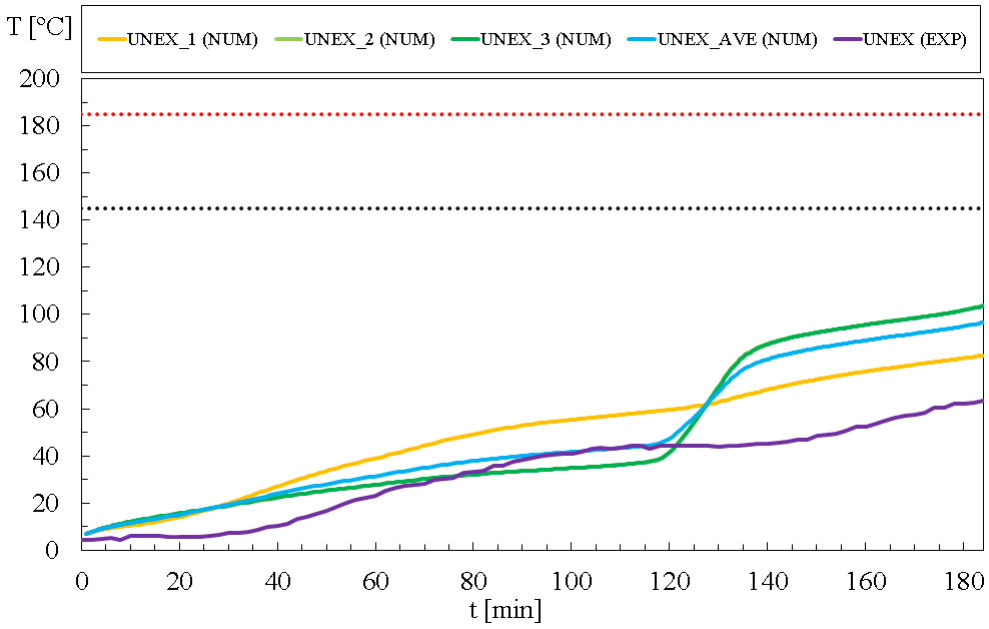

Figure 4.30: Maximum and Minimum Temperatures in the "S9" UNEX - Method 1.

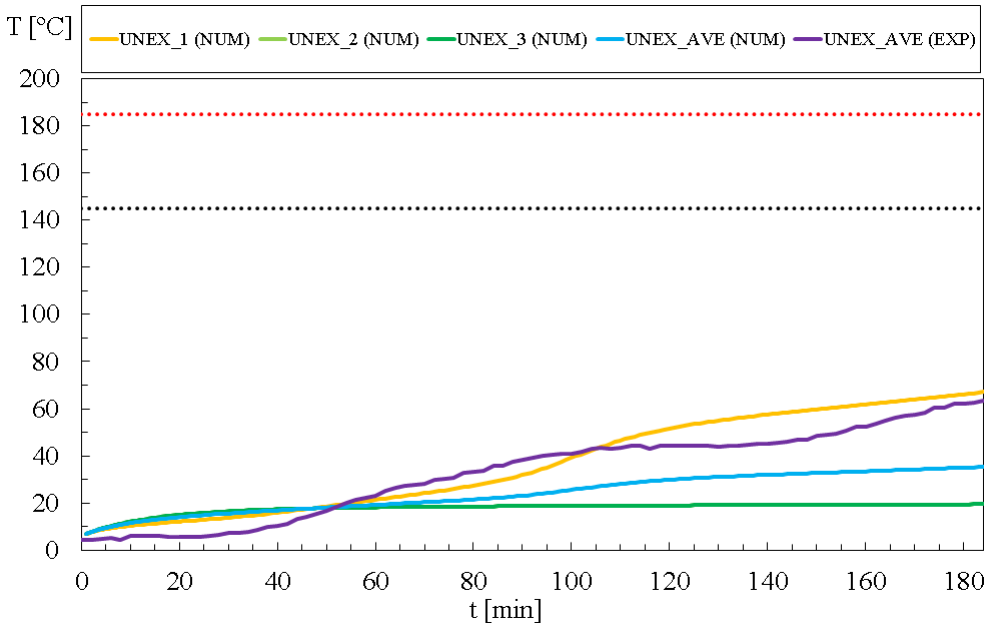

Figure 4.31: Maximum and Minimum Temperatures in the "S9" UNEX - Method 2.

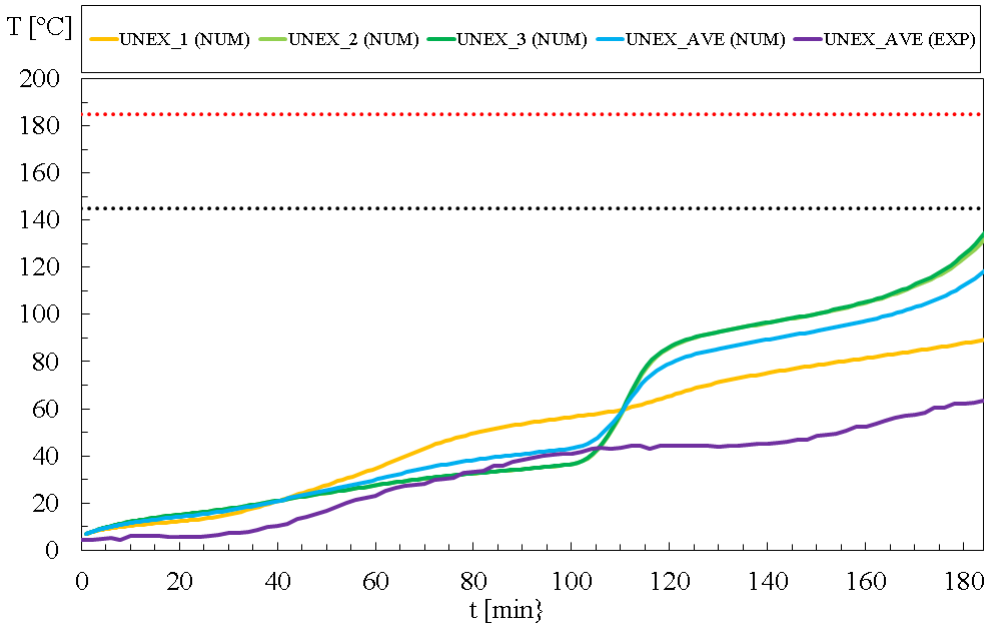

Figure 4.32: Maximum and Minimum Temperatures in the "S9" UNEX - Method 3.

hybrid method is also more suitable for structural resistance (R) analyses of LSF walls, as it yields better results for temperatures recorded in the studs (HF, WEB, and CF), which are crucial for verifying buckling effects along the steel profile [6], [7].

In this study, mesh convergence analyses were not conducted to ensure that the obtained results were not influenced by the mathematical model. Consequently, temperature values could have been closer to the obtained results. Furthermore, it is essential to highlight that the differences in RMSE results were more pronounced in the regions of plasterboards facing the cavity or between the plasterboards themselves. These differences in RMSE results can be explained by the singularities in the behaviour of materials during experiments, as well as in numerical simulations, where perfect contact between materials is assumed.

Given the good agreement between experimental and numerical results, the developed FEM was extended to study the fire performance of LSF wall panels under different configurations and materials.

Chapter 5

Parametric Analysis

After the model development, a series of parametric analyses were conducted to identify the effects of plasterboard thickness and type, as well as rockwool density, on the fire behaviour of standard fire curve and hydrocarbon fire of the Light Steel Frame walls studied. In total, 80 parametric analyses were performed, with 20 for each of the four specimens ("S1", "S5", "S9", and "S13") studied in this dissertation. This chapter presents these studies, their conclusions, and proposes simplified calculation methods to allow a practical assessment of the fire resistance of the walls.

To analyse the influence of plasterboards, simulations were carried out by altering the thickness of the plasterboards from 12mm to 16mm and changing from gypsum Type 1 to gypsum Type 2, following the thermal properties established in the study conducted by Sultan (1996) [15]. For the analysis of the influence of rockwool insulation density, several densities of 30, 90, 150, and 175 kg/m^3 were considered, in addition to the density of 60 kg/m^3 used in previous studies. The choice of plasterboard thickness and type, as well as rockwool densities, was made according to the most common parameters in the Portuguese market.

Table 5.1 displays all possible configurations of the specimens to be examined in the study.

For standardisation, the initial temperature adopted for the analyses was 20^{o}C, while the rest of the boundary conditions remained the same, such as convection and radiation,

Table 5.1: Configurations used in the parametric analysis of Specimens "S1", "S5", "S9", and "S13".

Case	Gypsum Thickness [mm]	Gypsum Type	Rockwool Density [kg/m^3]
1	12	1	30
2	12	1	60
3	12	1	90
4	12	1	150
5	12	1	175
6	12	2	30
7	12	2	60
8	12	2	90
9	12	2	150
10	12	2	175
11	16	1	30
12	16	1	60
13	16	1	90
14	16	1	150
15	16	1	175
16	16	2	30
17	16	2	60
18	16	2	90
19	16	2	150
20	16	2	175

Table 5.2: Fire resistance time from the parametric study for Specimen "S1".

Case	Gypsum Thickness [mm]	Gypsum Type [mm]	Rockwool Density [kg/m^3]	Tmax [min]	Tave [min]	Tfi [min]
1	12	1	30	178.33	181.54	178.33
2	12	1	60	217.89	242.31	217.89
3	12	1	90	240.78	282.36	240.78
4	12	1	150	266.69	319.35	266.69
5	12	1	175	275.8	331.06	275.8
6	12	2	30	149.08	151.39	149.08
7	12	2	60	187.78	210.41	187.78
8	12	2	90	212.73	249.69	212.73
9	12	2	150	243.96	291.3	243.96
10	12	2	175	255.32	305.25	255.32
11	16	1	30	247.53	250.25	247.53
12	16	1	60	307.56	329.36	307.56
13	16	1	90	337.17	369.72	337.17
14	16	1	150	369.34	410.63	369.34
15	16	1	175	379.91	423.15	379.91
16	16	2	30	212.38	209.49	209.49
17	16	2	60	265.21	277.98	265.21
18	16	2	90	301.35	325.75	301.35
19	16	2	150	335.82	368.24	335.82
20	16	2	175	349.05	383.62	349.05

according to the fire events under study (standard fire or hydrocarbon fire). The solution method (non-linear transient), convergence tolerance (heat flow), and time increment were the same as those adopted during Chapter 4, except for the final time that needed to be modified to find the isulation resistance time (I) for each alteration.

The results obtained for the analyses of each Specimen are presented in the following Tables 5.2, 5.3, 5.4 and 5.5:

The graphs displaying the temperature curves of the analysed walls are provided in more detail in Appendix B.

Table 5.3: Fire resistance time from the parametric study for Specimen "S5".

Case	Gypsum Thickness [mm]	Gypsum Type [mm]	Rockwool Density [kg/m^3]	Tmax [min]	Tave [min]	Tfi [min]
1	12	1	30	78.32	77.82	77.82
2	12	1	60	83.02	82.49	82.49
3	12	1	90	88.71	88.13	88.13
4	12	1	150	98.47	98.52	98.47
5	12	1	175	102.3	102.58	102.3
6	12	2	30	71.76	70.93	70.93
7	12	2	60	79.45	79.19	79.19
8	12	2	90	85.43	87.49	85.43
9	12	2	150	98.16	102.75	98.16
10	12	2	175	103.64	108.99	103.64
11	16	1	30	125.28	124.02	124.02
12	16	1	60	132.5	131.01	131.01
13	16	1	90	138.97	137.56	137.56
14	16	1	150	152.71	151.56	151.56
15	16	1	175	157.68	156.77	156.77
16	16	2	30	117.68	114.42	114.42
17	16	2	60	126.32	124.8	124.8
18	16	2	90	134.49	136.01	134.49
19	16	2	150	152.21	156.58	152.21
20	16	2	175	159.54	165.07	159.54

Table 5.4: Fire resistance time from the parametric study for Specimen "S9".

Case	Gypsum Thickness [mm]	Gypsum Type [mm]	Rockwool Density [kg/m^3]	Tmax [min]	Tave [min]	Tfi [min]
1	12	1	30	160.83	160.74	160.74
2	12	1	60	188.3	188.48	188.3
3	12	1	90	202.9	203.02	202.9
4	12	1	150	211.48	211.54	211.48
5	12	1	175	213.57	213.71	213.57
6	12	2	30	133.2	134.07	133.2
7	12	2	60	157.77	158.25	157.77
8	12	2	90	171.81	171.6	171.6
9	12	2	150	182.1	181.68	181.68
10	12	2	175	184.83	184.25	184.25
11	16	1	30	220.02	220.17	220.02
12	16	1	60	250.12	250.37	250.12
13	16	1	90	265.9	265.91	265.9
14	16	1	150	276	275.89	275.89
15	16	1	175	278.09	278.09	278.09
16	16	2	30	191.88	192.6	191.88
17	16	2	60	220.51	220.44	220.44
18	16	2	90	236.07	234.98	234.98
19	16	2	150	247.46	245.83	245.83
20	16	2	175	250.64	249.1	249.1

Table 5.5: Fire resistance time from the parametric study for Specimen "S13".

Case	Gypsum Thickness [mm]	Gypsum Type [mm]	Rockwool Density [kg/m^3]	Tmax [min]	Tave [min]	Tfi [min]
1	12	1	30	108.24	108.75	108.24
2	12	1	60	136.38	136.83	136.38
3	12	1	90	151.52	151.67	151.52
4	12	1	150	160.99	161.03	160.99
5	12	1	175	163.41	163.48	163.41
6	12	2	30	93.1	93.98	93.1
7	12	2	60	115.35	115.93	115.35
8	12	2	90	128.3	128.6	128.3
9	12	2	150	138.3	138.16	138.16
10	12	2	175	140.6	140.44	140.44
11	16	1	30	170.42	170.61	170.42
12	16	1	60	206.08	206.16	206.08
13	16	1	90	224.63	224.43	224.43
14	16	1	150	236.54	235.92	235.92
15	16	1	175	239.32	238.81	238.81
16	16	2	30	148.33	149.08	148.33
17	16	2	60	178.54	178.37	178.37
18	16	2	90	196.95	195.08	195.08
19	16	2	150	210.3	207.89	207.89
20	16	2	175	214.22	211.52	211.52

5.1 Parametric Analysis of Gypsum Thickness and Type

The comparison between the results obtained for the change in thickness of the sheathing panels for LSF walls with cavity insulation is represented in the graph in Fig. 5.1.

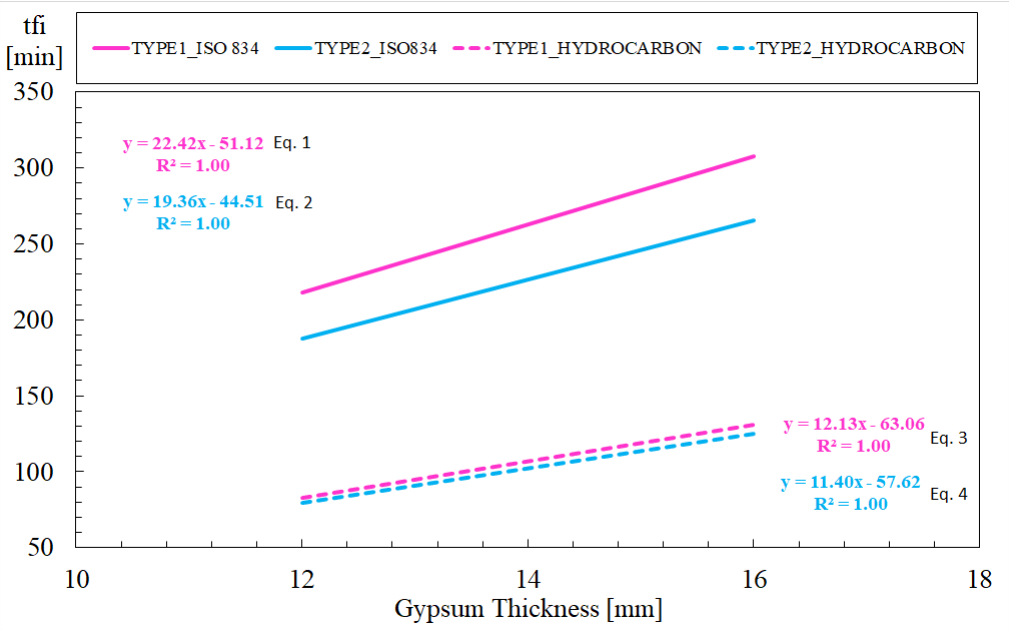

Figure 5.1: Comparison of results for Gypsum 1 and Gypsum 2 with 12mm and 16mm - Cavity Insulated Wall.

Analysing the results obtained, it is possible to observe similar rates of growth in the fire resistance time for the use of Gypsum Type 1 and Type 2 boards. The same trend can be observed for standard fire and hydrocarbon fire conditions. Thus, it is concluded that, for the LSF wall with rockwool insulation in the cavity, the fire resistance time increases by approximately 21 minutes and 12 minutes for every 1 mm increase in the thickness of the plasterboards for standard fire and hydrocarbon fire conditions, respectively. These proportions are valid for both types of gypsum analysed.

For walls with rockwool insulation between the two plasterboards, the comparison of the results is shown in the Fig. 5.2.

Similarly to the case of walls with the first geometry, the growth rates in fire resistance

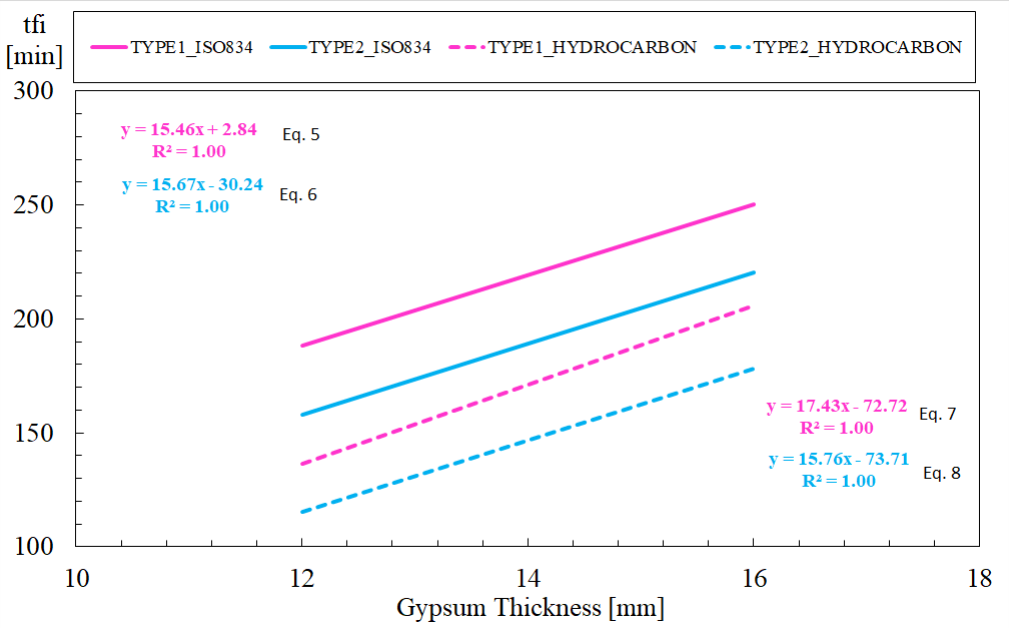

Figure 5.2: Comparison of results for Gypsum 1 and Gypsum 2 with 12mm and 16mm - External Insulated Wall.

time were similar for the use of different plasterboards under different fire conditions. For the LSF wall with rockwool insulation between the plasterboards, the fire resistance time increases by approximately 16 minutes and 17 minutes for every 1 mm increase in the thickness of the plasterboards for standard fire and hydrocarbon fire conditions, respectively. These proportions are valid for both types of gypsum analysed.

5.2 Parametric Analysis of Rockwool Density

The comparison between the results obtained for LSF walls with cavity insulation using different densities of rockwool insulation is shown in Fig. 5.3.

Given the obtained results, the rates of growth in fire resistance time for LSF walls with rockwool insulation in the cavity increase by approximately 7 minutes and 2 minutes for every 10 kg/m^3 of rockwool insulation density for standard fire and hydrocarbon fire conditions, respectively. The calculated proportions are valid for the two types of gypsum analysed.

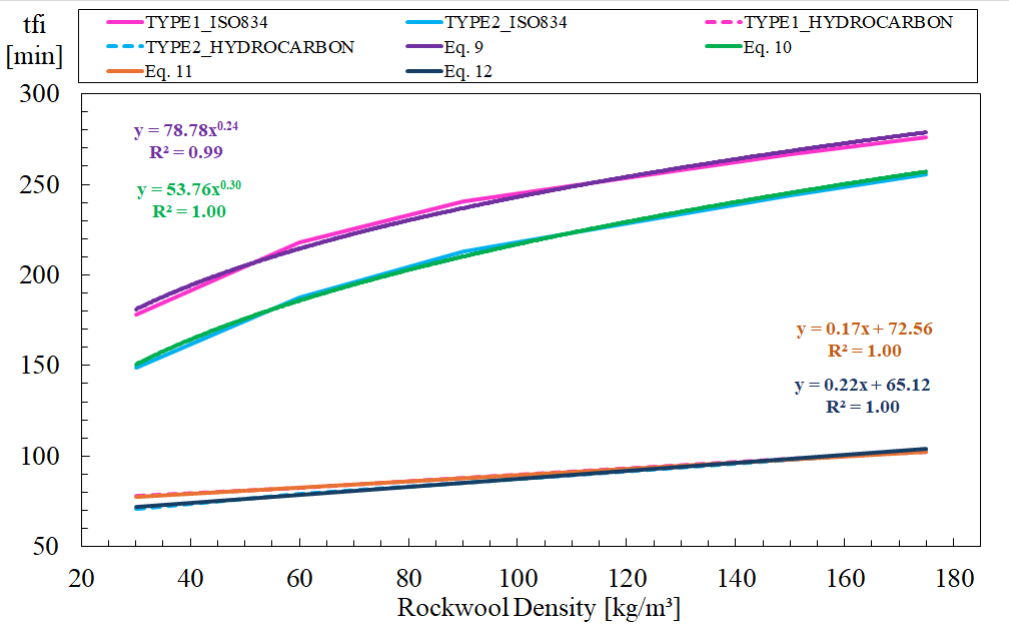

Figure 5.3: Comparison of results for Gypsum 1 and Gypsum 2 with different insulation densities - Cavity Insulated Wall.

As for the second geometry of walls where the rockwool insulation is located between the two gypsum boards, the comparison of results is shown in Fig. 5.4.

For this case, the rates of fire resistance time growth were similar for the use of different plasterboards subjected to different fire conditions. The results indicated an increase of approximately 9 minutes for every 10 kg/m^3 of insulation density for both standard fire and hydrocarbon fire conditions.

5.3 Conclusions

Analysing the growth rates obtained for the fire resistance time when altering the materials of LSF walls, it can be concluded that increasing the thickness of the cladding has a greater impact than choosing higher-density rockwool insulation. Furthermore, the results showed that walls subjected to the standard fire curve have a more pronounced impact than those subjected to hydrocarbon fire. The proportions obtained for material alterations under hydrocarbon fire analysis were nearly the same, while for alterations under standard fire

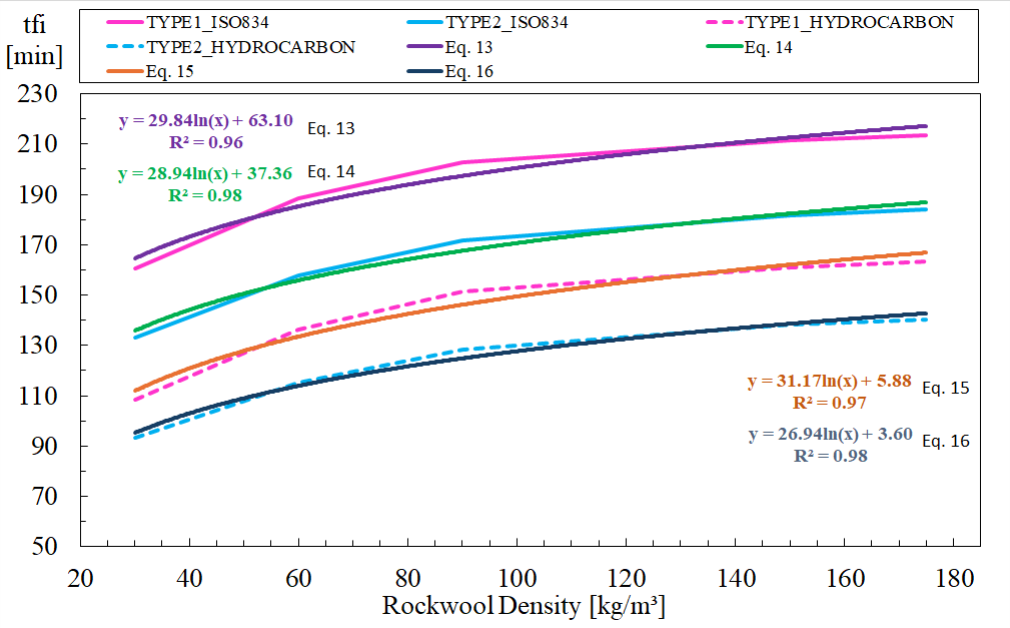

Figure 5.4: Comparison of results for Gypsum 1 and Gypsum 2 with different insulation densities - External Insulated Wall.

analysis, they varied significantly according to the modifications made. Additionally, in all simulations conducted, Gypsum Type 1 exhibited better fire performance than Gypsum Type 2.

Based on these findings, a new proposal is presented to determine the fire resistance insulation as a function of cladding thickness, rockwool density, wall geometry, and fire condition. The proposed equations are valid only for the materials and wall configurations used.

The regression coefficients R2 determine the accuracy of the result approximations, with 1.00 considered as the closest to reality.

Table 5.6: Proposal for Light Steel Frame Cavity Insulated Walls.

Equation	Parameter Range	Analysis	Gypsum Type	Fire
y = 22.42x - 51.12 R^2 = 1.00	12 ≤ x ≤ 16	Gypsum Thickness	1	ISO 834
y = 19.36x - 44.51 R^2 = 1.00	12 ≤ x ≤ 16	Gypsum Thickness	2	ISO 834
y = 12.13x - 63.06 R^2 = 1.00	12 ≤ x ≤ 16	Gypsum Thickness	1	Hydrocarbon
y = 11.40x - 57.62 R^2 = 1.00	12 ≤ x ≤ 16	Gypsum Thickness	2	Hydrocarbon
$y = 78.78x^{0.24}$ R^2 = 0.99	30 ≤ x ≤ 175	Rockwool Density	1	ISO 834
$y = 53.76x^{0.30}$ R^2 = 1.00	30 ≤ x ≤ 175	Rockwool Density	2	ISO 834
y = 0.17x + 72.56 R^2 = 1.00	30 ≤ x ≤ 175	Rockwool Density	1	Hydrocarbon
y = 0.22x + 65.12 R^2 = 1.00	30 ≤ x ≤ 175	Rockwool Density	2	Hydrocarbon

Table 5.7: Proposal for Light Steel Frame External Insulated Walls.

Equation	Parameter Range	Analysis	Gypsum Type	Fire
y = 15.46x + 2.84 R^2 = 1.00	12 ≤ x ≤ 16	Gypsum Thickness	1	ISO 834
y = 15.67x - 30.26 R^2 = 1.00	12 ≤ x ≤ 16	Gypsum Thickness	2	ISO 834
y = 17.43x - 72.73 R^2 = 1.00	12 ≤ x ≤ 16	Gypsum Thickness	1	Hydrocarbon
y = 15.76x - 73.72 R^2 = 1.00	12 ≤ x ≤ 16	Gypsum Thickness	2	Hydrocarbon
y = 29.84ln(x) + 63.10 R^2 = = 0.96	30 ≤ x ≤ 175	Rockwool Density	1	ISO 834
y = 028.94ln(x) + 37.36 R^2 = 0.98	30 ≤ x ≤ 175	Rockwool Density	2	ISO 834
y = 31.17ln(x) + 5.88 R^2 = 0.97	30 ≤ x ≤ 175	Rockwool Density	1	Hydrocarbon
y = 26.94ln(x) + 3.60 R^2 = 0.98	30 ≤ x ≤ 175	Rockwool Density	2	Hydrocarbon

Chapter 6

Conclusions and Future Work

6.1 Conclusions

This dissertation investigated the fire performance of non-load bearing walls constructed using the Light Steel Frame (LSF) methodology. The analysis covered ISO 834 and hydrocarbon fire conditions, employing three numerical modelling methods to calculate the fire resistance of LSF walls without insulation in the cavity. The hybrid method (solution 1) proved to be more effective in simulating fire-related phenomena, providing a better approximation to experimental results, both in terms of thermal insulation and structural resistance.

For walls with insulation in the cavity, adjustments to the thermal properties of gypsum boards and rockwool were necessary to approximate the experimental results. However, it was observed that the results for the unexposed surface to fire were satisfactory, while other layers showed RMSE exceeding 100ºC. This discrepancy could be attributed to singularities in the behaviour of materials during experiments and simulations.

Parametric analyses revealed that an increase in the thickness of the cladding boards has a more significant influence on fire resistance than the choice of the density of rockwool insulation. Additionally, simulations indicated that walls exposed to the standard fire curve show more pronounced variations in resistance than those exposed to hydrocarbon

fire when wall materials are modified. It is noteworthy that Gypsum Type 1 consistently demonstrated better fire performance than Gypsum Type 2 in all evaluated conditions.

These conclusions offer valuable insights into understanding the fire behaviour of LSF walls, contributing to advancing the understanding of this construction system. Suggestions for future research may include exploring additional variables and improving models for a better representation of experimental conditions.

6.2 Future Work

Evaluate the accuracy of the results when using the "birth and death" command in the numerical model to simulate the dropping of cladding panels and the melting of insulation.

In addition to the LINK31, SURF151, and SURF152 elements, the ANSYS software suggests the Radiosity Solver and AUX12 Radiation Matrix methods for radiation analysis. It is recommended to use these methods in simulations of radiation heat transfer in the cavity region without insulation in Light Steel Frame (LSF) walls.

Utilise the hybrid method, which incorporates temperatures from the cavity region obtained from experimental tests, to develop numerical models applicable to load bearing walls.

Bibliography

[1] T. Suntharalingam, I. Upasiri, P. Gatheeshgar, *et al.*, "Fire resistance of 3d printed concrete composite wall panels exposed to various fire scenarios," *Journal of Structural Fire Engineering*, vol. 12, pp. 377–409, 3 2021.

[2] M. Gravit and E. Golub, "The fire resistant ceiling construction in a hydrocarbon fire," *MATEC Web Conf.*, vol. 245, 2018.

[3] V. Kodur, "Role of fire resistance issues in the collapse of the twin towers," vol. 8, 2003, p. 10.

[4] P. V. Real, *Incêndio em Estruturas Metálicas: cálculo estrutural*. Editora Orion, 2003.

[5] S. Kesawan and M. Mahendran, "Fire tests of load-bearing lsf walls made of hollow flange channel sections," *Journal of Constructional Steel Research*, vol. 115, pp. 191–205, 2015.

[6] W. Chen, J. Jiang, J. Ye, Q. Zhao, K. Liu, and C. Xu, "Thermal behavior of external-insulated cold-formed steel non-load-bearing walls exposed to different fire conditions," *Structures*, vol. 25, pp. 631–645, 2020.

[7] S. Kesawan and M. Mahendran, "A review of parameters influencing the fire performance of light gauge steel frame walls," *Fire Technology*, vol. 54, pp. 3–35, 1 2018.

[8] K. V.K.R. and S. M.A, "Factors influencing fire resistance of load-bearing steel stud walls.," *Fire Technol 42, 5–26 (2006).*, 2005.

[9] P. Kolarkar and M. Mahendran, "Experimental studies of non-load bearing steel wall systems under fire conditions," *Fire Safety Journal*, vol. 53, pp. 85–104, Oct. 2012.

[10] H. Magarabooshanam, A. Ariyanayagam, and M. Mahendran, "Fire resistance of non-load bearing lsf walls with varying cavity depth," *Thin-Walled Structures*, vol. 150, p. 106 675, 2020.

[11] S. Gnanachelvam, A. Ariyanayagam, and M. Mahendran, "Effects of insulation materials and their location on the fire resistance of lsf walls," *Journal of Building Engineering*, vol. 44, p. 103 323, 2021.

[12] S. Gunalan, P. Kolarkar, and M. Mahendran, "Experimental study of load bearing cold-formed steel wall systems under fire conditions," *Thin-Walled Structures*, vol. 65, pp. 72–92, 2013.

[13] S. Gunalan and M. Mahendran, "Finite element modelling of load bearing cold-formed steel wall systems under fire conditions," *Engineering Structures*, vol. 56, pp. 1007–1027, 2013.

[14] S. Gunalan and M. Mahendran, "Development of a simplified design method to predict the fire rating of lsf walls," in *Research and Applications in Structural Engineering, Mechanics and Computation: Proceedings of the Fifth International Conference on Structural Engineering, Mechanics and Computation (SEMC 2013)*, A. Zingoni, Ed., Netherlands: CRC Press/Balkema, 2013, pp. 2009–2014.

[15] M. A. Sultan and M. A. Sultan, "A model for predicting heat transfer through noninsulated unloaded steel-stud gypsum board wall assemblies exposed to fire," *Fire Technology*, 1996.

[16] J. T. Gerlich, P. C. R. Collier, and A. H. Buchanan, "Design of light steel-framed walls for fire resistance," *Fire and Materials*, vol. 20, no. 2, pp. 79–96, 1996.

[17] P. Keerthan and M. Mahendran, "Numerical modelling of non-load-bearing light gauge cold-formed steel frame walls under fire conditions," *Journal of Fire Sciences*, vol. 30, no. 5, pp. 375–403, 2012.

[18] A. D. Ariyanayagam, "Fire performance and design of light gauge steel frame wall systems exposed to realistic design fires," Ph.D. dissertation, Queensland University of Technology, 2013.

[19] E. C. for Standardization, *En 1991-1-2:2002 - eurocode 1: Actions on structures part 1-2: General actions-actions on structures exposed to fire*, 2002.

[20] C. Barnett, "Bfd curve: A new empirical model for fire compartment temperatures," *Fire Safety Journal*, vol. 37, no. 5, pp. 437–463, 2002.

[21] W. Chen, J. Ye, and Q. Zhao, "Thermal performance of non-load-bearing cold-formed steel walls under different design fire conditions," *Thin-Walled Structures*, vol. 143, p. 106 242, 2019.

[22] W. Chen, J. Ye, Q. Zhao, and J. Jiang, "Full-scale experiments of gypsum-sheathed cavity-insulated cold-formed steel walls under different fire conditions," *Journal of Constructional Steel Research*, vol. 164, p. 105 809, 2020.

[23] I. Upasiri, K. Konthesigha, S. Nanayakkara, K. Poologanathan, P. Gatheeshgar, and D. Perera, "Fire performance of lightweight concrete-filled lsf wall panels," *Structures*, vol. 40, pp. 1039–1055, 2022.

[24] P. Piloto, M. S. Khetata, and A. B. Ramos Gavilán, "Fire performance of non-loadbearing light steel framing walls - numerical simulation," 2017.

[25] M. S. Khetata, L. Fernandes, C. Marinho, P. A. G. Piloto, A. B. R. Gavilán, and H. Razuk, "Fire resistance of non-loadbearing light steel framing walls: Numerical validation," 2017, pp. 853–862.

[26] P. Piloto, M. S. Khetata, and A. B. Ramos Gavilán, "Fire performance of non-loadbearing light steel framing walls - numerical and simple calculation methods," 2017.

[27] P. Piloto, "Fire resistance of cold-formed steel walls with composite panels: Results from insulation rating (i) and loadbearing prediction rating (r)," 2018.

[28] P. A. G. Piloto, M. S. Khetata, and A. B. R. Gavilán, "Loadbearing capacity of lsf walls under fire exposure," *MATTER: International Journal of Science and Technology*, vol. 4, no. 3, pp. 104–124, Nov. 2018.

[29] S. M. Khetata, P. A. Piloto, and A. B. Gavilán, "Fire resistance of composite non-load bearing light steel framing walls," *Journal of Fire Sciences*, vol. 38, no. 2, pp. 136–155, 2020.

[30] M. Alves, G. Constantini, A. Ianni, E. F. A. Kimura, A. Meda, and P. Piloto, "Fire performance of non-load-bearing double-stud light steel frame walls: Experimental tests, numerical simulation, and simplified method," *Fire and Materials*, vol. 46, no. 1, pp. 227–250, 2022.

[31] P. A. Piloto, M. S. Khetata, and A. B. Ramos-Gavilán, "Analysis of the critical temperature on load bearing lsf walls under fire," *Engineering Structures*, vol. 270, p. 114 858, 2022.

[32] L. Torres, C. Couto, P. Vila Real, and P. Piloto, "Numerical study of the fire behaviour of external walls in light steel framing," *Fire Safety Journal*, vol. 141, p. 103 946, 2023.

[33] P. A. Piloto, S. Gomes, L. Torres, C. Couto, and P. Vila Real, "Accuracy of 2d numerical models towards the prediction of the fire resistance on lsf partition walls," *International Journal of Thermal Sciences*, vol. 193, p. 108 511, 2023.

[34] C. Costa and V. Silva, *Estruturas de concreto armado em situação de incêndio*. University of São Paulo, Jan. 2002.

[35] V. Silva and P. Pimenta, "Estruturas de aço em situação de incêndio.," Feb. 2016.

[36] E. C. for Standardization, *En 1363-1:2020 - fire resistance tests part 1 : General requirements*, 2020.

[37] E. C. for Standardization, *En 1364-1:1999 - fire resistance tests for non-loadbearing elements - part 1: Walls*, 1999.

[38] E. C. for Standardization, *En 13501-2:2007+a1:2009 - fire classification of construction products and building elements - part 2: Classification using data from fire resistance tests, excluding ventilation services*, 2009.

[39] E. Madenci and I. Guven, *The finite element method and applications in engineering using ANSYS®*. Springer, 2015.

[40] A. Inc., "Ansys academic research mechanical," Help System, version 23.2.

[41] J. E. Mason, "Heat transfer programs for the design of structures exposed to fire," 2000.

[42] T. Stolarski, Y. Nakasone, and S. Yoshimoto, *Engineering analysis with ANSYS software*. Butterworth-Heinemann, 2018.

[43] E. C. for Standardization, *En 1993-1-2:2005 - eurocode 3: Design of steel structures part 1-2: General rules — structural fire design*, 2005.

[44] E. C. for Standardization, *Pren 1995-1-2:2023 - eurocode 5: Design of timber structures - part 1-2: Structural fire design*, 2023.

Appendix A

Material Properties

A.1 Carbon Steel Properties

A.1.1 Specific Heat [J/kgK]

For 20°C $\leq \theta_a \leq$ 600°C:

$$c_a = 425 + 7.73x10^{-1}\theta_a - 1.69x10^{-3}{\theta_a}^3 \tag{A.1}$$

For 600°C $\leq \theta_a \leq$ 735°C

$$c_a = 666 + \frac{13002}{738 - \theta_a} \tag{A.2}$$

For 735°C $\leq \theta_a \leq$ 900°C

$$c_a = 545 + \frac{17820}{\theta_a - 731} \tag{A.3}$$

For 900°C $\leq \theta_a \leq$ 1200°C

$$c_a = 650 \tag{A.4}$$

Where θ_a is the steel temperature [°C].

A.1.2 Thermal conductivity [W/mK]

For 20°C $\leq \theta_a \leq$ 800°C:

$$\lambda_a = 54 - 3.33x10^{-2}\theta_a \tag{A.5}$$

For 800°C $\leq \theta_a \leq$ 1200°C:

$$\lambda_a = 27.3 \tag{A.6}$$

A.2 Gypsum Plasterboards

A.2.1 Type 1

Thermal properties of gypsum plasterboards [44].

T [°C]	λ [W/mK]	c [kJ/kgK]	$\rho/\rho 20$ [-]
20	0,40	0,96	1,0
70	0,40	0,96	1,0
100	0,27	0,96	1,0
130	0,13	14,9	0,926
140	0,13	25,2	0,902
150	0,13	21,7	0,877
170	0,13	0,96	0,828
600	0,13	0,96	0,827
720	0,33	4,36	0,826
750	0,38	0,96	0,776
1000	0,80	0,96	0,776
1200	2,37	0,96	0,776

A.2.2 Type 2

Specific Heat

For 20°C $\leq$ T $\leq$ 78°C

$$c_g = 6.146T + 1.377 \tag{A.7}$$

For 78°C ≤ T ≤ 75°C

$$c_g = 150T - 9.858 \tag{A.8}$$

For 85°C ≤ T ≤ 97°C

$$c_g = 262T - 1.9501 \tag{A.9}$$

For 97°C ≤ T ≤ 124°C

$$c_g = 476T - 40311 \tag{A.10}$$

For 124°C ≤ T ≤ 139°C

$$c_g = 154.507 - 1.097T \tag{A.11}$$

For 139°C ≤ T ≤ 148°C

$$c_g = 16.601 - 105T \tag{A.12}$$

For 148°C ≤ T ≤ 373°C

$$c_g = 1.189 - 1.27T \tag{A.13}$$

For 373°C ≤ T ≤ 430°C

$$c_g = 714 \tag{A.14}$$

For 430°C ≤ T ≤ 571°C

$$c_g = 1.151 - 1014T \tag{A.15}$$

For 571°C $\leq$ T $\leq$ 609°C

$$c_g = 1877T - 501 \tag{A.16}$$

For 609°C $\leq$ T $\leq$ 662°C

$$c_g = 44.2T - 26300 \tag{A.17}$$

For 662°C $\leq$ T $\leq$ 670°C

$$c_g = 3000 \tag{A.18}$$

For 670°C $\leq$ T $\leq$ 685°C

$$c_g = 103.570 - 150T \tag{A.19}$$

For T $\geq$ 685°C

$$c_g = 571 \tag{A.20}$$

Thermal Conductivity

For 20°C $\leq$ T $\leq$ 100°C

$$k_g = 0.25 \tag{A.21}$$

For 100°C $\leq$ T $\leq$ 400°C

$$k_g = 0.12 \tag{A.22}$$

For 400°C $\leq$ T $\leq$ 800°C

$$k_g = 0.00035t - 0.01 \tag{A.23}$$

For T $\geq$ 800°C

$$k_g = 0.0013t - 0.77 \tag{A.24}$$

Density

For 20°C $\leq$ T $\leq$ 80°C

$$\rho_g = 698 \tag{A.25}$$

For T $\geq$ 80°C

$$\rho_g = 576 \tag{A.26}$$

A.3 Mineral Wool (Rockwool)

Thermal properties of mineral wool insulation [44].

T [°C]	λ [W/mK]	c [kJ/kgK]	$\rho/\rho 20$ [-]
20	0,036	0,880	1,00
100	0,047	1,040	1,00
200	*	1,160	0,980
400	0,05	$0.09\times(11\times\ e^{-0.05\times\rho 20}+1.9)$	0,977
600	0,05	$0.15\times(11\times\ e^{-0.05\times\rho 20}+1.9)$	0,973
800	0,05	$0.23\times(11\times\ e^{-0.05\times\rho 20}+1.9)$	0,970
925	0,05	$0.30\times(11\times\ e^{-0.05\times\rho 20}+1.9)$	0,960
1200	0,05	$0.45\times(11\times\ e^{-0.05\times\rho 20}+1.9)$	0,887

* Linear interpolation may apply.

Appendix B

Technical Files

Specimen “S1” : Case 1.

STRUCTURE:
Studs: C140 (140x50x13x1.2mm)
Track: U142 (142x50x1.2 mm)
CFS wall: 1200x1200 mm
Gypsum: Type 1 (12 mm)
Rock wool: 30 kg/m^3

FIRE: Hydrocarbon
Tfi (Tmax) = 178.33 min
Tfi (Tave) = 181.54 min

Temperature x Time:

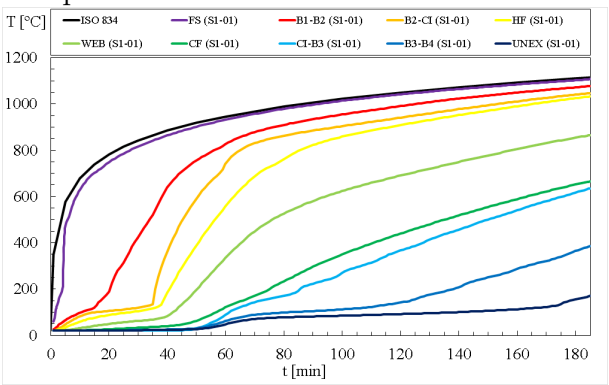

LSF Wall Configuration:

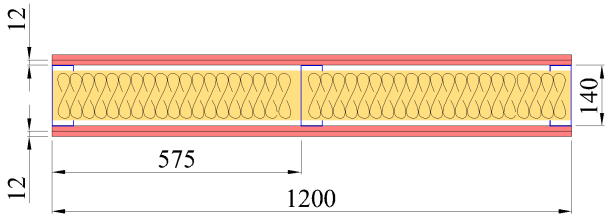

Mesh Complete Wall:

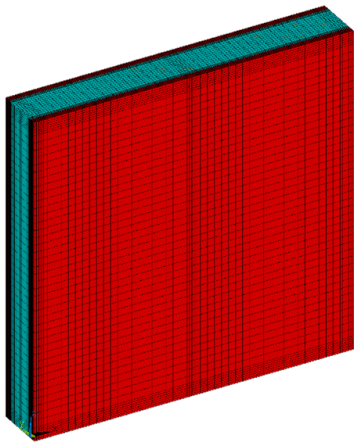

Temperature at t=3600s:

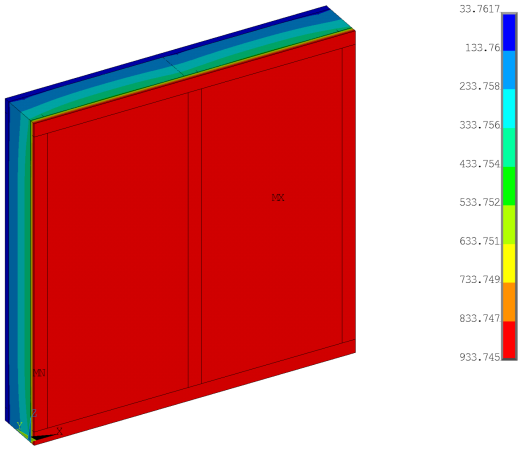

Mesh Half Wall:

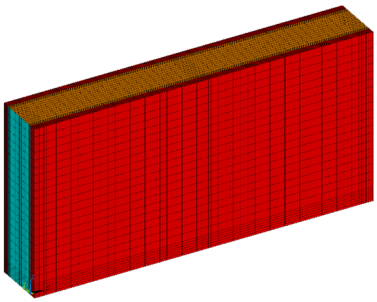

Temperature at t=3600s:

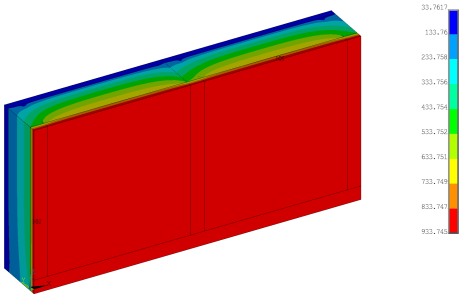

Specimen “S1” : Case 2.

STRUCTURE:
Studs: C140 (140x50x13x1.2mm)
Track: U142 (142x50x1.2 mm)
CFS wall: 1200x1200 mm
Gypsum: Type 1 (12 mm)
Rock wool: 60 kg/m^3

FIRE: Hydrocarbon
Tfi (Tmax) = 217.89 min
Tfi (Tave) = 242.31 min

Temperature x Time:

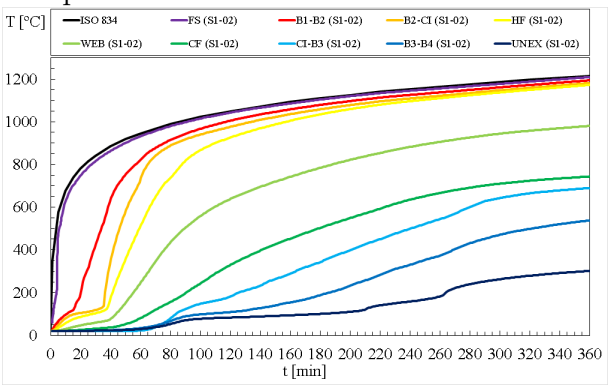

LSF Wall Configuration:

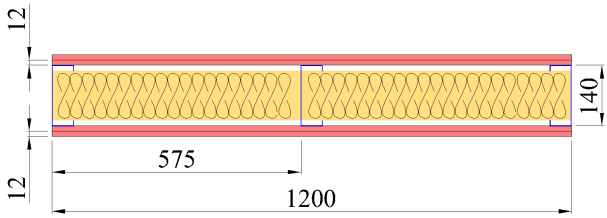

Mesh Complete Wall:

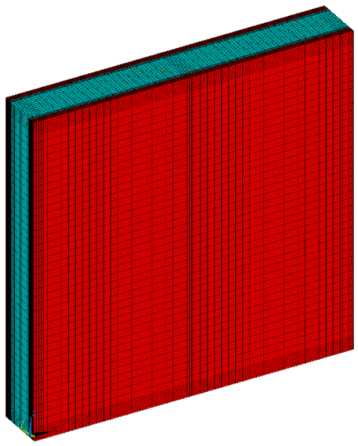

Temperature at t=3600s:

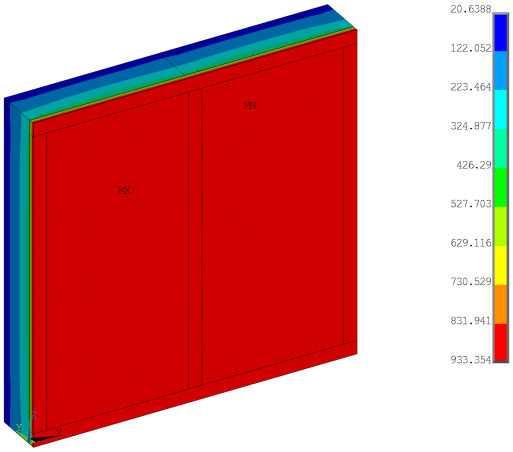

Mesh Half Wall:

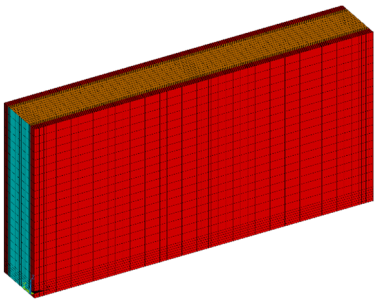

Temperature at t=3600s:

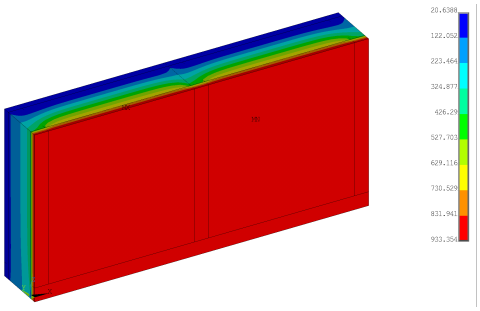

Specimen “S1” : Case 3.

STRUCTURE:
Studs: C140 (140x50x13x1.2mm)
Track: U142 (142x50x1.2 mm)
CFS wall: 1200x1200 mm
Gypsum: Type 1 (12 mm)
Rock wool: 90 kg/m^3

FIRE: Hydrocarbon
Tfi (Tmax) = 240.78 min
Tfi (Tave) = 282.36 min

Temperature x Time:

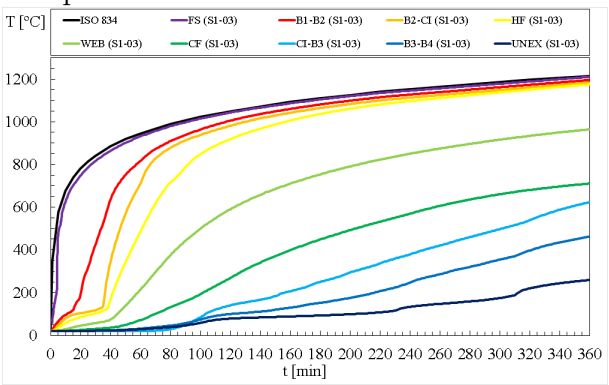

LSF Wall Configuration:

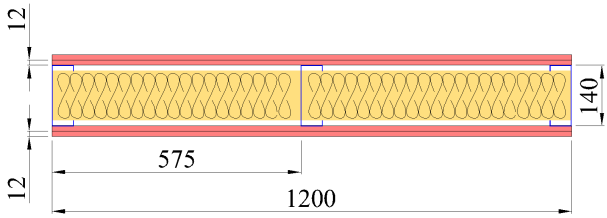

Mesh Complete Wall:

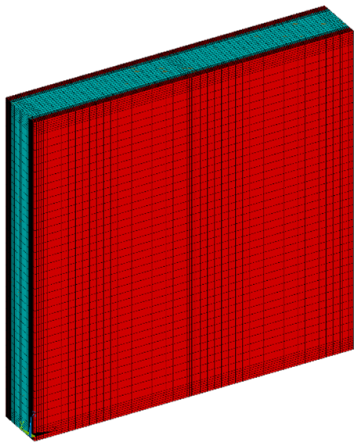

Temperature at t=3600s:

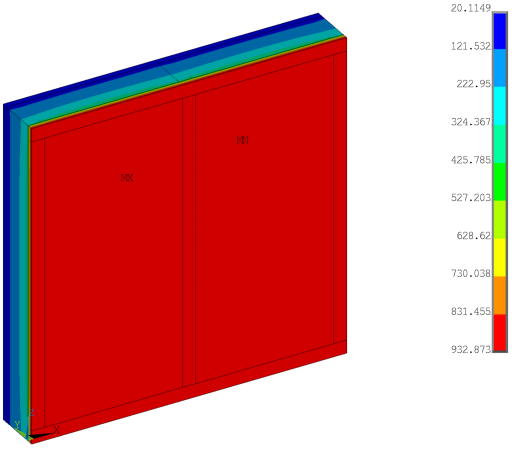

Mesh Half Wall:

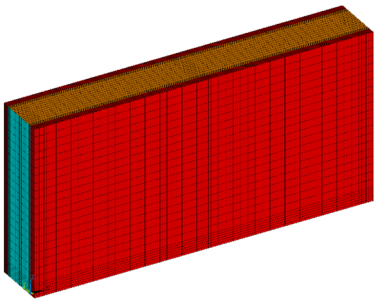

Temperature at t=3600s:

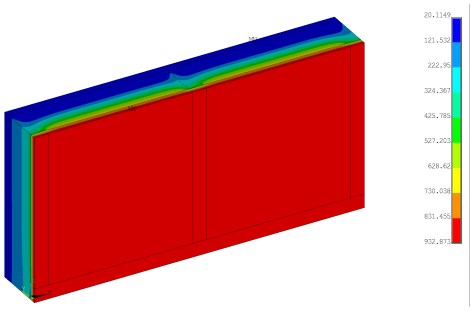

Specimen “S1” : Case 4.

STRUCTURE:
Studs: C140 (140x50x13x1.2mm)
Track: U142 (142x50x1.2 mm)
CFS wall: 1200x1200 mm
Gypsum: Type 1 (12 mm)
Rock wool: 150 kg/m^3

FIRE: Hydrocarbon
Tfi (Tmax) = 266.69 min
Tfi (Tave) = 319.35 min

Temperature x Time:

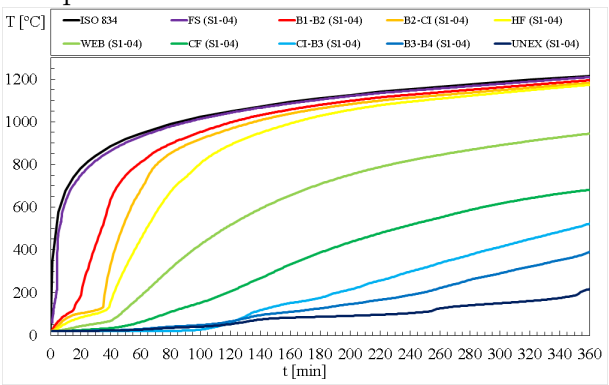

LSF Wall Configuration:

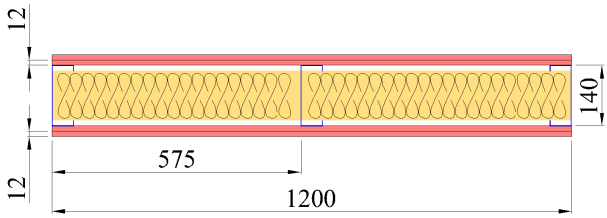

Mesh Complete Wall:

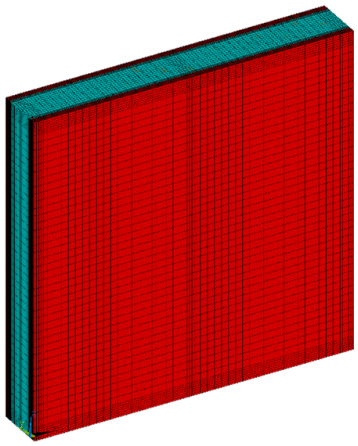

Temperature at t=3600s:

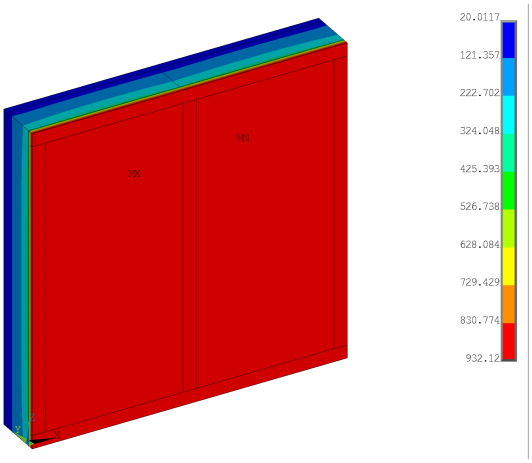

Mesh Half Wall:

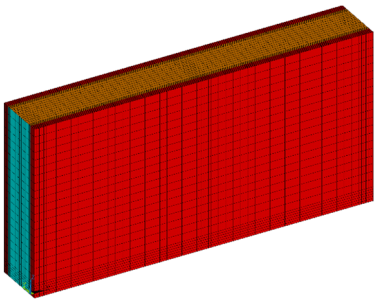

Temperature at t=3600s:

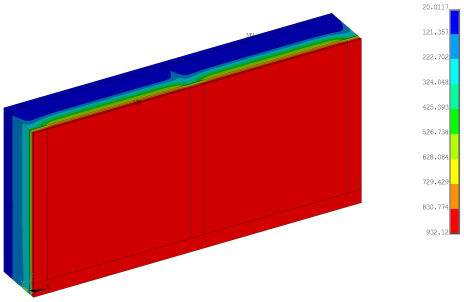

Specimen “S1” : Case 5.

STRUCTURE:
Studs: C140 (140x50x13x1.2mm)
Track: U142 (142x50x1.2 mm)
CFS wall: 1200x1200 mm
Gypsum: Type 1 (12 mm)
Rock wool: 175 kg/m^3

FIRE: Hydrocarbon
Tfi (Tmax) = 275.80 min
Tfi (Tave) = 331.06 min

Temperature x Time:

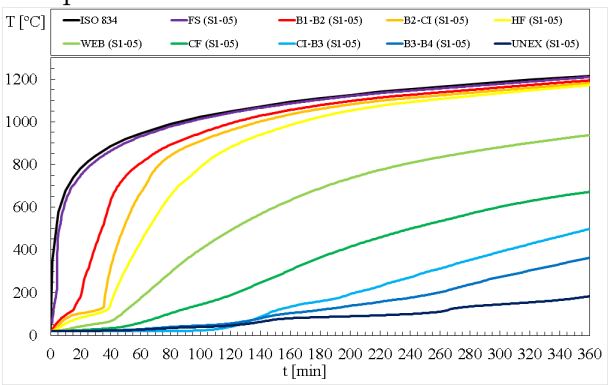

LSF Wall Configuration:

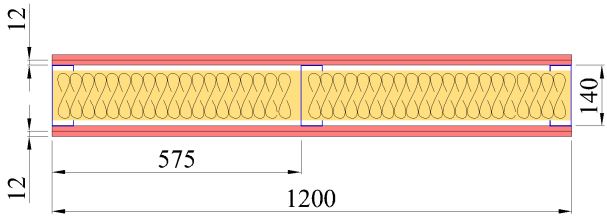

Mesh Complete Wall:

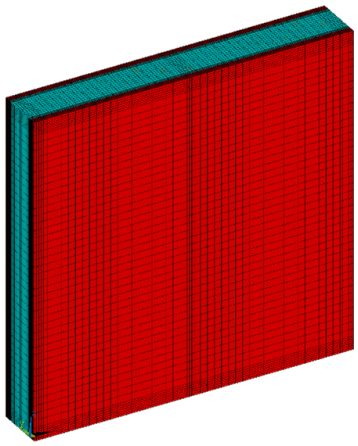

Temperature at t=3600s:

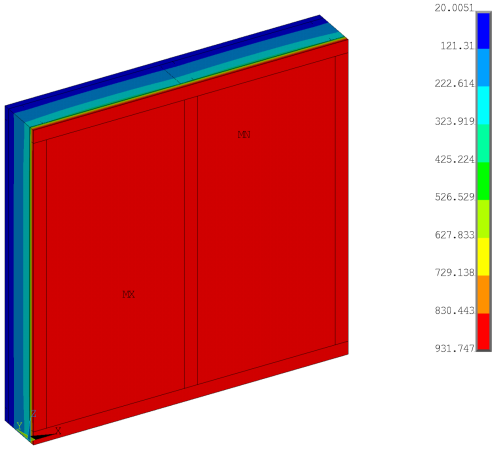

Mesh Half Wall:

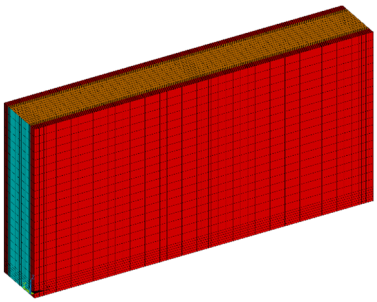

Temperature at t=3600s:

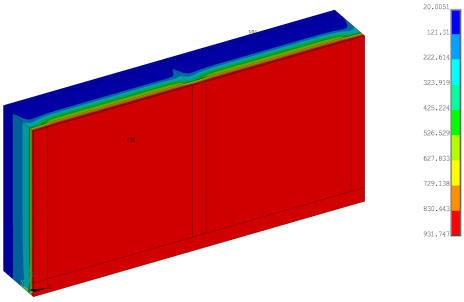

Specimen “S1” : Case 6.

STRUCTURE:
Studs: C140 (140x50x13x1.2mm)
Track: U142 (142x50x1.2 mm)
CFS wall: 1200x1200 mm
Gypsum: Type 2 (12 mm)
Rock wool: 30 kg/m^3

FIRE: Hydrocarbon
Tfi (Tmax) = 149.08 min
Tfi (Tave) = 151.39 min

Temperature x Time:

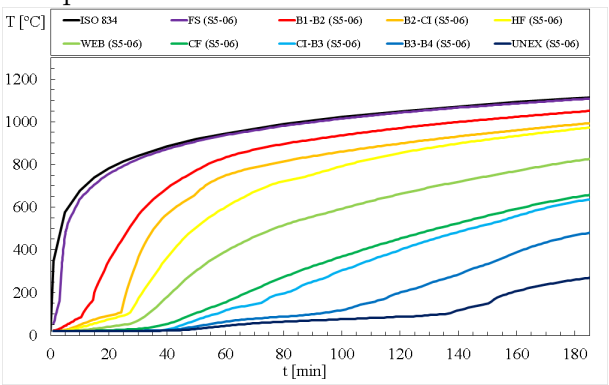

LSF Wall Configuration:

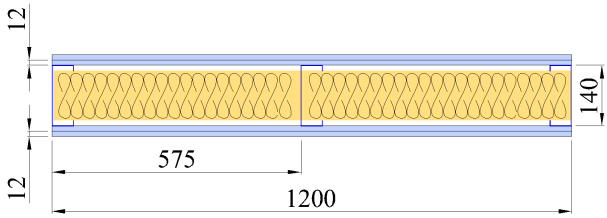

Mesh Complete Wall:

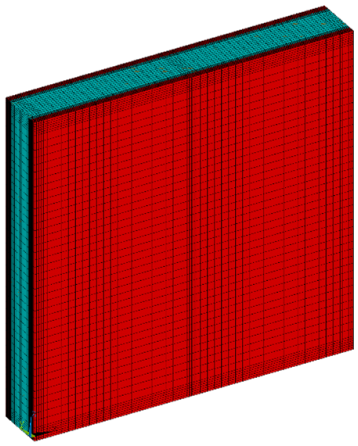

Temperature at t=3600s:

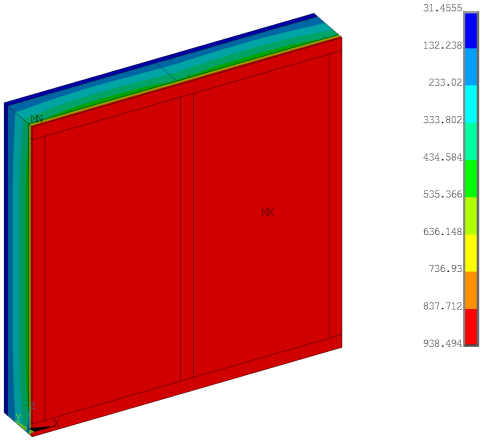

Mesh Half Wall:

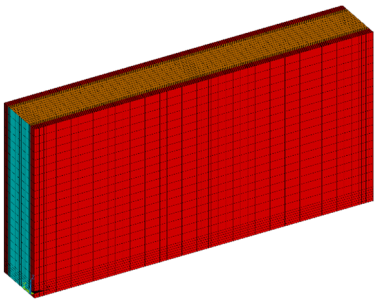

Temperature at t=3600s:

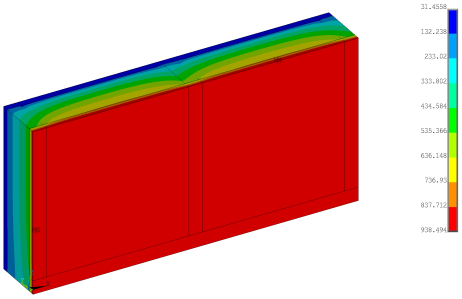

Specimen “S1” : Case 7.

STRUCTURE:
Studs: C140 (140x50x13x1.2mm)
Track: U142 (142x50x1.2 mm)
CFS wall: 1200x1200 mm
Gypsum: Type 2 (12 mm)
Rock wool: 60 kg/m^3

FIRE: Hydrocarbon
Tfi (Tmax) = 187.78 min
Tfi (Tave) = 210.41 min

Temperature x Time:

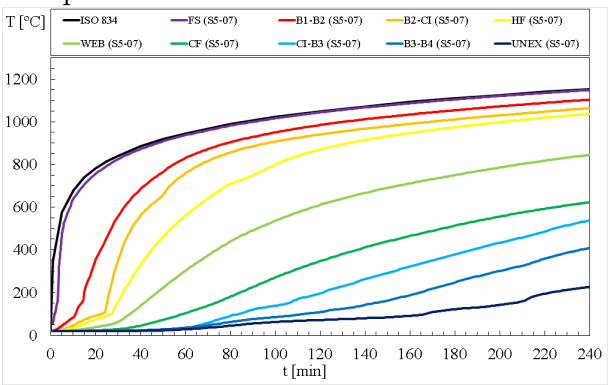

LSF Wall Configuration:

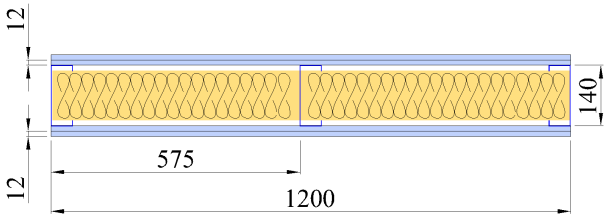

Mesh Complete Wall:

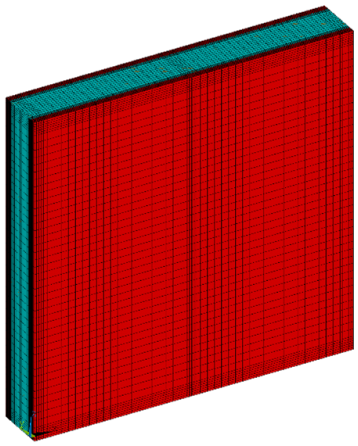

Temperature at t=3600s:

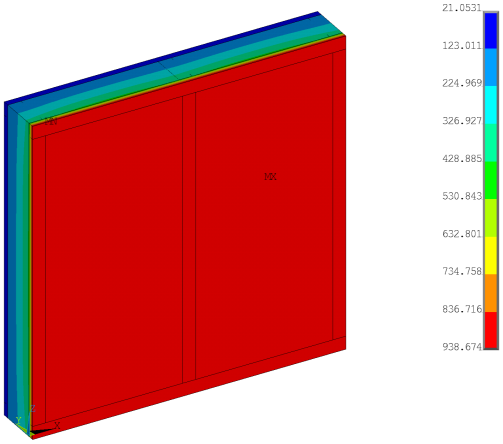

Mesh Half Wall:

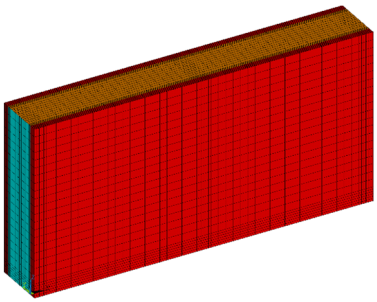

Temperature at t=3600s:

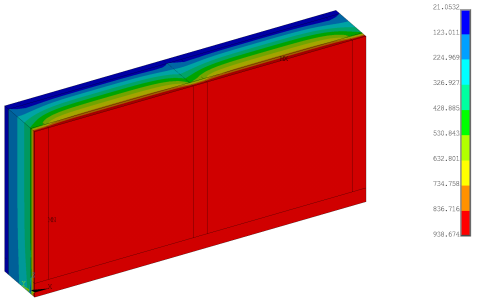

Specimen “S1” : Case 8.

STRUCTURE:
Studs: C140 (140x50x13x1.2mm)
Track: U142 (142x50x1.2 mm)
CFS wall: 1200x1200 mm
Gypsum: Type 2 (12 mm)
Rock wool: 90 kg/m^3

FIRE: Hydrocarbon
Tfi (Tmax) = 212.73 min
Tfi (Tave) = 249.69 min

Temperature x Time:

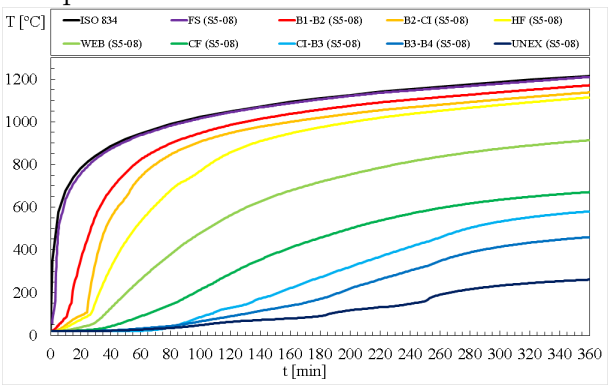

LSF Wall Configuration:

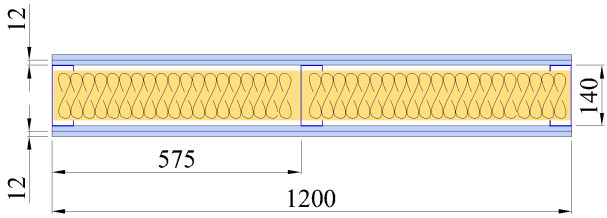

Mesh Complete Wall:

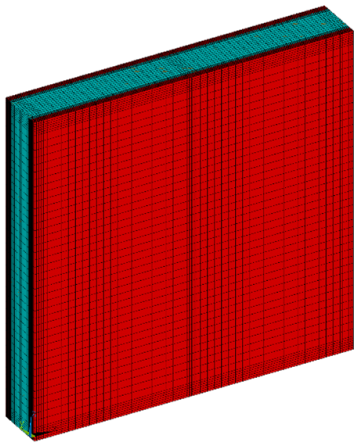

Temperature at t=3600s:

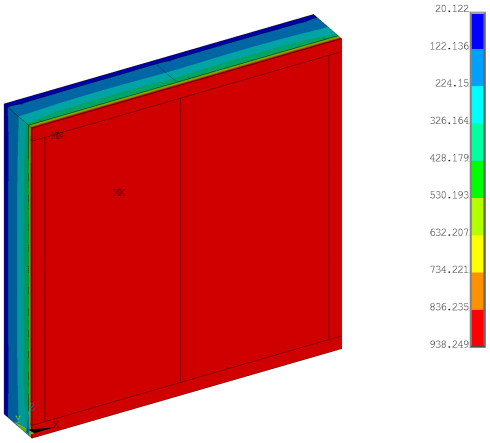

Mesh Half Wall:

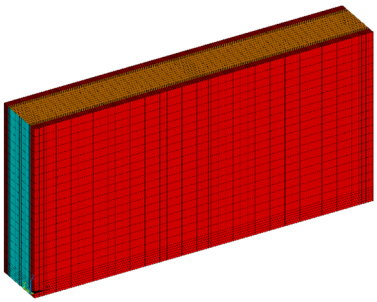

Temperature at t=3600s:

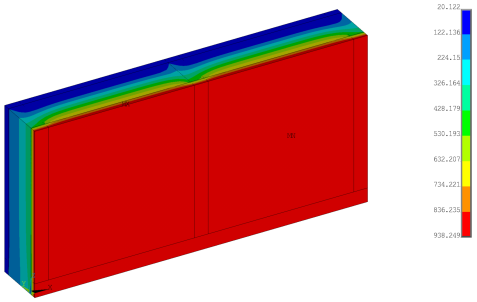

Specimen “S1” : Case 9.

STRUCTURE:
Studs: C140 (140x50x13x1.2mm)
Track: U142 (142x50x1.2 mm)
CFS wall: 1200x1200 mm
Gypsum: Type 2 (12 mm)
Rock wool: 150 kg/m^3

FIRE: Hydrocarbon
Tfi (Tmax) = 243.96 min
Tfi (Tave) = 291.3 min

Temperature x Time:

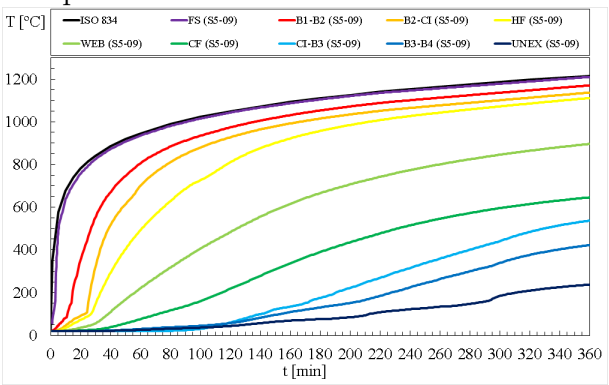

LSF Wall Configuration:

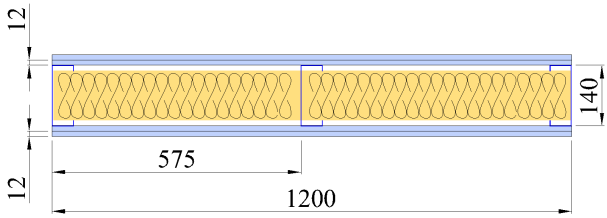

Mesh Complete Wall:

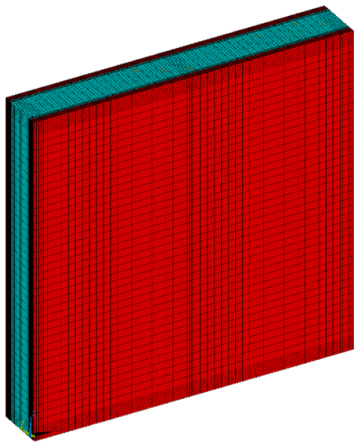

Temperature at t=3600s:

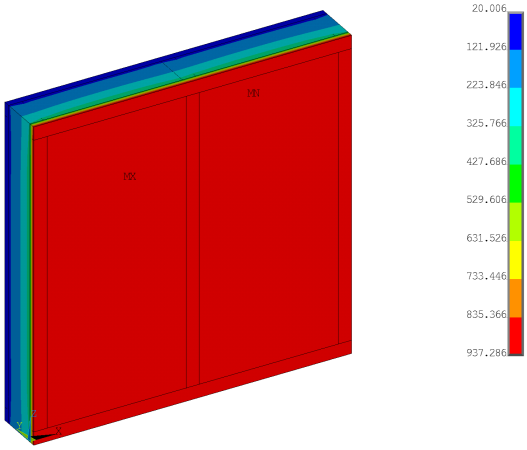

Mesh Half Wall:

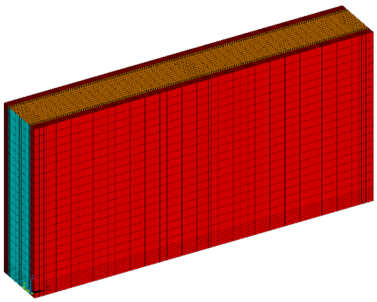

Temperature at t=3600s:

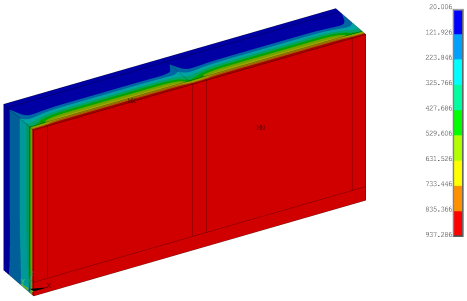

Specimen “S1” : Case 10.

STRUCTURE:
Studs: C140 (140x50x13x1.2mm)
Track: U142 (142x50x1.2 mm)
CFS wall: 1200x1200 mm
Gypsum: Type 2 (12 mm)
Rock wool: 175 kg/m^3

FIRE: Hydrocarbon
Tfi (Tmax) = 255.32 min
Tfi (Tave) = 305.25 min

Temperature x Time:

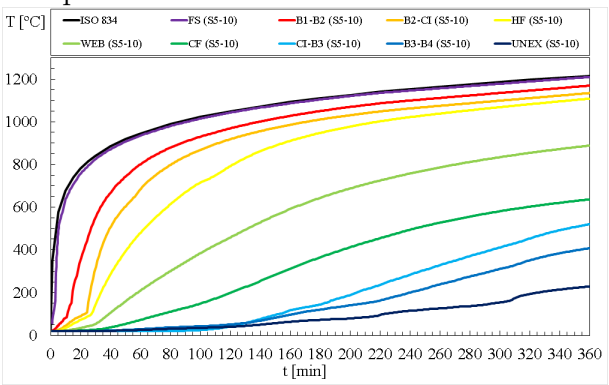

LSF Wall Configuration:

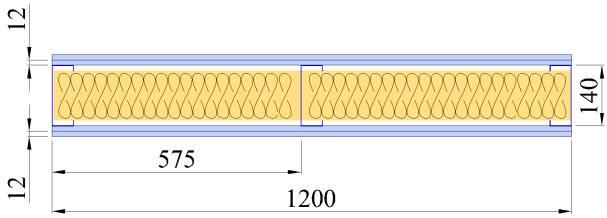

Mesh Complete Wall:

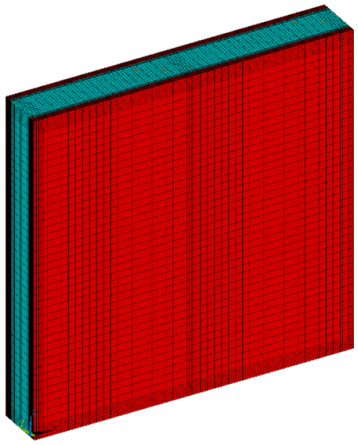

Temperature at t=3600s:

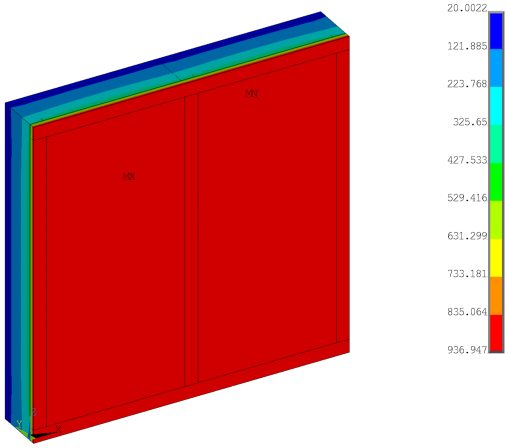

Mesh Half Wall:

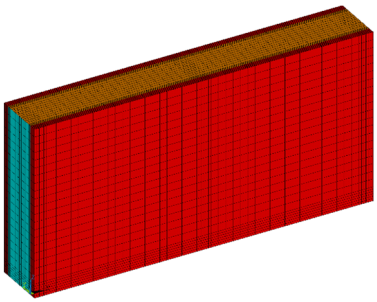

Temperature at t=3600s:

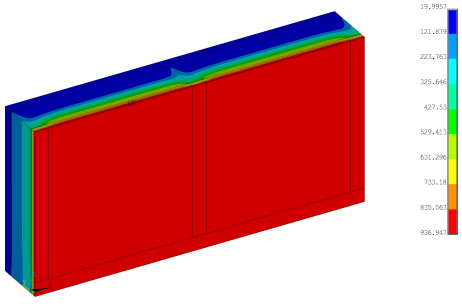

Specimen “S1” : Case 11.

STRUCTURE:
Studs: C140 (140x50x13x1.2mm)
Track: U142 (142x50x1.2 mm)
CFS wall: 1200x1200 mm
Gypsum: Type 1 (16 mm)
Rock wool: 30 kg/m^3

FIRE: Hydrocarbon
Tfi (Tmax) = 247.53 min
Tfi (Tave) = 250.25 min

Temperature x Time:

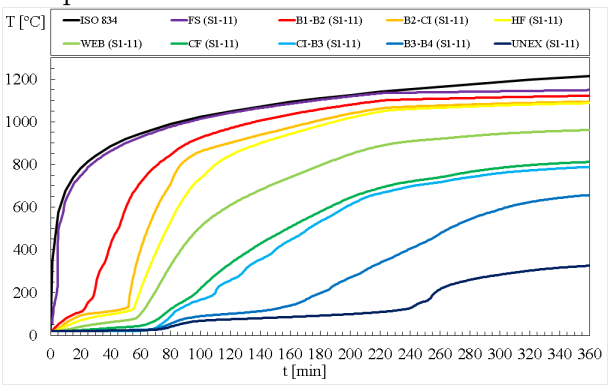

LSF Wall Configuration:

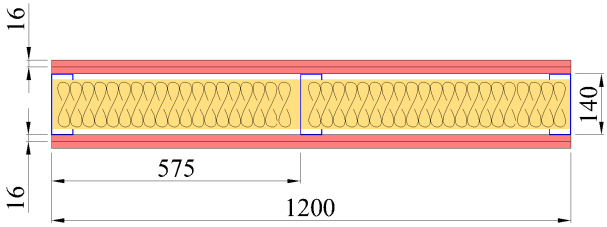

Mesh Complete Wall:

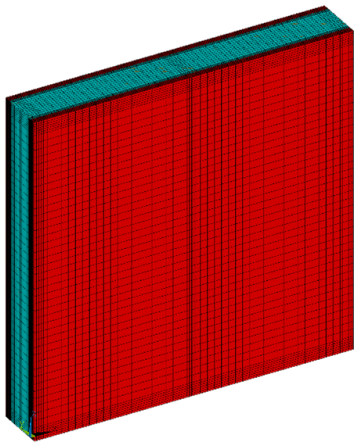

Temperature at t=3600s:

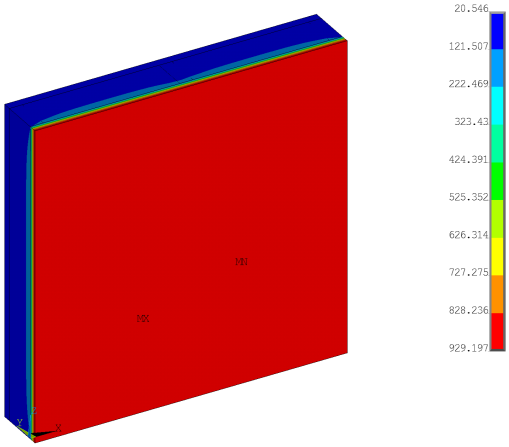

Mesh Half Wall:

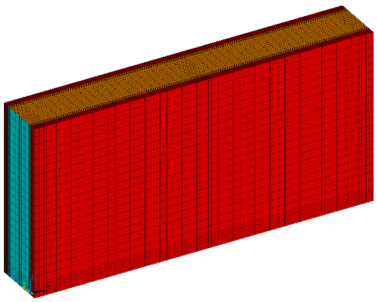

Temperature at t=3600s:

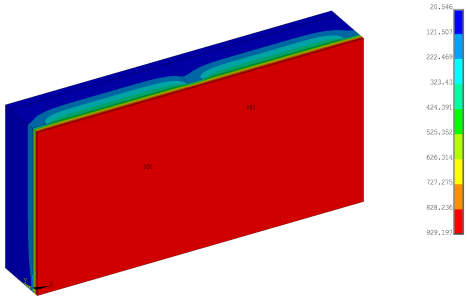

Specimen “S1” : Case 12.

STRUCTURE:
Studs: C140 (140x50x13x1.2mm)
Track: U142 (142x50x1.2 mm)
CFS wall: 1200x1200 mm
Gypsum: Type 1 (16 mm)
Rock wool: 60 kg/m^3

FIRE: Hydrocarbon
Tfi (Tmax) = 307.56 min
Tfi (Tave) = 329.36 min

Temperature x Time:

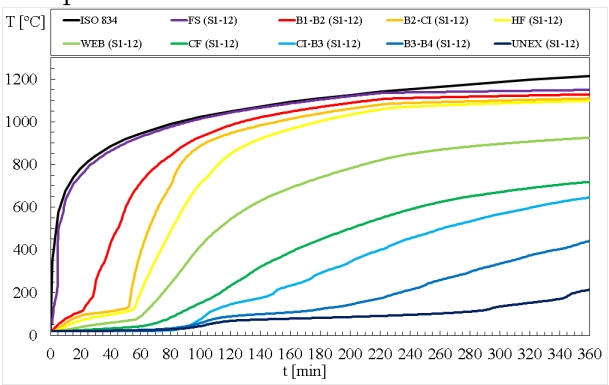

LSF Wall Configuration:

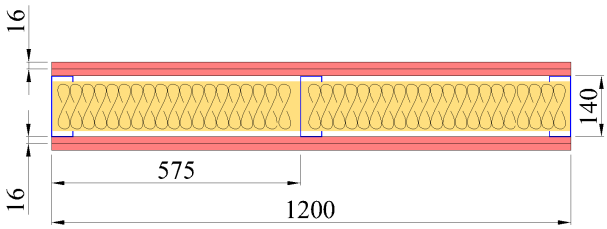

Mesh Complete Wall:

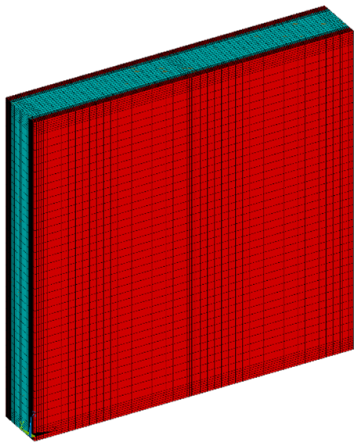

Temperature at t=3600s:

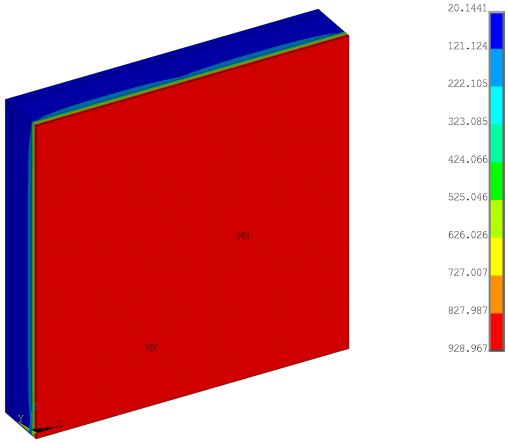

Mesh Half Wall:

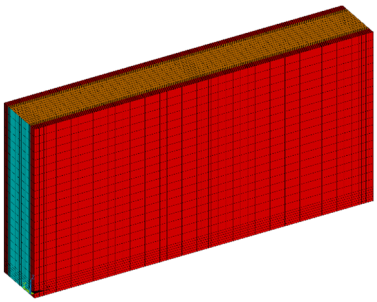

Temperature at t=3600s:

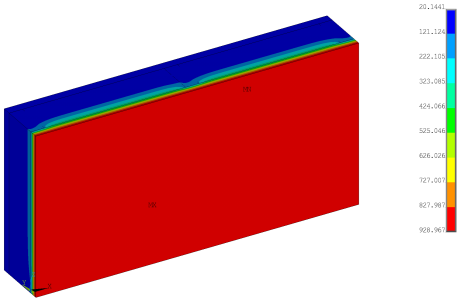

Specimen “S1” : Case 13.

STRUCTURE: Studs: C140 (140x50x13x1.2mm) Track: U142 (142x50x1.2 mm) CFS wall: 1200x1200 mm Gypsum: Type 1 (16 mm) Rock wool: 90 kg/m^3	FIRE: Hydrocarbon Tfi (Tmax) = 337.17 min Tfi (Tave) = 369.72 min
Temperature x Time: 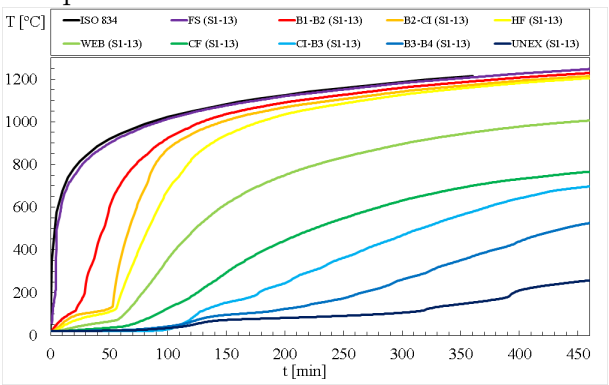	LSF Wall Configuration: 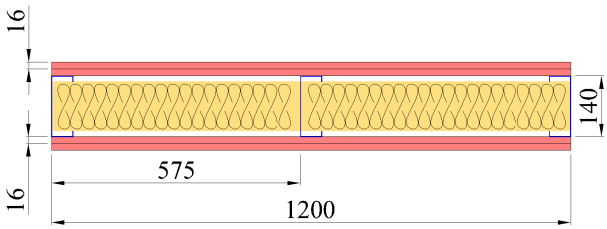
Mesh Complete Wall: 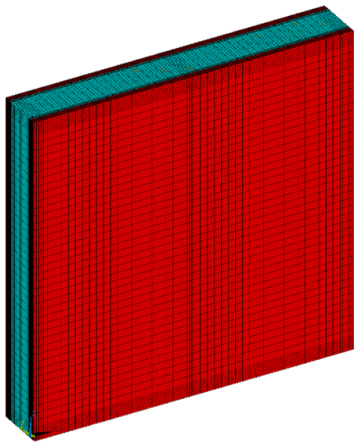	Temperature at t=3600s: 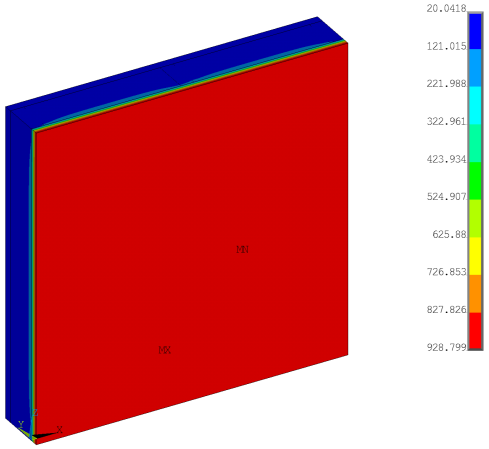
Mesh Half Wall: 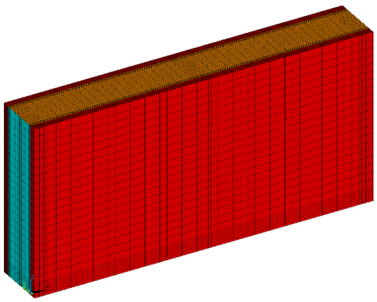	Temperature at t=3600s: 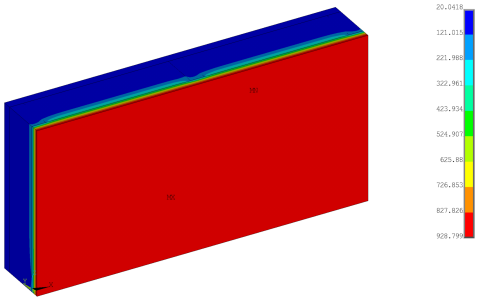

Specimen “S1” : Case 14.

STRUCTURE:
Studs: C140 (140x50x13x1.2mm)
Track: U142 (142x50x1.2 mm)
CFS wall: 1200x1200 mm
Gypsum: Type 1 (16 mm)
Rock wool: 150 kg/m^3

FIRE: Hydrocarbon
Tfi (Tmax) = 369.34 min
Tfi (Tave) = 410.63 min

Temperature x Time:

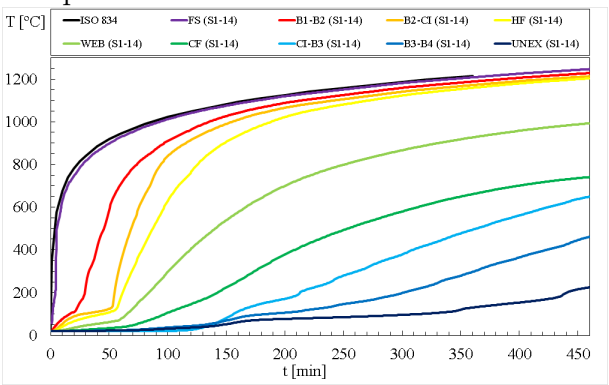

LSF Wall Configuration:

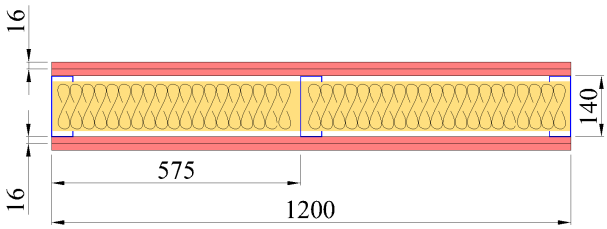

Mesh Complete Wall:

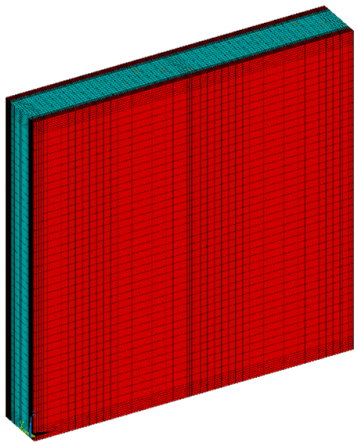

Temperature at t=3600s:

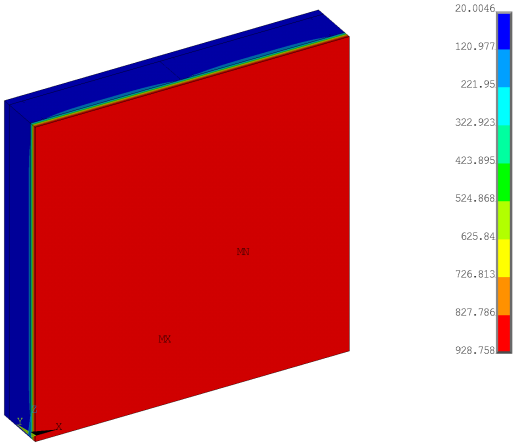

Mesh Half Wall:

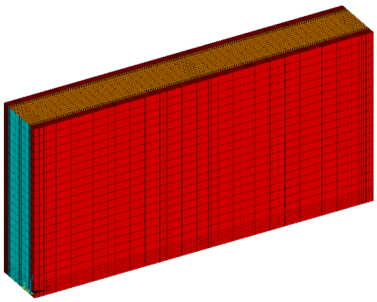

Temperature at t=3600s:

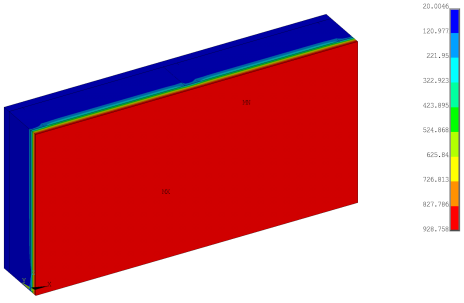

Specimen “S1” : Case 15.

STRUCTURE:
Studs: C140 (140x50x13x1.2mm)
Track: U142 (142x50x1.2 mm)
CFS wall: 1200x1200 mm
Gypsum: Type 1 (16 mm)
Rock wool: 175 kg/m^3

FIRE: Hydrocarbon
Tfi (Tmax) = 379.91 min
Tfi (Tave) = 423.15 min

Temperature x Time:

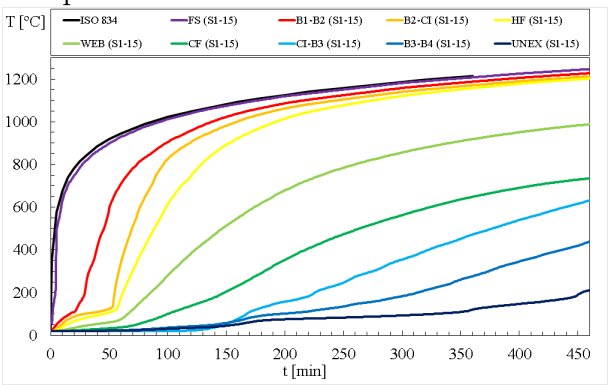

LSF Wall Configuration:

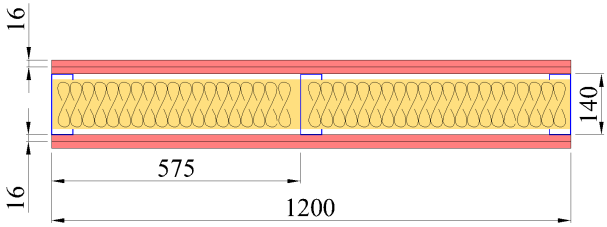

Mesh Complete Wall:

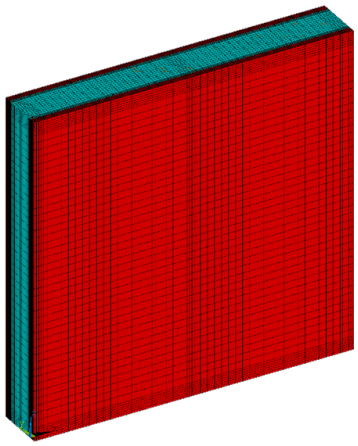

Temperature at t=3600s:

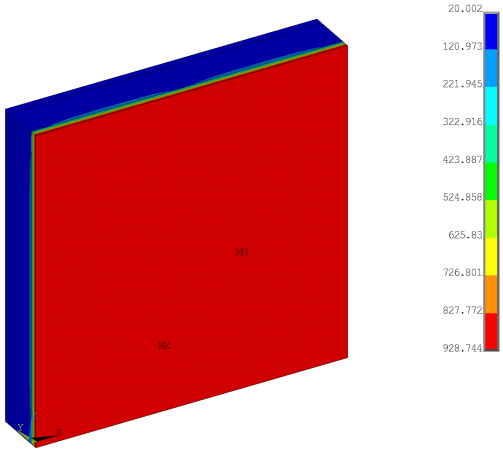

Mesh Half Wall:

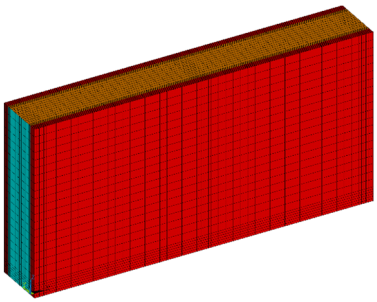

Temperature at t=3600s:

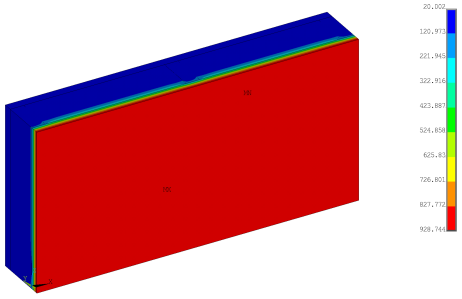

Specimen “S1” : Case 16.

STRUCTURE:
Studs: C140 (140x50x13x1.2mm)
Track: U142 (142x50x1.2 mm)
CFS wall: 1200x1200 mm
Gypsum: Type 2 (16 mm)
Rock wool: 30 kg/m^3

FIRE: Hydrocarbon
Tfi (Tmax) = 212.38 min
Tfi (Tave) = 209.49 min

Temperature x Time:

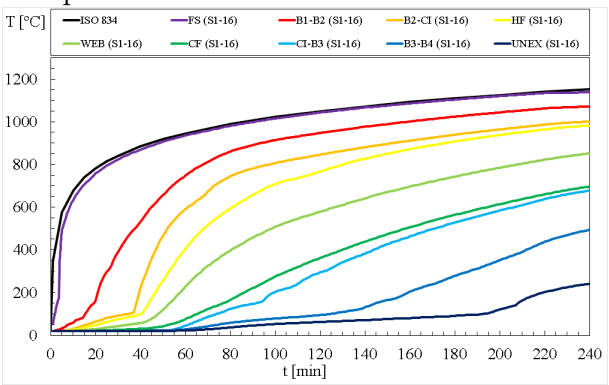

LSF Wall Configuration:

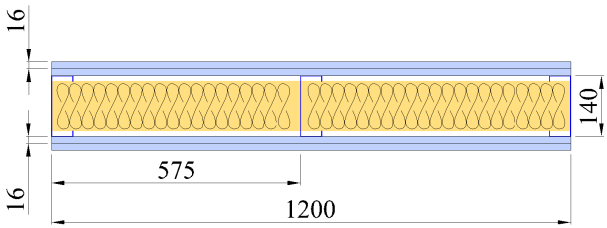

Mesh Complete Wall:

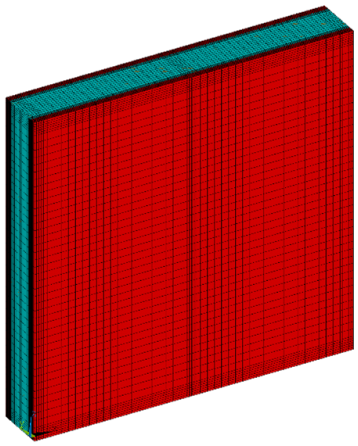

Temperature at t=3600s:

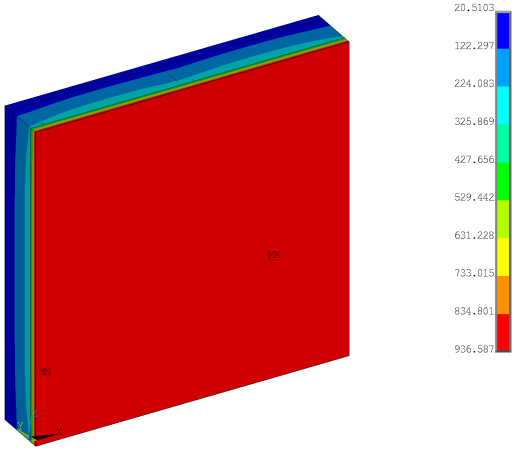

Mesh Half Wall:

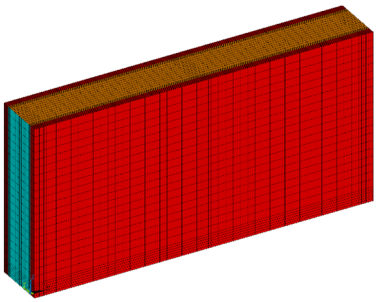

Temperature at t=3600s:

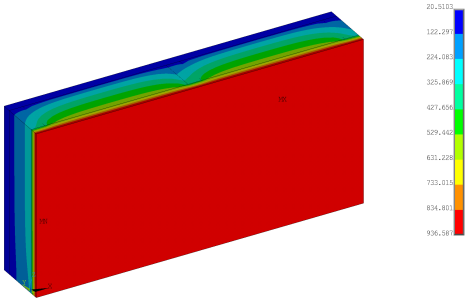

Specimen “S1” : Case 17.

STRUCTURE:
Studs: C140 (140x50x13x1.2mm)
Track: U142 (142x50x1.2 mm)
CFS wall: 1200x1200 mm
Gypsum: Type 2 (16 mm)
Rock wool: 60 kg/m^3

FIRE: Hydrocarbon
Tfi (Tmax) = 265.21 min
Tfi (Tave) = 277.98 min

Temperature x Time:

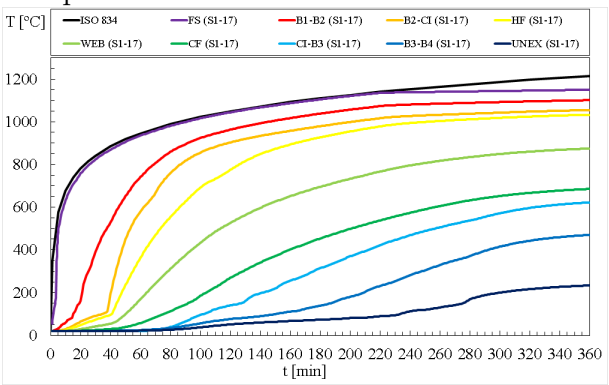

LSF Wall Configuration:

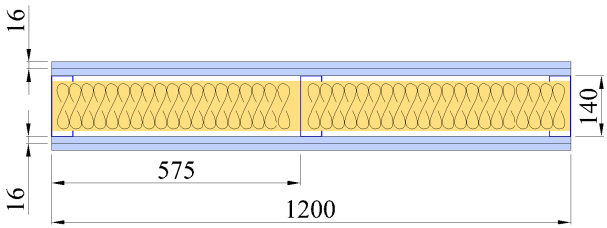

Mesh Complete Wall:

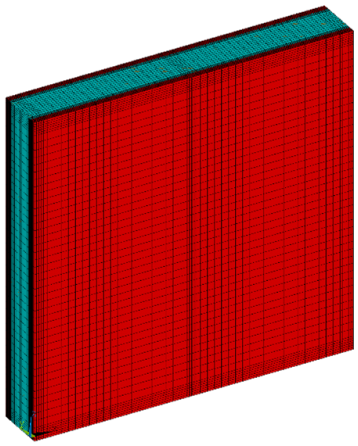

Temperature at t=3600s:

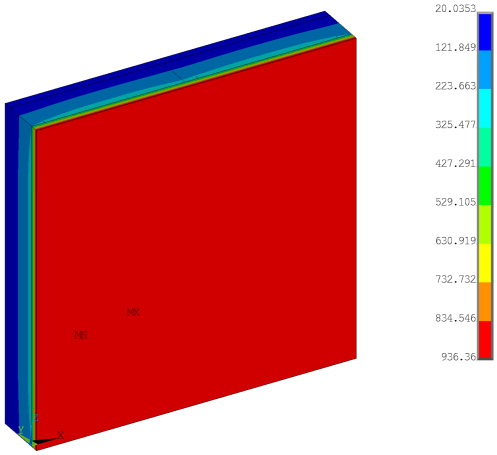

Mesh Half Wall:

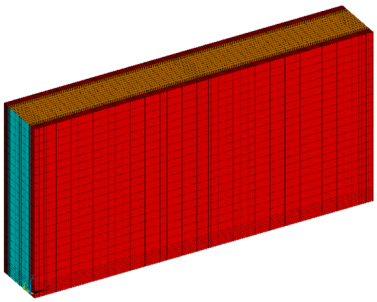

Temperature at t=3600s:

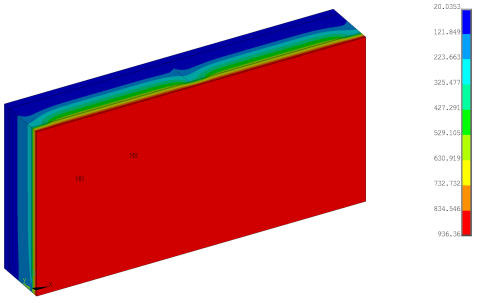

Specimen “S1” : Case 18.

STRUCTURE:
Studs: C140 (140x50x13x1.2mm)
Track: U142 (142x50x1.2 mm)
CFS wall: 1200x1200 mm
Gypsum: Type 2 (16 mm)
Rock wool: 90 kg/m^3

FIRE: Hydrocarbon
Tfi (Tmax) = 301.35 min
Tfi (Tave) = 325.75 min

Temperature x Time:

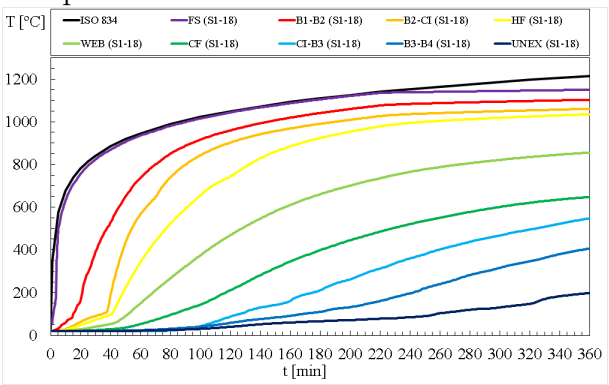

LSF Wall Configuration:

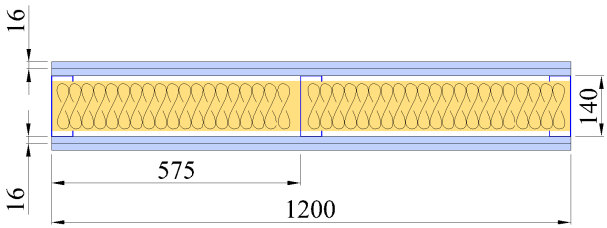

Mesh Complete Wall:

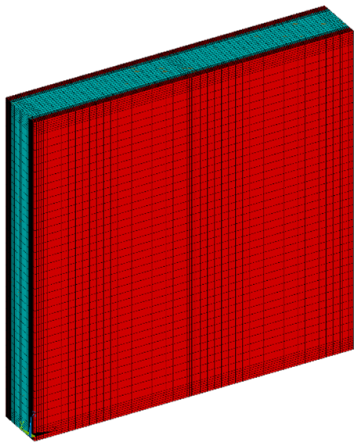

Temperature at t=3600s:

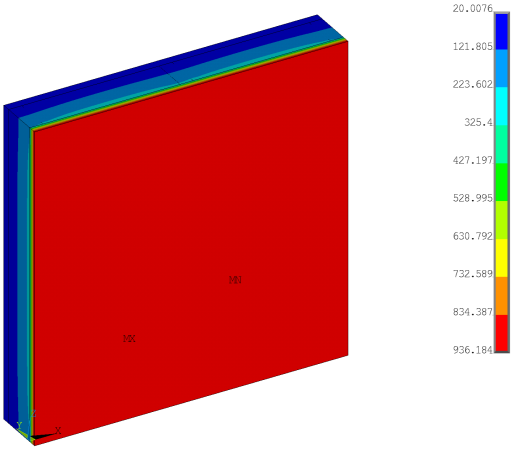

Mesh Half Wall:

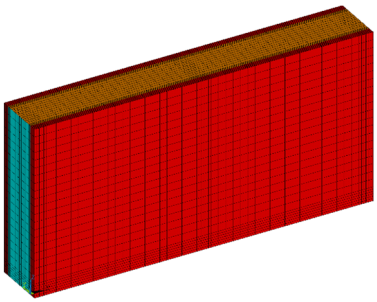

Temperature at t=3600s:

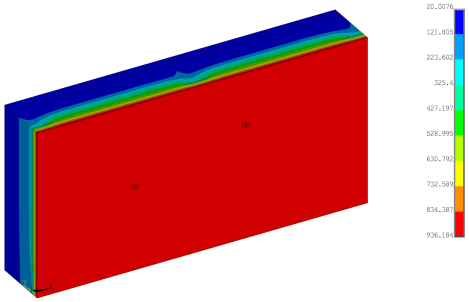

Specimen “S1” : Case 19.

STRUCTURE:
Studs: C140 (140x50x13x1.2mm)
Track: U142 (142x50x1.2 mm)
CFS wall: 1200x1200 mm
Gypsum: Type 2 (16 mm)
Rock wool: 150 kg/m^3

FIRE: Hydrocarbon
Tfi (Tmax) = 335.82 min
Tfi (Tave) = 368.24 min

Temperature x Time:

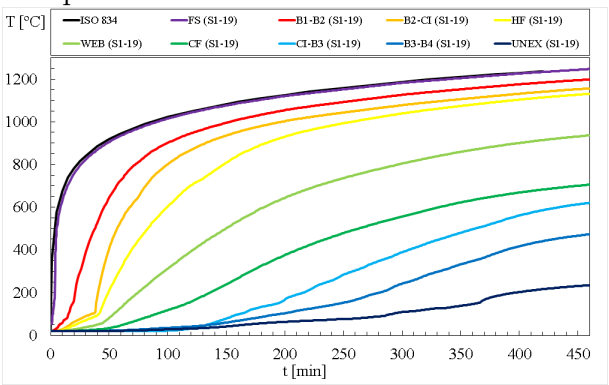

LSF Wall Configuration:

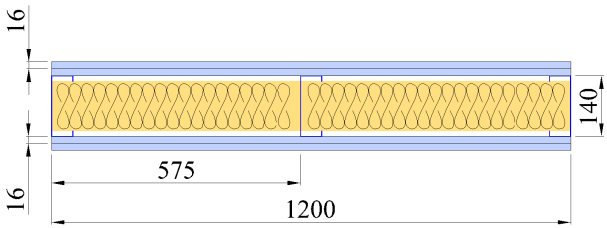

Mesh Complete Wall:

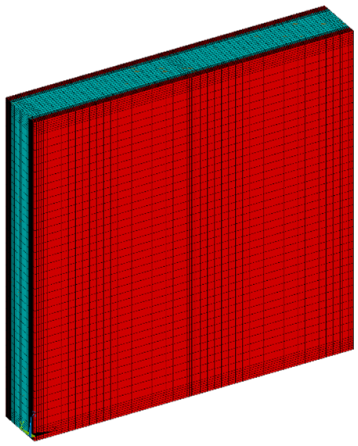

Temperature at t=3600s:

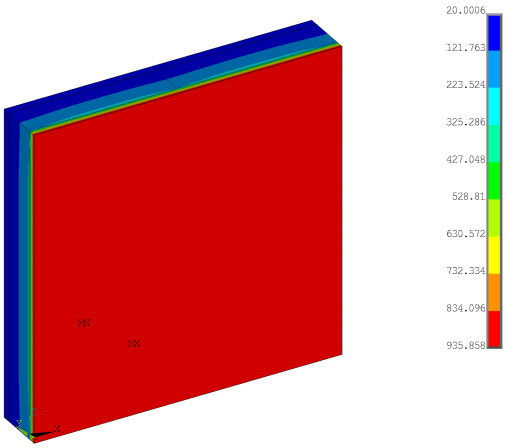

Mesh Half Wall:

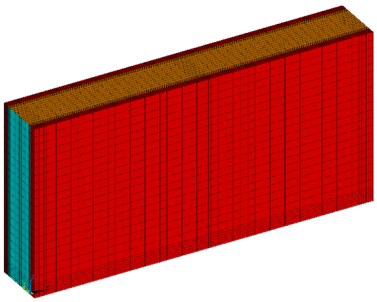

Temperature at t=3600s:

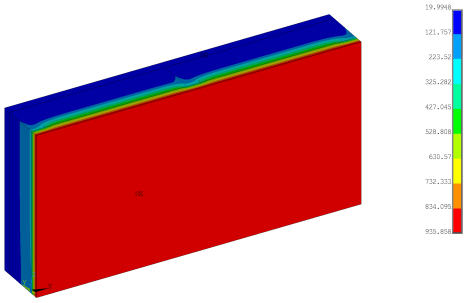

Specimen “S1” : Case 20.

STRUCTURE:
Studs: C140 (140x50x13x1.2mm)
Track: U142 (142x50x1.2 mm)
CFS wall: 1200x1200 mm
Gypsum: Type 2 (16 mm)
Rock wool: 175 kg/m^3

FIRE: Hydrocarbon
Tfi (Tmax) = 349.05 min
Tfi (Tave) = 383.62 min

Temperature x Time:

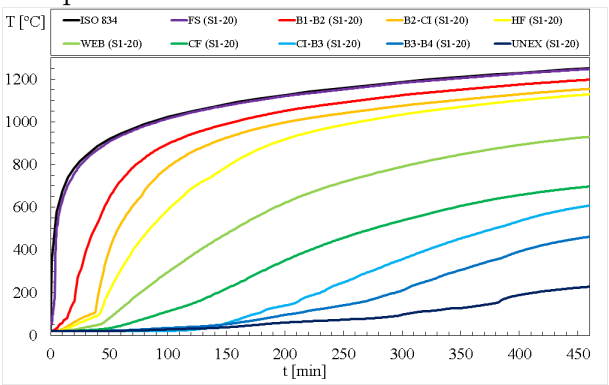

LSF Wall Configuration:

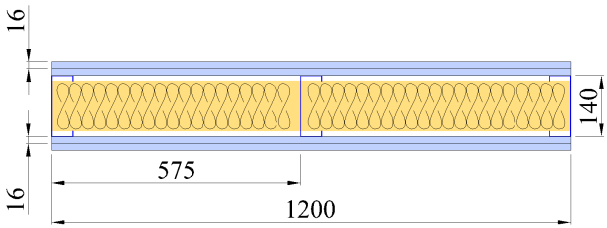

Mesh Complete Wall:

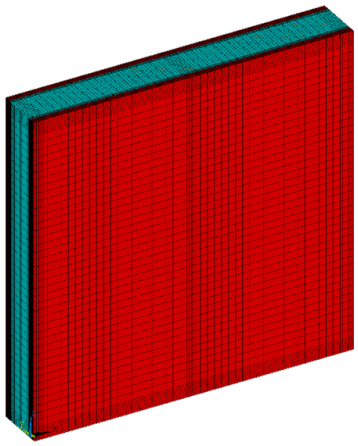

Temperature at t=3600s:

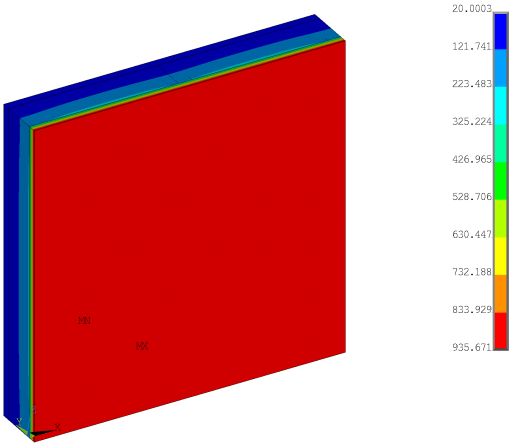

Mesh Half Wall:

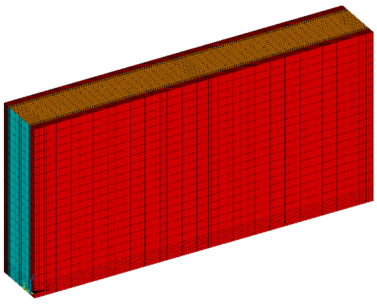

Temperature at t=3600s:

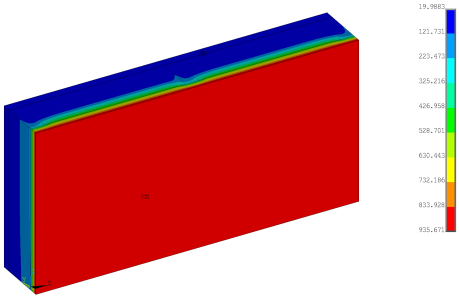

Specimen “S5” : Case 1.

STRUCTURE:
Studs: C140 (140x50x13x1.2mm)
Track: U142 (142x50x1.2 mm)
CFS wall: 1200x1200 mm
Gypsum: Type 1 (12 mm)
Rock wool: 30 kg/m^3

FIRE: Hydrocarbon
Tfi (Tmax) = 78.32 min
Tfi (Tave) = 77.82 min

Temperature x Time:

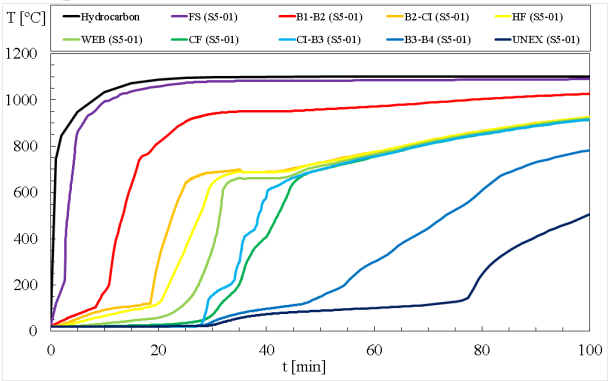

LSF Wall Configuration:

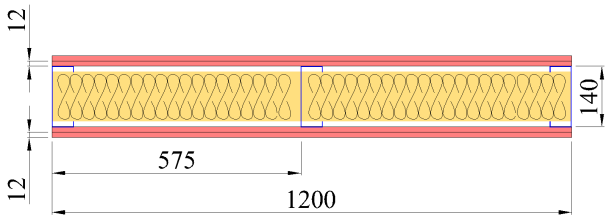

Mesh Complete Wall:

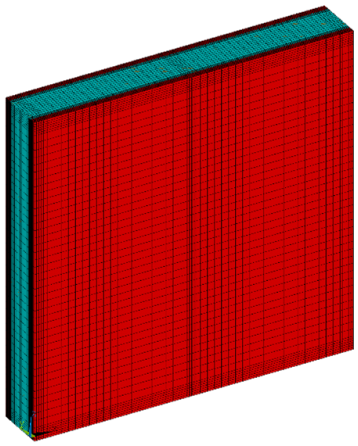

Temperature at t=3600s:

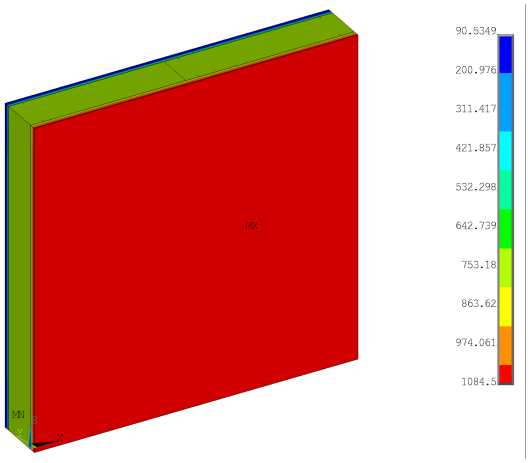

Mesh Half Wall:

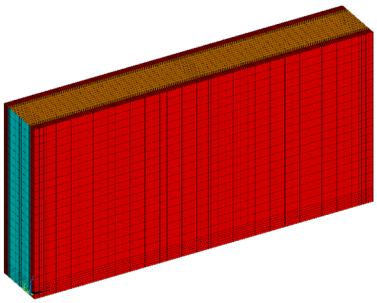

Temperature at t=3600s:

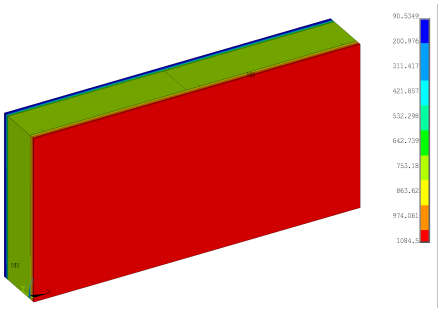

Specimen “S5” : Case 2.

STRUCTURE:
Studs: C140 (140x50x13x1.2mm)
Track: U142 (142x50x1.2 mm)
CFS wall: 1200x1200 mm
Gypsum: Type 1 (12 mm)
Rock wool: 60 kg/m^3

FIRE: Hydrocarbon
Tfi (Tmax) = 82.49 min
Tfi (Tave) = 83.02 min

Temperature x Time:

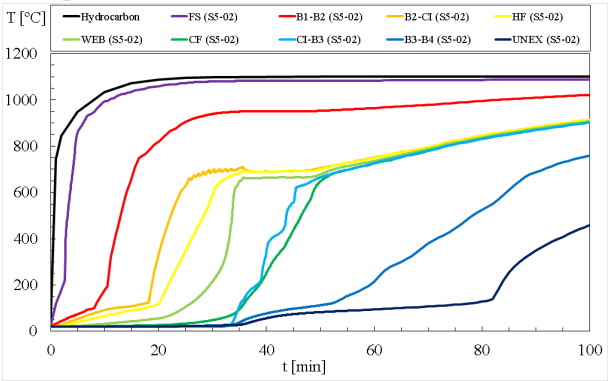

LSF Wall Configuration:

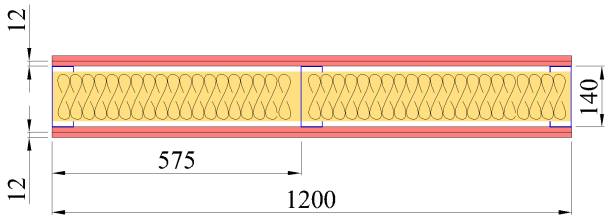

Mesh Complete Wall:

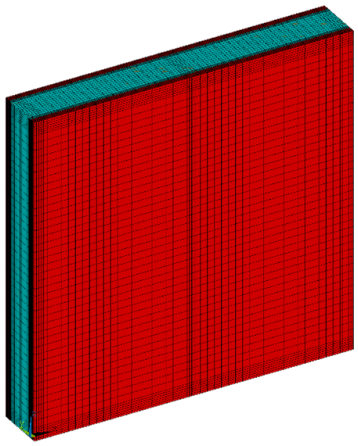

Temperature at t=3600s:

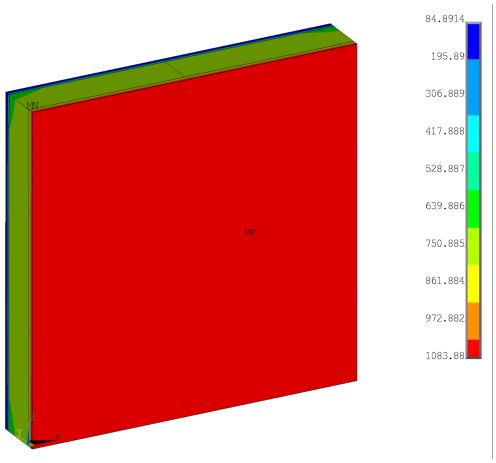

Mesh Half Wall:

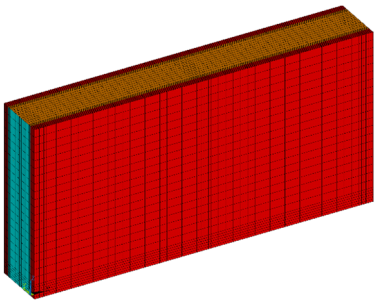

Temperature at t=3600s:

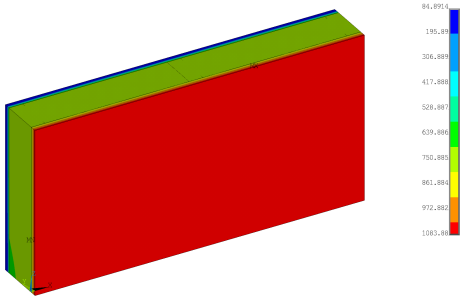

Specimen “S5” : Case 3.

STRUCTURE:
Studs: C140 (140x50x13x1.2mm)
Track: U142 (142x50x1.2 mm)
CFS wall: 1200x1200 mm
Gypsum: Type 1 (12 mm)
Rock wool: 90 kg/m^3

FIRE: Hydrocarbon
Tfi (Tmax) = 88.71 min
Tfi (Tave) = 88.13 min

Temperature x Time:

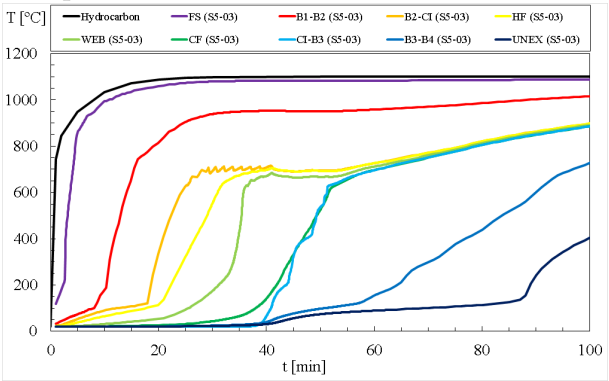

LSF Wall Configuration:

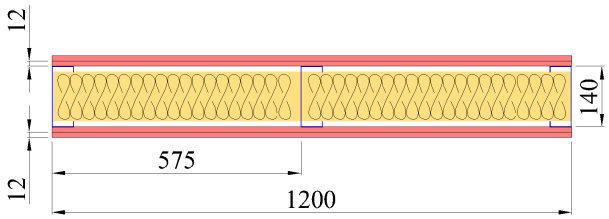

Mesh Complete Wall:

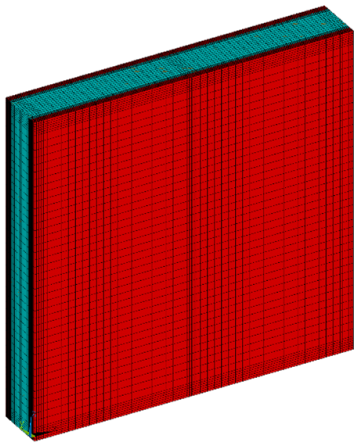

Temperature at t=3600s:

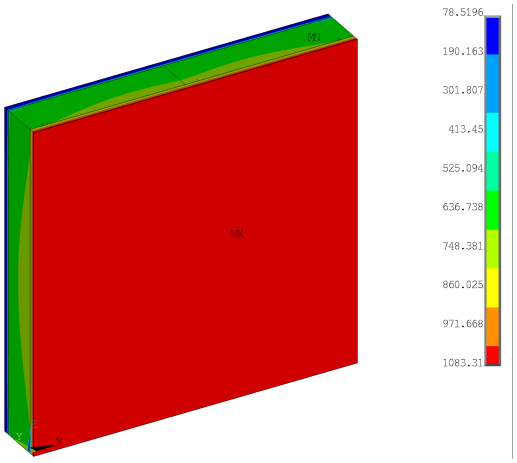

Mesh Half Wall:

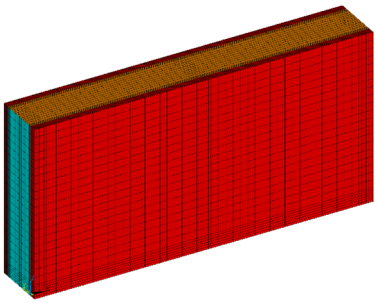

Temperature at t=3600s:

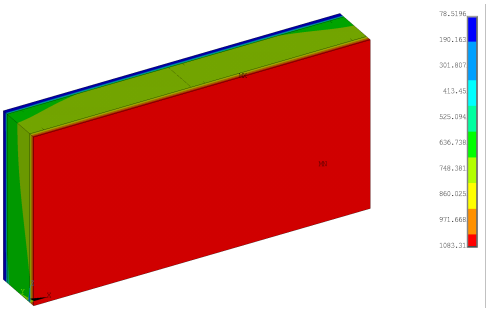

Specimen “S5” : Case 4.

STRUCTURE:
Studs: C140 (140x50x13x1.2mm)
Track: U142 (142x50x1.2 mm)
CFS wall: 1200x1200 mm
Gypsum: Type 1 (12 mm)
Rock wool: 150 kg/m^3

FIRE: Hydrocarbon
Tfi (Tmax) = 98.47 min
Tfi (Tave) = 98.52 min

Temperature x Time:

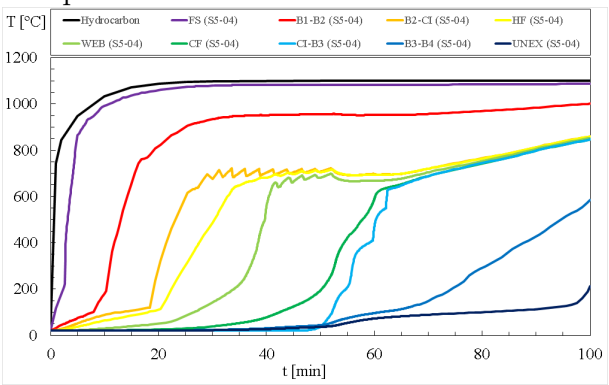

LSF Wall Configuration:

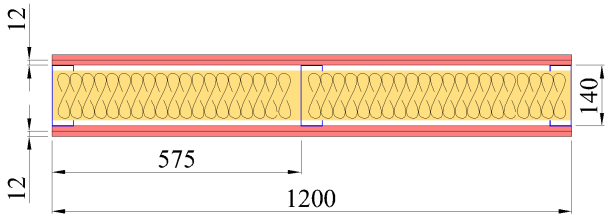

Mesh Complete Wall:

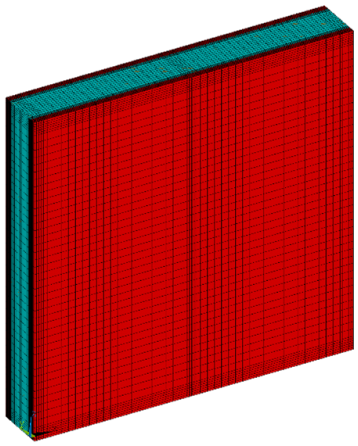

Temperature at t=3600s:

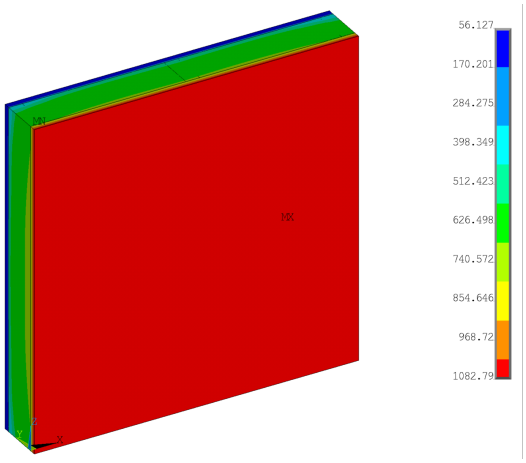

Mesh Half Wall:

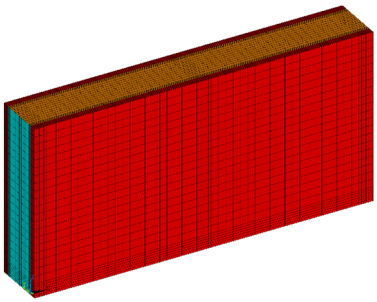

Temperature at t=3600s:

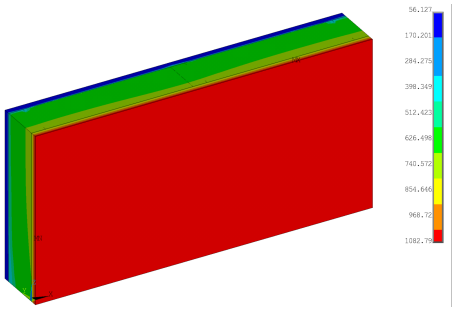

Specimen “S5” : Case 5.

STRUCTURE:
Studs: C140 (140x50x13x1.2mm)
Track: U142 (142x50x1.2 mm)
CFS wall: 1200x1200 mm
Gypsum: Type 1 (12 mm)
Rock wool: 175 kg/m^3

FIRE: Hydrocarbon
Tfi (Tmax) = 102.3 min
Tfi (Tave) = 102.58 min

Temperature x Time:

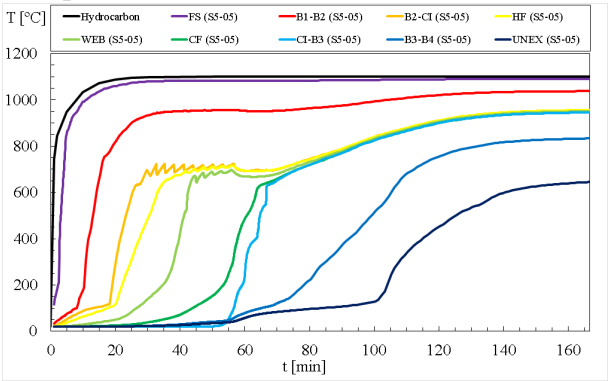

LSF Wall Configuration:

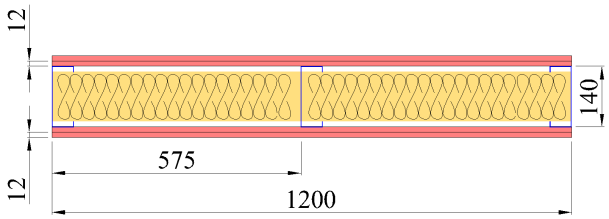

Mesh Complete Wall:

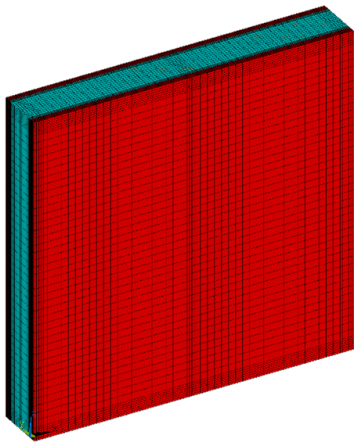

Temperature at t=3600s:

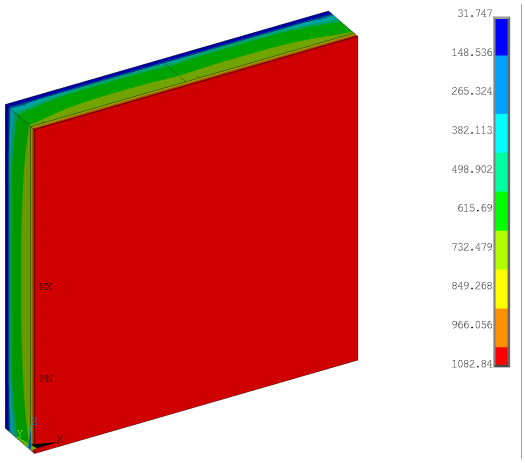

Mesh Half Wall:

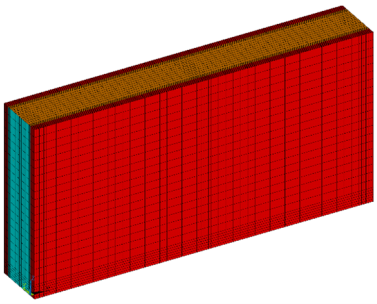

Temperature at t=3600s:

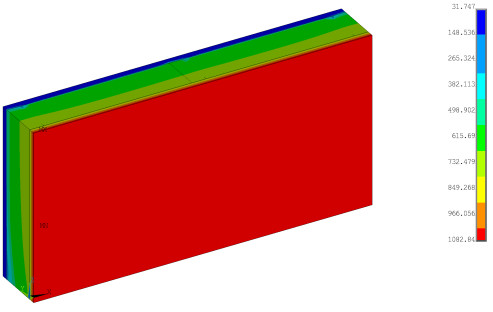

Specimen “S5” : Case 6.

STRUCTURE:
Studs: C140 (140x50x13x1.2mm)
Track: U142 (142x50x1.2 mm)
CFS wall: 1200x1200 mm
Gypsum: Type 2 (12 mm)
Rock wool: 30 kg/m^3

FIRE: Hydrocarbon
Tfi (Tmax) = 71.76 min
Tfi (Tave) = 70.93 min

Temperature x Time:

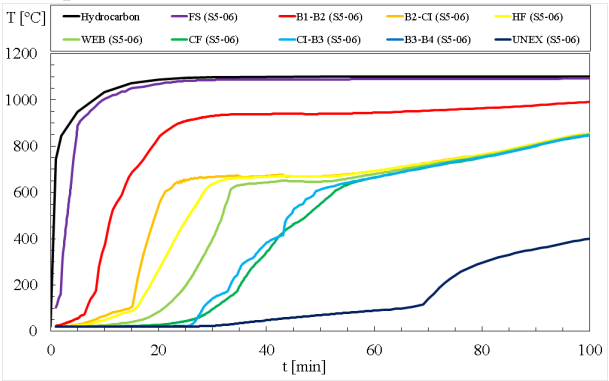

LSF Wall Configuration:

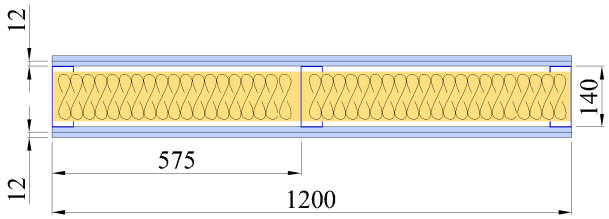

Mesh Complete Wall:

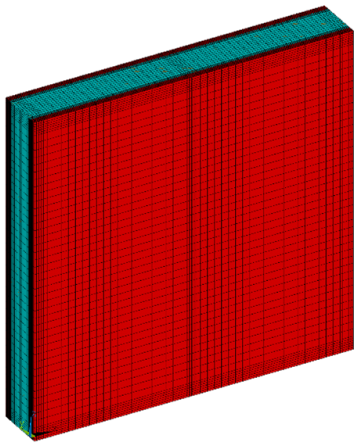

Temperature at t=3600s:

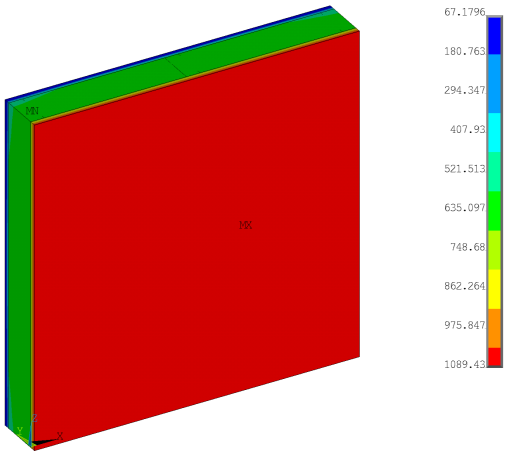

Mesh Half Wall:

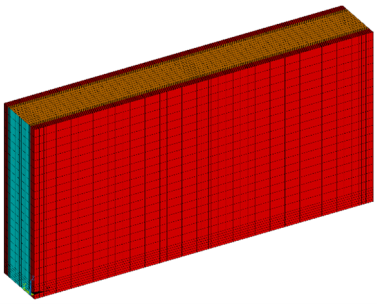

Temperature at t=3600s:

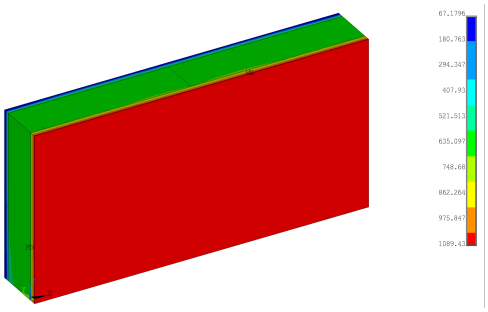

Specimen “S5” : Case 7.

STRUCTURE:
Studs: C140 (140x50x13x1.2mm)
Track: U142 (142x50x1.2 mm)
CFS wall: 1200x1200 mm
Gypsum: Type 2 (12 mm)
Rock wool: 60 kg/m^3

FIRE: Hydrocarbon
Tfi (Tmax) = 79.45 min
Tfi (Tave) = 79.19 min

Temperature x Time:

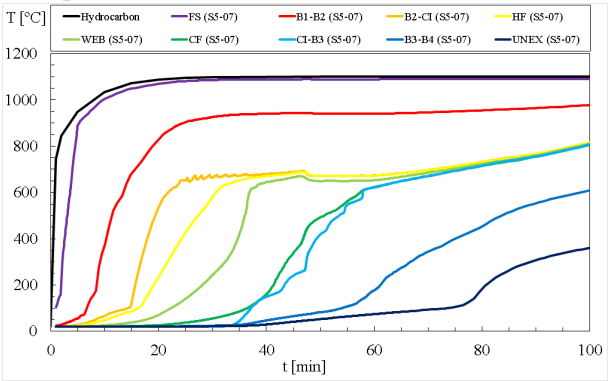

LSF Wall Configuration:

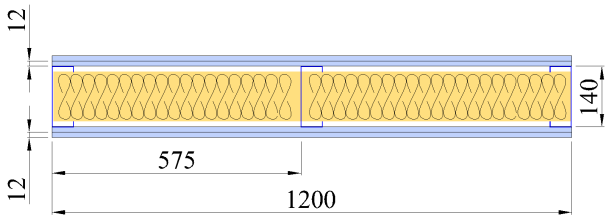

Mesh Complete Wall:

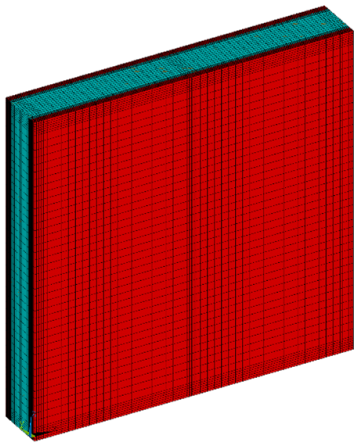

Temperature at t=3600s:

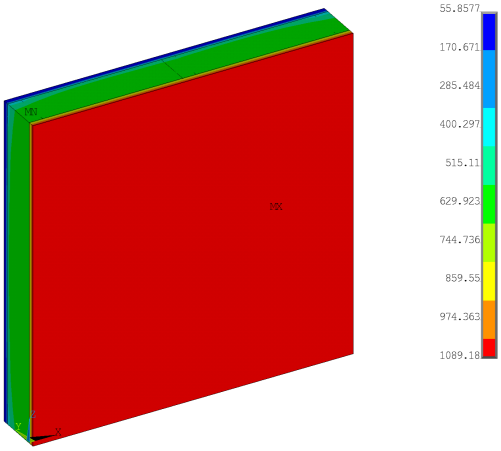

Mesh Half Wall:

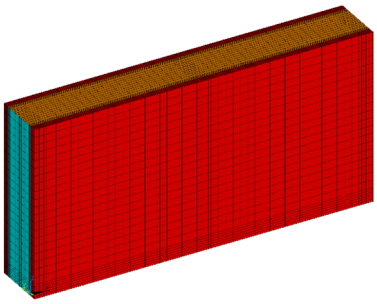

Temperature at t=3600s:

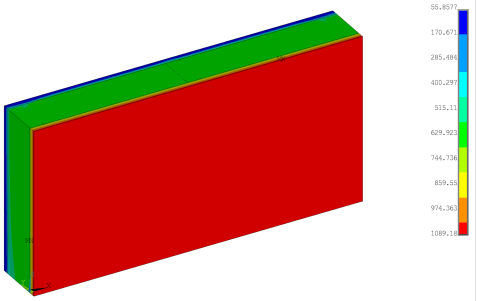

Specimen “S5” : Case 8.

STRUCTURE:
Studs: C140 (140x50x13x1.2mm)
Track: U142 (142x50x1.2 mm)
CFS wall: 1200x1200 mm
Gypsum: Type 2 (12 mm)
Rock wool: 90 kg/m^3

FIRE: Hydrocarbon
Tfi (Tmax) = 85.43 min
Tfi (Tave) = 87.49 min

Temperature x Time:

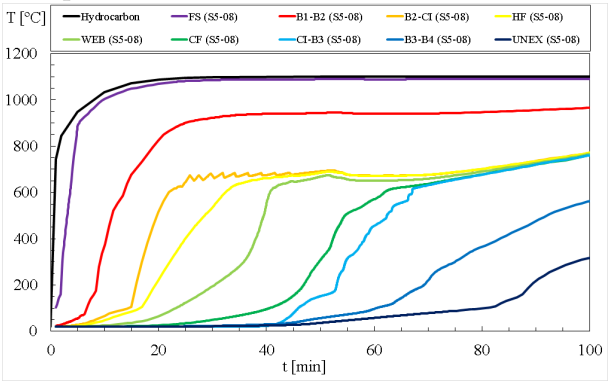

LSF Wall Configuration:

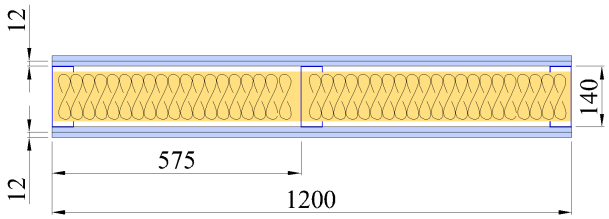

Mesh Complete Wall:

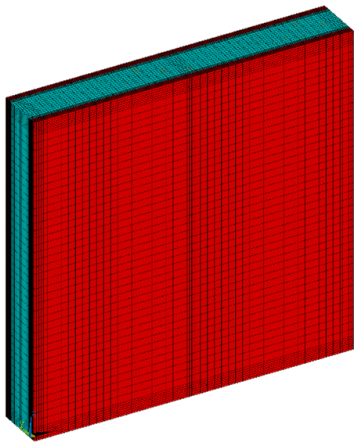

Temperature at t=3600s:

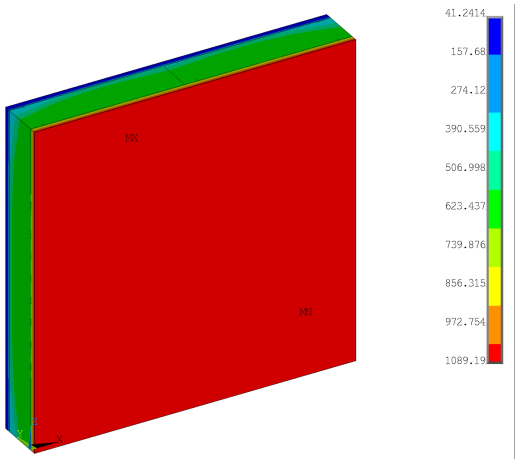

Mesh Half Wall:

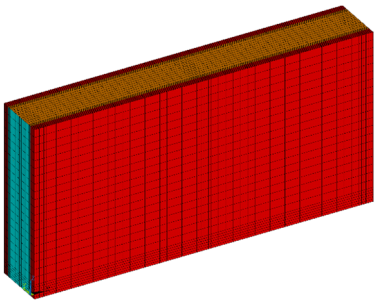

Temperature at t=3600s:

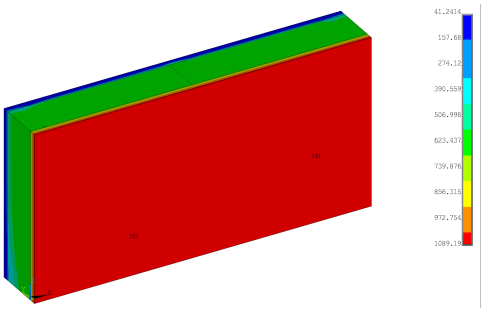

Specimen “S5” : Case 9.

STRUCTURE:
Studs: C140 (140x50x13x1.2mm)
Track: U142 (142x50x1.2 mm)
CFS wall: 1200x1200 mm
Gypsum: Type 2 (12 mm)
Rock wool: 150 kg/m^3

FIRE: Hydrocarbon
Tfi (Tmax) = 98.16 min
Tfi (Tave) = 102.75 min

Temperature x Time:

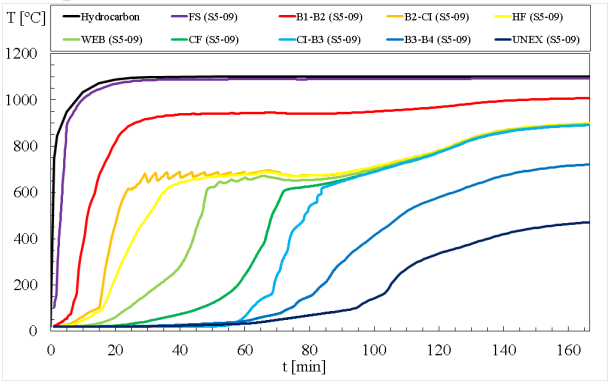

LSF Wall Configuration:

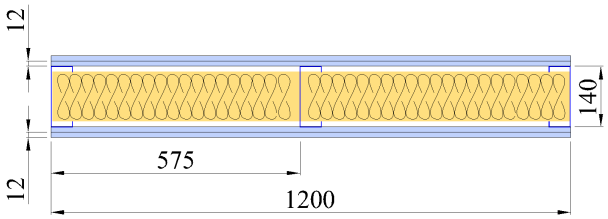

Mesh Complete Wall:

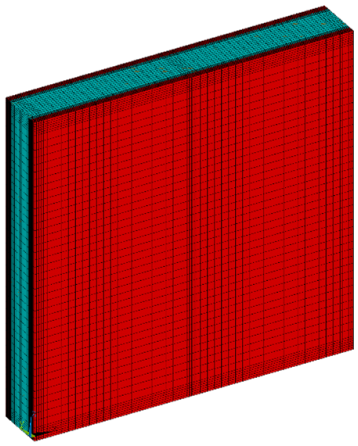

Temperature at t=3600s:

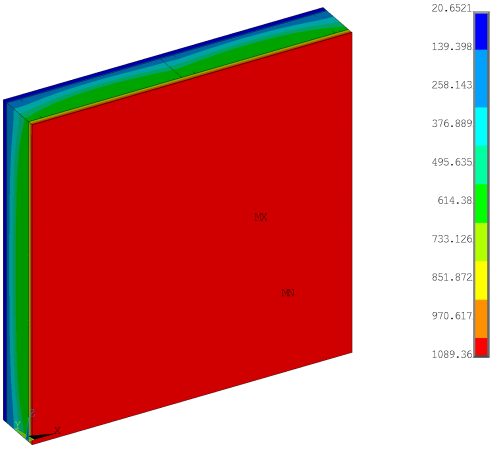

Mesh Half Wall:

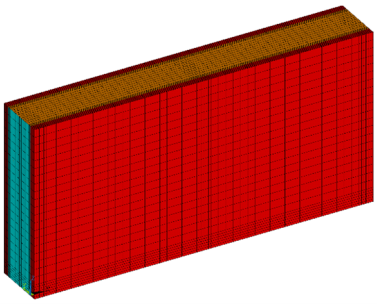

Temperature at t=3600s:

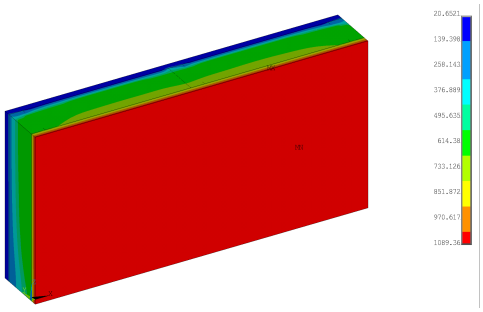

Specimen “S5” : Case 10.

STRUCTURE:
Studs: C140 (140x50x13x1.2mm)
Track: U142 (142x50x1.2 mm)
CFS wall: 1200x1200 mm
Gypsum: Type 2 (12 mm)
Rock wool: 175 kg/m^3

FIRE: Hydrocarbon
Tfi (Tmax) = 103.64 min
Tfi (Tave) = 108.99 min

Temperature x Time:

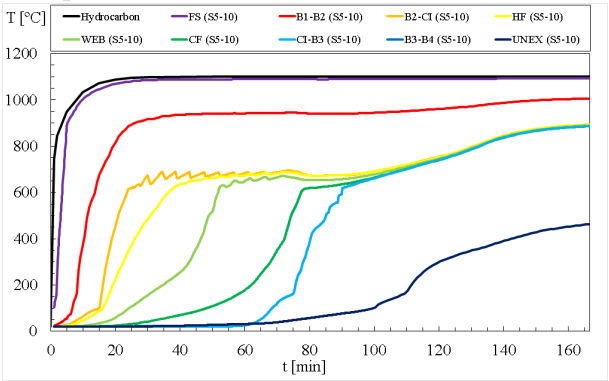

LSF Wall Configuration:

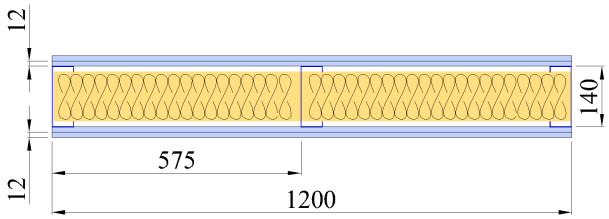

Mesh Complete Wall:

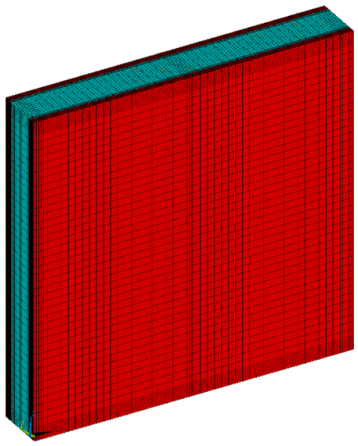

Temperature at t=3600s:

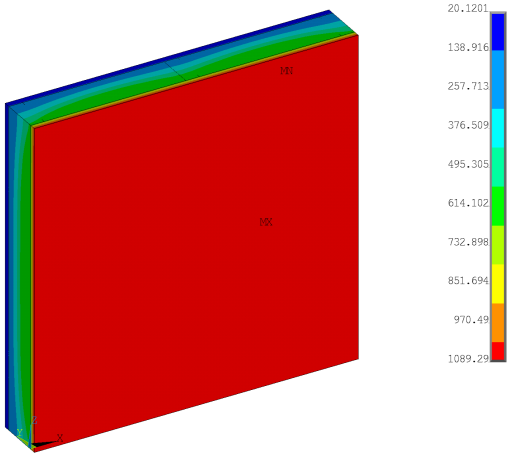

Mesh Half Wall:

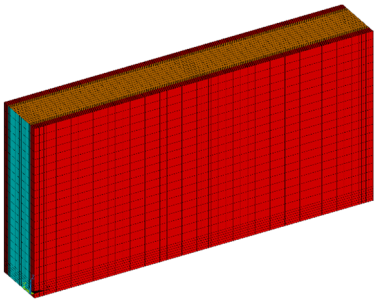

Temperature at t=3600s:

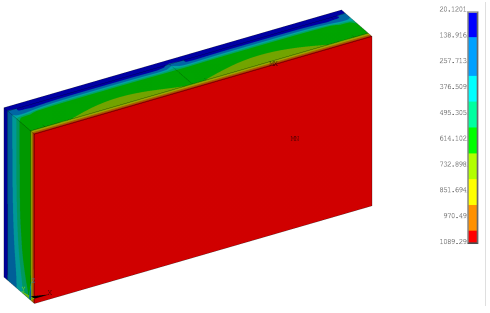

Specimen “S5” : Case 11.

STRUCTURE:
Studs: C140 (140x50x13x1.2mm)
Track: U142 (142x50x1.2 mm)
CFS wall: 1200x1200 mm
Gypsum: Type 1 (16 mm)
Rock wool: 30 kg/m^3

FIRE: Hydrocarbon
Tfi (Tmax) = 125.28 min
Tfi (Tave) = 124.02 min

Temperature x Time:

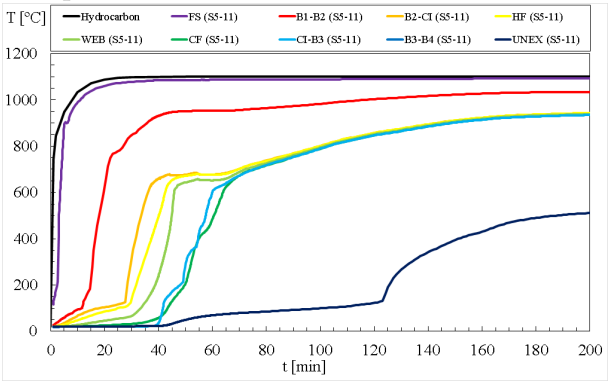

LSF Wall Configuration:

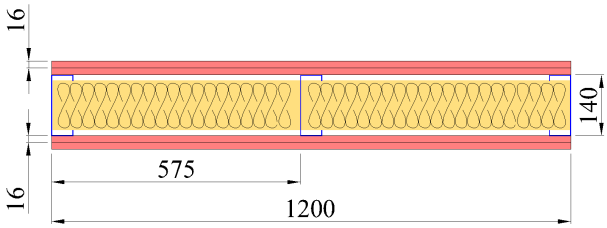

Mesh Complete Wall:

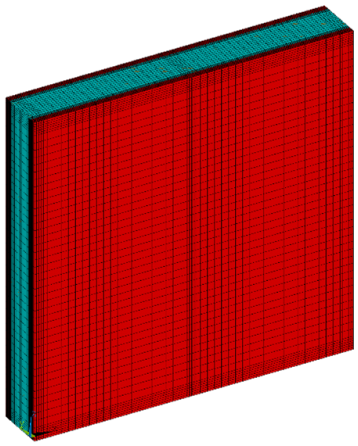

Temperature at t=3600s:

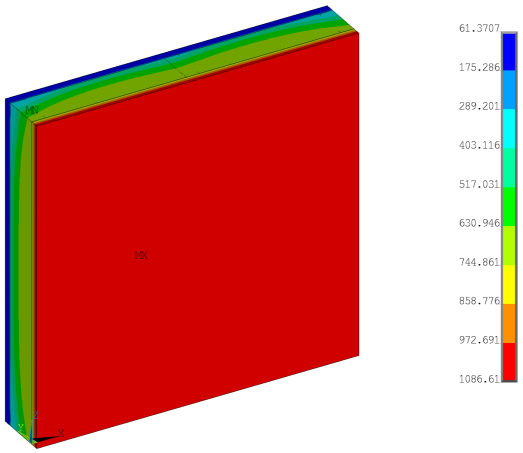

Mesh Half Wall:

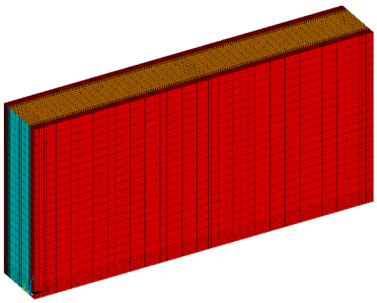

Temperature at t=3600s:

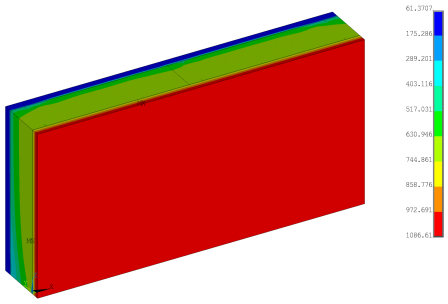

Specimen “S5” : Case 12.

STRUCTURE:
Studs: C140 (140x50x13x1.2mm)
Track: U142 (142x50x1.2 mm)
CFS wall: 1200x1200 mm
Gypsum: Type 1 (16 mm)
Rock wool: 60 kg/m^3

FIRE: Hydrocarbon
Tfi (Tmax) = 132.5 min
Tfi (Tave) = 131.01 min

Temperature x Time:

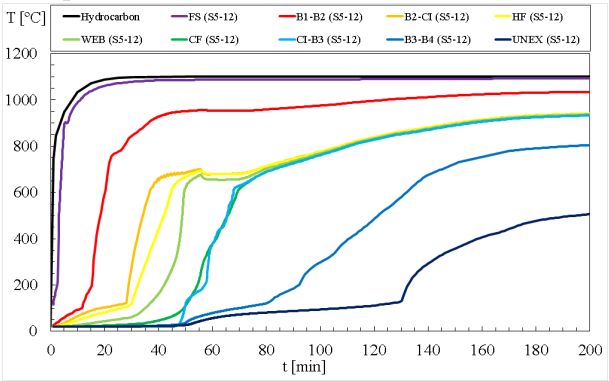

LSF Wall Configuration:

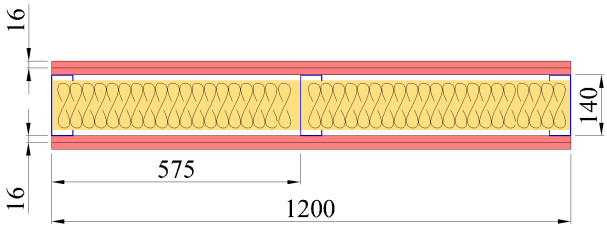

Mesh Complete Wall:

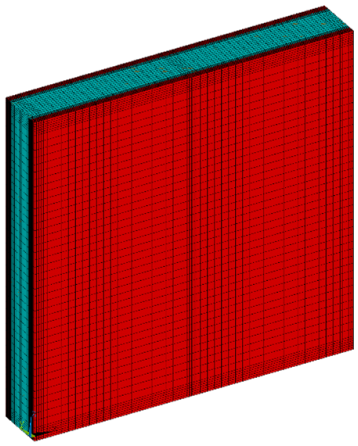

Temperature at t=3600s:

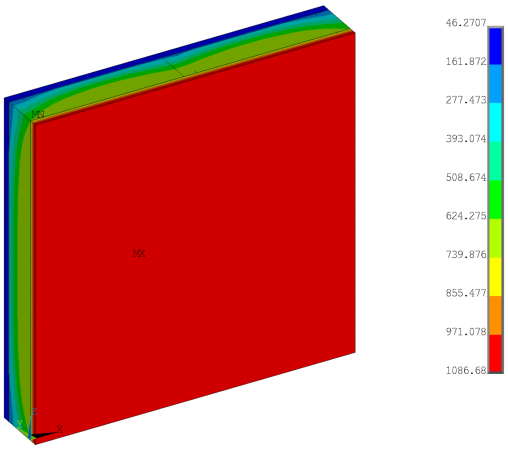

Mesh Half Wall:

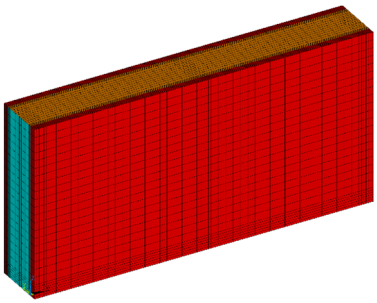

Temperature at t=3600s:

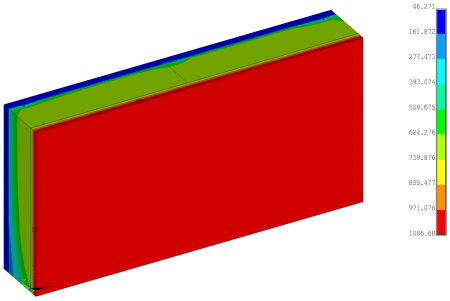

Specimen “S5” : Case 13.

STRUCTURE:
Studs: C140 (140x50x13x1.2mm)
Track: U142 (142x50x1.2 mm)
CFS wall: 1200x1200 mm
Gypsum: Type 1 (16 mm)
Rock wool: 90 kg/m^3

FIRE: Hydrocarbon
Tfi (Tmax) = 138.97 min
Tfi (Tave) = 137.56 min

Temperature x Time:

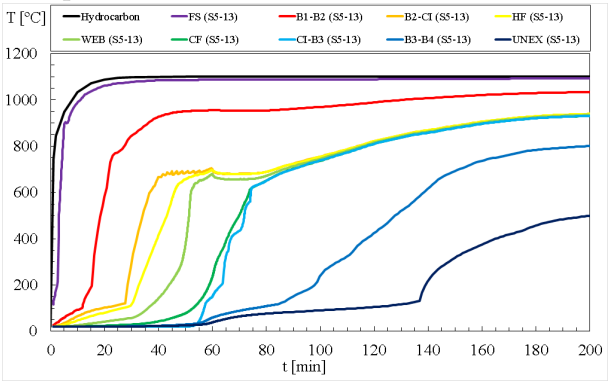

LSF Wall Configuration:

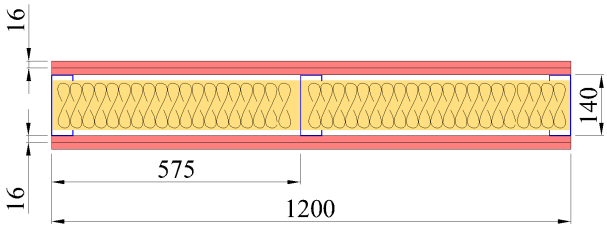

Mesh Complete Wall:

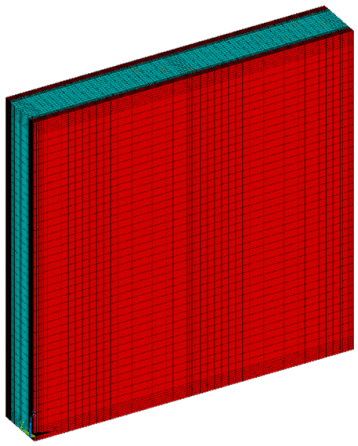

Temperature at t=3600s:

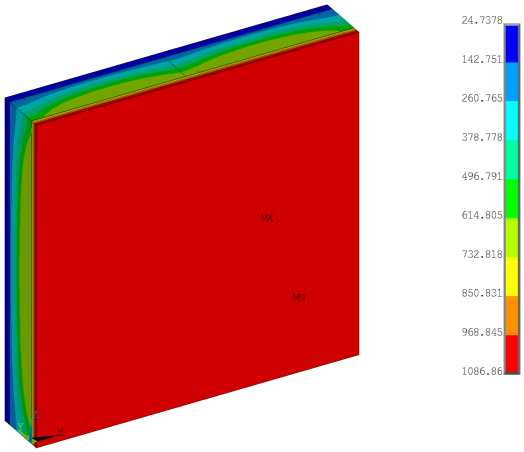

Mesh Half Wall:

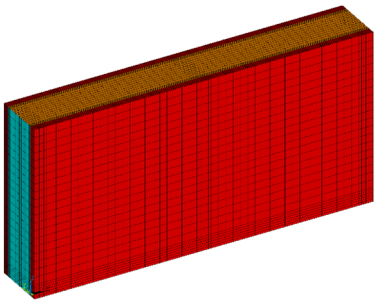

Temperature at t=3600s:

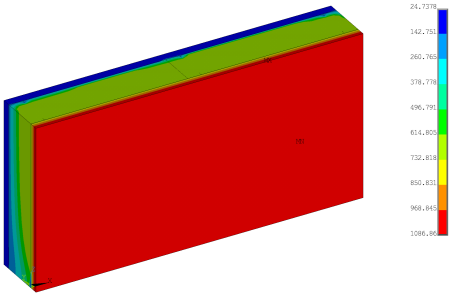

Specimen “S5” : Case 14.

STRUCTURE:
Studs: C140 (140x50x13x1.2mm)
Track: U142 (142x50x1.2 mm)
CFS wall: 1200x1200 mm
Gypsum: Type 1 (16 mm)
Rock wool: 150 kg/m^3

FIRE: Hydrocarbon
Tfi (Tmax) = 152.71 min
Tfi (Tave) = 151.56 min

Temperature x Time:

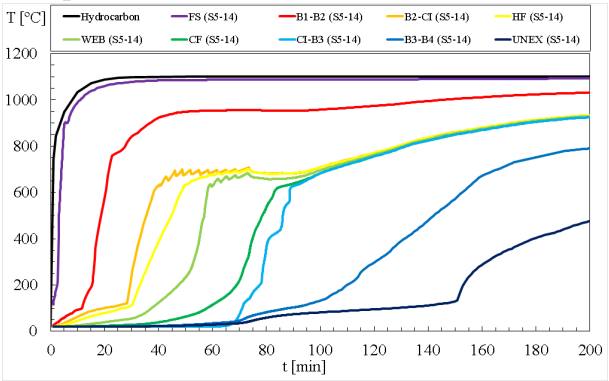

LSF Wall Configuration:

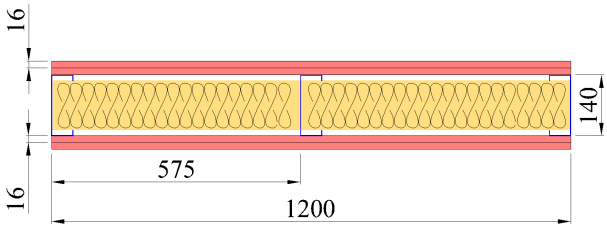

Mesh Complete Wall:

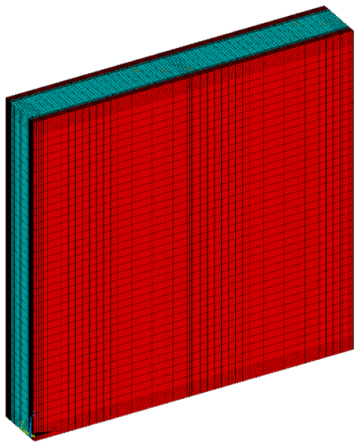

Temperature at t=3600s:

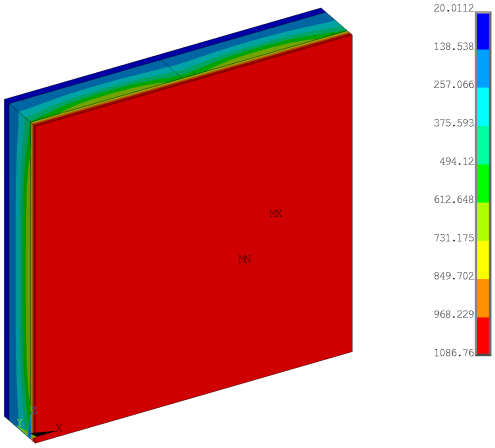

Mesh Half Wall:

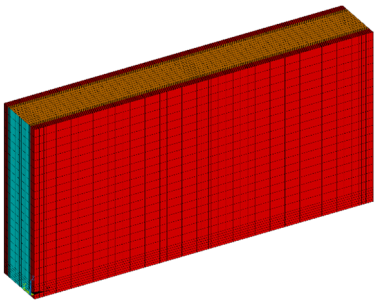

Temperature at t=3600s:

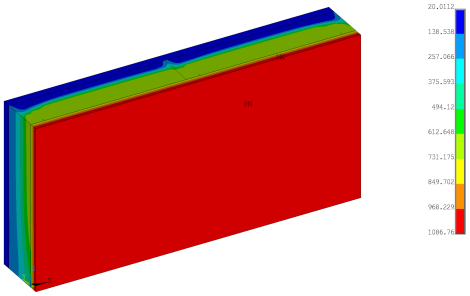

Specimen “S5” : Case 15.

STRUCTURE:
Studs: C140 (140x50x13x1.2mm)
Track: U142 (142x50x1.2 mm)
CFS wall: 1200x1200 mm
Gypsum: Type 1 (16 mm)
Rock wool: 175 kg/m^3

FIRE: Hydrocarbon
Tfi (Tmax) = 157.68 min
Tfi (Tave) = 156.77 min

Temperature x Time:

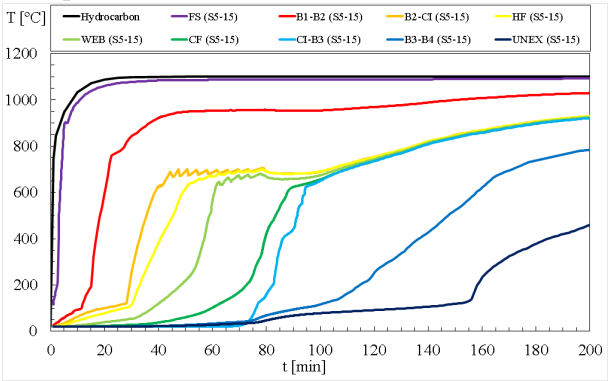

LSF Wall Configuration:

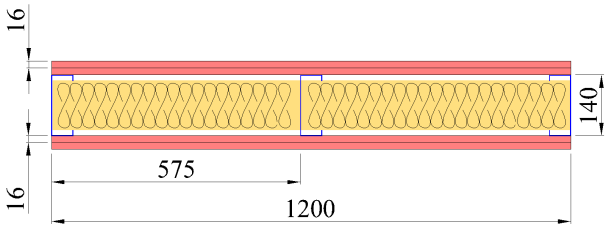

Mesh Complete Wall:

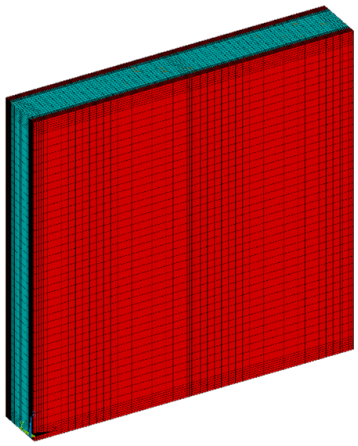

Temperature at t=3600s:

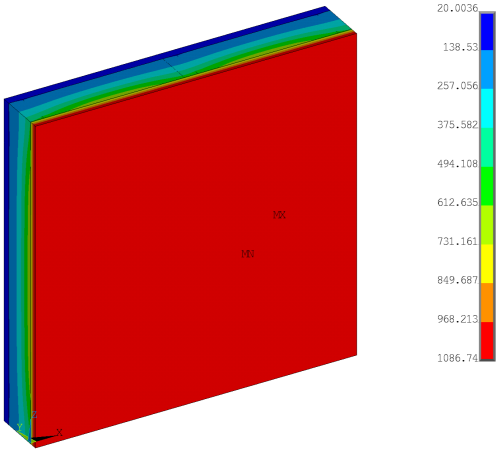

Mesh Half Wall:

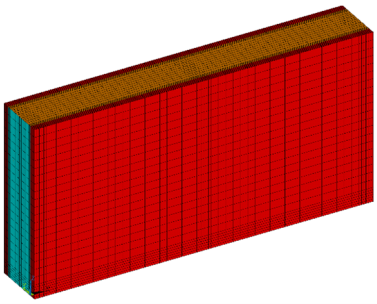

Temperature at t=3600s:

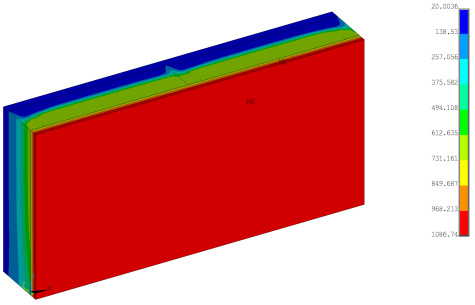

Specimen “S5” : Case 16.

STRUCTURE:
Studs: C140 (140x50x13x1.2mm)
Track: U142 (142x50x1.2 mm)
CFS wall: 1200x1200 mm
Gypsum: Type 2 (16 mm)
Rock wool: 30 kg/m^3

FIRE: Hydrocarbon
Tfi (Tmax) = 117.68 min
Tfi (Tave) = 114.42 min

Temperature x Time:

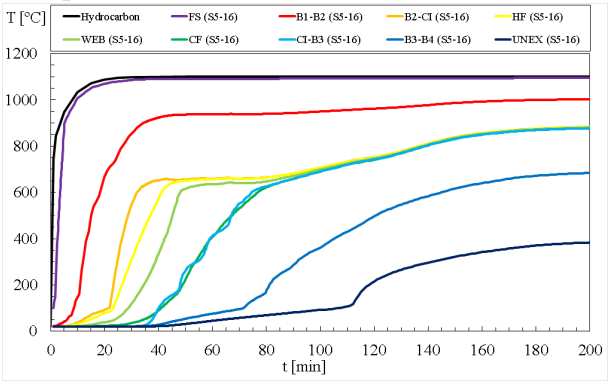

LSF Wall Configuration:

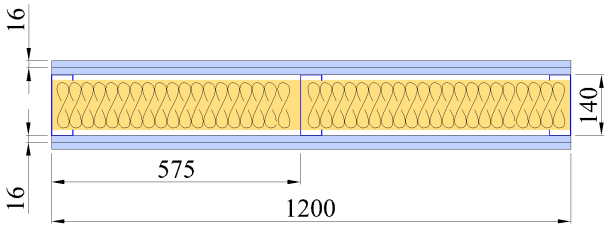

Mesh Complete Wall:

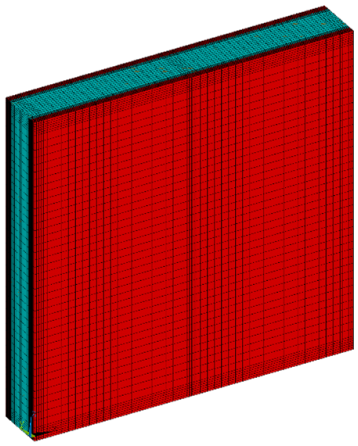

Temperature at t=3600s:

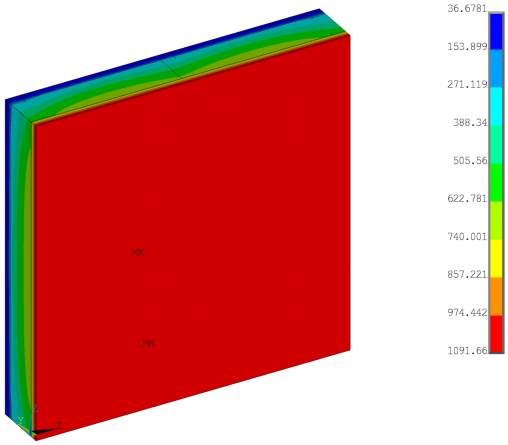

Mesh Half Wall:

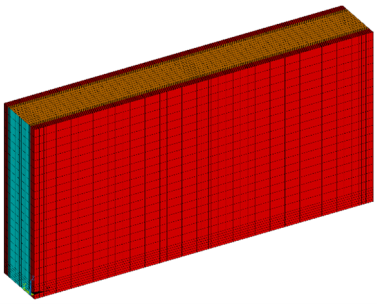

Temperature at t=3600s:

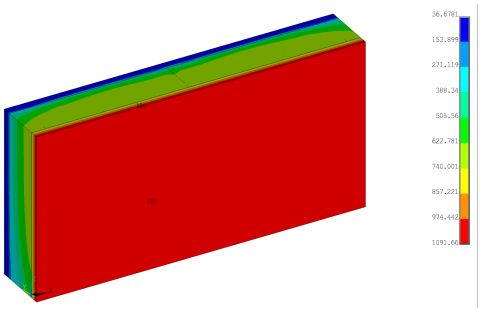

Specimen “S5” : Case 17.

STRUCTURE:
Studs: C140 (140x50x13x1.2mm)
Track: U142 (142x50x1.2 mm)
CFS wall: 1200x1200 mm
Gypsum: Type 2 (16 mm)
Rock wool: 60 kg/m^3

FIRE: Hydrocarbon
Tfi (Tmax) = 126.32 min
Tfi (Tave) = 124.8 min

Temperature x Time:

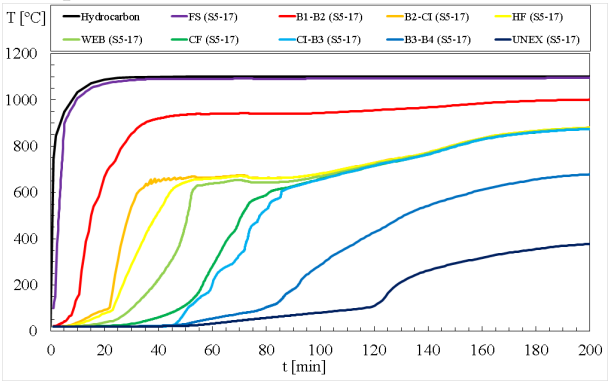

LSF Wall Configuration:

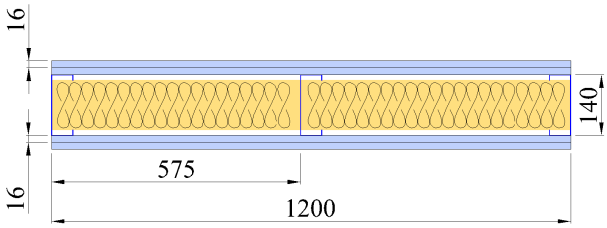

Mesh Complete Wall:

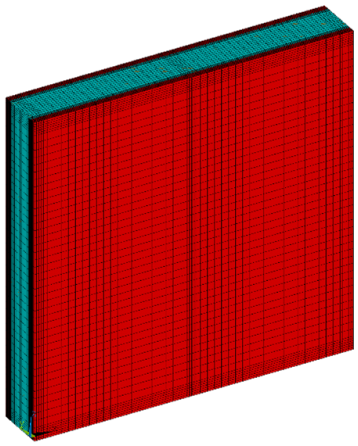

Temperature at t=3600s:

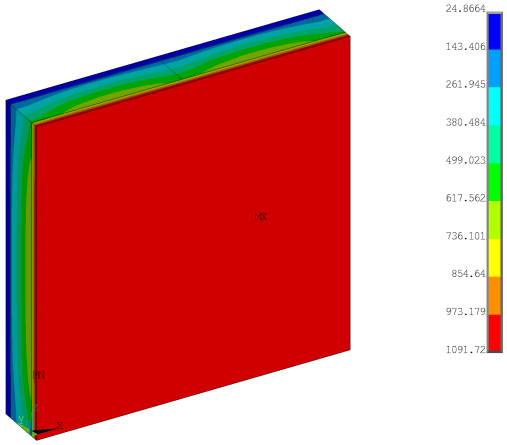

Mesh Half Wall:

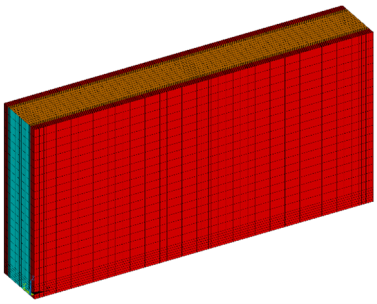

Temperature at t=3600s:

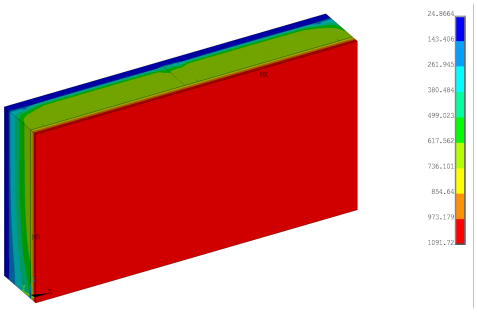

Specimen “S5” : Case 18.

STRUCTURE:
Studs: C140 (140x50x13x1.2mm)
Track: U142 (142x50x1.2 mm)
CFS wall: 1200x1200 mm
Gypsum: Type 2 (16 mm)
Rock wool: 90 kg/m^3

FIRE: Hydrocarbon
Tfi (Tmax) = 134.49 min
Tfi (Tave) = 136.01 min

Temperature x Time:

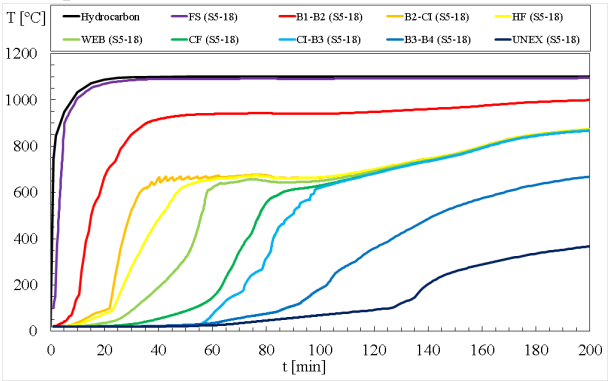

LSF Wall Configuration:

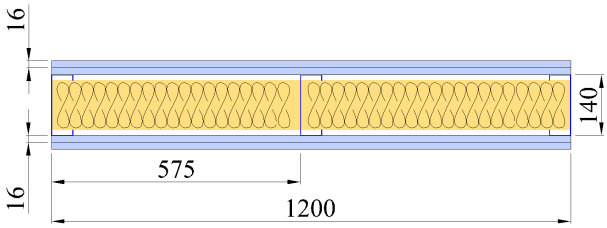

Mesh Complete Wall:

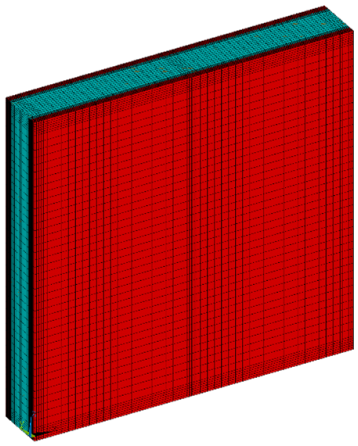

Temperature at t=3600s:

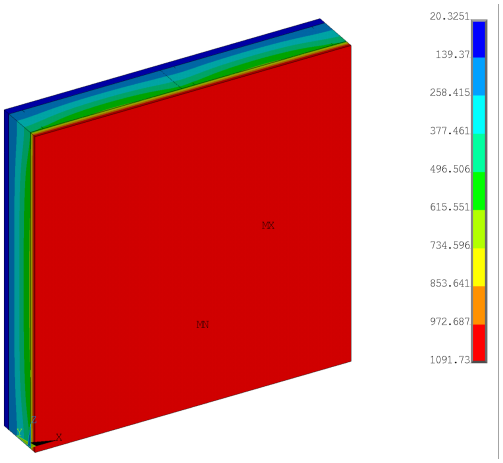

Mesh Half Wall:

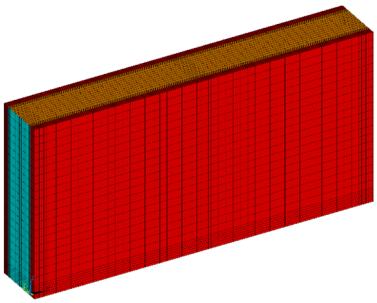

Temperature at t=3600s:

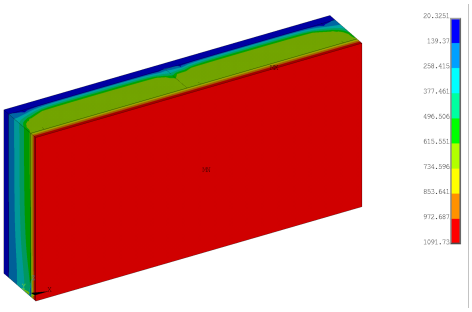

Specimen “S5” : Case 19.

STRUCTURE:
Studs: C140 (140x50x13x1.2mm)
Track: U142 (142x50x1.2 mm)
CFS wall: 1200x1200 mm
Gypsum: Type 2 (16 mm)
Rock wool: 150 kg/m^3

FIRE: Hydrocarbon
Tfi (Tmax) = 152.21 min
Tfi (Tave) = 156.58 min

Temperature x Time:

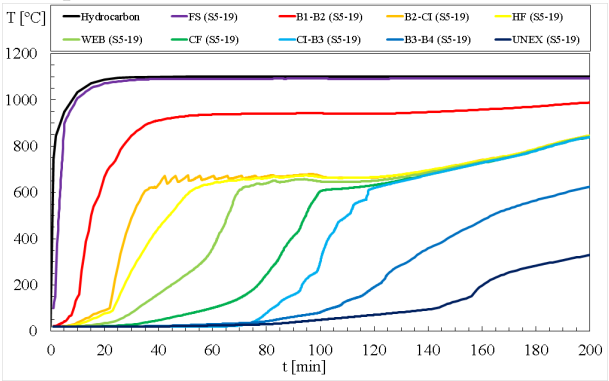

LSF Wall Configuration:

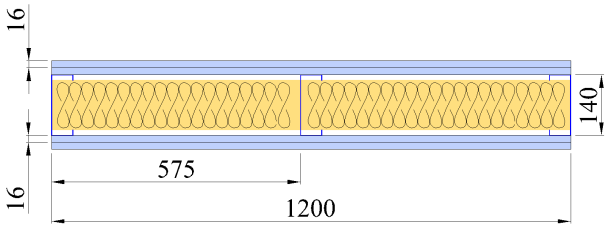

Mesh Complete Wall:

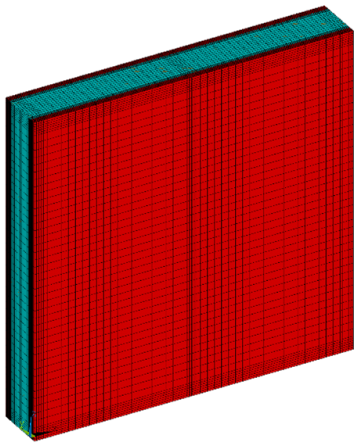

Temperature at t=3600s:

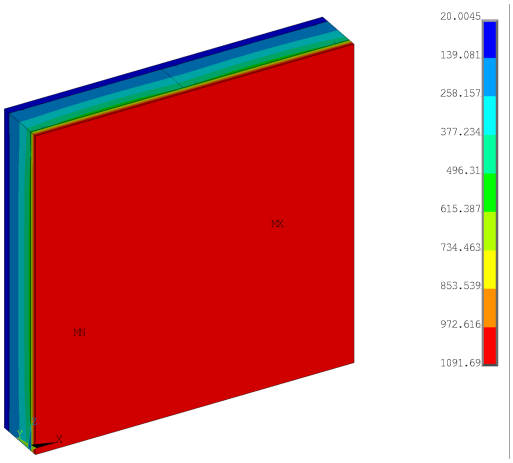

Mesh Half Wall:

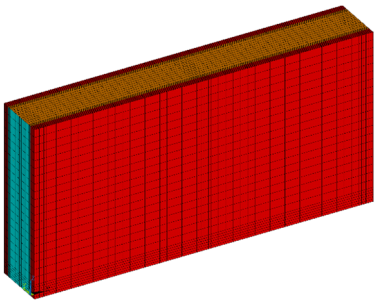

Temperature at t=3600s:

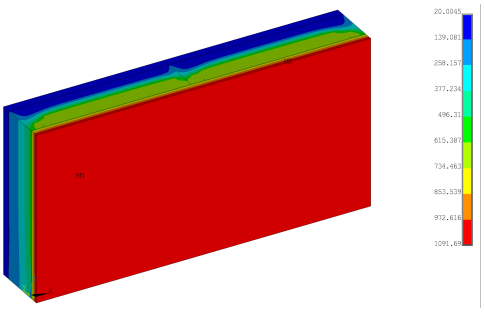

Specimen “S5” : Case 20.

STRUCTURE:
Studs: C140 (140x50x13x1.2mm)
Track: U142 (142x50x1.2 mm)
CFS wall: 1200x1200 mm
Gypsum: Type 2 (16 mm)
Rock wool: 175 kg/m^3

FIRE: Hydrocarbon
Tfi (Tmax) = 159.54 min
Tfi (Tave) = 165.07 min

Temperature x Time:

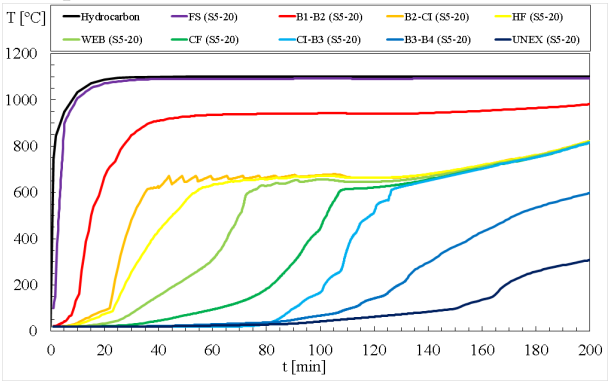

LSF Wall Configuration:

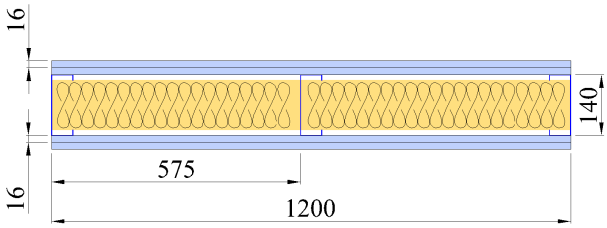

Mesh Complete Wall:

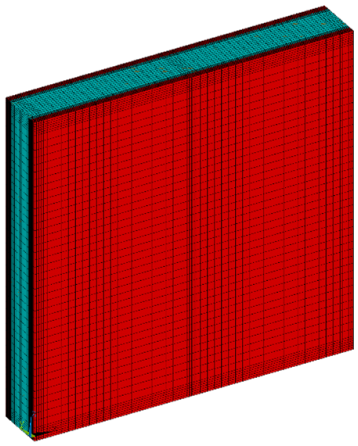

Temperature at t=3600s:

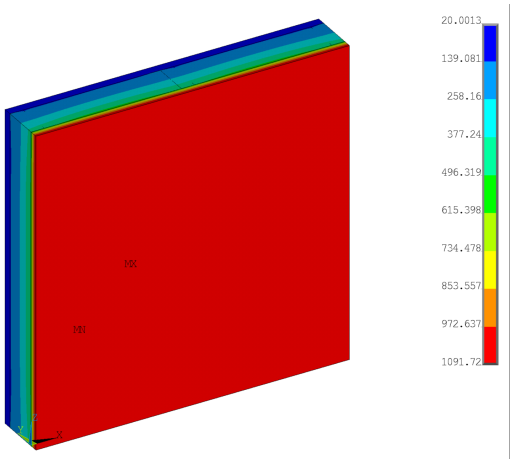

Mesh Half Wall:

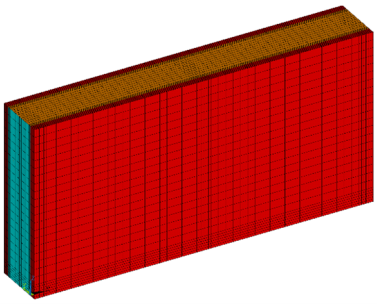

Temperature at t=3600s:

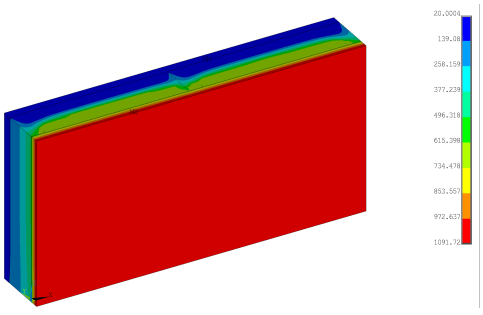

Specimen “S9” : Case 1.

STRUCTURE: Studs: C140 (140x50x13x1.2mm) Track: U142 (142x50x1.2 mm) CFS wall: 1200x1200 mm Gypsum: Type 1 (12 mm) Rock wool: 30 kg/m^3	FIRE: Hydrocarbon Tfi (Tmax) = 160.83 min Tfi (Tave) = 160.74 min
Temperature x Time: 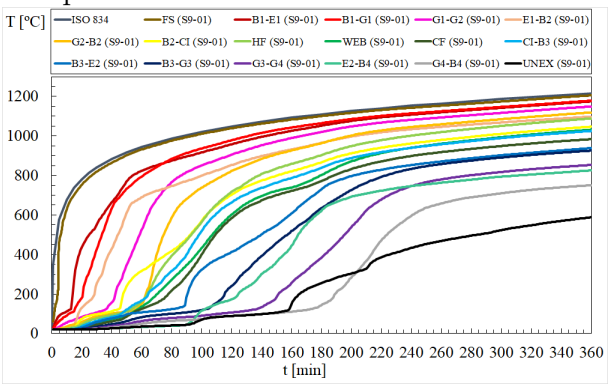	LSF Wall Configuration: 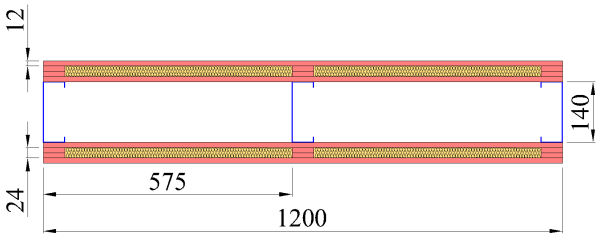
Mesh Complete Wall: 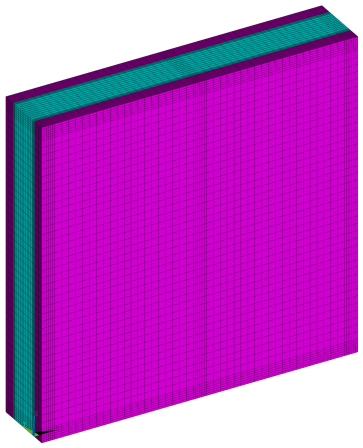	Temperature at t=3600s: 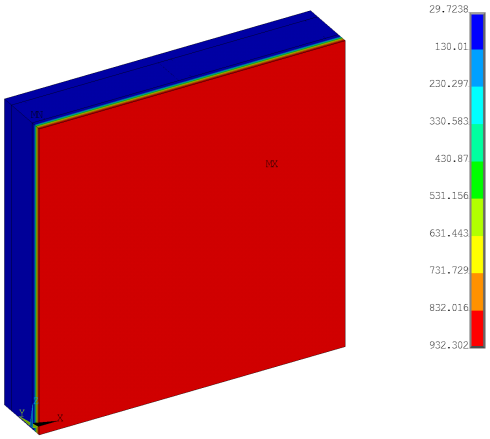
Mesh Half Wall: 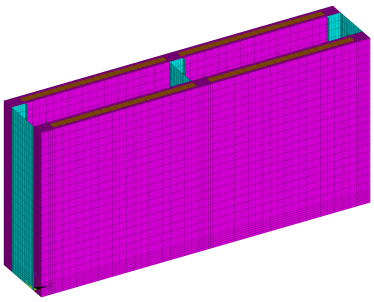	Temperature at t=3600s: 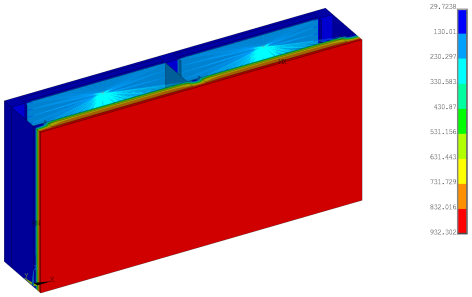

Specimen “S9” : Case 2.

STRUCTURE:
Studs: C140 (140x50x13x1.2mm)
Track: U142 (142x50x1.2 mm)
CFS wall: 1200x1200 mm
Gypsum: Type 1 (12 mm)
Rock wool: 60 kg/m^3

FIRE: Hydrocarbon
Tfi (Tmax) = 188.3 min
Tfi (Tave) = 188.48 min

Temperature x Time:

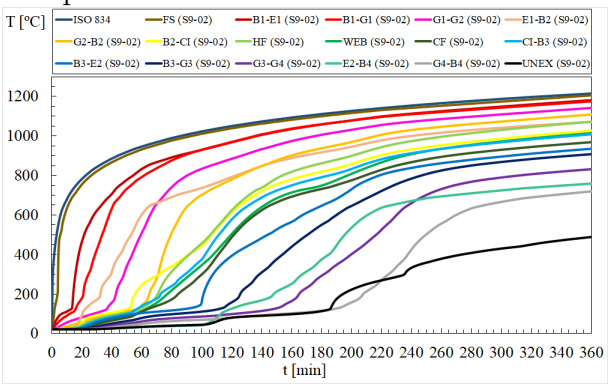

LSF Wall Configuration:

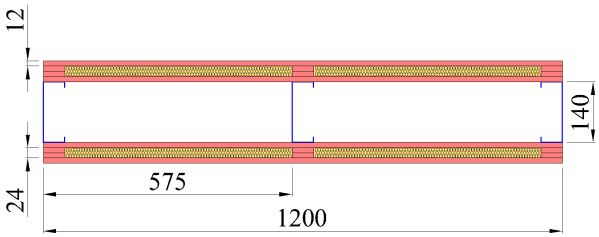

Mesh Complete Wall:

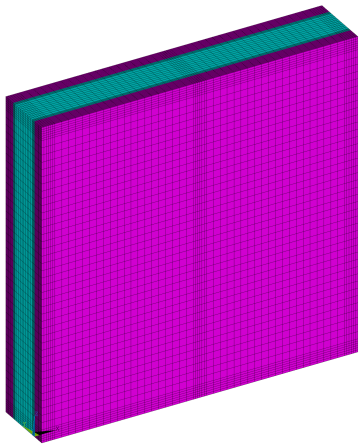

Temperature at t=3600s:

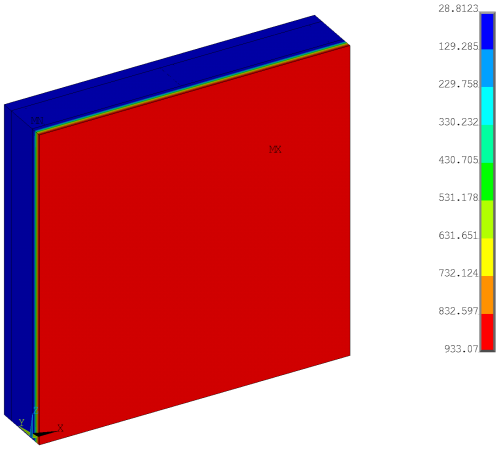

Mesh Half Wall:

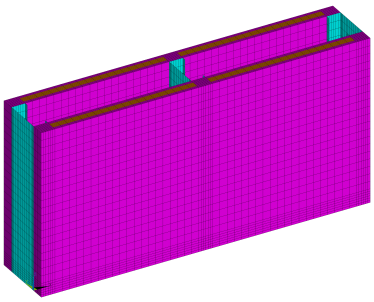

Temperature at t=3600s:

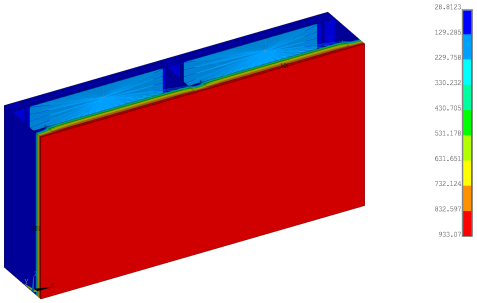

Specimen “S9” : Case 3.

STRUCTURE:
Studs: C140 (140x50x13x1.2mm)
Track: U142 (142x50x1.2 mm)
CFS wall: 1200x1200 mm
Gypsum: Type 1 (12 mm)
Rock wool: 90 kg/m^3

FIRE: Hydrocarbon
Tfi (Tmax) = 202.9 min
Tfi (Tave) = 203.02 min

Temperature x Time:

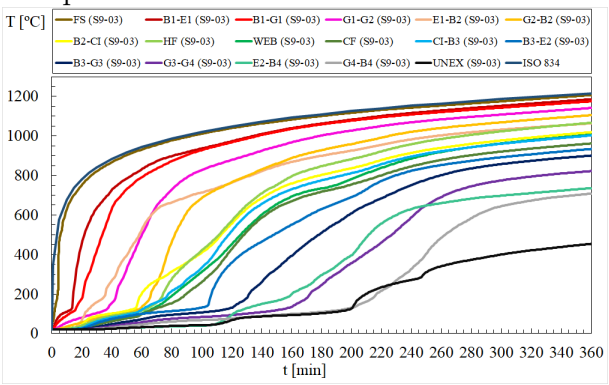

LSF Wall Configuration:

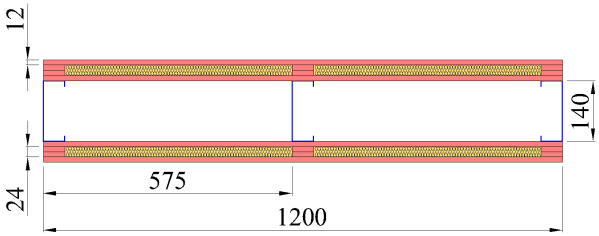

Mesh Complete Wall:

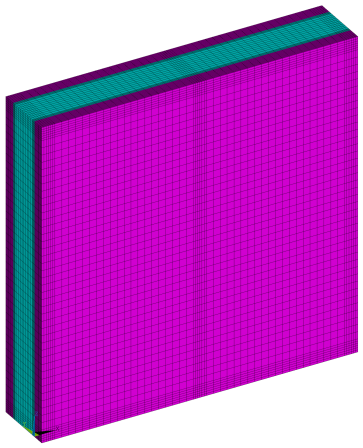

Temperature at t=3600s:

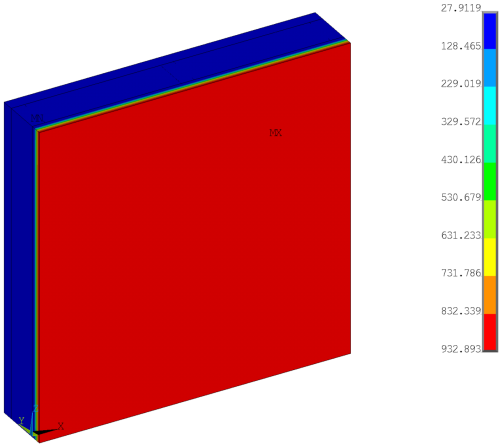

Mesh Half Wall:

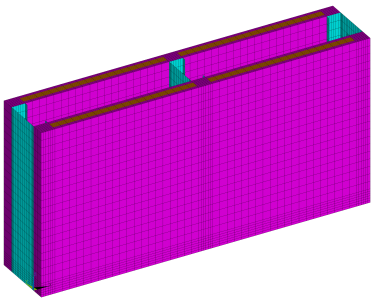

Temperature at t=3600s:

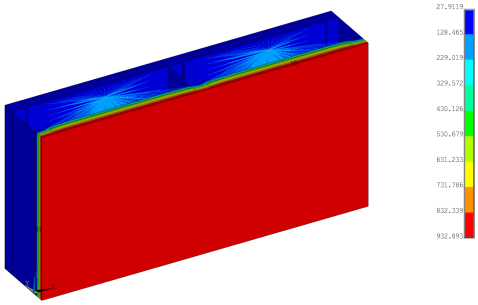

Specimen “S9” : Case 4.

STRUCTURE:
Studs: C140 (140x50x13x1.2mm)
Track: U142 (142x50x1.2 mm)
CFS wall: 1200x1200 mm
Gypsum: Type 1 (12 mm)
Rock wool: 150 kg/m^3

FIRE: Hydrocarbon
Tfi (Tmax) = 211.48 min
Tfi (Tave) = 211.54 min

Temperature x Time:

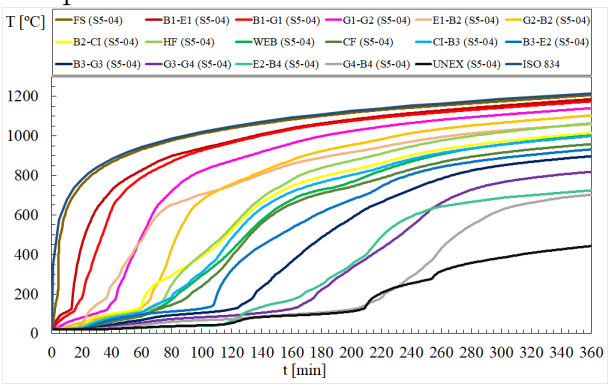

LSF Wall Configuration:

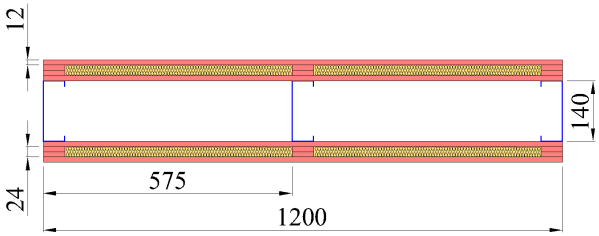

Mesh Complete Wall:

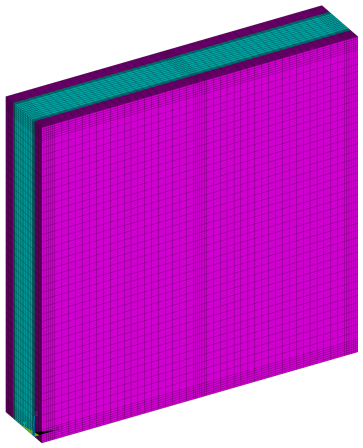

Temperature at t=3600s:

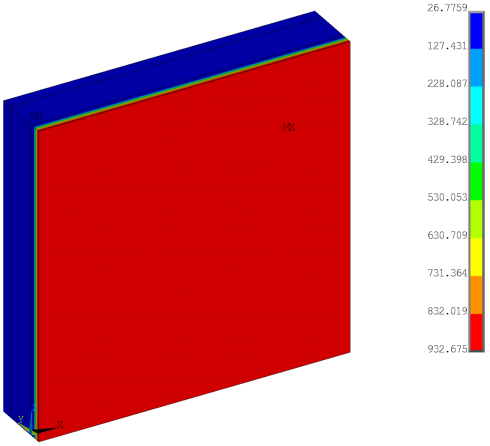

Mesh Half Wall:

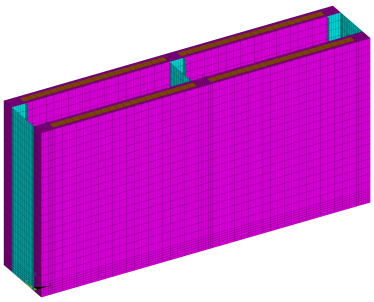

Temperature at t=3600s:

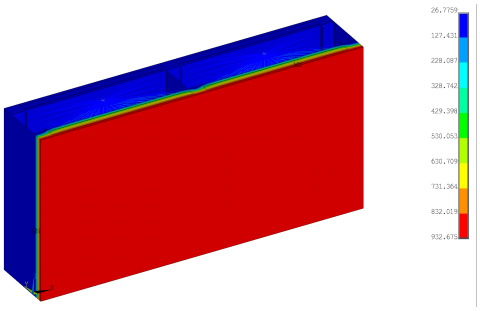

Specimen “S9” : Case 5.

STRUCTURE:
Studs: C140 (140x50x13x1.2mm)
Track: U142 (142x50x1.2 mm)
CFS wall: 1200x1200 mm
Gypsum: Type 1 (12 mm)
Rock wool: 175 kg/m^3

FIRE: Hydrocarbon
Tfi (Tmax) = 213.57 min
Tfi (Tave) = 213.71 min

Temperature x Time:

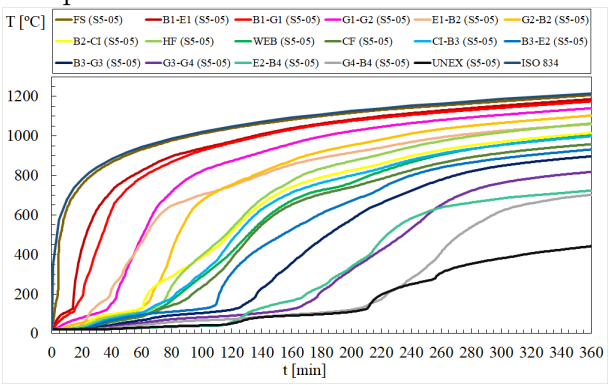

LSF Wall Configuration:

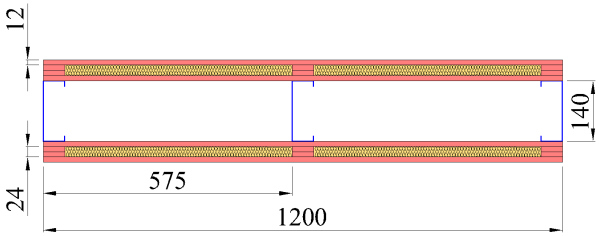

Mesh Complete Wall:

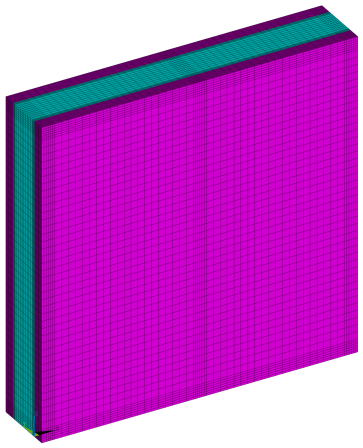

Temperature at t=3600s:

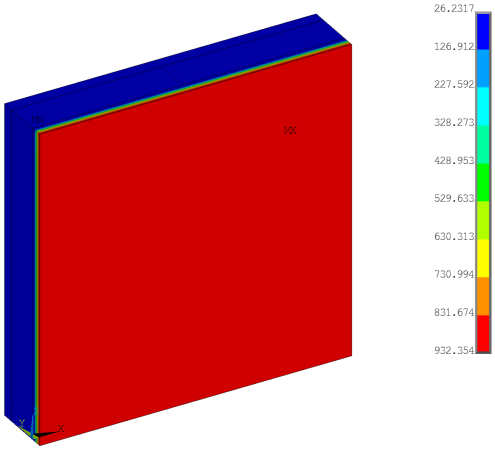

Mesh Half Wall:

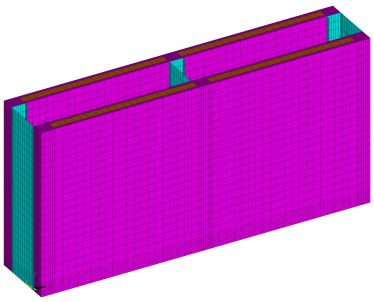

Temperature at t=3600s:

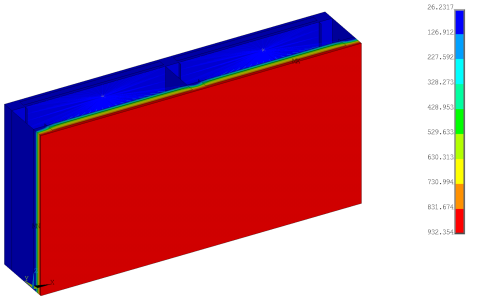

Specimen “S9” : Case 6.

STRUCTURE:
Studs: C140 (140x50x13x1.2mm)
Track: U142 (142x50x1.2 mm)
CFS wall: 1200x1200 mm
Gypsum: Type 2 (12 mm)
Rock wool: 30 kg/m^3

FIRE: Hydrocarbon
Tfi (Tmax) = 133.2 min
Tfi (Tave) = 134.07 min

Temperature x Time:

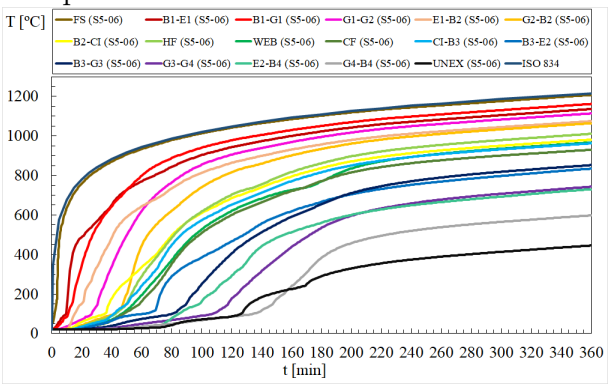

LSF Wall Configuration:

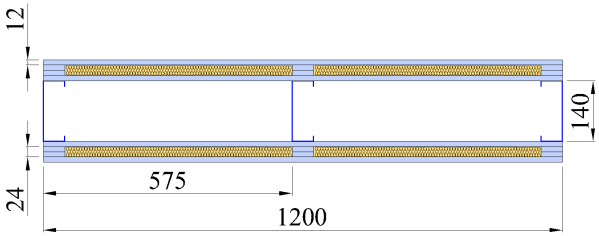

Mesh Complete Wall:

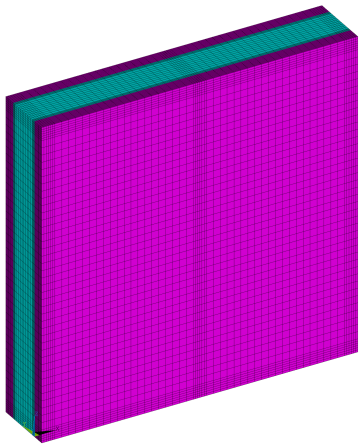

Temperature at t=3600s:

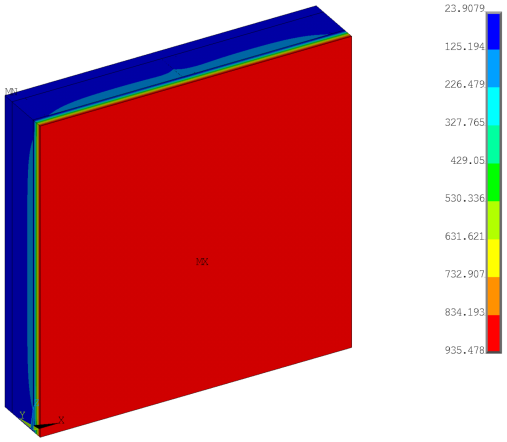

Mesh Half Wall:

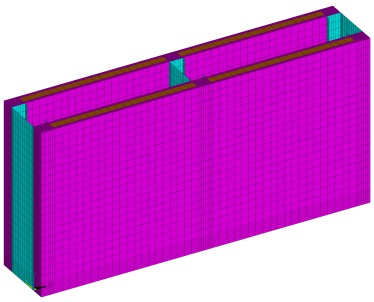

Temperature at t=3600s:

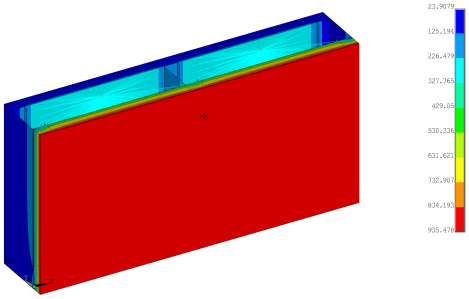

Specimen “S9” : Case 7.

STRUCTURE:
Studs: C140 (140x50x13x1.2mm)
Track: U142 (142x50x1.2 mm)
CFS wall: 1200x1200 mm
Gypsum: Type 2 (12 mm)
Rock wool: 60 kg/m^3

FIRE: Hydrocarbon
Tfi (Tmax) = 157.77 min
Tfi (Tave) = 158.25 min

Temperature x Time:

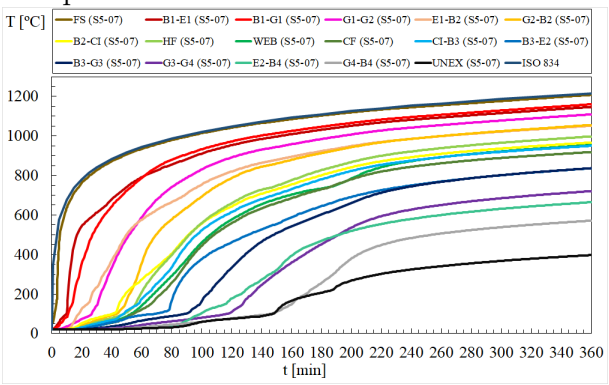

LSF Wall Configuration:

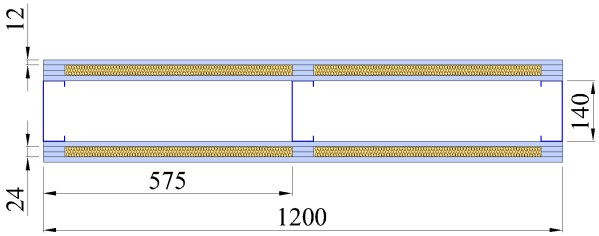

Mesh Complete Wall:

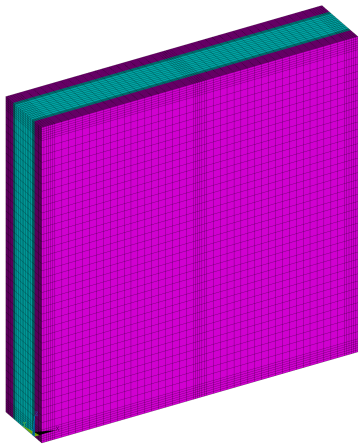

Temperature at t=3600s:

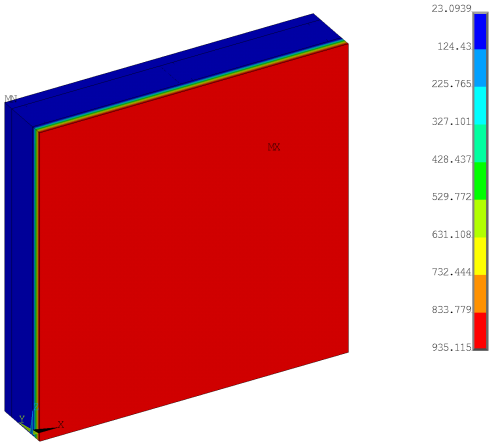

Mesh Half Wall:

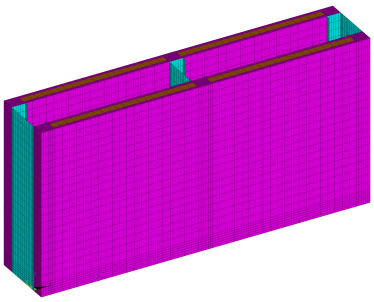

Temperature at t=3600s:

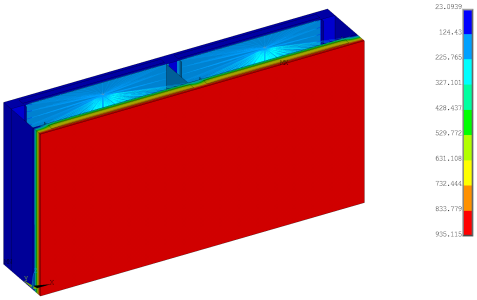

Specimen “S9” : Case 8.

STRUCTURE:
Studs: C140 (140x50x13x1.2mm)
Track: U142 (142x50x1.2 mm)
CFS wall: 1200x1200 mm
Gypsum: Type 2 (12 mm)
Rock wool: 90 kg/m^3

FIRE: Hydrocarbon
Tfi (Tmax) = 171.81 min
Tfi (Tave) = 171.6 min

Temperature x Time:

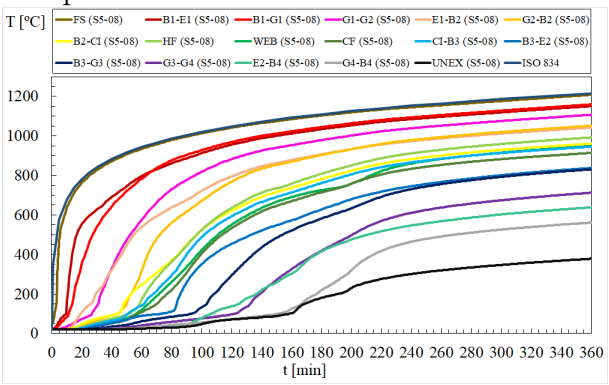

LSF Wall Configuration:

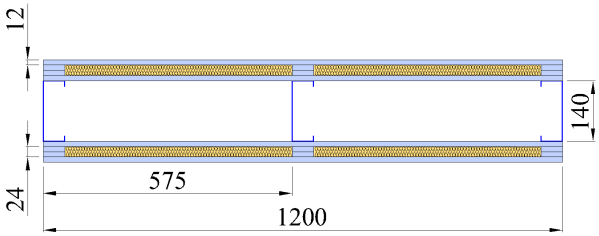

Mesh Complete Wall:

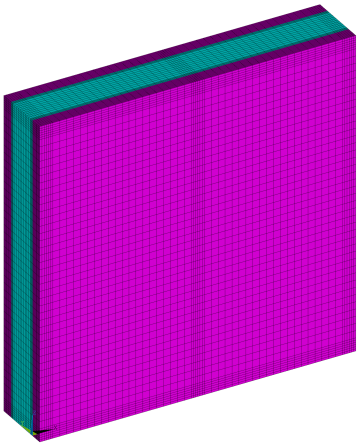

Temperature at t=3600s:

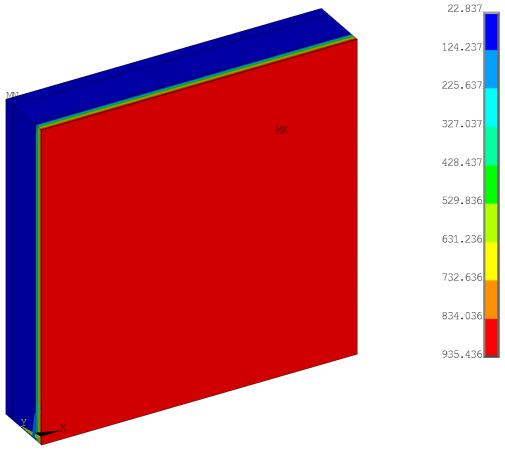

Mesh Half Wall:

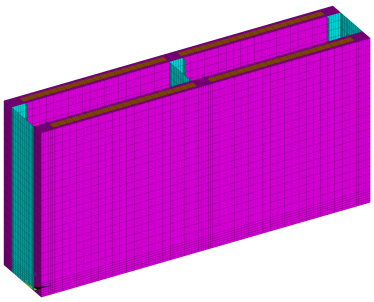

Temperature at t=3600s:

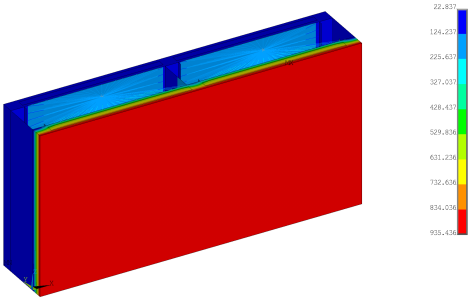

Specimen “S9” : Case 9.

STRUCTURE: Studs: C140 (140x50x13x1.2mm) Track: U142 (142x50x1.2 mm) CFS wall: 1200x1200 mm Gypsum: Type 2 (12 mm) Rock wool: 150 kg/m^3	FIRE: Hydrocarbon Tfi (Tmax) = 182.1 min Tfi (Tave) = 181.68 min
Temperature x Time: 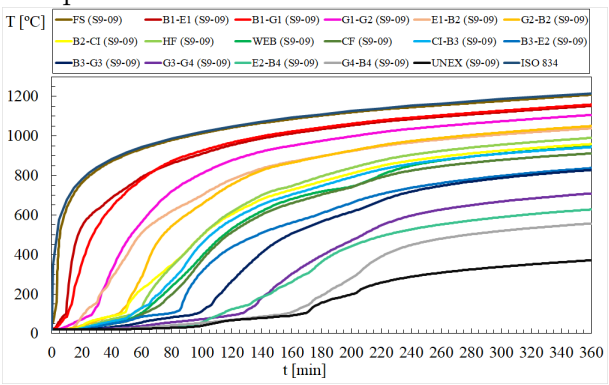	LSF Wall Configuration: 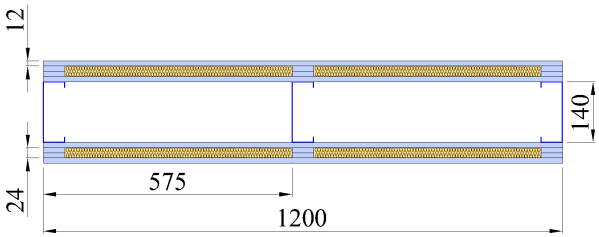
Mesh Complete Wall: 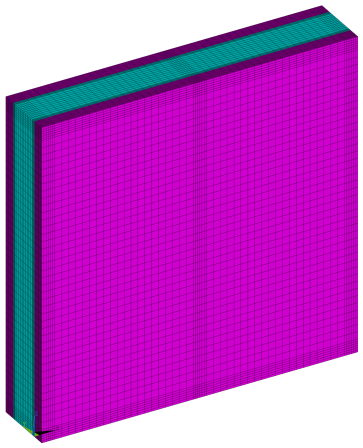	Temperature at t=3600s: 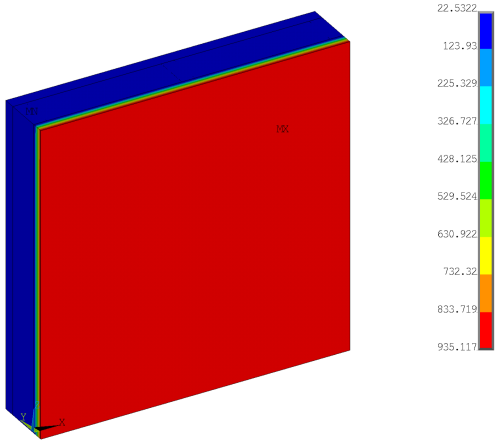
Mesh Half Wall: 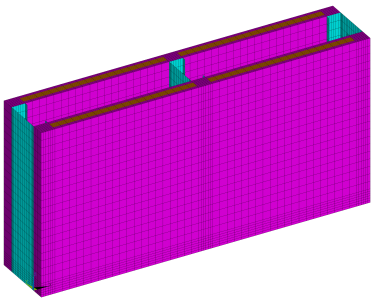	Temperature at t=3600s: 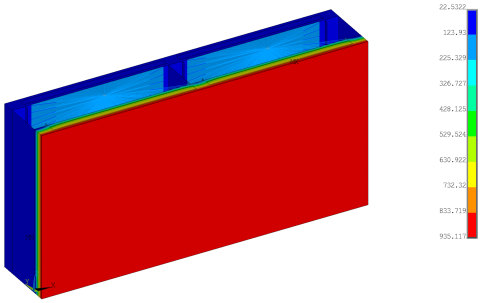

Specimen “S9” : Case 10.

STRUCTURE:
Studs: C140 (140x50x13x1.2mm)
Track: U142 (142x50x1.2 mm)
CFS wall: 1200x1200 mm
Gypsum: Type 2 (12 mm)
Rock wool: 175 kg/m^3

FIRE: Hydrocarbon
Tfi (Tmax) = 184.83 min
Tfi (Tave) = 184.25 min

Temperature x Time:

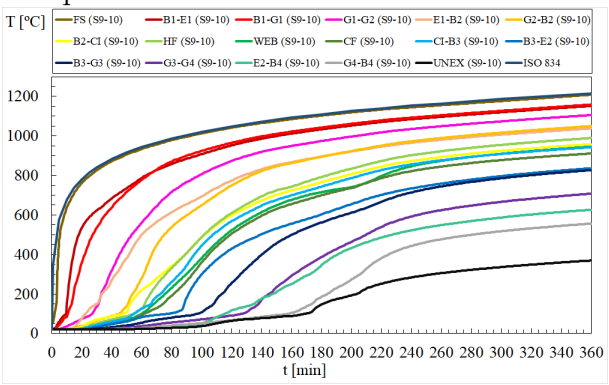

LSF Wall Configuration:

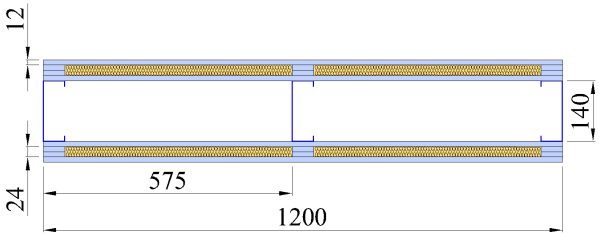

Mesh Complete Wall:

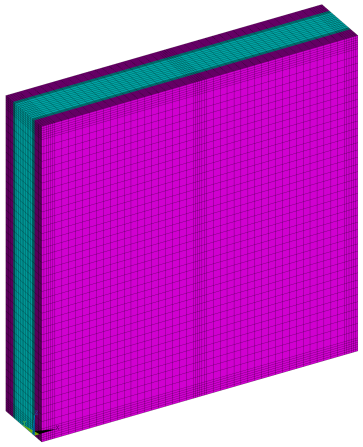

Temperature at t=3600s:

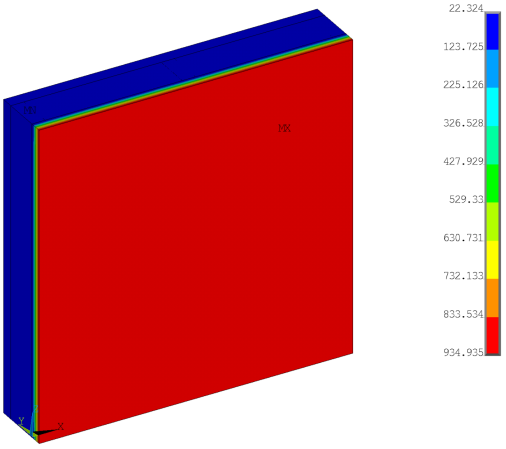

Mesh Half Wall:

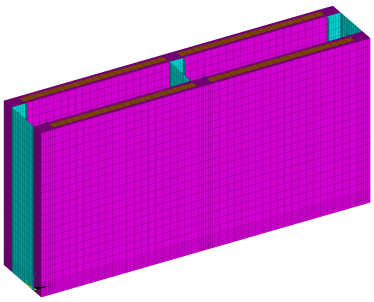

Temperature at t=3600s:

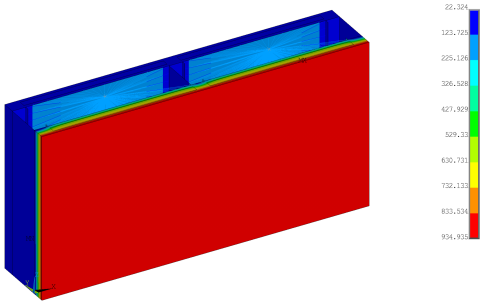

Specimen “S9” : Case 11.

STRUCTURE:
Studs: C140 (140x50x13x1.2mm)
Track: U142 (142x50x1.2 mm)
CFS wall: 1200x1200 mm
Gypsum: Type 1 (16 mm)
Rock wool: 30 kg/m^3

FIRE: Hydrocarbon
Tfi (Tmax) = 220.02 min
Tfi (Tave) = 220.17 min

Temperature x Time:

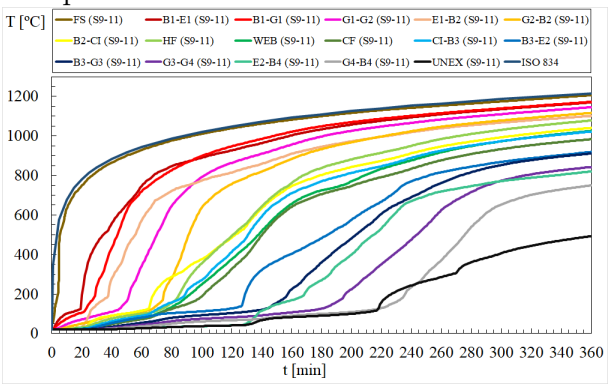

LSF Wall Configuration:

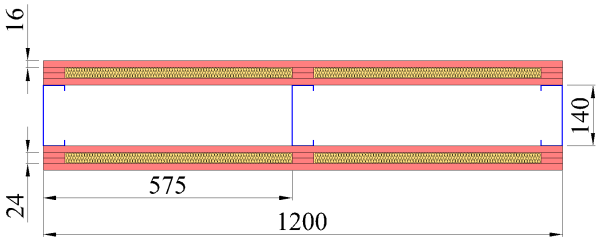

Mesh Complete Wall:

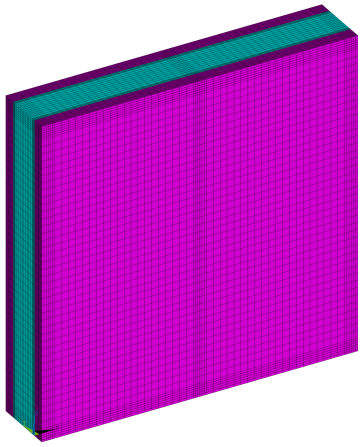

Temperature at t=3600s:

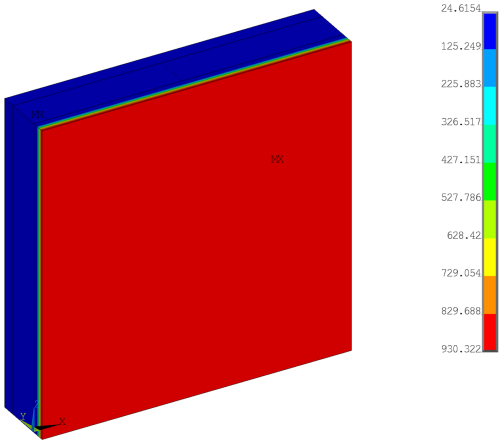

Mesh Half Wall:

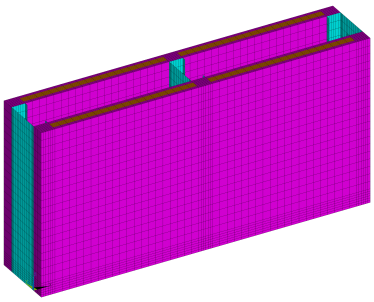

Temperature at t=3600s:

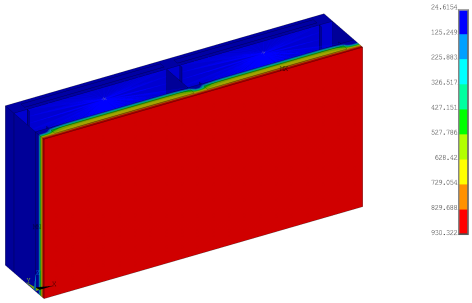

Specimen “S9” : Case 12.

STRUCTURE: Studs: C140 (140x50x13x1.2mm) Track: U142 (142x50x1.2 mm) CFS wall: 1200x1200 mm Gypsum: Type 1 (16 mm) Rock wool: 60 kg/m^3	FIRE: Hydrocarbon Tfi (Tmax) = 250.12 min Tfi (Tave) = 250.37 min
Temperature x Time: 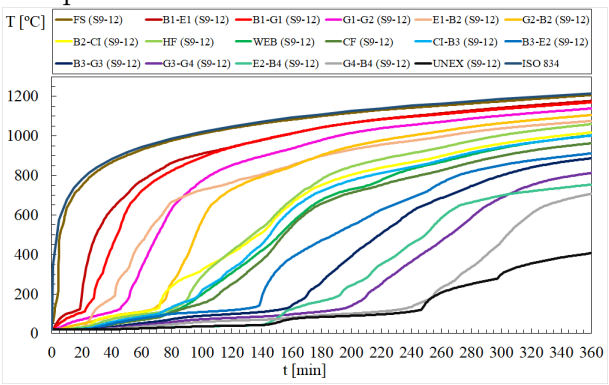	LSF Wall Configuration: 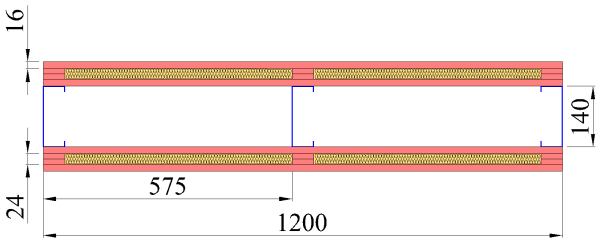
Mesh Complete Wall: 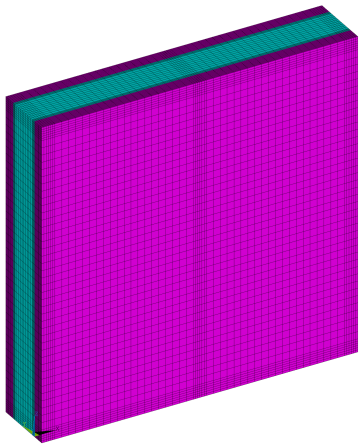	Temperature at t=3600s: 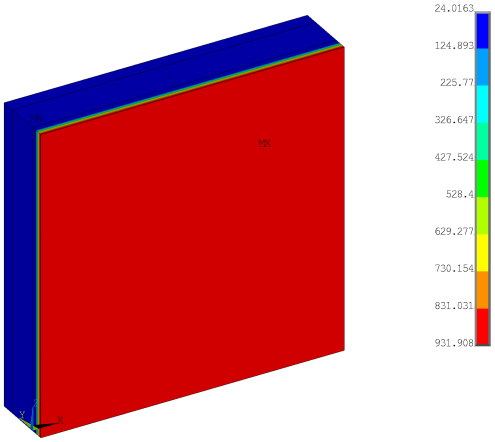
Mesh Half Wall: 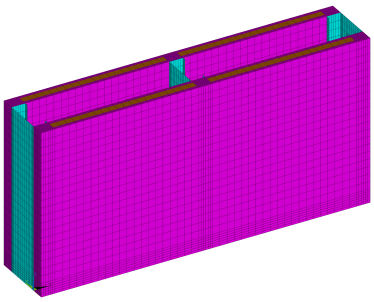	Temperature at t=3600s: 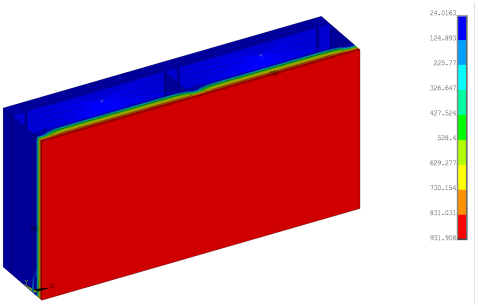

Specimen “S9” : Case 13.

STRUCTURE: Studs: C140 (140x50x13x1.2mm) Track: U142 (142x50x1.2 mm) CFS wall: 1200x1200 mm Gypsum: Type 1 (16 mm) Rock wool: 90 kg/m^3	FIRE: Hydrocarbon Tfi (Tmax) = 265.9 min Tfi (Tave) = 265.91 min
Temperature x Time: 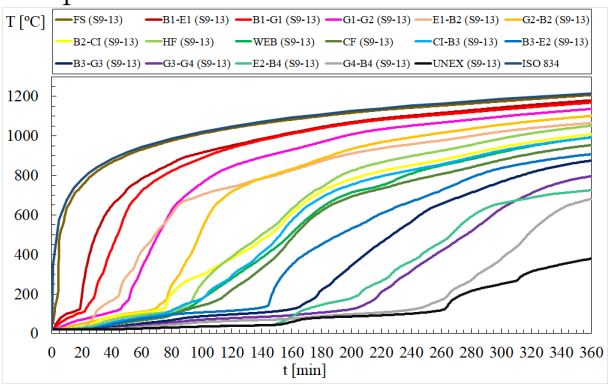	LSF Wall Configuration: 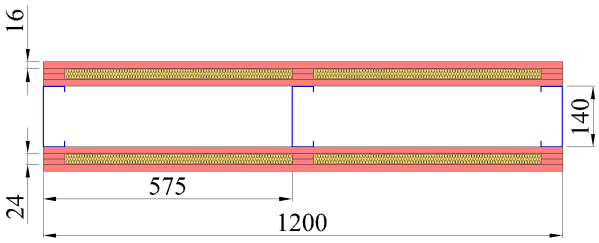
Mesh Complete Wall: 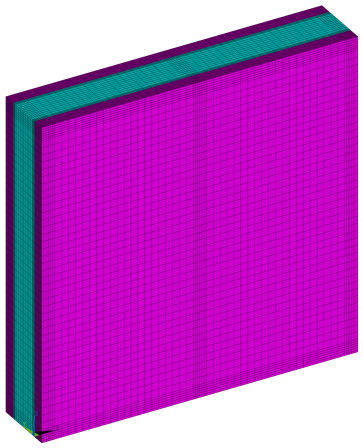	Temperature at t=3600s: 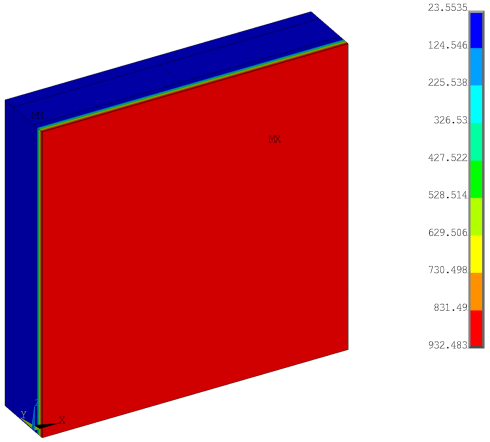
Mesh Half Wall: 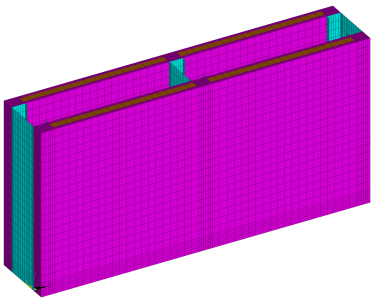	Temperature at t=3600s: 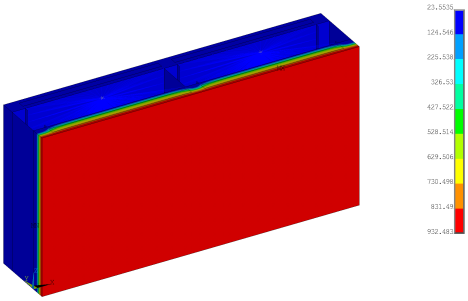

Specimen “S9” : Case 14.

STRUCTURE:
Studs: C140 (140x50x13x1.2mm)
Track: U142 (142x50x1.2 mm)
CFS wall: 1200x1200 mm
Gypsum: Type 1 (16 mm)
Rock wool: 150 kg/m^3

FIRE: Hydrocarbon
Tfi (Tmax) = 276 min
Tfi (Tave) = 275.89 min

Temperature x Time:

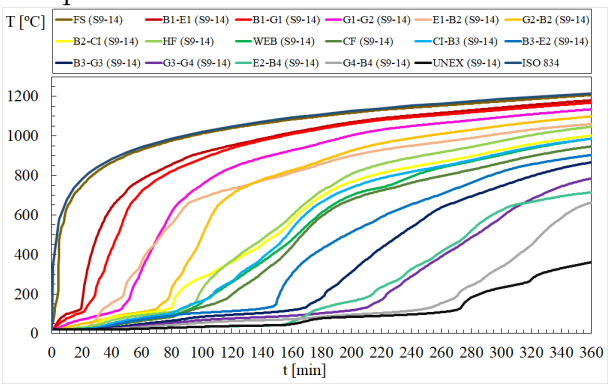

LSF Wall Configuration:

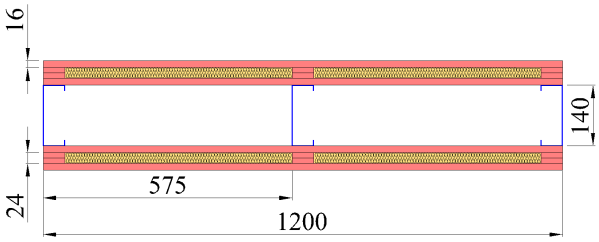

Mesh Complete Wall:

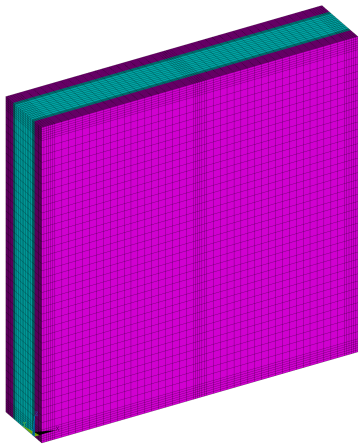

Temperature at t=3600s:

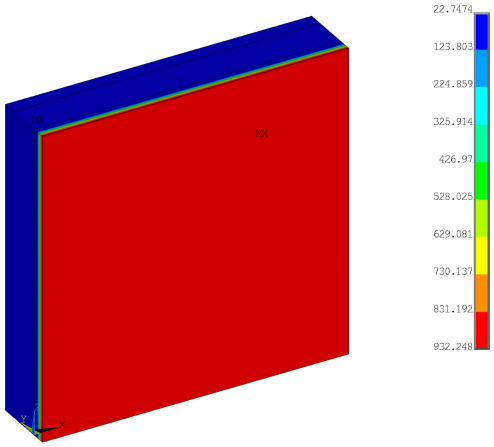

Mesh Half Wall:

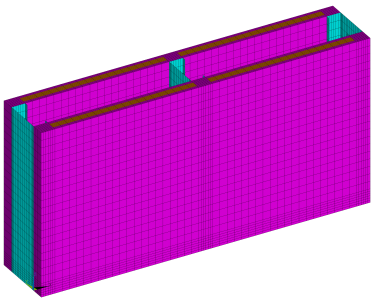

Temperature at t=3600s:

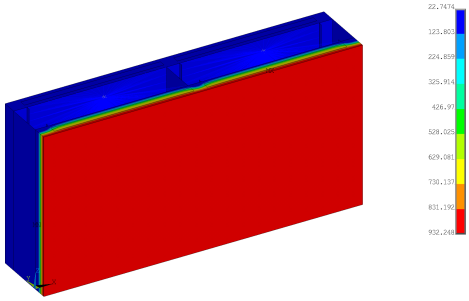

Specimen “S9” : Case 15.

STRUCTURE:
Studs: C140 (140x50x13x1.2mm)
Track: U142 (142x50x1.2 mm)
CFS wall: 1200x1200 mm
Gypsum: Type 1 (16 mm)
Rock wool: 175 kg/m^3

FIRE: Hydrocarbon
Tfi (Tmax) = 278.09 min
Tfi (Tave) = 278.09 min

Temperature x Time:

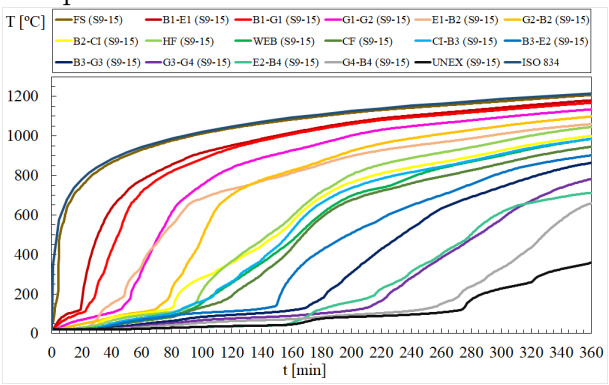

LSF Wall Configuration:

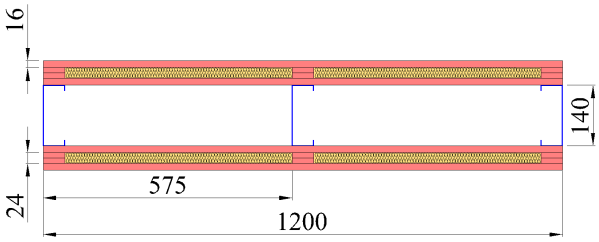

Mesh Complete Wall:

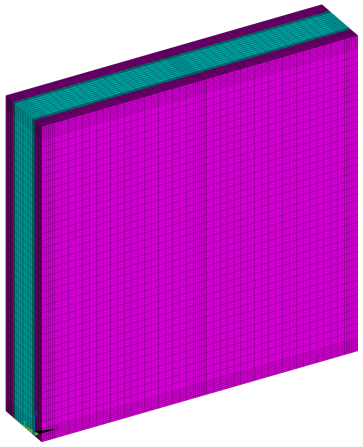

Temperature at t=3600s:

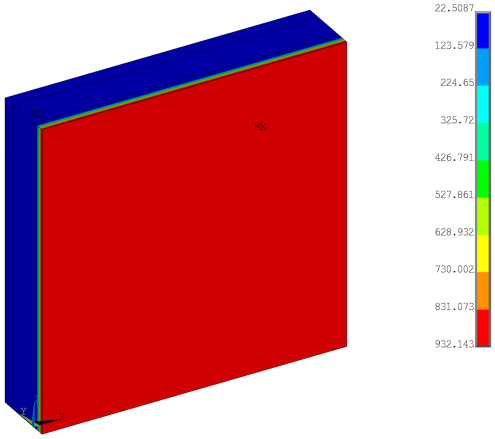

Mesh Half Wall:

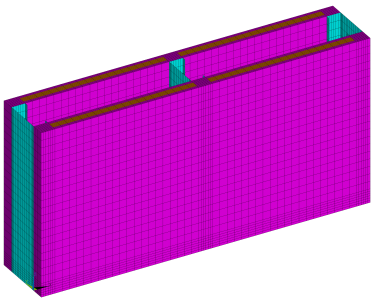

Temperature at t=3600s:

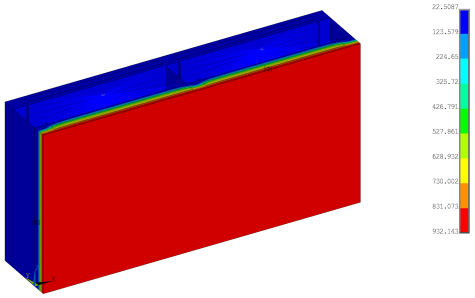

Specimen “S9” : Case 16.

STRUCTURE:
Studs: C140 (140x50x13x1.2mm)
Track: U142 (142x50x1.2 mm)
CFS wall: 1200x1200 mm
Gypsum: Type 2 (16 mm)
Rock wool: 30 kg/m^3

FIRE: Hydrocarbon
Tfi (Tmax) = 191.88 min
Tfi (Tave) = 192.6 min

Temperature x Time:

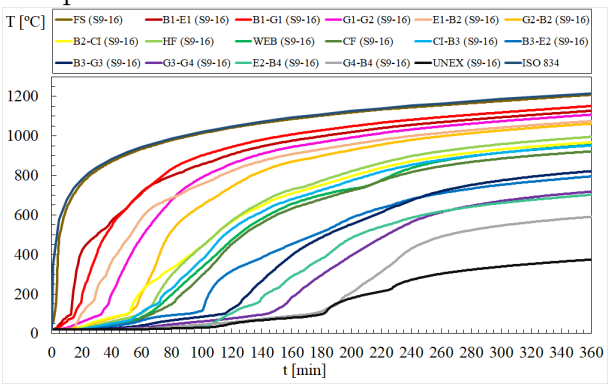

LSF Wall Configuration:

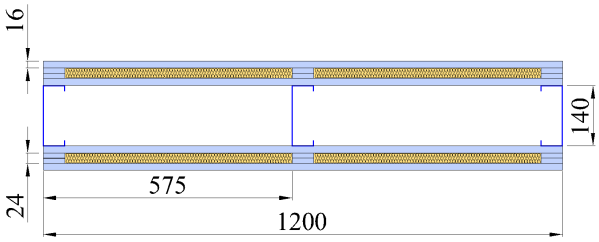

Mesh Complete Wall:

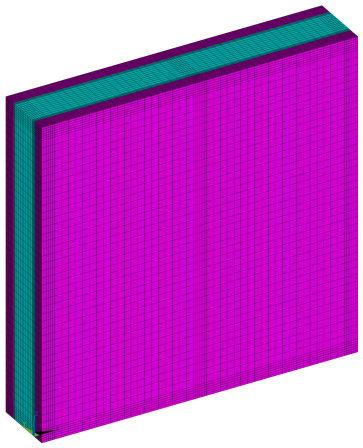

Temperature at t=3600s:

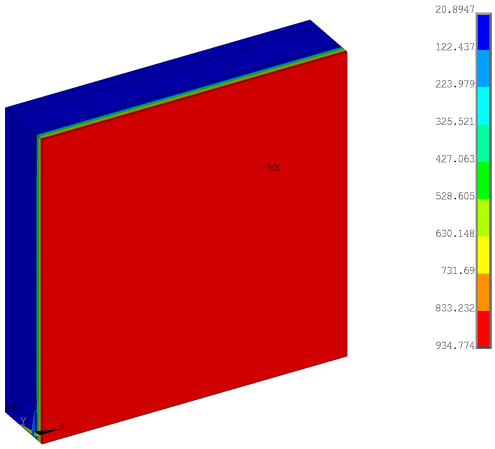

Mesh Half Wall:

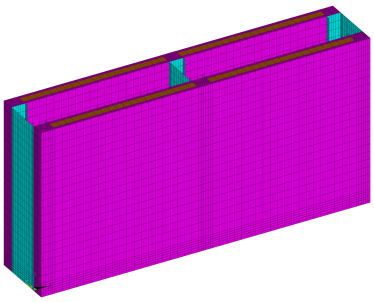

Temperature at t=3600s:

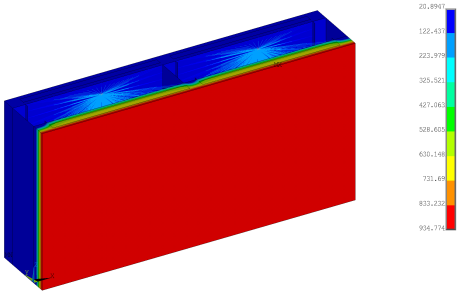

Specimen “S9” : Case 17.

STRUCTURE:
Studs: C140 (140x50x13x1.2mm)
Track: U142 (142x50x1.2 mm)
CFS wall: 1200x1200 mm
Gypsum: Type 2 (16 mm)
Rock wool: 60 kg/m^3

FIRE: Hydrocarbon
Tfi (Tmax) = 220.51 min
Tfi (Tave) = 220.44 min

Temperature x Time:

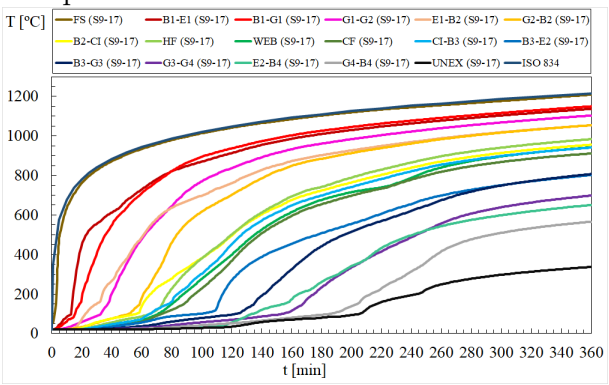

LSF Wall Configuration:

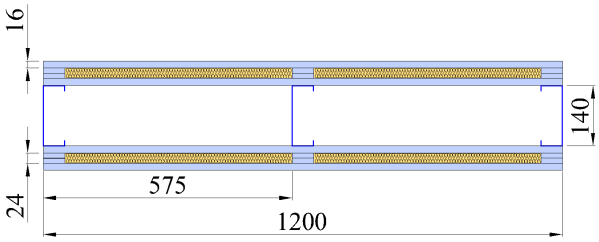

Mesh Complete Wall:

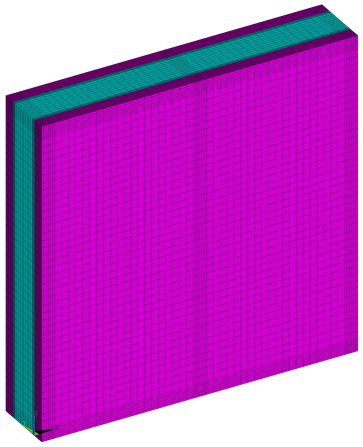

Temperature at t=3600s:

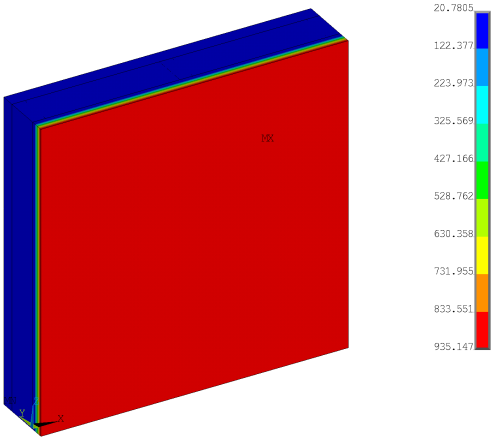

Mesh Half Wall:

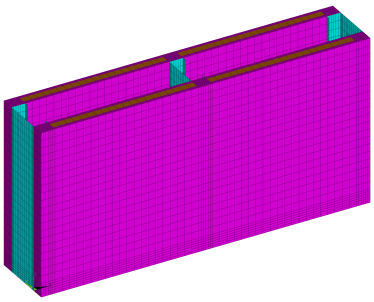

Temperature at t=3600s:

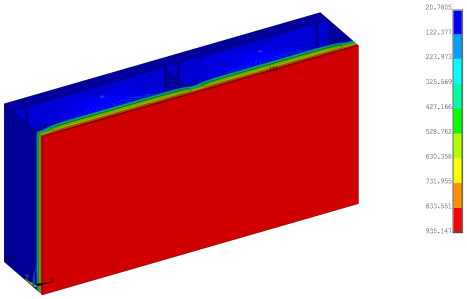

Specimen “S9” : Case 18.

STRUCTURE:
Studs: C140 (140x50x13x1.2mm)
Track: U142 (142x50x1.2 mm)
CFS wall: 1200x1200 mm
Gypsum: Type 2 (16 mm)
Rock wool: 90 kg/m^3

FIRE: Hydrocarbon
Tfi (Tmax) = 236.07 min
Tfi (Tave) = 234.98 min

Temperature x Time:

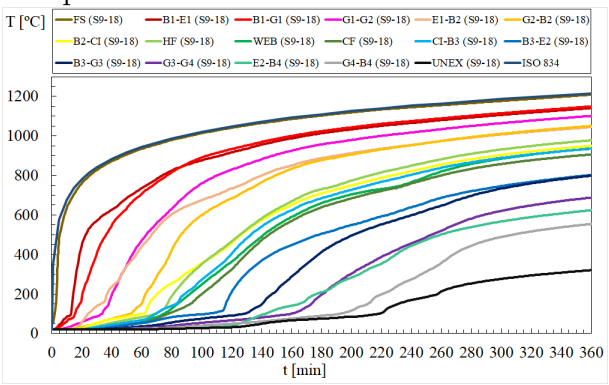

LSF Wall Configuration:

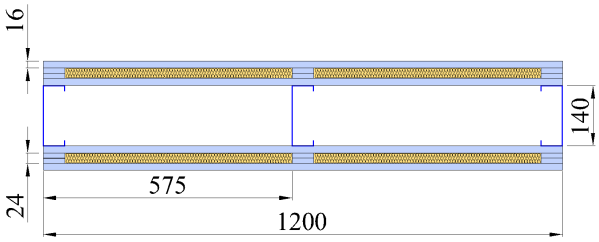

Mesh Complete Wall:

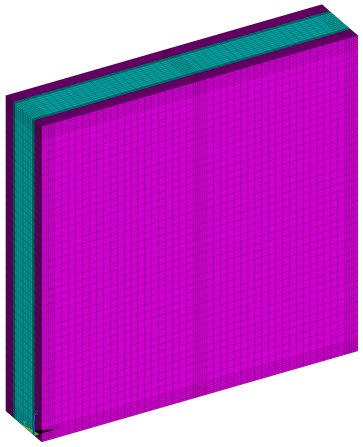

Temperature at t=3600s:

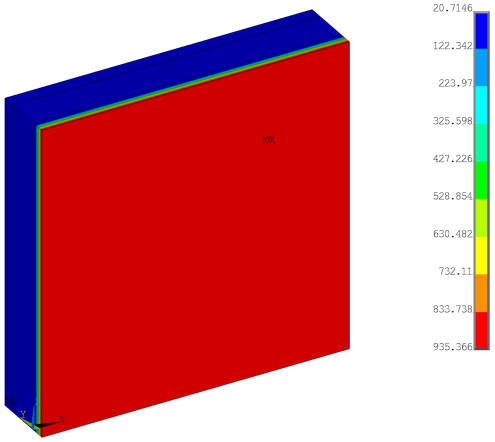

Mesh Half Wall:

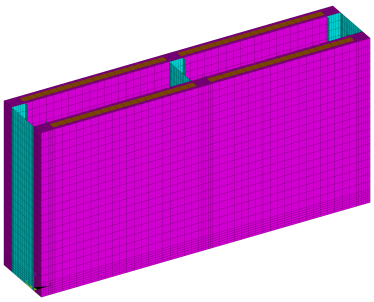

Temperature at t=3600s:

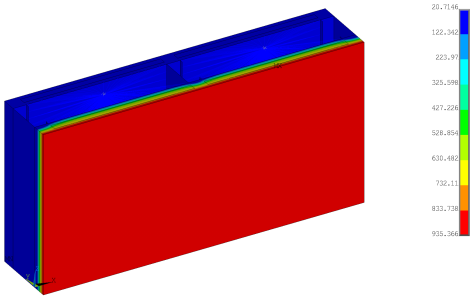

Specimen “S9” : Case 19.

STRUCTURE:
Studs: C140 (140x50x13x1.2mm)
Track: U142 (142x50x1.2 mm)
CFS wall: 1200x1200 mm
Gypsum: Type 2 (16 mm)
Rock wool: 150 kg/m^3

FIRE: Hydrocarbon
Tfi (Tmax) = 247.46 min
Tfi (Tave) = 245.83 min

Temperature x Time:

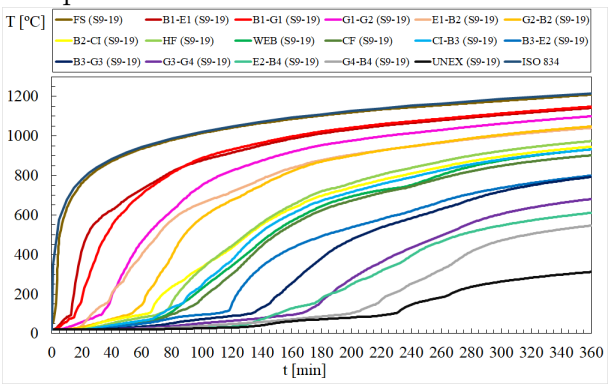

LSF Wall Configuration:

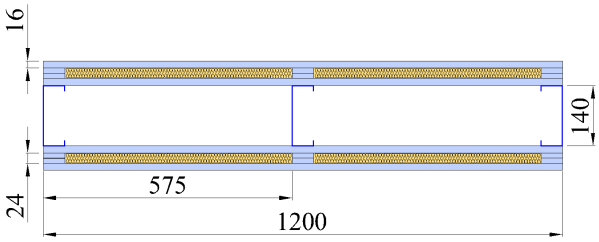

Mesh Complete Wall:

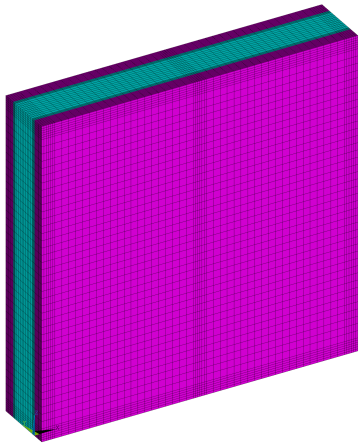

Temperature at t=3600s:

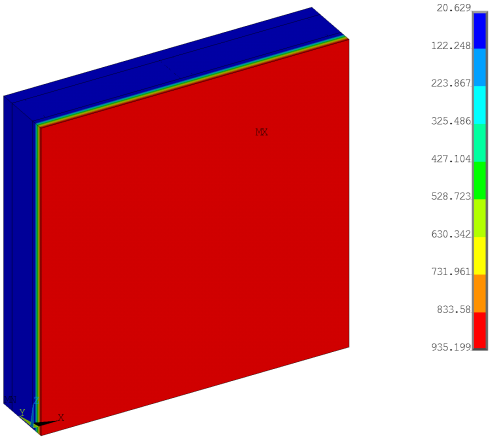

Mesh Half Wall:

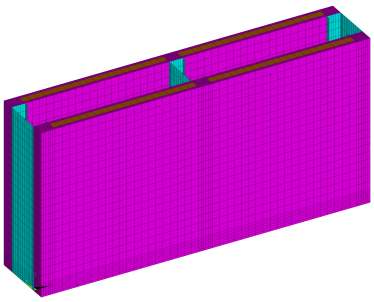

Temperature at t=3600s:

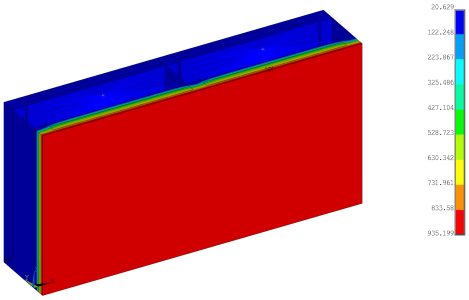

Specimen “S9” : Case 20.

STRUCTURE:
Studs: C140 (140x50x13x1.2mm)
Track: U142 (142x50x1.2 mm)
CFS wall: 1200x1200 mm
Gypsum: Type 2 (16 mm)
Rock wool: 175 kg/m^3

FIRE: Hydrocarbon
Tfi (Tmax) = 250.64 min
Tfi (Tave) = 249.1 min

Temperature x Time:

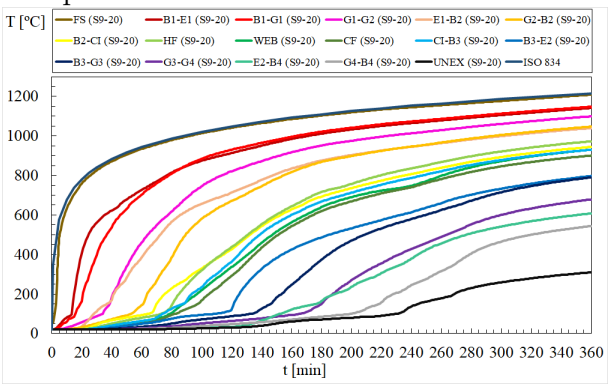

LSF Wall Configuration:

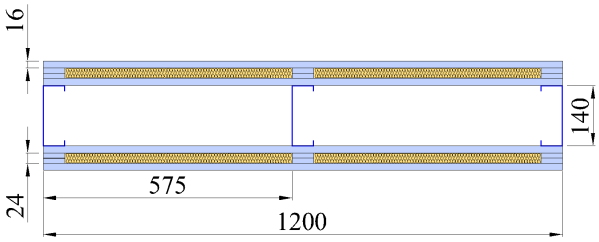

Mesh Complete Wall:

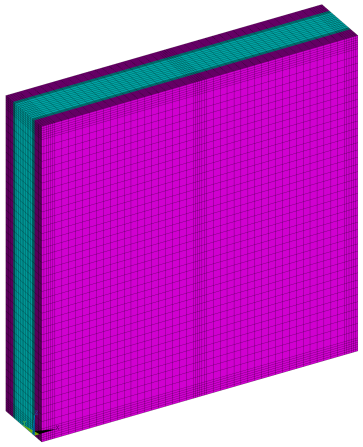

Temperature at t=3600s:

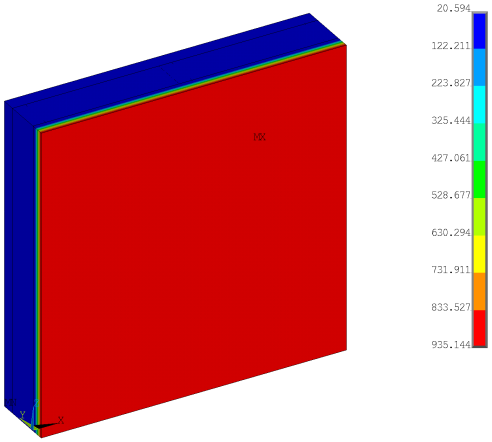

Mesh Half Wall:

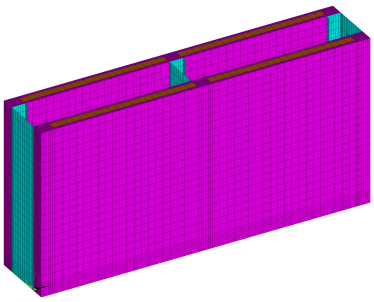

Temperature at t=3600s:

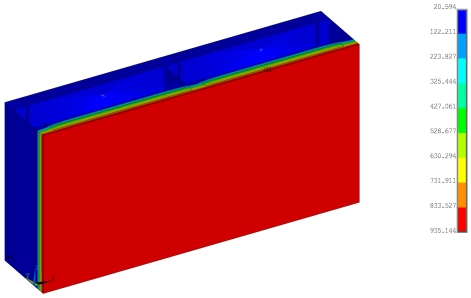

Specimen “S13” : Case 1.

STRUCTURE:
Studs: C140 (140x50x13x1.2mm)
Track: U142 (142x50x1.2 mm)
CFS wall: 1200x1200 mm
Gypsum: Type 1 (12 mm)
Rock wool: 30 kg/m^3

FIRE: Hydrocarbon
Tfi (Tmax) = 108.24 min
Tfi (Tave) = 108.75 min

Temperature x Time:

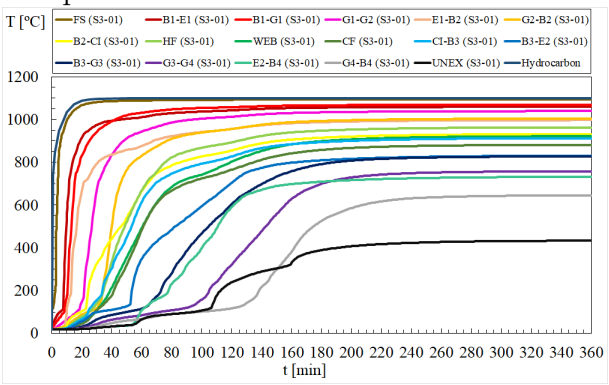

LSF Wall Configuration:

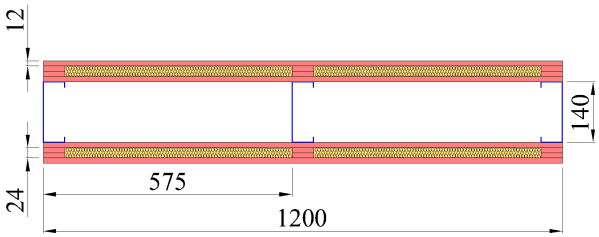

Mesh Complete Wall:

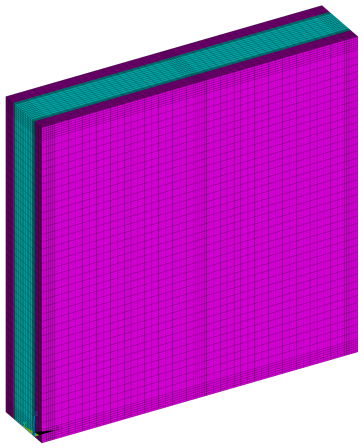

Temperature at t=3600s:

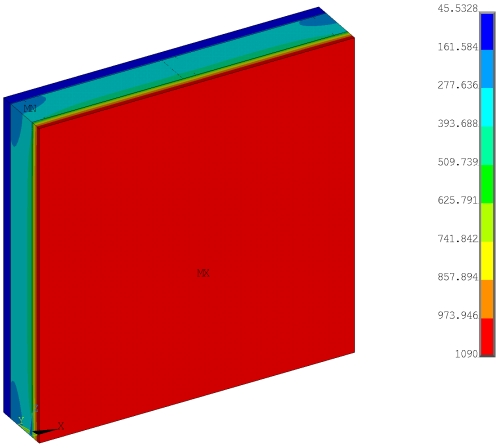

Mesh Half Wall:

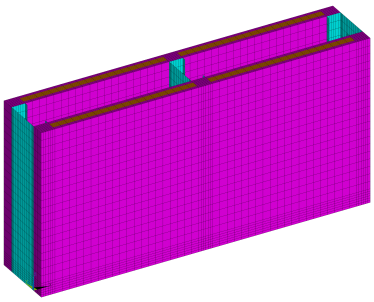

Temperature at t=3600s:

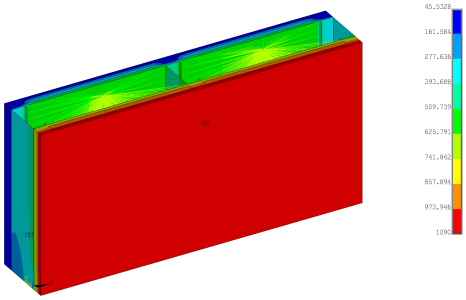

Specimen “S13” : Case 2.

STRUCTURE:
Studs: C140 (140x50x13x1.2mm)
Track: U142 (142x50x1.2 mm)
CFS wall: 1200x1200 mm
Gypsum: Type 1 (12 mm)
Rock wool: 60 kg/m^3

FIRE: Hydrocarbon
Tfi (Tmax) = 136.38 min
Tfi (Tave) = 136.83 min

Temperature x Time:

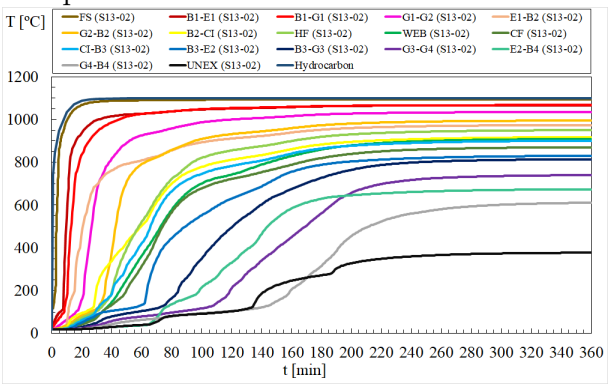

LSF Wall Configuration:

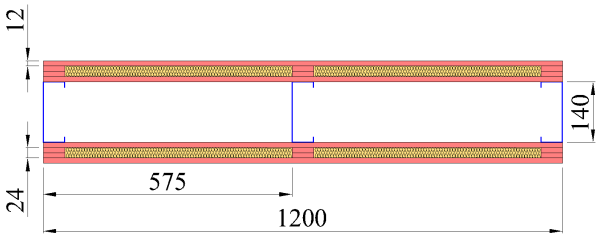

Mesh Complete Wall:

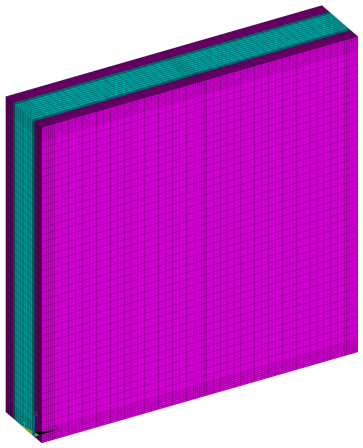

Temperature at t=3600s:

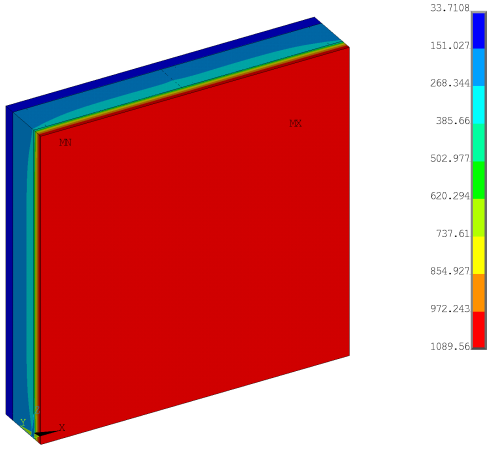

Mesh Half Wall:

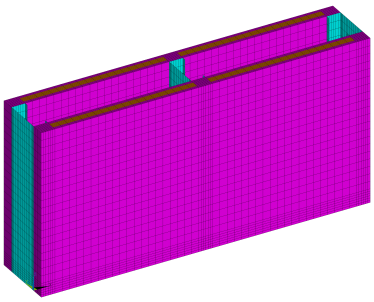

Temperature at t=3600s:

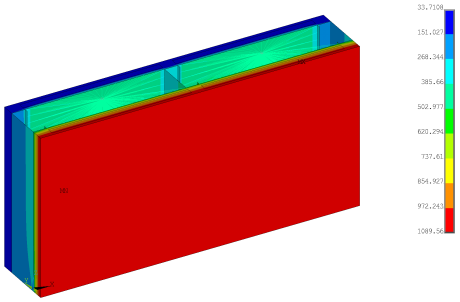

Specimen “S13” : Case 3.

STRUCTURE:
Studs: C140 (140x50x13x1.2mm)
Track: U142 (142x50x1.2 mm)
CFS wall: 1200x1200 mm
Gypsum: Type 1 (12 mm)
Rock wool: 90 kg/m^3

FIRE: Hydrocarbon
Tfi (Tmax) = 151.52 min
Tfi (Tave) = 151.67 min

Temperature x Time:

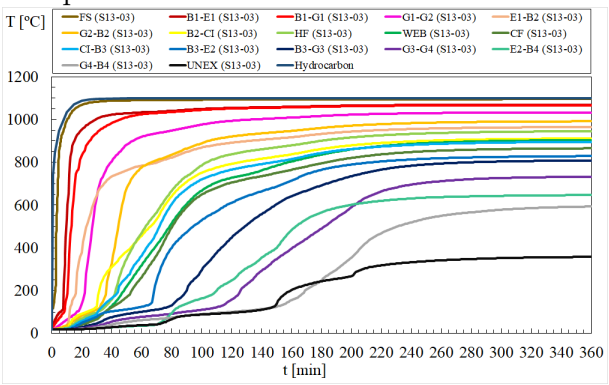

LSF Wall Configuration:

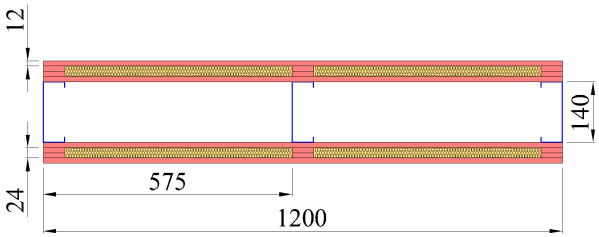

Mesh Complete Wall:

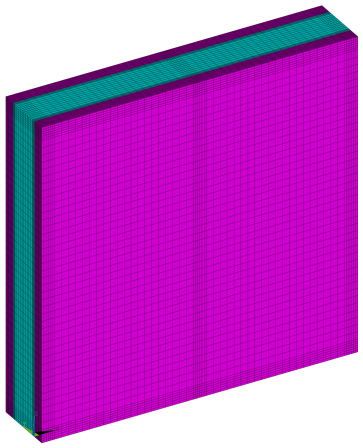

Temperature at t=3600s:

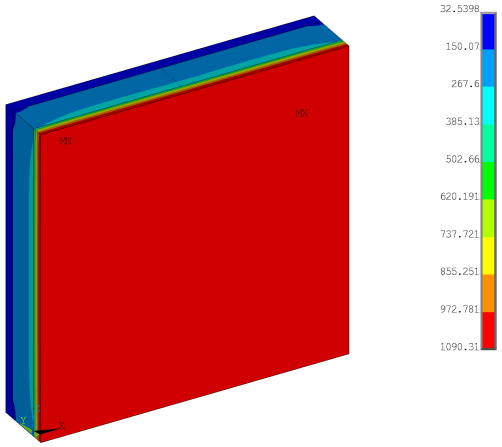

Mesh Half Wall:

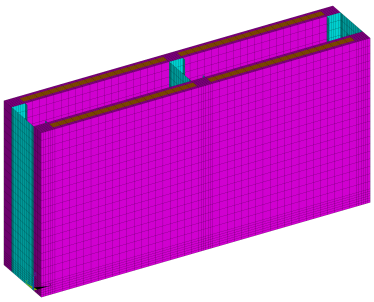

Temperature at t=3600s:

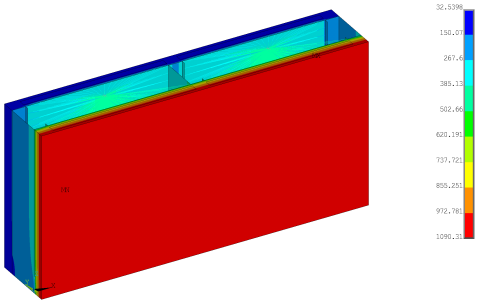

Specimen “S13” : Case 4.

STRUCTURE:
Studs: C140 (140x50x13x1.2mm)
Track: U142 (142x50x1.2 mm)
CFS wall: 1200x1200 mm
Gypsum: Type 1 (12 mm)
Rock wool: 150 kg/m^3

FIRE: Hydrocarbon
Tfi (Tmax) = 160.99 min
Tfi (Tave) = 161.03 min

Temperature x Time:

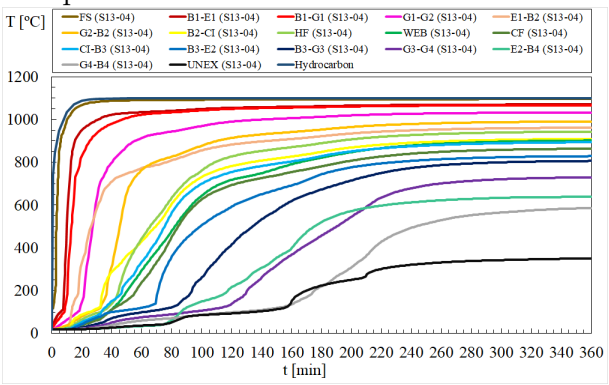

LSF Wall Configuration:

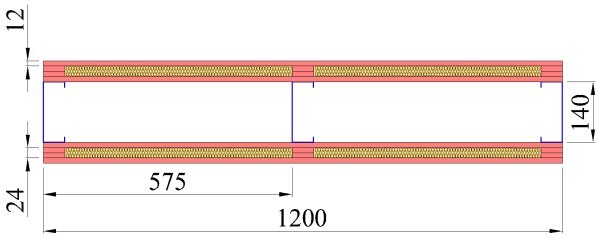

Mesh Complete Wall:

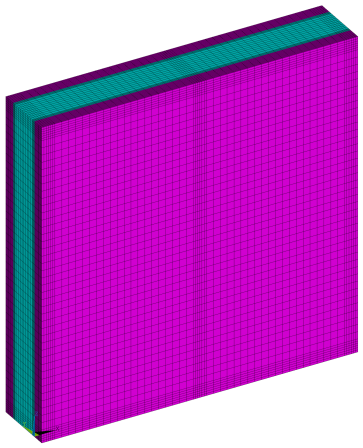

Temperature at t=3600s:

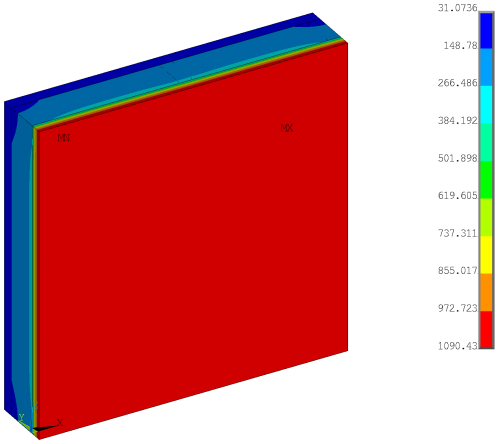

Mesh Half Wall:

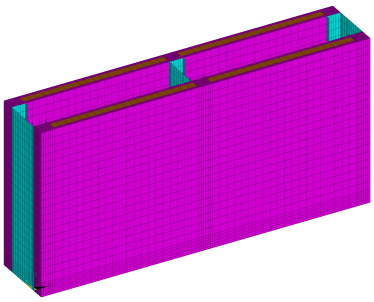

Temperature at t=3600s:

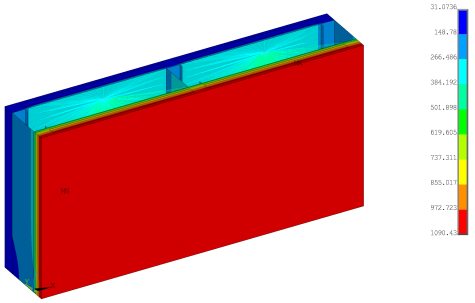

Specimen “S13” : Case 5.

STRUCTURE:
Studs: C140 (140x50x13x1.2mm)
Track: U142 (142x50x1.2 mm)
CFS wall: 1200x1200 mm
Gypsum: Type 1 (12 mm)
Rock wool: 175 kg/m^3

FIRE: Hydrocarbon
Tfi (Tmax) = 163.41 min
Tfi (Tave) = 163.48 min

Temperature x Time:

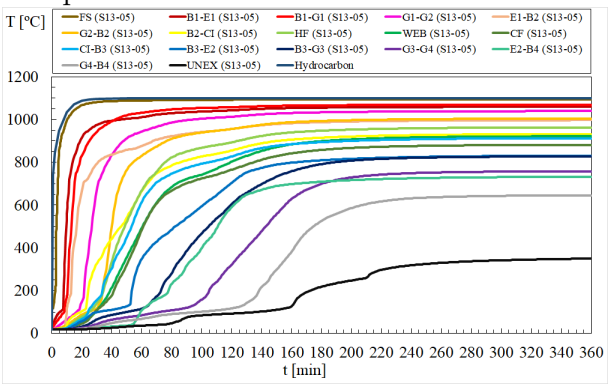

LSF Wall Configuration:

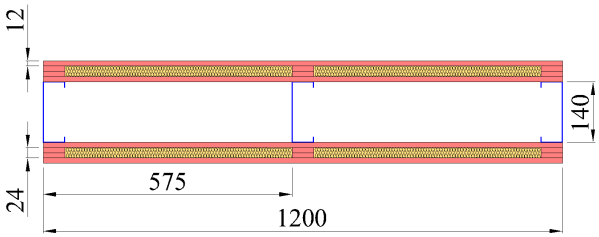

Mesh Complete Wall:

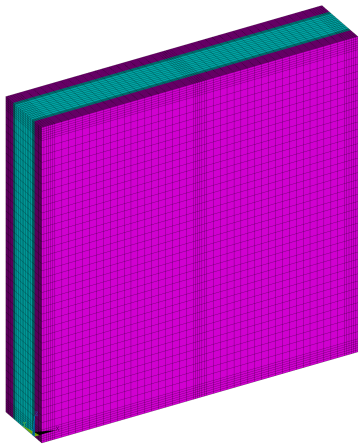

Temperature at t=3600s:

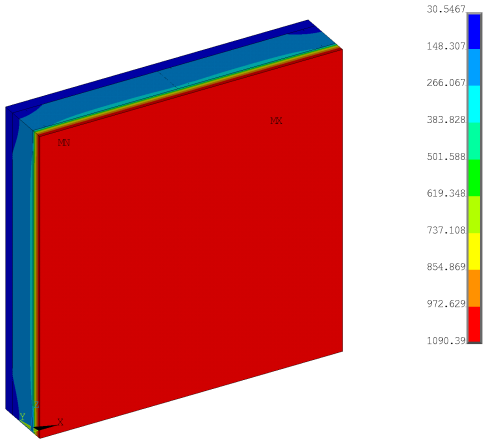

Mesh Half Wall:

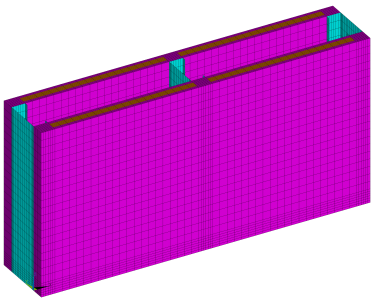

Temperature at t=3600s:

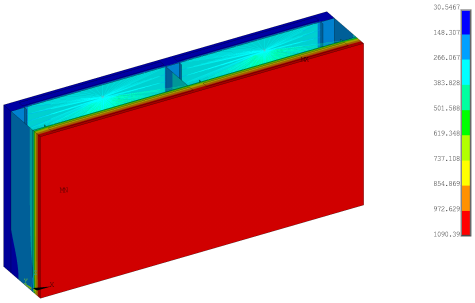

Specimen “S13” : Case 6.

STRUCTURE:
Studs: C140 (140x50x13x1.2mm)
Track: U142 (142x50x1.2 mm)
CFS wall: 1200x1200 mm
Gypsum: Type 2 (12 mm)
Rock wool: 30 kg/m^3

FIRE: Hydrocarbon
Tfi (Tmax) = 93.1 min
Tfi (Tave) = 93.98 min

Temperature x Time:

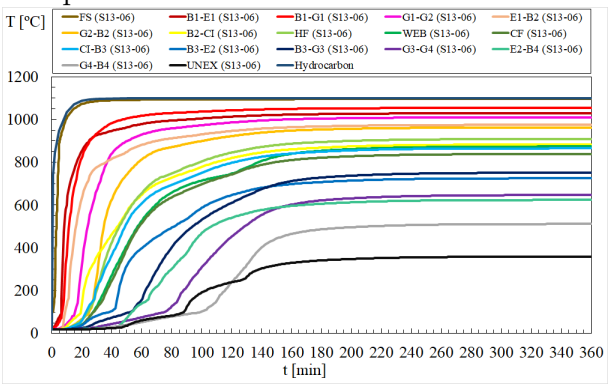

LSF Wall Configuration:

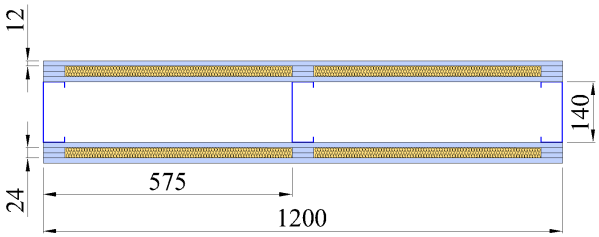

Mesh Complete Wall:

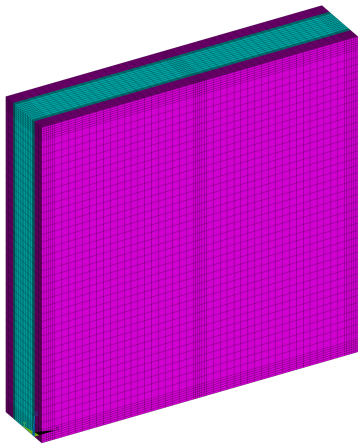

Temperature at t=3600s:

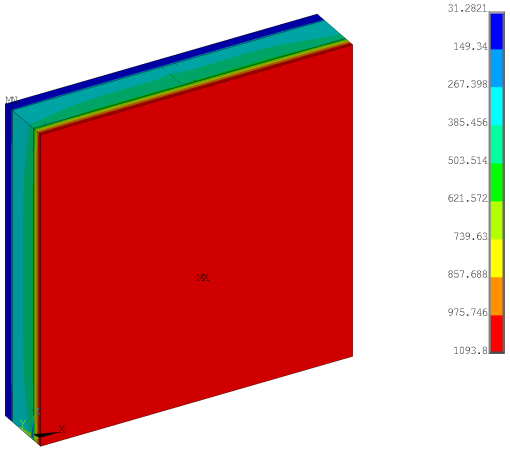

Mesh Half Wall:

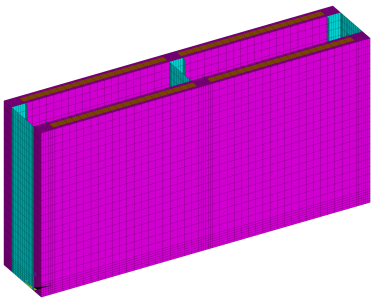

Temperature at t=3600s:

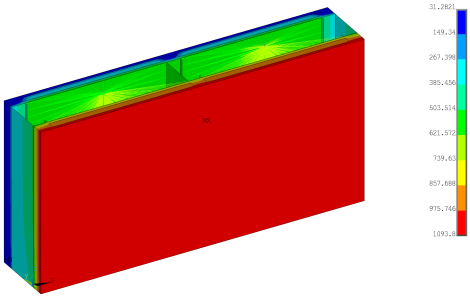

Specimen “S13” : Case 7.

STRUCTURE:
Studs: C140 (140x50x13x1.2mm)
Track: U142 (142x50x1.2 mm)
CFS wall: 1200x1200 mm
Gypsum: Type 2 (12 mm)
Rock wool: 60 kg/m^3

FIRE: Hydrocarbon
Tfi (Tmax) = 115.35 min
Tfi (Tave) = 115.93 min

Temperature x Time:

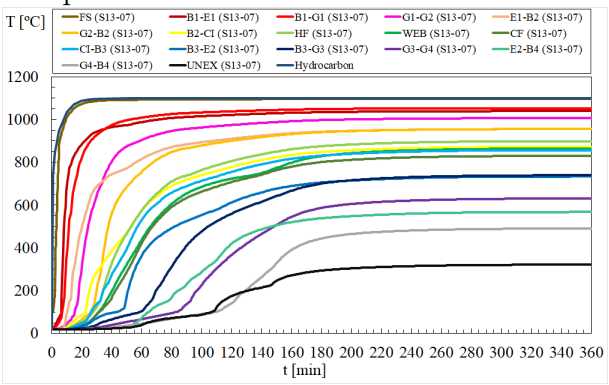

LSF Wall Configuration:

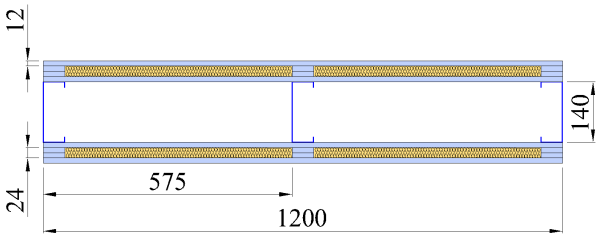

Mesh Complete Wall:

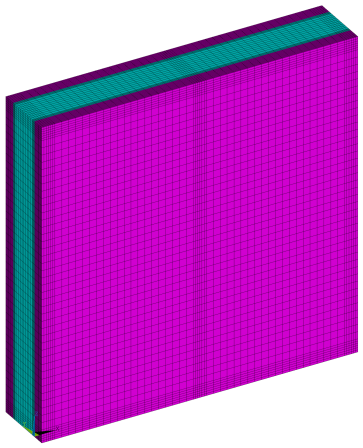

Temperature at t=3600s:

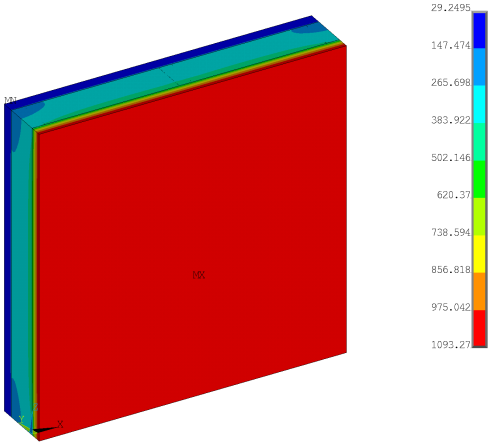

Mesh Half Wall:

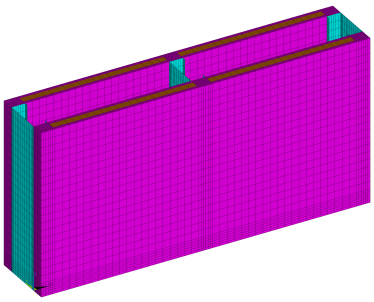

Temperature at t=3600s:

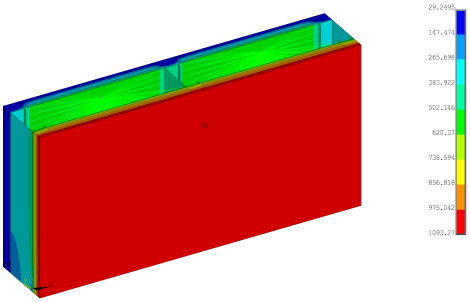

Specimen “S13” : Case 8.

STRUCTURE:
Studs: C140 (140x50x13x1.2mm)
Track: U142 (142x50x1.2 mm)
CFS wall: 1200x1200 mm
Gypsum: Type 2 (12 mm)
Rock wool: 90 kg/m^3

FIRE: Hydrocarbon
Tfi (Tmax) = 128.3 min
Tfi (Tave) = 128.6 min

Temperature x Time:

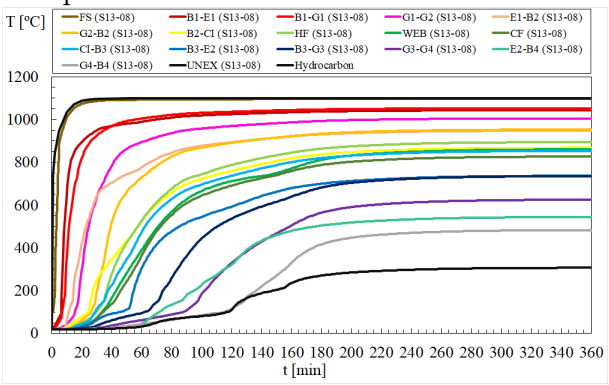

LSF Wall Configuration:

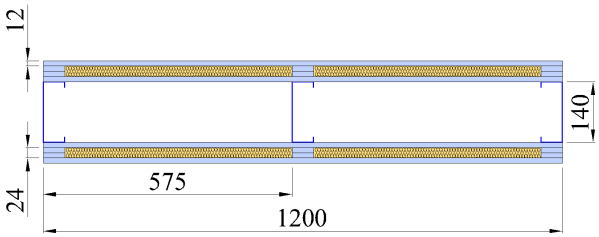

Mesh Complete Wall:

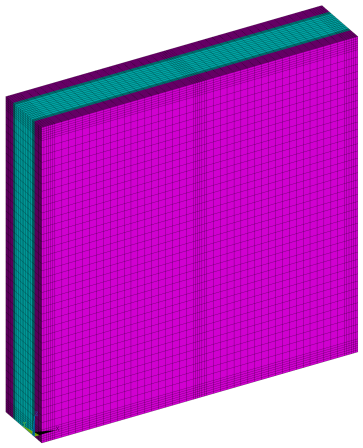

Temperature at t=3600s:

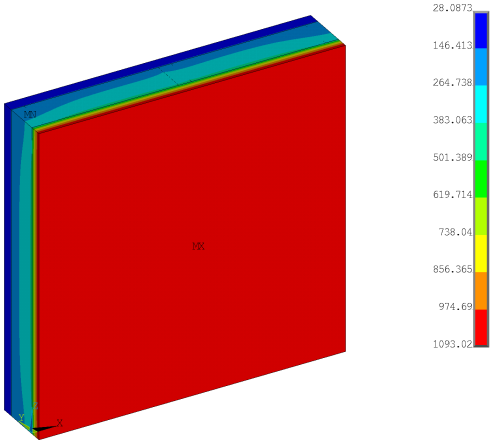

Mesh Half Wall:

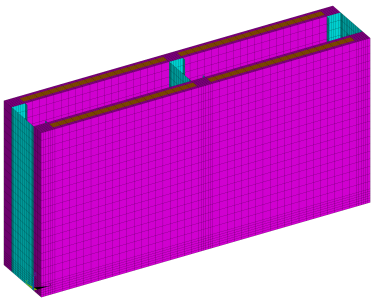

Temperature at t=3600s:

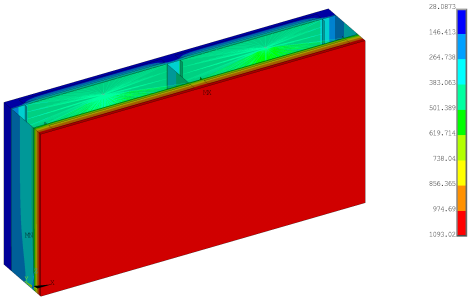

Specimen “S13” : Case 9.

STRUCTURE:
Studs: C140 (140x50x13x1.2mm)
Track: U142 (142x50x1.2 mm)
CFS wall: 1200x1200 mm
Gypsum: Type 2 (12 mm)
Rock wool: 150 kg/m^3

FIRE: Hydrocarbon
Tfi (Tmax) = 138.3 min
Tfi (Tave) = 138.16 min

Temperature x Time:

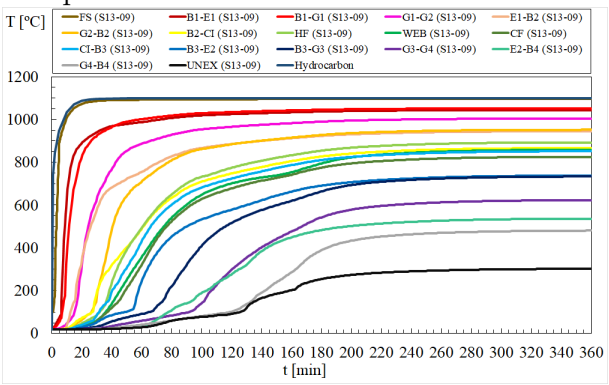

LSF Wall Configuration:

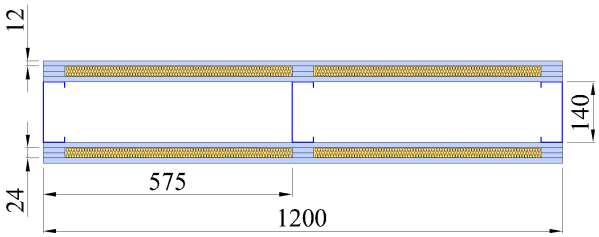

Mesh Complete Wall:

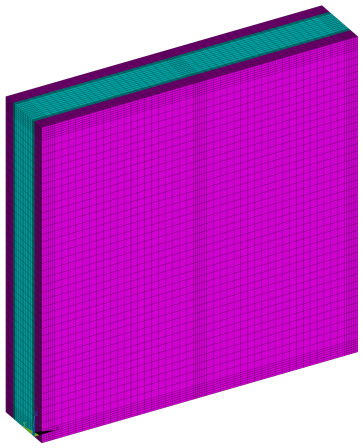

Temperature at t=3600s:

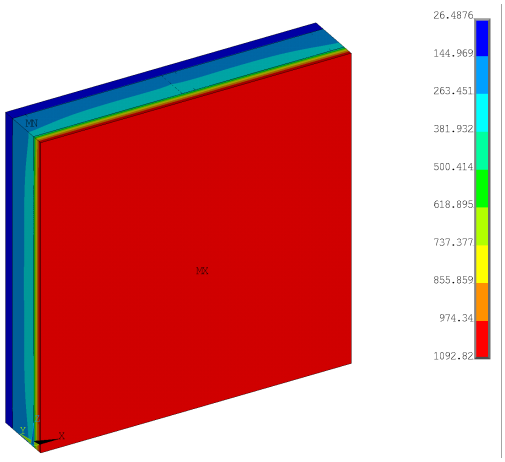

Mesh Half Wall:

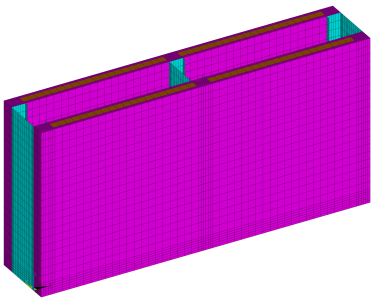

Temperature at t=3600s:

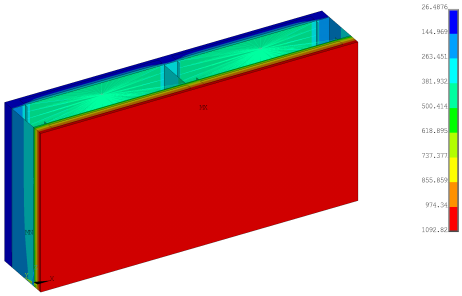

Specimen “S13” : Case 10.

STRUCTURE:
Studs: C140 (140x50x13x1.2mm)
Track: U142 (142x50x1.2 mm)
CFS wall: 1200x1200 mm
Gypsum: Type 2 (12 mm)
Rock wool: 175 kg/m^3

FIRE: Hydrocarbon
Tfi (Tmax) = 140.6 min
Tfi (Tave) = 140.44 min

Temperature x Time:

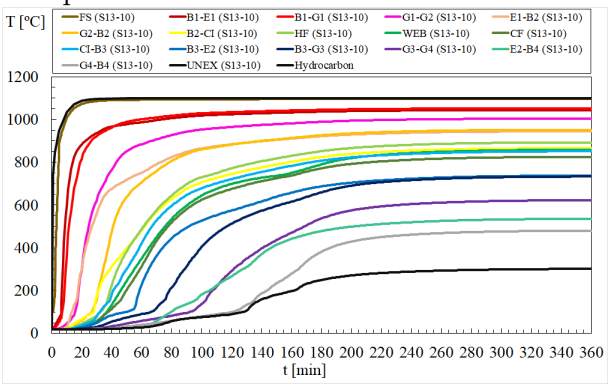

LSF Wall Configuration:

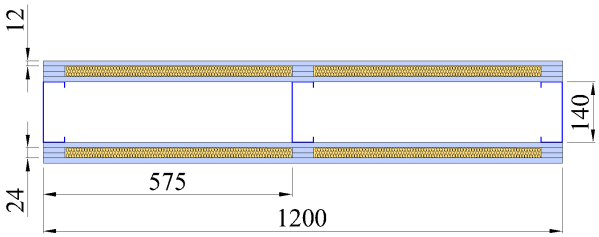

Mesh Complete Wall:

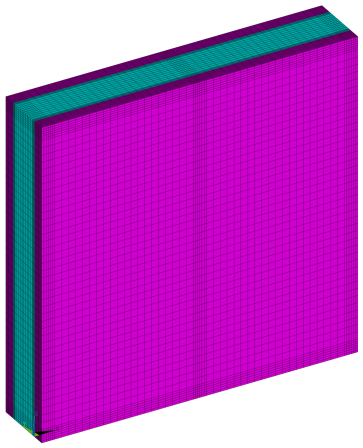

Temperature at t=3600s:

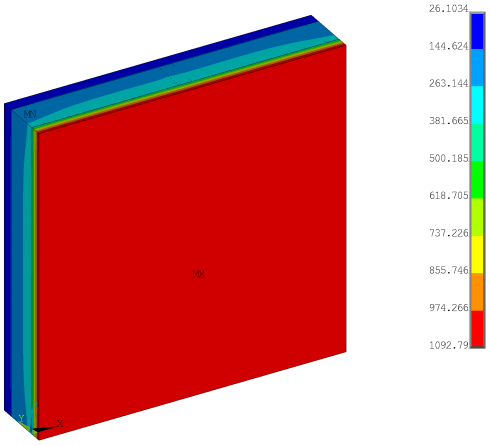

Mesh Half Wall:

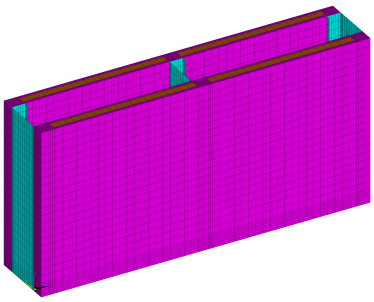

Temperature at t=3600s:

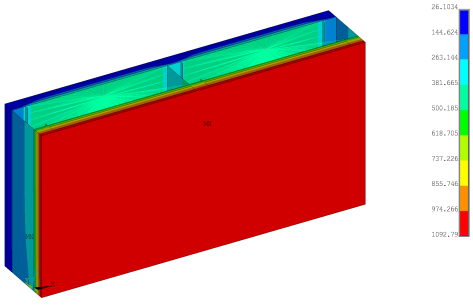

Specimen “S13” : Case 11.

STRUCTURE:
Studs: C140 (140x50x13x1.2mm)
Track: U142 (142x50x1.2 mm)
CFS wall: 1200x1200 mm
Gypsum: Type 1 (16 mm)
Rock wool: 30 kg/m^3

FIRE: Hydrocarbon
Tfi (Tmax) = 170.42 min
Tfi (Tave) = 170.61 min

Temperature x Time:

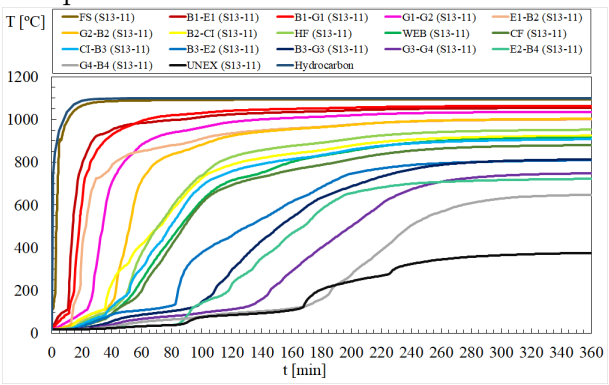

LSF Wall Configuration:

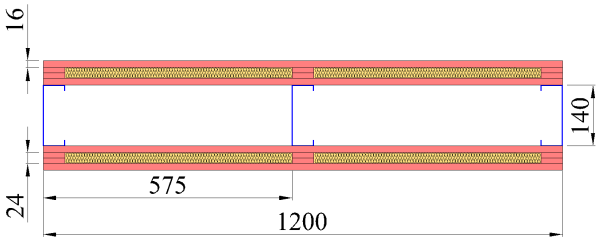

Mesh Complete Wall:

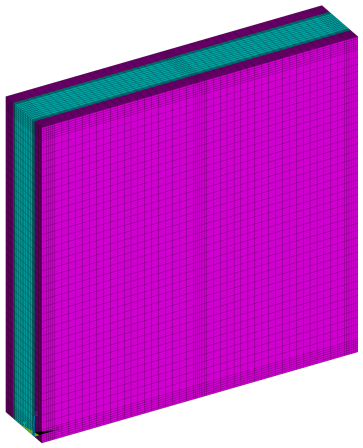

Temperature at t=3600s:

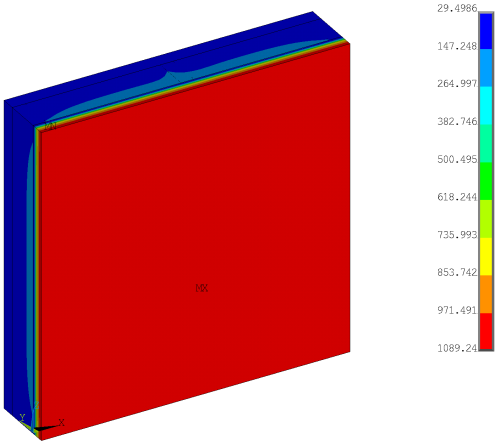

Mesh Half Wall:

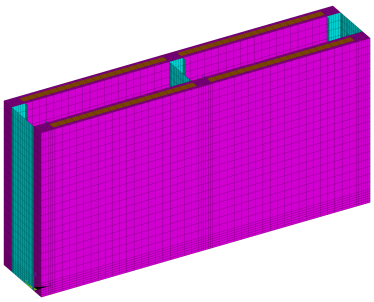

Temperature at t=3600s:

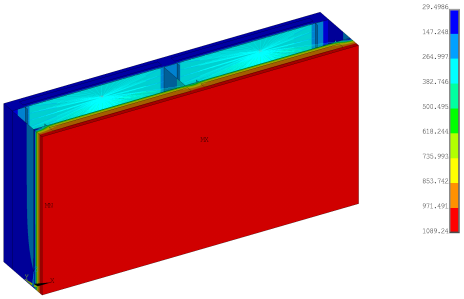

Specimen “S13” : Case 12.

STRUCTURE:
Studs: C140 (140x50x13x1.2mm)
Track: U142 (142x50x1.2 mm)
CFS wall: 1200x1200 mm
Gypsum: Type 1 (16 mm)
Rock wool: 60 kg/m^3

FIRE: Hydrocarbon
Tfi (Tmax) = 206.08 min
Tfi (Tave) = 206.16 min

Temperature x Time:

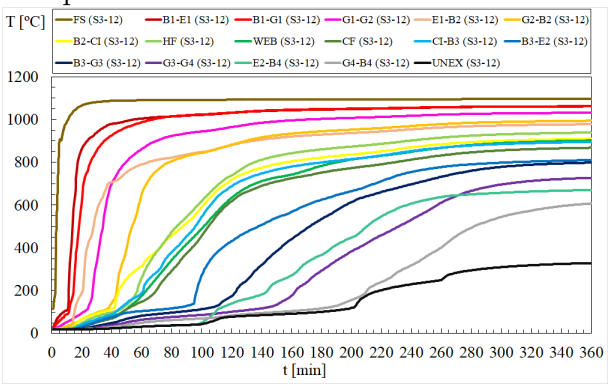

LSF Wall Configuration:

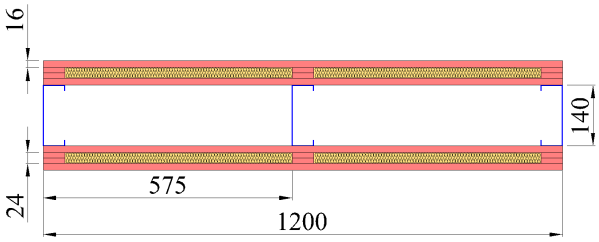

Mesh Complete Wall:

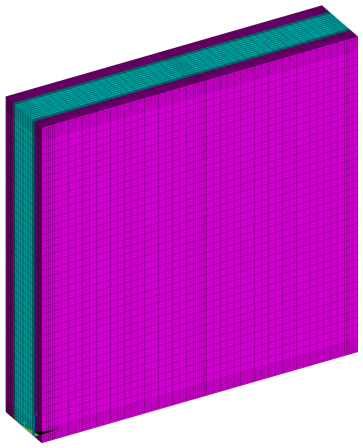

Temperature at t=3600s:

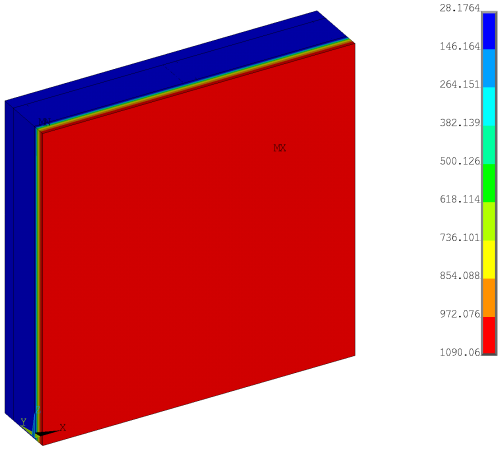

Mesh Half Wall:

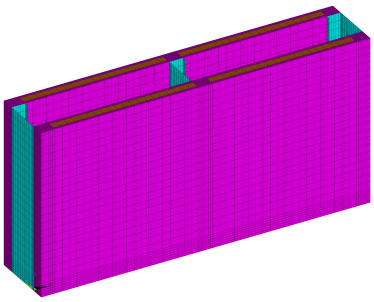

Temperature at t=3600s:

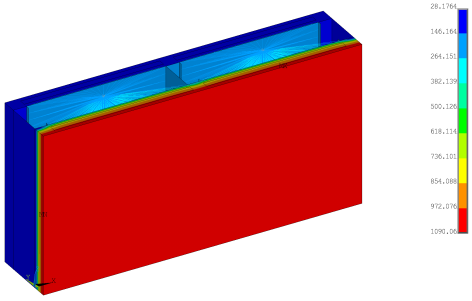

Specimen “S13” : Case 13.

STRUCTURE:
Studs: C140 (140x50x13x1.2mm)
Track: U142 (142x50x1.2 mm)
CFS wall: 1200x1200 mm
Gypsum: Type 1 (16 mm)
Rock wool: 90 kg/m^3

FIRE: Hydrocarbon
Tfi (Tmax) = 224.63 min
Tfi (Tave) = 224.43 min

Temperature x Time:

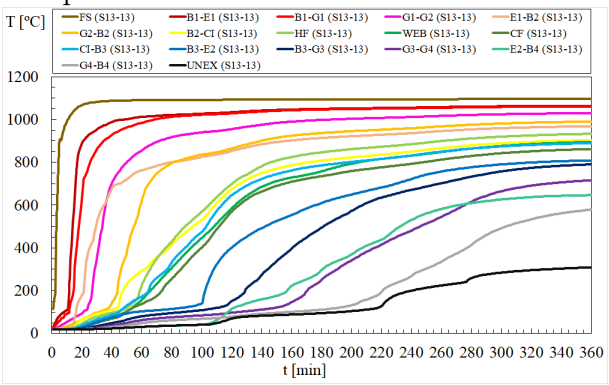

LSF Wall Configuration:

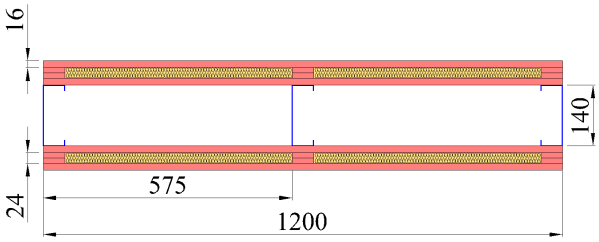

Mesh Complete Wall:

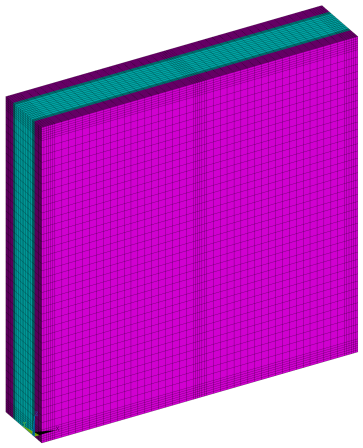

Temperature at t=3600s:

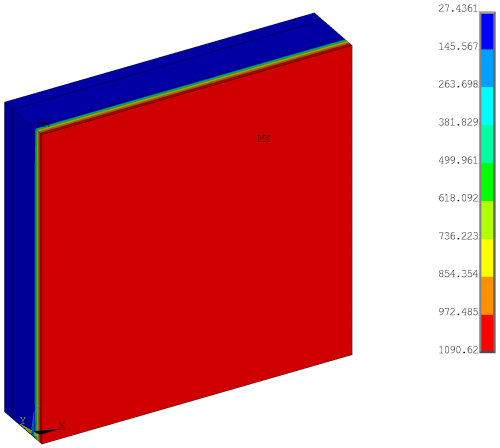

Mesh Half Wall:

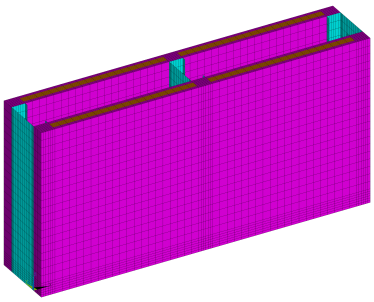

Temperature at t=3600s:

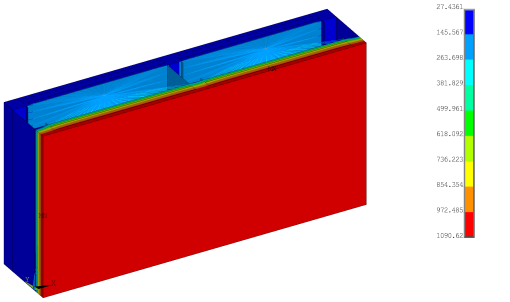

Specimen “S13” : Case 14.

STRUCTURE:
Studs: C140 (140x50x13x1.2mm)
Track: U142 (142x50x1.2 mm)
CFS wall: 1200x1200 mm
Gypsum: Type 1 (16 mm)
Rock wool: 150 kg/m^3

FIRE: Hydrocarbon
Tfi (Tmax) = 236.54 min
Tfi (Tave) = 235.92 min

Temperature x Time:

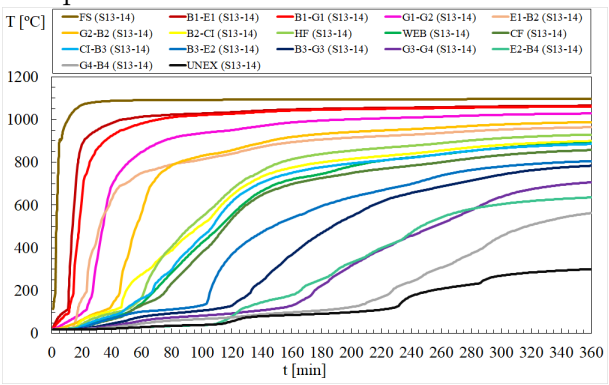

LSF Wall Configuration:

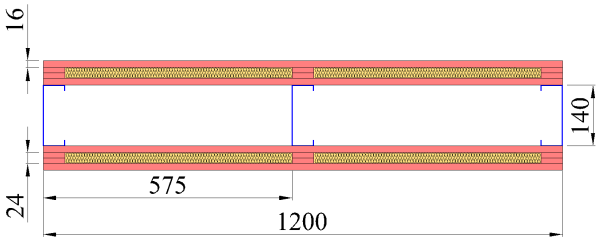

Mesh Complete Wall:

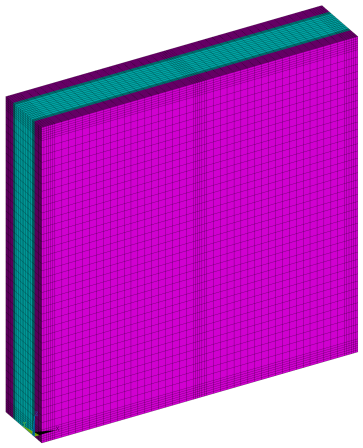

Temperature at t=3600s:

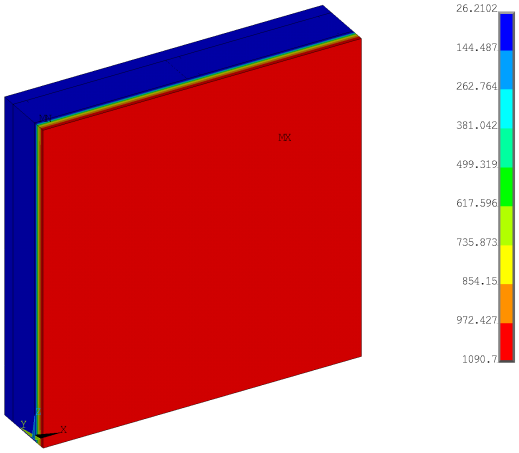

Mesh Half Wall:

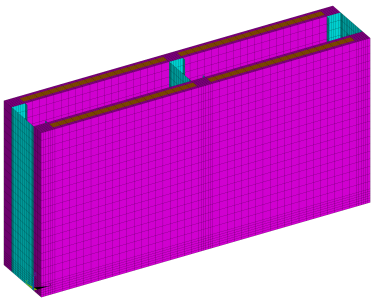

Temperature at t=3600s:

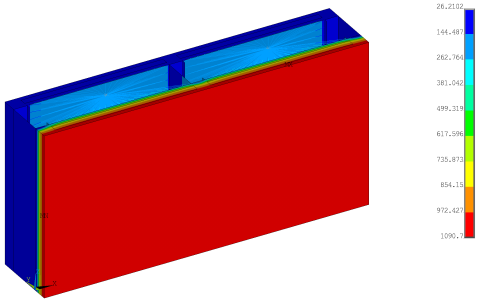

Specimen “S13” : Case 15.

STRUCTURE:
Studs: C140 (140x50x13x1.2mm)
Track: U142 (142x50x1.2 mm)
CFS wall: 1200x1200 mm
Gypsum: Type 1 (16 mm)
Rock wool: 175 kg/m^3

FIRE: Hydrocarbon
Tfi (Tmax) = 239.32 min
Tfi (Tave) = 238.81 min

Temperature x Time:

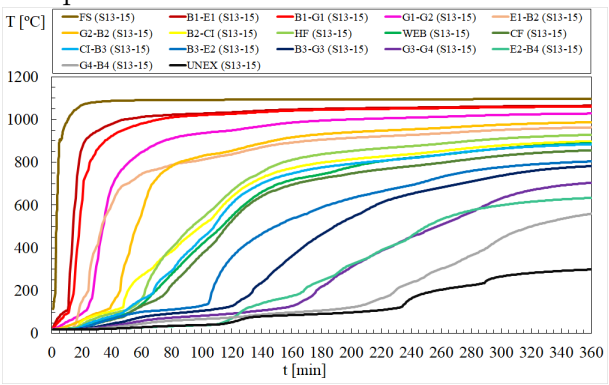

LSF Wall Configuration:

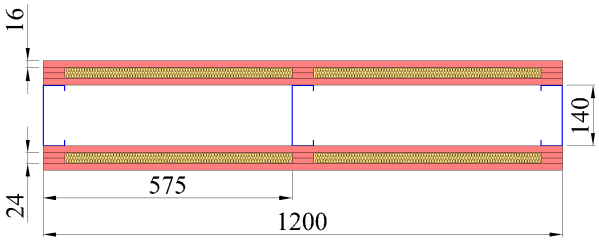

Mesh Complete Wall:

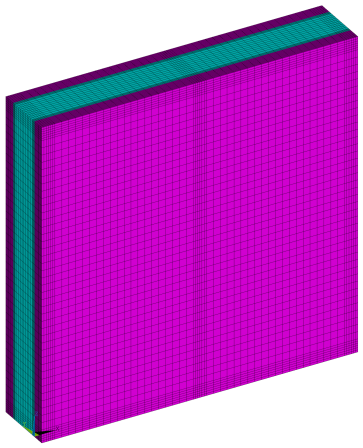

Temperature at t=3600s:

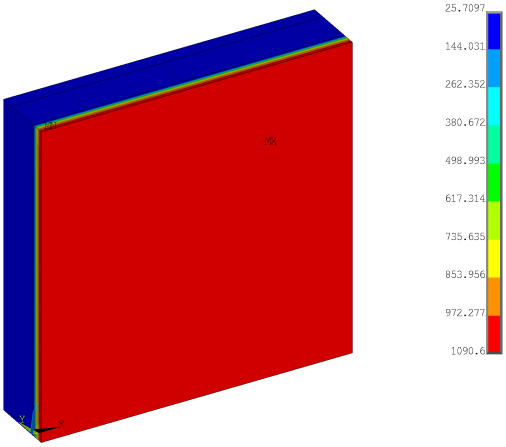

Mesh Half Wall:

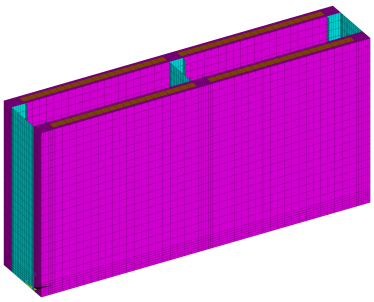

Temperature at t=3600s:

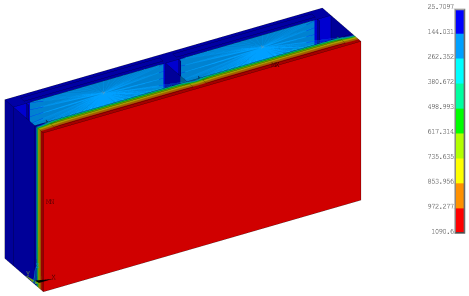

Specimen “S13” : Case 16.

STRUCTURE:
Studs: C140 (140x50x13x1.2mm)
Track: U142 (142x50x1.2 mm)
CFS wall: 1200x1200 mm
Gypsum: Type 2 (16 mm)
Rock wool: 30 kg/m^3

FIRE: Hydrocarbon
Tfi (Tmax) = 148.33 min
Tfi (Tave) = 149.08 min

Temperature x Time:

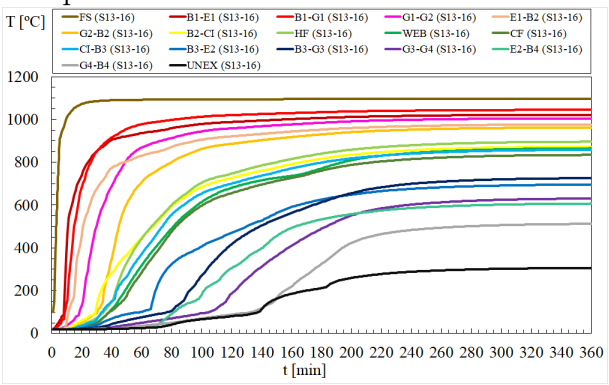

LSF Wall Configuration:

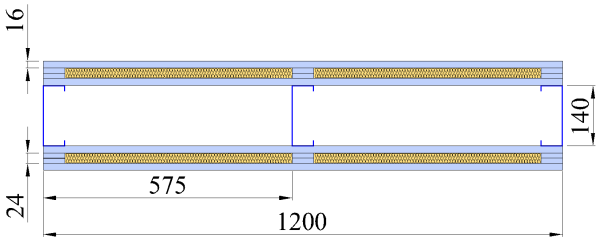

Mesh Complete Wall:

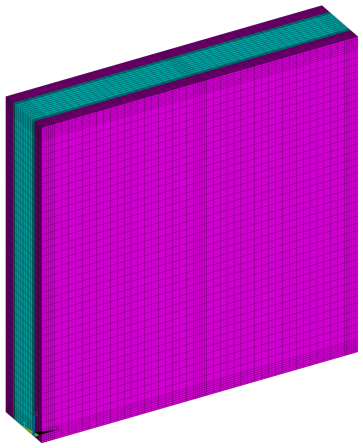

Temperature at t=3600s:

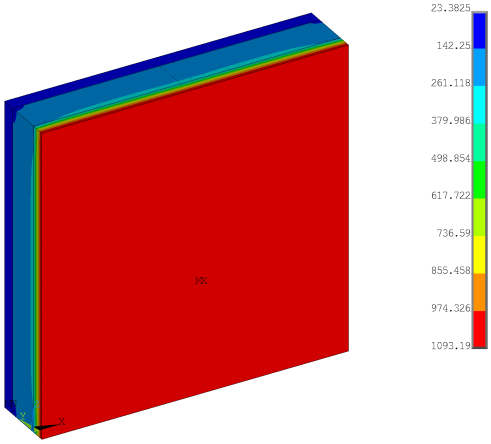

Mesh Half Wall:

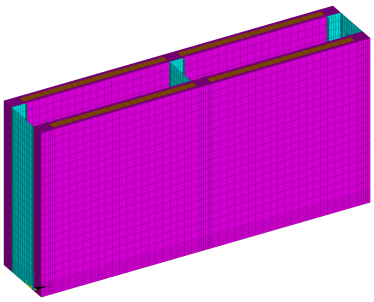

Temperature at t=3600s:

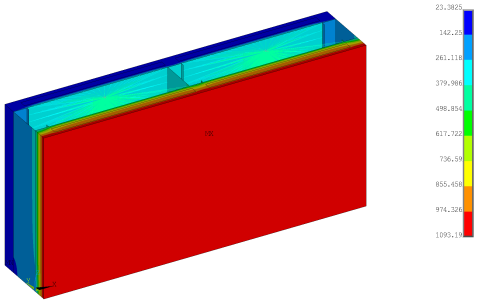

Specimen “S13” : Case 17.

STRUCTURE:
Studs: C140 (140x50x13x1.2mm)
Track: U142 (142x50x1.2 mm)
CFS wall: 1200x1200 mm
Gypsum: Type 2 (16 mm)
Rock wool: 60 kg/m^3

FIRE: Hydrocarbon
Tfi (Tmax) = 178.54 min
Tfi (Tave) = 178.37 min

Temperature x Time:

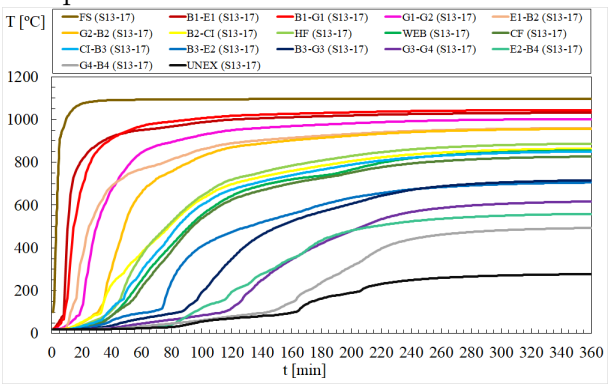

LSF Wall Configuration:

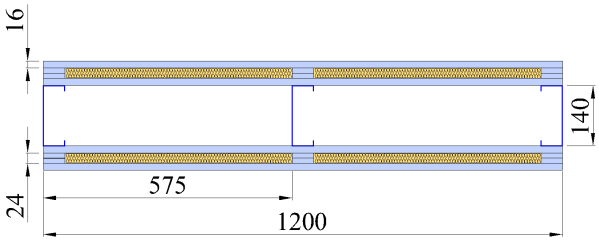

Mesh Complete Wall:

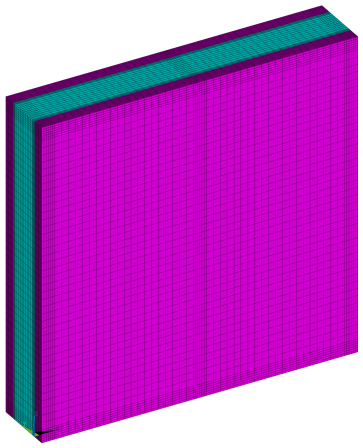

Temperature at t=3600s:

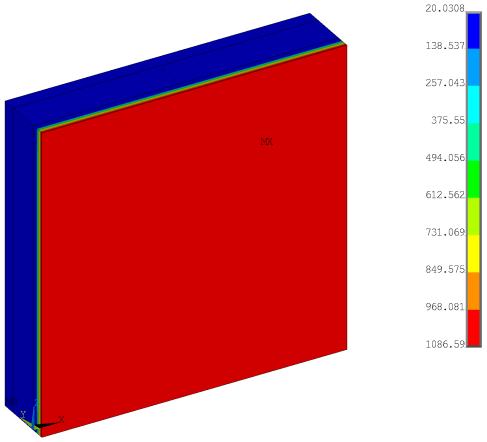

Mesh Half Wall:

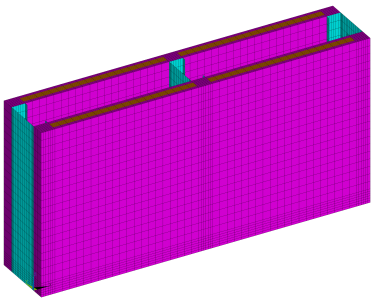

Temperature at t=3600s:

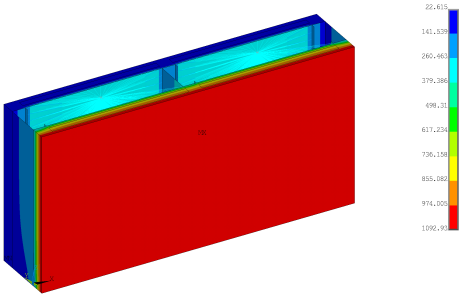

Specimen “S13” : Case 18.

STRUCTURE:
Studs: C140 (140x50x13x1.2mm)
Track: U142 (142x50x1.2 mm)
CFS wall: 1200x1200 mm
Gypsum: Type 2 (16 mm)
Rock wool: 90 kg/m^3

FIRE: Hydrocarbon
Tfi (Tmax) = 196.95 min
Tfi (Tave) = 195.08 min

Temperature x Time:

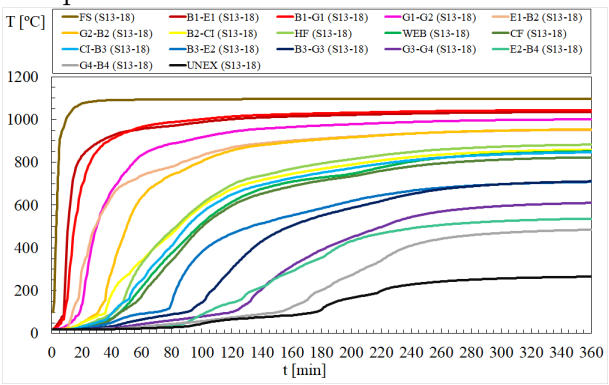

LSF Wall Configuration:

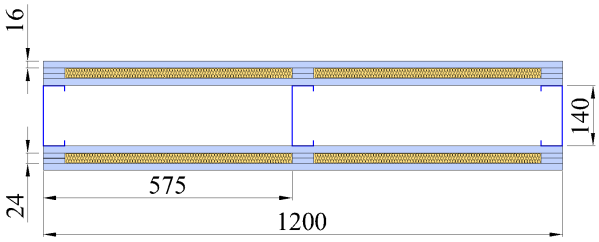

Mesh Complete Wall:

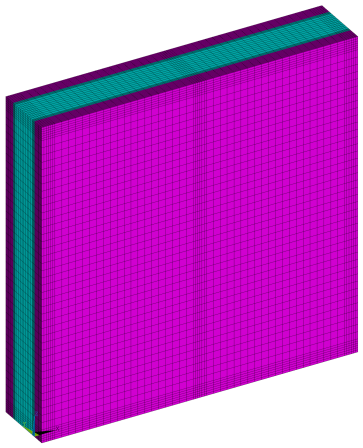

Temperature at t=3600s:

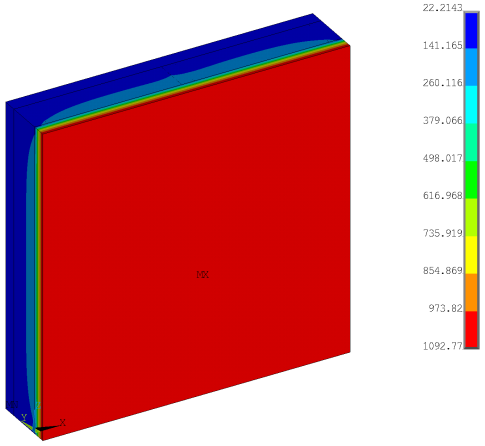

Mesh Half Wall:

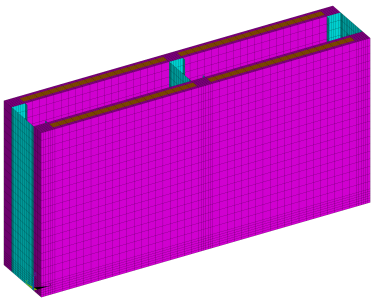

Temperature at t=3600s:

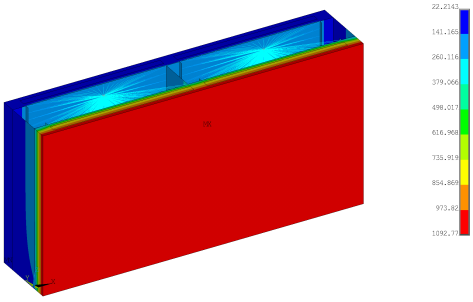

Specimen “S13” : Case 19.

STRUCTURE:
Studs: C140 (140x50x13x1.2mm)
Track: U142 (142x50x1.2 mm)
CFS wall: 1200x1200 mm
Gypsum: Type 2 (16 mm)
Rock wool: 150 kg/m^3

FIRE: Hydrocarbon
Tfi (Tmax) = 210.3 min
Tfi (Tave) = 207.89 min

Temperature x Time:

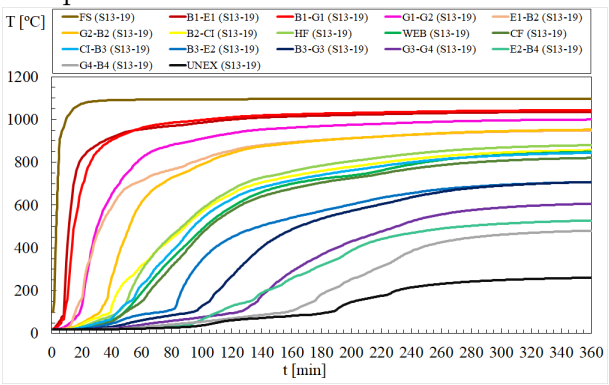

LSF Wall Configuration:

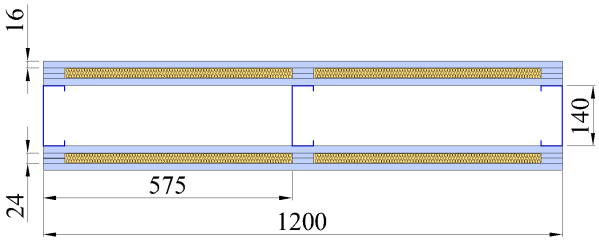

Mesh Complete Wall:

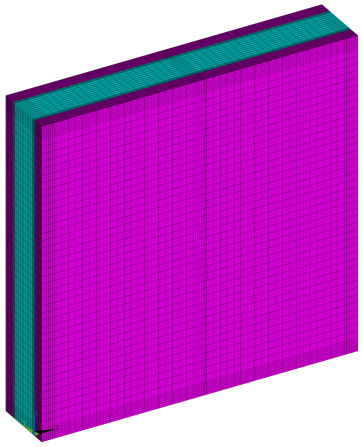

Temperature at t=3600s:

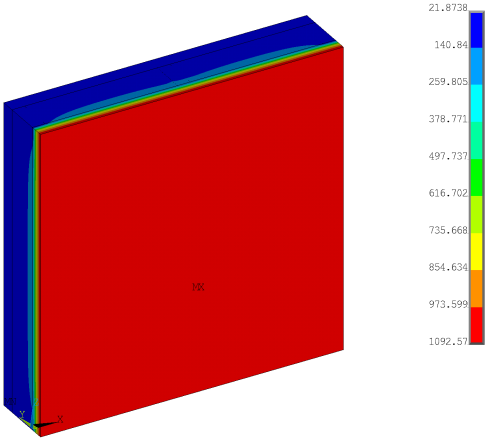

Mesh Half Wall:

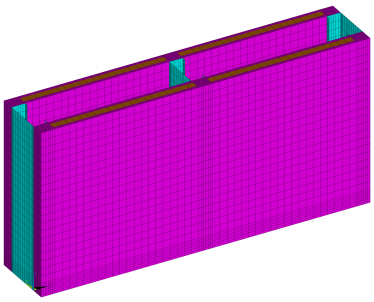

Temperature at t=3600s:

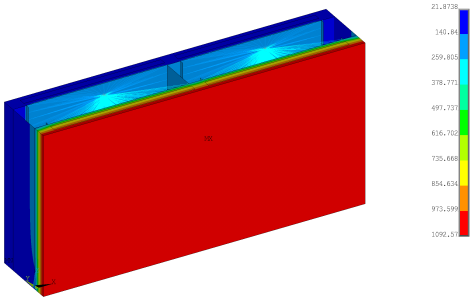

Specimen “S13” : Case 20.

STRUCTURE:
Studs: C140 (140x50x13x1.2mm)
Track: U142 (142x50x1.2 mm)
CFS wall: 1200x1200 mm
Gypsum: Type 2 (16 mm)
Rock wool: 175 kg/m^3

FIRE: Hydrocarbon
Tfi (Tmax) = 214.22 min
Tfi (Tave) = 211.52 min

Temperature x Time:

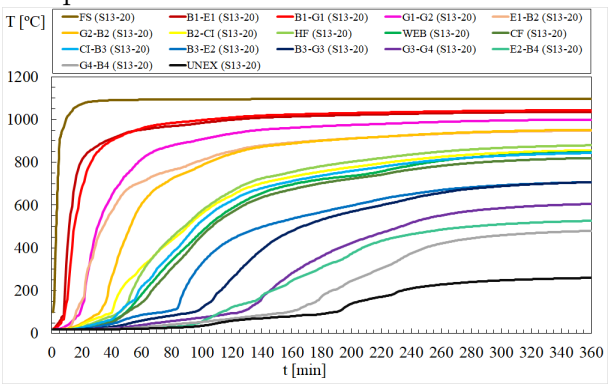

LSF Wall Configuration:

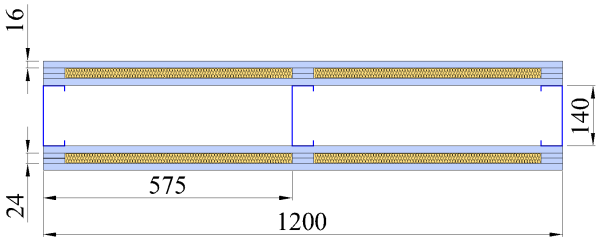

Mesh Complete Wall:

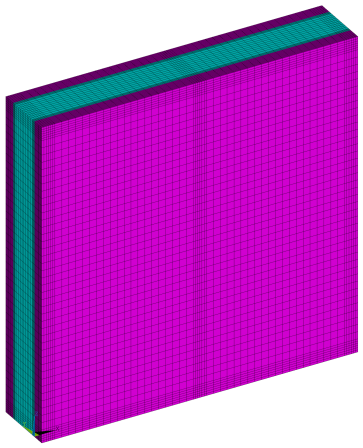

Temperature at t=3600s:

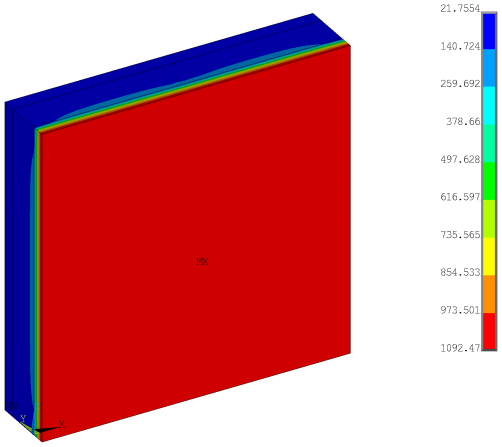

Mesh Half Wall:

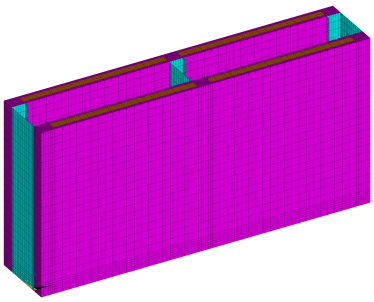

Temperature at t=3600s: